University of Alberta

Nanoengineered Glancing Angle Deposition Thin Films for Ultrathin-Layer Chromatography

by

Steven Richard Jim

A thesis submitted to the Faculty of Graduate Studies and Research
in partial fulfillment of the requirements for the degree of

Doctor of Philosophy

in

Microsystems and Nanodevices

Department of Electrical and Computer Engineering

Spring 2014
Edmonton, Alberta

Dedicated to my mom, dad, and sister,
always loving and supportive.

Abstract

Analytical separations are important methods of identifying and quantifying molecular compounds present in complex sample mixtures. These approaches are popular in biochemistry, medical diagnostics, quality control, and numerous other applications. In these techniques, constituent analytes are separated according to their characteristic physical and chemical properties. Planar chromatography analytical separations leverage the effects of these properties on competing interactions between the compounds, moving liquids, and stationary flat porous solids. Engineered solid-liquid interfaces can improve performance since these interactions occur at the nanoscale.

Ultrathin-layer chromatography (UTLC) is a miniature form of planar chromatography in which sample analytes are carried by solvents that wick through < 10 μm thick solids with extraordinarily fine pores. The technique achieves fast separations (minutes) over short distances (millimetres to centimetres) with high sensitivity. The strong dependence of UTLC performance on layer microstructure motivates pursuit of new chromatographic media.

This dissertation studies UTLC layers produced using glancing angle deposition (GLAD). GLAD is an excellent platform for engineering nanostructured thin films of varied material, porosity, and architecture. It can achieve ~ 5 μm thick columnar morphologies well-suited for UTLC that are unattainable or impractical using other techniques. Unique anisotropic media exhibited channel features that strongly influenced analyte migration direction

and velocity. Further control of chromatographic behaviours was achieved using post-deposition enhancements. Fluorocarbon reactive ion etching (RIE) selectively modifies film microstructure, increases porosity, and decreases the surface area over which analytes may interact. Atomic layer deposition (ALD) applies extremely thin < 10 nm conformal coatings that produce alternative chromatographic surface chemistries over GLAD UTLC film scaffolds. These investigations required invention of new instrumentation and analysis techniques since conventional planar chromatography equipment is unoptimized for miniaturized GLAD UTLC plates.

Approaches to fabricating, utilizing, characterizing, and enhancing nanoengineered GLAD UTLC media are considered in this thesis. The intriguing behaviours described within provide insight into the manner in which the microscopic features of GLAD films impact macroscopic development phenomena. These investigations simultaneously advanced both the capabilities of the UTLC planar chromatography technique and the understanding of GLAD nanostructured thin film materials.

Acknowledgements

(See also the first appendix, **A Names and faces**.) For some, graduate thesis writing is to be completed as soon as possible; it's just one of the final obstacles to earning letters to put behind their name. However, I took it as an opportunity to reflect on technical knowledge attained, difficult lessons learned, and the impact of this work on myself and others. It's also a chance to pause and recognize the support that enabled such an instructive and enjoyable experience.

My parents and sister have shown me unlimited and unconditional love and support. I am forever grateful for the compassion of our exceptionally close family. I proudly dedicate my thesis to them as a small token of my appreciation.

I have my fantastic supervisor, Professor Michael J. Brett, to thank for my life in academia. He created the best possible environment for his students; one where they can work, fail, recover, learn, succeed, and thrive. This environment is a product of strong funding and enviable facilities but most importantly his leadership and selection of the Glancing Angle Deposition (GLAD) research group members. Although many of these people are named further in **A Names and faces**, Dr. Michael T. Taschuk, Mike Brett's "second in command," deserves special recognition. He is an extraordinary research associate, manager, and mentor to students. I attribute much of my productivity, academic success, growth as a researcher, and growth as a professional to my interactions with him. Mike Brett's excellent administrative assistant Audrey Lin was also critical to the GLAD group's smooth operation. Her efforts simplified the complex logistics of securing equipment and materials required for research and dissemination.

Mike Taschuk led the GLAD ultrathin-layer chromatography (UTLC) team assembled from group members with strong and varied backgrounds: Louis W. Bezuidenhout, Anthony J. Oko, Dr. Jane Hall (née Zhen Wang), Dr. Ali Foroughi-Abari, and Dr. Viktor Leontyev. "Dr. Dr." Louis Bezuidenhout (PhD 2011 and future medical doctor) was an excellent mentor and trainer that offered

early guidance and expert support. He shared his GLAD UTLC concept that evolved into my research project and into the work of others. Anthony Oko (MSc 2013) was a bright and motivated summer student that eventually became a graduate student. He was a quick study and always eager to discuss new ideas. We worked closely and multiplied each other's productivity. Jane Hall, Ali Foroughi-Abari, and Viktor Leontyev applied their respective backgrounds in analytical chemistry, nanomaterials engineering, and fundamental physics. All contributed to discussions and ideas about combining GLAD with UTLC.

Professor Gertrud E. Morlock was essential to the GLAD UTLC program. Although an exceptionally busy academic, she kindly allowed me to visit her food chemistry thin layer chromatography laboratory (2009 and 2011) in the Institut für Lebensmittelchemie (Institute for Food Chemistry, directed by Professor Wolfgang Schwack) at Universität Hohenheim (Stuttgart, Germany). My brief experiences collaborating with this gracious host and champion for planar chromatography techniques were highlights of my program. The GLAD UTLC team grew two people larger when the "Troublemakers" visited for three months in 2012. Gerda Morlock sent German diplom thesis students, Simone Kirchert and Julia Wannenmacher to visit the GLAD group. Both were intelligent, diligent, and a pleasure to train and support during and after their visits.

Several organizations in Edmonton, Canada enabled the research described in this thesis: the University of Alberta, NRC National Institute for Nanotechnology, U of A NanoFab (Micro & Nanofabrication Facility), U of A Electrical and Computer Engineering (ECE) Department, U of A ECE Machine Shop, U of A Earth and Atmospheric Sciences Scanning Electron Microscopy Laboratory (George Braybrook), and Cadien Nanofabrication Group (Professor Kenneth C. Cadien, Chemical and Materials Engineering, U of A). Generous financial support was provided by the Natural Sciences and Engineering Research Council (NSERC) of Canada, Alberta Innovates – Technology Futures, the Informatics Centre of Research Excellence (iCORE), and Micralyne, Inc. (Edmonton, Canada).

For more than 12 years, I have eagerly looked forward to my always enjoyable weekend shifts as a part-time staff science interpreter at the local science museum, TELUS World of Science – Edmonton. I hope that my passion for science literacy is contagious and motivates members of the public to become and stay interested in science. I feel that my own chosen career in science, technology, and engineering is tied closely to my involvement with this institution as a visitor, volunteer, and as a staff member.

Finally, I'm appreciative for the continued friendship and support of my family, friends, labmates, science museum colleagues, recreational soccer teammates, and others close to me. Thanks also to you, the reader, for your interest in this research — research only possible with the involvement of so many.

Contents

List of tables

List of figures

Symbols and nomenclature

This table lists frequently used symbols, terminology, abbreviations, typical measurement units, and brief descriptions. Page numbers for detailed explanations are also provided when applicable.

… | … : Notation to compactly describe GLAD ALD nanocomposites. For example, "SiO_2 | Al_2O_3" denotes a GLAD SiO_2 film coated with ALD Al_2O_3. **130**

Analyte: Compound separated from a sample mixture. **8**

Atomic layer deposition (ALD): A method of creating very thin conformal coatings. **52, 130**

Automatic TLC Sampler 4 (ATS 4): The current state-of-the art TLC sample application robot manufactured by CAMAG. **25, 58**

ϕ **Azimuthal angle (°):** Angle of incident vapour flux with respect to initial orientation (0-360°) in GLAD process. **31**

Chevron: A "zig-zag." GLAD UTLC films with chevron morphologies are composed of alternating inclined column sections. **32, 51**

Chromatogram: Representation of chromatographic separation; typically a 2D image of the separation pattern or a 1D signal produced by integrating an intensity signal across the width of a separation track. See also **Densitogram** below. **11, 65, 115**

β **Column inclination angle (°):** Angle of GLAD column tilt with respect to substrate normal. **30**

Comma separated values (*.csv): Platform independent text file format used to store arrays of (numerical) values. **118**

Concentration zone: A highly porous region on a planar chromatography plate to which sample mixtures are applied. Eluting the sample into the less porous separation zone produces sharp bands. "UTLC-CZ" plates are UTLC plates prepared with concentration zones. **13, 94, 101**

d **Darkness:** A colour-independent measure of the pixel intensity defined over the inclusive range (0-1). It is related to the pixel lightness value (*l*). **67**

α **Deposition angle (°):** Angle of incident vapour flux with respect to substrate normal (0-90°). GLAD films fabricated at high α have higher porosity. **30**

Densitogram: A 1D signal produced by integrating signal intensity across the width of a separation track. (This term is sometimes used synonymously with "chromatogram.") **11, 65, 115**

ρ **Density (g cm^{-3}):** The density of a given material. **31**

Development: Chromatographic separation. **8**

Digital single-lens reflex (DSLR): A type of digital camera that uses a moveable mirror to reflect the light transmitted by the camera's lens into the viewfinder. When a photo is taken, the mirror retracts to allow this light to reach the digital imaging sensor. Some DSLR cameras can also record videos by locking the mirror in this position to enable sustained illumination of the imaging sensor. The TR-UTLC system records videos using one such DSLR camera. **65, 108**

Electron energy loss spectroscopy (EELS): A TEM technique used to analyze the chemical composition of a specimen. **132**

Focussed ion beam (FIB): A beam of ions (for example gallium) that may be used to cut and mill small specimens. **131**

Frames per second (fps): The rate at which video frames are recorded or extracted.

Full width at half maximum (FWHM): A measure of the width of a peak. **11**

Glancing angle deposition (GLAD): A physical vapour deposition technique for producing nanostructured columnar thin films. **29, 46**

Hue-saturation-lightness (hsl): A digital image colour mode that describes each pixel's colour according to its (hue, saturation, lightness). **65**

Hue-saturation-value (hsv): A digital image colour mode that describes each pixel's colour according to its (hue, saturation, value). Specific hue and saturation quantities are denoted as *h* and *s*, respectively. *h*' indicates the hue rounded to the nearest integer. **65**

High performance thin layer chromatography (HPTLC): A planar chromatography technique that employs stationary phases and instrumentation improved over traditional TLC. **17**

JPEG: A digital image standard created by the Joint Photographic Experts Group. The TR-UTLC analysis set uses 8-bit rgb JPEG images. **108**

Light emitting diode (LED): An electronic solid state light source.

l **Lightness:** A colour-independent measure of the pixel intensity defined over the inclusive range (0-1). It is related to the pixel darkness value (*d*). **67**

Limit of detection (LOD): A measure of the sensitivity of an analytical technique. High sensitivity systems have low LOD. **86**

MATLAB: Numerical analysis software package produced by Mathworks (Natick, Massachusetts, USA). Custom analysis scripts are saved in the *.m (text) file format. Numerical data are saved in the proprietary *.mat file format.

Macropore: A pore with width > 50 nm.

Mesopore: A pore with 2-50 nm width.

Micropore: A pore with width < 2 nm.

MA **Migration anisotropy:** The ratio of the migration distance in the along-channel direction to that in the across-channel direction on anisotropic media. GLAD UTLC layers with higher *MA* are considered to have stronger (macropore) anisotropy. **78**

χ **Migration constant ($mm^2\ s^{-1}$ or $pixels^2\ frame^{-1}$):** A constant used to describe the capillary-driven migration. **10, 113**

Z **Migration distance (mm or pixels):** Analyte position with respect to applied spot. Z_i is the position of the i^{th} analyte; Z_F is the position of the migration front. In anisotropic media, $Z_{i,along}$ and $Z_{i,across}$ may be used to denote migration parallel and perpendicular to the channel-like features. **78**

Migration front: The leading edge of the mobile phase advancing across the planar chromatography plate. Analytes not retained by the stationary phase move with the migration front and have $hR_F = 100$. Such analytes are said to "front migrate." **10, 112**

Mobile phase: Mixture of solvents that flows through the stationary phase. Weakly retained analytes are carried more rapidly by the mobile phase. **8, 61**

MOV: File format for digital videos (movies). The TR-UTLC imaging camera records MOV videos from which frames are extracted. **108**

Normal-phase separation: A type of (adsorption) chromatography separation mode in which the stationary phase is more polar than the mobile phase. Polar analytes are retained most strongly. **10**

Office Chromatography: An approach to employing consumer office peripherals (inkjet printers and flatbed scanners) as instrumentation for planar chromatography. **24, 59, 63**

Perfluoroalkoxy (PFA): A chemical resistant transparent plastic with properties similar to PTFE.

H **Plate height (μm):** A measure of analyte separation efficiency (smaller is more efficient). *H* should not be confused with *h*, a given image pixel's hue value. **12**

N **Plate number:** A measure of analyte separation efficiency (larger is more efficient). **12**

Polytetrafluoroethylene (PTFE): A chemical resistant white plastic; generic name for DuPont™ Teflon ®.

Recipe file: A MATLAB *.mat file used to initialize and store parameters required for TR-UTLC video analysis. **108, 112**

Red-green-blue (rgb): A digital image colour mode that describes each pixel's colour according to its (red, green, blue) components. **65**

Reactive ion etch (RIE): An anisotropic plasma etching method used in microfabrication. **52, 91, 92**

Relative humidity (% RH): An expression of water content in air at a given temeature.

Relative standard deviation (% RSD): The standard deviation of a set of measurements scaled against the average of those measurements. The RSD is typically expressed in percent and used to describe relative variation in a calculated value.

R_F, hR_F **Retention factor:** Analyte migration distance normalized against mobile phase front migration distance. Strongly retained analytes have low R_F. The retention factor is also commonly expressed in parts per hundred: $hR_F = 100R_F$. (The hR_F formulation is used throughout this thesis.) Strongly retained analytes have low hR_F. Alternative names include "retardation factor" and "ratio to front." **12**

Reversed-phase separation: A type of (adsorption) chromatography separation mode in which the stationary phase is less polar than the mobile phase. Non-polar analytes are retained most strongly. **10**

Scanning electron microscope (SEM): An electron microscope that produces an image by collecting secondary electrons produced near the surface of a specimen.

Serial bideposition (SBD): A GLAD motion algorithm used to produce anisotropic blade-like thin films that exhibit unique channel-like features. ϕ changes periodically from 0° → 180° → 360° → … **32, 51**

Separation track (a.k.a development track): A region of the chromatography plate containing the applied spot position, all separated spots, and the migration front. Chromatograms are produced by integrating across the width of the track.

$\Delta\theta$ **Separation track deviation angle (°):** The angle between the channel feature orientation in anisotropic GLAD UTLC layers (θ_C) and the resultant separation track orientation (θ_T). **79**

Separation zone: A region on a planar chromatography plate in which analytes are separated. This region is less porous than the adjacent concentration zone on UTLC-CZ plates. **13, 101**

Signal-to-noise-ratio (SNR): A description of the signal intensity relative to the noise in a system. **86**

1 Introduction

1.1 Analytical separations and miniaturization

Analytical separations are popular approaches of identifying and quantifying molecular compounds present in complex chemical mixtures. These techniques are commonly applied to biochemistry [1,2], environmental monitoring [3], quality control [4,5], medical diagnostics [2], and other uses. While there are numerous types of analytical separation mechanisms, all exploit the unique physical and chemical properties associated with individual compounds in the sample mixture. Molecules in these mixtures can be forced through tortuous porous materials, adsorb and desorb at fluid-solid interfaces, and move at speeds dependent upon their particular attributes. The exact manner in which they separate is a result of interactions at the nanoscale.

Several of these analytical separation techniques have accordingly become more powerful upon miniaturization. Microfabricated devices (such as so-called Lab-on-a-Chip devices [2,6–9]) and porous nanomaterials increase surface areas

while reducing volumes, pronouncing the interactions on which analytical separations rely. Their advantageous geometries therefore increase analysis speed, sensitivity, and overall performance [6–8,10–12]. Many of these benefits apply to the chromatography analytical separation technique.

1.2 Engineering GLAD nanomaterials for planar chromatography

Investigations described in this thesis took place at the intersection between two vastly different scientific fields: planar chromatography and nanostructured thin films. The former is a powerful and well-established family of analytical techniques used to separate and characterize a sample mixture's constituent analyte compounds. It leverages the varying 'preference' of molecules in moving with a migrating liquid or remaining stationary on a flat porous layer [13–16]. The latter method is a comparatively new way of fabricating high surface area porous coatings with engineered microstructure. This glancing angle deposition (GLAD) approach is an excellent platform for creating unique nanostructured columnar thin films of controlled porosity and architecture with characteristic features spanning the ~ 10-1000 nm size range [17–22]. These diverse disciplines overlap because chromatographic performance is influenced strongly by the properties of the separation medium. Miniature nanostructured GLAD thin film media (25.4 mm x 25.4 mm or 50.8 mm x 25.4 mm) are particularly well-suited to an emerging form of planar chromatography called ultrathin-layer chromatography (UTLC) – a form that achieves excellent performance using exceptionally thin layers with remarkably small pores.

1.3 Thesis structure and contributions

The dissertation presents knowledge obtained by applying miniaturized nanoengineered GLAD thin film media to analytical UTLC techniques. It describes challenges encountered and capabilities gained by combining these two methods together.

The following chapter, **2 Theory and Background**, reviews concepts critical to the rest of the thesis. Key definitions and mechanisms in planar chromatography, the UTLC variant, and GLAD film fabrication are summarized.

3 GLAD UTLC methods describes practices adopted, modified, and invented to create and utilize new nanostructured chromatography plates. In particular, the chapter outlines general procedures for depositing and post-processing GLAD UTLC plates, employing them in chromatographic separations, and extracting meaningful quantitative data.

4 Anisotropic UTLC microstructures[1] explores the performance of characteristic GLAD SiO_2 film architectures. Coloured dye separations performed on isotropic vertical post, anisotropic chevron, and anisotropic blade-like media offer insight into the manner that separated compounds migrate in the unique channel-features practical only by GLAD.

The strong dependence of separation quality on film microstructure motivated subsequent investigations into methods of fine-tuning. **5 Modified morphology and development**[2] evaluates structural changes possible through reactive ion etch (RIE) post-deposition processing and their effects on chromatography.

6 Time-resolved UTLC[3] describes new instrumentation and analyses invented to improve characterization of GLAD UTLC performance. This chapter focusses on the imaging and numerical analysis approach developed in partnership with Anthony Oko [23,24] and subsequent enhancements required to generalize its utility to any (GLAD) UTLC coloured compound separation.

[1] Chapter incorporates material from S.R. Jim, M.T. Taschuk, G.E. Morlock, L.W. Bezuidenhout, W. Schwack, M.J. Brett, Engineered anisotropic microstructures for ultrathin-layer chromatography, Analytical Chemistry. 82 (2010) 5349–5356; and A.J. Oko, S.R. Jim, M.T. Taschuk, M.J. Brett, Analyte migration in anisotropic nanostructured ultrathin-layer chromatography media, Journal of Chromatography A. 1218 (2011) 2661–2667.

[2] Chapter incorporates material from S.R. Jim, A.J. Oko, M.T. Taschuk, M.J. Brett, Morphological modification of nanostructured ultrathin-layer chromatography stationary phases, Journal of Chromatography A. 1218 (2011) 7203–7210.

[3] Chapter describes S.R. Jim's unpublished enhancements to the method developed in partnership with A.J. Oko: A.J. Oko, S.R. Jim, M.T. Taschuk, M.J. Brett, Time resolved chromatograms in ultra-thin layer chromatography, Journal of Chromatography A. 1249 (2012) 226–232.

7 Surfaces modified by atomic layer deposition[4] shifts attention back to the chromatographic media and techniques for changing surface chemistry. Atomic layer deposition (ALD) covers the columnar features of SiO_2 GLAD films with exceptionally thin coatings of Al_2O_3, ZrO_2, and ZnO to dramatically change chromatographic performance.

8 Customized GLAD UTLC chamber[5] describes a preliminary attempt at optimizing a development chamber for miniaturized GLAD UTLC media. The time-resolved UTLC methods discussed earlier provide a rich study of the new chamber's effectiveness and insights into improvements required in future design iterations.

The final chapter, **9 Summary, evaluation, future directions, and remarks**, reviews and reflects on work described in earlier chapters. Comparisons of the GLAD UTLC approach against the first UTLC reports by Hauck *et al.* (2001, 2002, and 2003) [10–12] provide context to this dissertation's research contributions. The chapter further suggests potential extensions of the present work and evaluates the current state of the broader UTLC field.

Appendices **B Numerical analysis scripts**, **C Time-resolved UTLC scripts**, and **D Custom GLAD UTLC chamber schematics** present numerical analysis programing code excerpts and engineering drawings that would have caused the other chapters to burst at their seams if included therein. Permanent links to full copies of the MATLAB programming code are also provided. Future researchers will hopefully find this carefully prepared content useful in their own work.

The first appendix, **A Names and faces**, deserves special attention as it is unconventional. It matches faces to the names of the people responsible for making this graduate program so thoroughly instructive and enjoyable.

[4] Chapter incorporates material from S.R. Jim, A. Foroughi-Abari, K.M. Krause, P. Li, M. Kupsta, M.T. Taschuk, K.C. Cadien, and M.J. Brett, Ultrathin-layer chromatography nanostructures modified by atomic layer deposition, Journal of Chromatography A. 1299 (2013) 118–125.
[5] Chapter describes unpublished work with a new GLAD UTLC planar chromatography chamber.

Although certainly readable in printed form, readers may favour the electronic version of this dissertation. Most bolded in-text cross-references are hyperlinked to their corresponding figures, tables, equations, and sections. The **Contents**, **List of tables**, and **List of figures** are similarly hyperlinked to their respective entries. The listing of **Symbols and nomenclature** serves as both a glossary and index for specialized terminology. In any chapter, clicking the footer brings the reader to the beginning of that chapter and clicking the header brings the reader to the **Contents**.

References

[1] G.T. Roman, R.T. Kennedy, Fully integrated microfluidic separations systems for biochemical analysis., J. Chromatogr. A. 1168 (2007) 170–188.

[2] J. West, M. Becker, S. Tombrink, A. Manz, Micro total analysis systems: latest achievements., Anal. Chem. 80 (2008) 4403–4419.

[3] J. Sherma, Review of advances in the thin layer chromatography of pesticides: 2010-2012, J. Environ. Sci. Heal. B. 48 (2013) 417–30.

[4] G.E. Morlock, W. Schwack, The contribution of planar chromatography to food analysis, J. Planar Chromatogr. 20 (2007) 399–406.

[5] J. Sherma, Review of HPTLC in drug analysis: 1996-2009, J. AOAC Int. 93 (2010) 754–764.

[6] A. Manz, D.J. Harrison, E.M.J. Verpoorte, J.C. Fettinger, A. Paulus, H. Lüdi, et al., Planar chips technology for miniaturization and integration of separation techniques into monitoring systemsCapillary electrophoresis on a chip, J. Chromatogr. A. 593 (1992) 253–258.

[7] D.J. Harrison, A. Manz, Z.H. Fan, H. Luedi, H.M. Widmer, Capillary electrophoresis and sample injection systems integrated on a planar glass chip, Anal. Chem. 64 (1992) 1926–1932.

[8] D.J. Harrison, K. Fluri, K. Seiler, Z. Fan, C.S. Effenhauser, A. Manz, Micromachining a miniaturized capillary electrophoresis-based chemical analysis system on a chip., Science. 261 (1993) 895–897.

[9] M.L. Kovarik, D.M. Ornoff, A.T. Melvin, N.C. Dobes, Y. Wang, A.J. Dickinson, et al., Micro total analysis systems: fundamental advances and applications in the laboratory, clinic, and field, Anal. Chem. 85 (2013) 451–472.

[10] H.E. Hauck, O. Bund, W. Fischer, M. Schulz, Ultra-thin layer chromatography (UTLC) — A new dimension in thin-layer chromatography, J. Planar Chromatogr. 14 (2001) 234–236.

[11] H.E. Hauck, M. Schulz, Ultrathin-layer chromatography, J. Chromatogr. Sci. 40 (2002) 550–552.

[12] H.E. Hauck, M. Schulz, Ultra thin-layer chromatography, Chromatographia. 57 (2003) S313–S315.

[13] J. Sherma, B. Fried, Handbook of Thin-Layer Chromatography, 3rd ed., Marcel Dekker [Taylor and Francis], New York, 2003.

[14] E. Reich, A. Schibli, High-Performance Thin Layer Chromatography for the Analysis of Medicinal Plants, Thieme Medical Publishers, New York, 2007.

[15] P.E. Wall, Thin-Layer Chromatography: A modern practical approach, Royal Society of Chemistry, Cambridge, 2005.

[16] B. Spangenberg, C.F. Poole, C. Weins, Quantitative Thin-Layer Chromatography, Springer Berlin Heidelberg, Berlin, Heidelberg, 2011.

[17] K. Robbie, M.J. Brett, A. Lakhtakia, Chiral sculptured thin films, Nature. 384 (1996) 616–616.

[18] K. Robbie, J.C. Sit, M.J. Brett, Advanced techniques for glancing angle deposition, J. Vac. Sci. Technol. B. 16 (1998) 1115–1122.

[19] K. Robbie, M.J. Brett, Method of depositing shadow sculpted thin films, U.S. Patent 5,866,204, 1999.

[20] M.M. Hawkeye, M.J. Brett, Glancing angle deposition: Fabrication, properties, and applications of micro- and nanostructured thin films, J. Vac. Sci. Technol. A. 25 (2007) 1317–1335.

[21] M.T. Taschuk, M.M. Hawkeye, M.J. Brett, Glancing Angle Deposition, in: P. Martin (Ed.), Handbook of Deposition Technologies for Films and Coatings: Science, Applications and Technology, 3rd ed., William Andrew (Elsevier), Oxford, United Kingdom, 2010: pp. 621–678.

[22] M.M. Hawkeye, M.T. Taschuk, M.J. Brett, Glancing Angle Deposition: Engineering the Nanoscale (in-press), Wiley, 2014.

[23] A.J. Oko, S.R. Jim, M.T. Taschuk, M.J. Brett, Time resolved chromatograms in ultra-thin layer chromatography, J. Chromatogr. A. 1249 (2012) 226–232.

[24] A.J. Oko, Advanced Materials and Detection Methods in Ultrathin-Layer Chromatography, University of Alberta, 2013.

2 Theory and Background

Investigations discussed in this dissertation bridge the diverse disciplines of analytical chemistry and materials science. This chapter establishes the context for this research by reviewing fundamental concepts in these fields. It describes planar chromatography theory, practice, and motivations for improved materials. Special attention is given to recent advances in ultrathin-layer chromatography (UTLC) – one of the newest planar chromatography variants. The chapter concludes with an overview of the glancing angle deposition (GLAD) approach to fabricating nanostructured thin films and its applicability to UTLC.

2.1 Planar chromatography

Planar chromatography analytical separation techniques have advanced significantly since the invention of "spot chromatography" in 1938 by USSR chemists Izmailov and Shraiber [1–3]. The crude ~ 2 mm thick aluminum oxide layers first used to separate pharmaceutical plant extracts [1] have evolved into carefully engineered chromatographic materials applicable to many analytical problems [4]. Pesticide characterization [5], pharmaceutical analysis [6,7], and

food chemistry [8] are just some of the applications that capitalize upon planar chromatography's many attributes.

Simplicity is one of planar chromatography's greatest advantages over alternative separation techniques (especially those taking place in tube or capillary columns). Only limited instrumentation is required to achieve rapid parallel separations of several samples across flat porous media [3,6,9,10]. Users can also always start with new sorbents without concern for contaminants remaining on used materials since conventional thin-layer chromatography (TLC) and high-performance TLC (HPTLC) plates are relatively inexpensive and disposable. Separating compounds in unpurified sample mixtures using these open layers rather than enclosed chromatographic columns further enables coupling with numerous offline (post-separation) detection modes including optical densitometry, UV/Vis (ultraviolet and visible wavelengths) spectroscopy, fluorescence detection, mass spectrometry, and effect-directed (microbial detection) analysis [11–13]. While performance improvements are possible using newer forced-flow variants such as pressurized planar electrochromatography and over-pressure planar chromatography [3,6,9,10,14], the practicality of traditional capillary-driven TLC and HPTLC make these original techniques most common.

2.1.1 Method and mechanisms

In classical planar chromatography analytical techniques, a sample mixture containing compounds ("analytes") to be separated is applied as a spot or a band to an open dry porous separation medium ("stationary phase") fixed to a flat plate (**Figure 2-1a**). Small spots or bands are desirable because they maximize the attainable overall separation performance (see **3.3 Sample spot application** for further discussion). A solution of solvents ("mobile phase") introduced to one side of this plate then carries analyte compounds in the sample mixture through the stationary phase as it wicks across the plate (**Figure 2-1b**). (This process is called the chromatographic "development.") Analytes within the sample mixture are separated from each other based on their competing chemical and physical

interactions with the mobile and the stationary phases (**Figure 2-1c**). Compounds that prefer to interact with the mobile phase are carried faster along a separation track than those that prefer to interact with the stationary phase.

Capillary-driven (wicking) mobile phase flow through the chromatography plate is both an advantage and liability for planar chromatography. The obvious advantage is that expensive high pressure column chromatography pump equipment is not required. As the leading edge of the wicking solvent ("mobile phase front") spans the full width of the plate, multiple separations can occur in parallel on the same medium. However, capillary-driven flow across the open surface is also less uniform and more sensitive to evaporation effects [3].

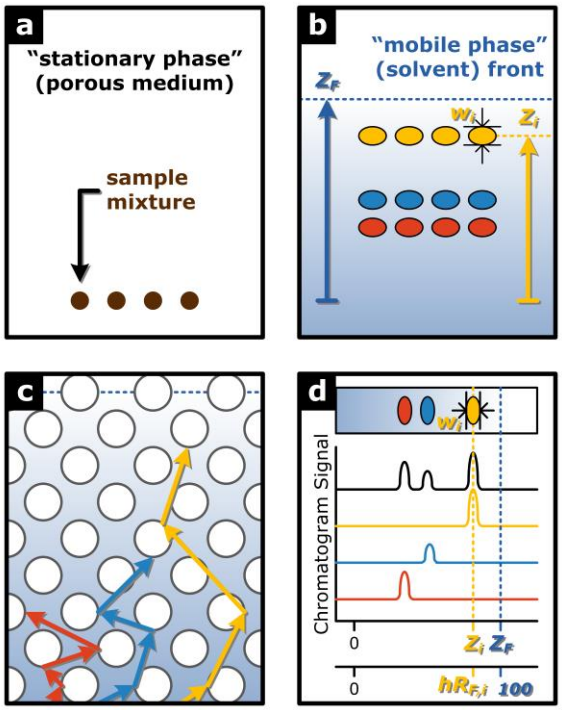

Figure 2-1 Planar chromatography definitions and mechanisms. (a) Sample mixture spots are applied to the porous "stationary phase." (b) Analytes within the sample are separated as the solvent "mobile phase" wicks through the stationary phase. (c) Analytes are separated based on their varied interactions with the stationary and mobile phases. (d) Chromatogram signals may be extracted from separation tracks with or without colour filtering. The position of the mobile phase front (Z_F) as well as the position (Z_i), width (w_i), and retention factor (hR_F) of a given analyte spot are indicated.

Advancement of the liquid mobile phase migration front is commonly modelled using an adaptation of the Lucas-Washburn equation [3,4,10,15]:

$$Z_F = \sqrt{\chi t} \quad \textbf{(2-1)}$$

$$\chi = \frac{2k_0 d_p \gamma \cos\theta}{\eta} \quad \textbf{(2-2)}$$

Where Z_F is the distance from the immersion line and t is the elapsed time. The flow constant χ combines the permeability of the layer k_0, average particle size in the stationary phase d_p, liquid surface tension γ and viscosity η, and contact angle between liquid and the medium θ. This equation implies that flow through a given stationary phase will depend upon mobile phase composition and several other factors. It further describes the reduction in flow velocity over the course of the development.

Analyte compounds may interact with the mobile and stationary phases through different mechanisms [3,10]. "Normal-phase" and "reversed-phase" separations are two common types of adsorption chromatography. Both of these modes separate analytes based on their varied polarity. Normal-phase separations employ a polar stationary phase (such as silica gel) and non-polar mobile phase (often organic solvents). Analytes with higher polarity adsorb more strongly to these stationary phases while those with lower polarity migrate faster with the mobile phase. These separations are typically appropriate for low-polarity analytes. Investigations described in this thesis generally employed normal-phase separations of lipophilic (low polarity) coloured dyes (see **3.4.1 Model dye system**). In comparison, reversed-phase separations employ a non-polar stationary phase (such as silane or C18 functionalized silica gel) and polar mobile phase (sometimes an aqueous solution) to separate polar (often water soluble) analytes. Regardless of separation mechanism type, all analyte spots undergo diffusion broadening during the chromatographic development. The worsening of separation performance with spot broadening is apparent in several chromatographic figures of merit (**below**). Methods of minimizing this

undesirable but unavoidable effect remain active areas of research in all analytical separation fields.

2.1.2 Chromatograms and performance metrics

Resultant analyte spot positions and widths are typically presented in the form of a chromatogram (densitogram)[1] plot (**Figure 2-1d**) [3,10]. This numerical signal records analyte optical density (visible or UV light) at different positions along the development track. Measurements may be performed with scanning slit densitometers [3] or from images captured using dedicated TLC imaging booths (TLC Scanner 4, CAMAG, Muttenz, Switzerland), digital cameras [16–19], or flatbed scanners [20,21]. Chromatographers may use commercial software packages such as CAMAG Video Scan or Sorbfil TLC Videodensitometer (OOO IMID, Krasnodar, Russia) to extract these signals. The density of invisible analytes may be measured directly under UV illumination, indirectly using UV fluorescent chromatography plates, or with the help of various visualization chemical reactions [3,6,9,10,22].

Calculation of analyte peak position and width from the extracted chromatograms permits separation quality to be assessed using several figures of merit. (See also graphical definitions in **Figure 2-1**.) For the i^{th} analyte, Z_i denotes the position of the peak centre with respect to the applied spot position and w_b is the base width of the peak. The width may also be expressed using the "full width at half maximum" (FWHM).

In the special case of a chromatogram peak well-approximated by a Gaussian peak of the form:

$$y = A \exp\left(\frac{-(x - x_0)^2}{2\sigma^2}\right) \qquad \textbf{(2-3)}$$

[1] "Chromatogram" is often used to describe separated separation patterns and extracted intensity-position signals. "Densitogram" is only used to describe the extracted intensity-position signals.

The peak centre x_0 is used to calculate Z and the base width can be estimated from the standard deviation σ by assuming $w_b = 4\sigma$ in the below formulae [3,6]. The FWHM of a Gaussian peak is FWHM = $2\sqrt{2\ln 2}\,\sigma$. Alternative models may also be used to describe asymmetric chromatographic peaks [23,24].

Retention factor (R_F or hR_F)

A particular analyte's preference in interacting with the mobile phase over the stationary phase is characterized in terms of a dimensionless retention factor, R_F ($0 \leq R_F \leq 1$) [3,6,9,25]:

$$R_{F,i} = \frac{Z_i}{Z_F} \tag{2-4}$$

Where Z_i and Z_F are respectively the migration distances of the i^{th} analyte and the mobile phase mobile phase front as measured from the applied spot position. This retention factor can also be written in parts per hundred as the hR_F ($0 \leq hR_F \leq 100$) [3,9,25]:

$$hR_{F,i} = 100\left(\frac{Z_i}{Z_F}\right) = 100R_{F,i} \tag{2-5}$$

The latter formulation, **Equation (2-5)**, will be used throughout this thesis. Compounds with a low hR_F value have a strong preference in interacting with the stationary phase and are said to be strongly retained. Meanwhile, compounds with a high hR_F value have a strong preference in interacting with the mobile phase and are considered weakly retained. The hR_F value is independent of development time but may depend upon applied spot position [6].

Plate number (N) and height (H)

Separation efficiency is described in terms of the plate number (N) and plate height (H) [3,9,25]:

$$N_i = 16\left(\frac{Z_i}{w_{b,i}}\right)^2 \quad \textbf{(2-6)}$$

$$H_i = \frac{Z_i}{N_i} = \frac{w_{b,i}^2}{16Z_i} \quad \textbf{(2-7)}$$

Where Z_i and $w_{b,i}$ are the migration distance and base width for the peak corresponding to the i^{th} component in the dye mixture. Greater plate numbers and smaller plate heights indicate higher separation efficiency. It is important to note that this classical treatment does not take into account the detrimental effects of large spot size on plate numbers and heights; alternative formulations attempt to factor out this contribution [3,4].

2.2 Motivations for stationary phase advancement

2.2.1 Concentration zones for improved starting spots[2]

Applied sample spot quality significantly affects overall chromatographic performance [3,10]. Large non-uniform starting spots result in broad analyte peaks, reduced separation efficiency (small plate numbers and large plate heights), and poor resolution. Careful consideration of sample dissolution solvent and application instrumentation can improve the size and uniformity of applied spots (see **3.3 Sample spot application**). Spotted samples can also be focussed using multiple development techniques. These methods can employ repeated developments with a given mobile phase to iteratively compress analyte spots as they are separated [26]. Alternatively, a short preliminary development using a strong solvent can focus the applied sample spot into a narrow band prior to chromatographic separation [3,10].

[2] Portions of this section were reproduced with permission from S.R. Jim, A.J. Oko, M.T. Taschuk, M.J. Brett, Morphological modification of nanostructured ultrathin-layer chromatography stationary phases, Journal of Chromatography A. 1218 (2011) 7203–7210. Copyright (2011) Elsevier.

The stationary phase itself can also be modified to improve spot shape prior to separation. Concentration zones (sometimes known as "kieselguhr" zones) exhibit high porosity, exceedingly low specific surface area, and low analyte retention [28–31]. These regions make TLC and HPTLC plates more tolerant to large and poorly applied samples. Sample spots applied to these regions focus into sharp lines as they migrate across the interface between the concentration and separation zones [6,10] (**Figure 2-2**). Each line then separates into a series of well-resolved bands as the chromatographic development continues into the separation zone. Concentration zones therefore permit application of large volume, low concentration samples with less precision in spot placement. Beesley (1972) reported TLC concentration zone plates that permitted spot volumes up to 100 μL [30]. Halpaap and Krebs (1977) found that concentration zones also improved resistance to sample overloading on TLC and HPTLC plates [31]. In some cases, these zones may also be used in the simultaneous purification and analysis of unpurified samples [28,30,31]. See also **5.4 GLAD UTLC-CZ demonstration** for a successful application of the concentration zone concept to nanostructured chromatography layers.

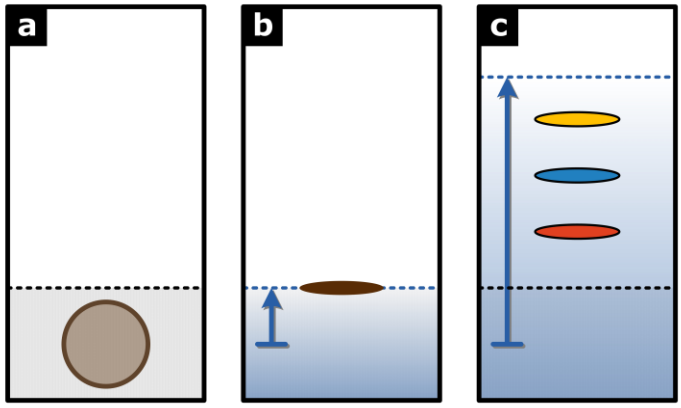

Figure 2-2 Planar chromatography concentration zone schematic. A sample mixture applied to a concentration zone (a) is compressed at the interface between the concentration and separation zones (b) prior to separation (c). Grey tinted regions are of increased porosity; blue arrow and blue tinted regions represent the advancing mobile phase during development. Reproduced with permission from [27]. Copyright (2011) Elsevier.

2.2.2 Van Deemter equation and evolution of HPTLC

The concept of plate height (**above**) is useful when considering the different contributions to undesirable analyte spot broadening during separation. These effects are captured in the van Deemter equation originally defined for column chromatography [32]:

$$H = A + \frac{B}{u} + Cu \quad \textbf{(2-8)}$$

Where u is the mobile phase flow velocity – a parameter that can be easily controlled in column chromatography. A describes the effects of stationary phase tortuosity, eddy diffusion, and mobile phase flow non-uniformity (especially at stationary phase interfaces). B describes longitudinal diffusion within the mobile phase. C describes the effects of stagnant mobile phase and analyte mass transfer between the stationary and mobile phases. The equation provides insight into the optimum flow velocity for a given column chromatography separation. A modified form of this equation has been defined in planar chromatography [3,25]:

$$H = A\sqrt[3]{u} + \frac{B}{u} + Cu \quad \textbf{(2-9)}$$

The A, B, and C coefficients here have similar meaning but the manner in which each is calculated is different. Note also that the flow velocity u decreases during the development (**Equation (2-1)**). However, this theoretical model suggests criteria for achieving high separation efficiency (small H). Homogenous layers with higher order, smaller pores, and narrower pore size distribution should decrease the A coefficient of the first term. Faster separations reduce the time during which diffusion broadening can occur and would decrease B/u. Cu is reduced if the time required for analytes to equilibrate between the stationary and mobile phases is small compared to the flow velocity. Although the C-term is difficult to control by changing the stationary phase alone, the A and B contributions may be addressed by improving the chromatographic layer quality.

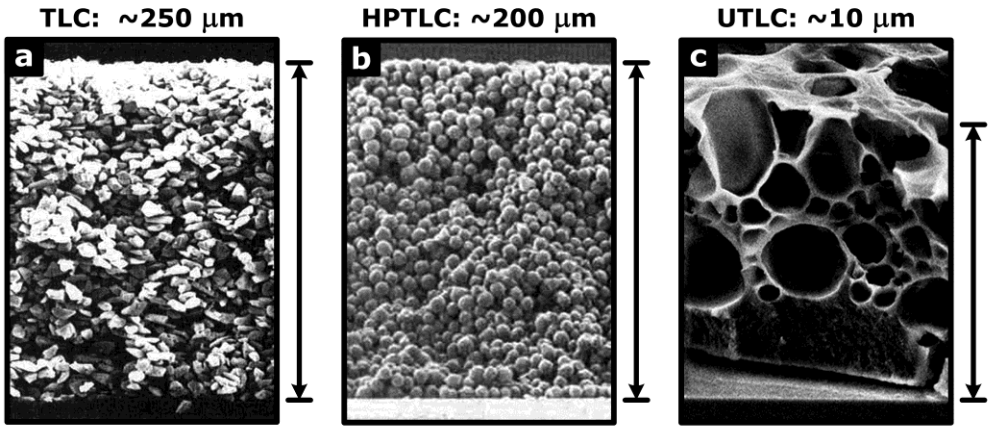

Figure 2-3 Cross-sectional scanning electron micrographs of (a) thin-layer chromatography (TLC), (b) high performance TLC (HPTLC), and (c) ultrathin-layer chromatography (UTLC) silica gel stationary phases. Representative sorbent thicknesses provided. Parts (a) and (b) modified with permission from [33], copyright (2003) Marcel Dekker [Taylor and Francis]. Part (c) modified with permission from [21], copyright (2010) American Chemical Society.

Table 2-1 Comparison of TLC, HPTLC, and Merck monolithic UTLC stationary phase properties and performance

Stationary Phase Layer Properties	**TLC** [4,34] **(particles, silica gel 60)**	**HPTLC** [4,34] **(particles, silica gel 60)**	**UTLC** [4,34,35] **(monolithic, silica gel)**
Typical Thickness (μm)	100 – 250	100 – 200	10
Characteristic Size (μm)	10 – 12 (particle size)	4 – 6 (particle size)	1 – 2 (macropore size)
Pore Size (Å)	60	60	30 – 40
Specific Surface Area ($m^2 g^{-1}$)	520	480 – 540	~ 350
Representative Developments	**TLC** [4,34,35]	**HTLC** [4,34]	**UTLC** [4,34,35]
Development Time (s)	> 900	> 180	60 – 360
Development Distance (mm)	70 – 150	30 – 70	10 – 30
Limit of Detection (ng, UV-visible, absorption)	1 – 5	0.1 – 0.5	0.5
Plate Height (μm)	30 – 75	12 – 25	80

High-performance thin-layer chromatography (HPTLC) media significantly improve upon the benefits of thin-layer chromatography (TLC) media [4,6,9]. The small size and spherical shape of modern HPTLC silica gel particles enables layers with improved homogeneity, lower tortuosity, finer pores, and narrower pore size distribution (**Figure 2-3** and **Table 2-1**) [4,9]. As a result, separations on HPTLC plates also occur more rapidly than on TLC plates. These properties cause the *A*- and *B*-terms in **Equation (2-9)** and resultant plate heights of HPTLC media to be smaller than those TLC layers. The strong dependence of separation efficiency upon microstructure motivates continued improvements in planar chromatography stationary phases from TLC, to HPTLC, and ultimately ultrathin-layer chromatography [4].

2.3 Ultrathin-layer chromatography[3]

The invention of monolithic silica gel ultrathin-layer chromatography (UTLC) sorbents in 2001 marked the beginning of a trend towards higher performing miniature planar chromatography plates with ultrathin and nanostructured stationary phases [35–38]. While traditional TLC and HPTLC layers are typically composed of silica gel particles fixed to a substrate using a binder, these isotropic monolithic layers generally have a single homogenous chromatographic surface [36]. Such materials therefore exhibit consistent surface chemistry and chromatographic interactions throughout since no competing analyte-binder interactions occur. Thinner UTLC sorbents with carefully selected morphologies achieve faster separations over shorter distances with higher sensitivity and lower reagent requirements [35]. These potential advantages motivate continued UTLC stationary phase innovation. The chromatographic merits of advanced selected ultrathin and nanostructured stationary phases including monolithic silica gels, monolithic polymers, electrospun nanofibrous mats, and carbon nanotube templated silica are summarized in **Table 2-2**[4]. Standard TLC and HPTLC

[3] Portions of this section are in-press as Chapter 3 "Ultrathin and Nanostructured Stationary Phases" by S.R. Jim and M.J. Brett in *Instrumental Thin Layer Chromatography* (Ed: C.F. Poole), Elsevier, 2014.

[4] **Table 9-4** is a version of this table modified to include GLAD UTLC performance data.

sample application, development, and documentation instrumentation are generally inappropriate for UTLC layers. This subsection therefore concludes with a discussion about recent progress towards specialized equipment designed to help these advanced chromatographic media approach their ultimate analytical potential.

2.3.1 Monolithic silica gels

Porous monolithic stationary phases exhibit a bimodal distribution in pore size [39] that affects both surface activity and migration velocities. Abundant small mesopores (2-50 nm [40]) ensure sufficient surface area over which analytes may interact with the sorbent while larger macropores (>50 nm [40]) enable rapid mobile phase migration.

The porosity and morphology of monolithic normal-phase silica layers are entirely dictated by the chemical reactions occurring during fabrication. Silica sol-gel monoliths are generally prepared from a mixture of silane precursors such as methyltrimethoxysilane (MTMOS) [41], tetraethoxysilane (TEOS) [39,42], tetramethoxysilane (TMOS) [39,42], or tetraalkoxysilane [35–37]. As in the synthesis of silica gel particles for traditional TLC and HPTLC layers, condensation of silicic acids in the mixture produces the mesoporous sol-gel. However, porogens (such as polyethylene glycol, PEG) added to this mixture serve as sacrificial templates during monolith fabrication [39,42]. Removing these porogens produces the macropores in the silica gel monoliths. Additives ensure a favourable pH during the condensation reaction and reduce cracking when drying the layer. An early study of 10-60 μm thick monoliths investigated the suitability of different silica gel mixtures in planar chromatography [41].

The first UTLC plates were prepared using similar methods optimized for exceptionally thin 10 μm monolithic layers [35–37]. These media were invented by Hauck *et al.* (Merck KGaA, Darmstadt, Germany) in 2001 [36] and were commercially available from Merck Darmstadt until 2011. (Factors contributing to their discontinuation are discussed below.) These binder-free UTLC layers

were prepared on 36 mm x 60 mm glass slides using tetraalkoxysilane precursors [36]. The resultant layers exhibit fine pores and a sponge-like appearance very different from that of traditional media composed of silica gel granules (**Figure 2-3**). **Table 2-1** compares the physical properties and representative separation performance of TLC, HPTLC, and UTLC layers. UTLC layers enables faster separations over shorter distances with higher sample detectability [35].

Monolithic silica UTLC plates possess sorbent layers that are thinner and have lower specific surface area than TLC and HPTLC plates. A consequence of the lower resultant total surface area is reduced sample capacity. Increasing the thickness of the monolithic silica gel to ~ 100 μm offers a method of increasing sample capacity but introduces other challenges [39,42]. Adhesion with the underlying substrate material and cracking within the silica gel can reduce the mechanical stability and influence mobile phase migration in these films. Careful optimization of glass substrate surface treatments and silica gel additives is required for these thicker monolithic layers.

2.3.2 Monolithic polymers

Porous polymer monoliths have also been used in reversed-phase planar chromatography. Superhydrophobic UV photopolymerized layers (50-200 μm thick) are better suited than silica gel monoliths in separations of peptides and other large molecules [43–45]. Complex mixtures of methacrylate monomers, styrene monomers, alcohols, and other additives are cast into a glass mold. These molds are constructed from a glass substrate, a Teflon gasket (to determine layer thickness), and a glass top plate. UV irradiation cures the mixture within the mold to create thin porous polymer slabs. The porosity and morphology of these hydrophobic monoliths (**Figure 2-4**) are influenced by the amount and type of alcohol porogens in the polymer mixture [44]. Polymer mixture composition must be optimized to produce a material dense enough to be mechanically stable but porous enough to allow rapid mobile phase migration. Surface treatments are again required to improve adhesion between the monolith and the glass substrate.

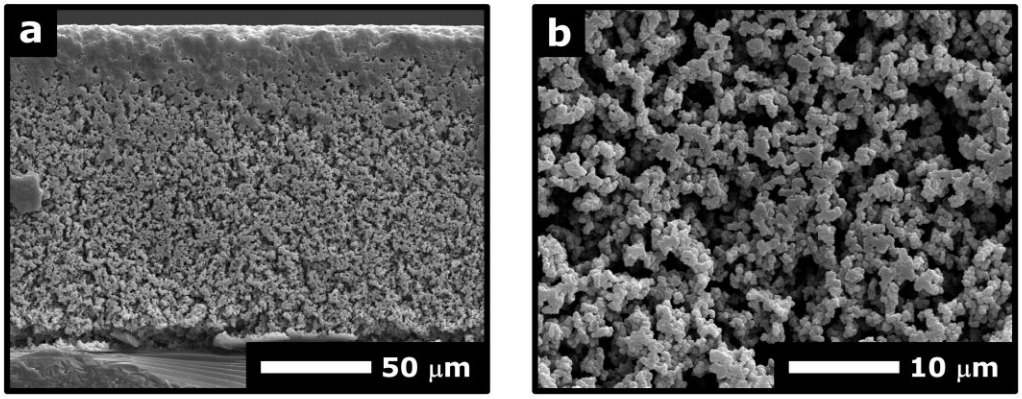

Figure 2-4 (a) Low and (b) high magnification cross-sectional scanning electron micrographs of a 150 μm thick poly(butyl acrylate-*co*-ethylene dimethacrylate) monolith. Figure modified with permission from [43]. Copyright (2007) American Chemical Society.

The hydrophobicity of the polymer monolith can also be selectively patterned to introduce interesting 2D separation behaviours. A narrow hydrophilic line optically patterned onto the hydrophobic monolith can act as a virtual channel [44]. Performing the first development along this channel (ion exchange chromatography) and the second development perpendicular to this channel (reversed-phase chromatography) improved separations of a peptide sample. Polymer monoliths with optically patterned hydrophobicity gradients can also improve 2D separation quality [45]. Similarly prepared polymer monoliths 125 μm thick have also been used in planar electrophoresis and pressurized planar electrochromatography [46]. Preliminary work on thermally-initiated polymer monoliths has also been recently reported [47].

2.3.3 Electrospun nanofibres

Electrospinning is a powerful method of microstructuring polymers [48]. A relatively simple apparatus enables rapid fabrication of nanofibrous stationary phase mats. Solutions containing dissolved polymers such as polyacrylonitrile (PAN) [49–52], polyvinyl alcohol (PVA) [53], SU-8 [50], and cellulose acetate [54] are injected into the setup using a syringe pump. A high voltage DC power supply generates a potential difference (for example, 9-20 kV [49–53]) between the syringe tip and a metal substrate (such as aluminum foil or sheets [49,52–54]

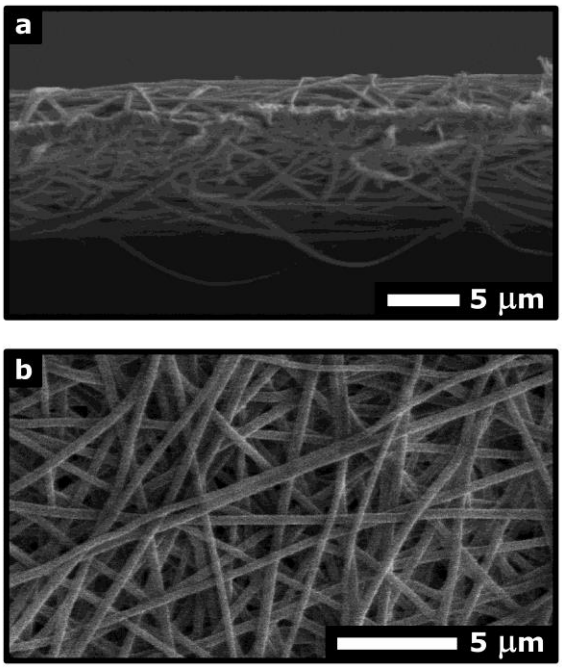

Figure 2-5 (a) Edge and (b) top scanning electron micrographs of electrospun nanofibrous PAN planar chromatography stationary phases. Figure modified with permission from [49]. Copyright (2009) American Chemical Society.

or stainless steel [50,51]). The resultant electric field produces a polymer jet that arrives at the substrate as a solid nanofibre. This nanofibre winds randomly across the substrate and can be metres in length. The nanofibre width (150-600 nm) and mat thickness (5-25 μm) are controlled by adjusting the polymer type, syringe pump flow rate, solution viscosity, power supply voltage, tip-substrate separation distance, electrospinning time, and other parameters [49–54]. An initial report of nanofibrous PAN mats studied the effects of electrospinning time on morphology (**Figure 2-5**) and UTLC separation performance [49]. Several recent advancements have increased the capabilities of this technique.

UTLC stationary phases with aligned nanofibres may be fabricated by moving the substrates on a rotating drum during electrospinning [51]. Careful selection of rotation speed increases nanofibre ordering and results in an anisotropic medium. Chromatographic separations performed along the aligned nanofibres occurred faster and more efficiently than on unordered materials. Incorporating cross-

linking additives made PVA stationary phases insoluble in water and allowed reversed-phase separations of amino acids [53]. High temperature pyrolysis of electrospun SU-8 layers produced glassy carbon UTLC sorbents appropriate for reversed-phase chromatography [50]. However, the dark colour of the resultant plates restricted their use to UV fluorescent laser dyes. Adding a photoluminescence indicator to the electrospun PAN nanofibres enabled detection of UV-active compounds [52]. Separated beverage preservative analytes absorbed UV and appeared as dark spots on the UTLC plates. The robustness of the electrospun nanofibrous UTLC plates also makes them appealing in electrospray ionization mass spectroscopy (ESI-MS) [52]. The elution head used to extract separated analytes can be pressed firmly against the layer during analyte extraction without causing substantial damage. The capabilities and relative simplicity of electrospun UTLC layers make them appealing in reversed-phase chromatography. However, significant structural and chemical differences prevent direct comparison with the normal-phase media described in this thesis.

2.3.4 Carbon nanotube templated layers

Chromatography media have also been microfabricated using processes employed in the microelectronics industry. A series of several thin film deposition, photolithography, and other steps enable complex media exhibiting herring-bone (zig-zag) channel features comprised of SiO_2 templated onto carbon nanotubes (CNTs) [55–58] (**Figure 2-6**). The initial report of these media [55] employed an iron thin film deposited onto an Al_2O_3 diffusion barrier that was patterned by photolithography (lift-off). The iron film catalyzes carbon nanotube chemical vapour deposition (CVD) growth. The resultant carbon nanotube "hedges" (4 μm wide, separated by 7 μm spaces) were then coated with low-pressure CVD (LPCVD) silicon. Thermal processing burned away the CNTs and oxidized the silicon into 50 μm tall SiO_2 nanowires < 200 nm in diameter. Mesopores in the hedges enabled access to high surface areas while macroporous channels between hedges permitted rapid mobile phase migration. The herring-bone pattern of the hedges had better mechanical stability than straight line hedges [59].

Subsequent work optimized the thickness of the iron thin film catalyst layer [57] and addressed pattern distortion problems associated with the thermal processing step [56,58]. The volume expansion that occurs upon oxidation distorted the herring-bone structures. This annealing step was eliminated by rapid direct deposition of an Al-doped SiO_2 film and amino-functionalization to cover the Al impurities [56,58]. The high temperature steps presently limit this process

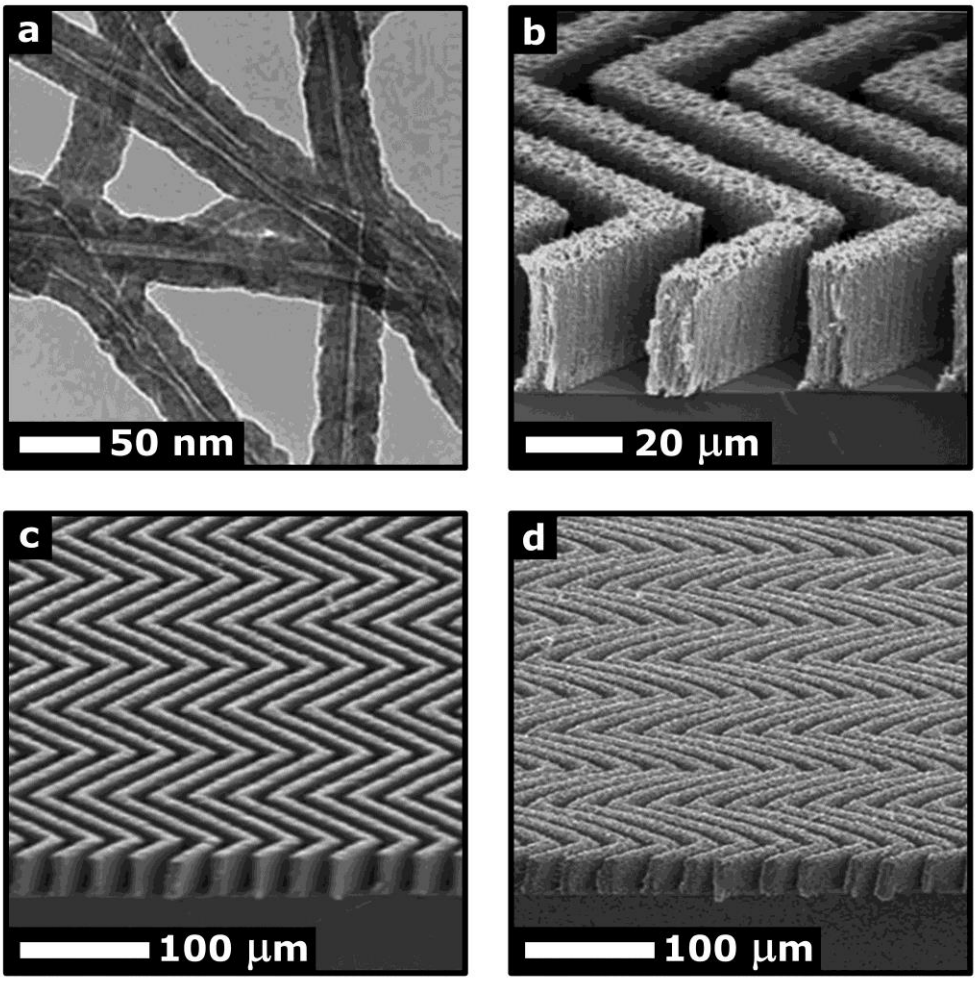

Figure 2-6 Microfabricated carbon nanotube templated planar chromatography media. (a) Transmission electron micrograph showing carbon nanotubes coated with Si using low pressure chemical vapour deposition. (b,c) High and low magnification scanning electron micrographs of patterned Si coated carbon nanotube hedges. (d) Scanning electron micrograph of structures after oxidizing Si to SiO_2 and burning out the carbon nanotubes. Figure modified with permission from [55]. Copyright (2011) Wiley.

to Si wafer substrates. While the multi-step CNT-template approach is complicated, it can achieve unique and interesting microstructures very different from those possible by other techniques, including the thin film deposition and microfabrication methods described in this thesis.

2.3.5 Advanced instrumentation and techniques

The size and unconventional development characteristics of UTLC plates introduce unique challenges and capabilities. The small format (the shortest dimension can be ~ 25 mm) and exceptionally thin layers on these miniaturized planar chromatography plates can make them difficult to handle and easy to damage. Conventional HPTLC sample application systems, development chambers, and documentation tools are often incompatible with these plates. Modified or entirely new instruments are required if UTLC media are to reach their ultimate performance. For instance, the "Office Chromatography" concept advanced by G.E. Morlock *et al.* incorporates repurposed high-performance inexpensive consumer inkjet printers and flatbed scanners into the UTLC process flow [21,60,61]. Ultrathin layers can also improve hyphenation with post-separation characterization methods such as mass spectroscopy. These factors must be considered carefully when applying miniaturized media to analytical problems.

Sample application

Sample application significantly affects the overall separation performance in all forms of planar chromatography [10]. This dependence is pronounced on miniaturized plates. Large applied spot sizes can negate improvements in separation efficiency and analyte resolution. Reduced thickness and lower specific surface areas also make UTLC stationary phases more susceptible to sample overloading than TLC or HPTLC layers. In their first report, Hauck *et al.* (2001) recognized this limitation and recommended sample volumes < 20 nL to maximize UTLC's benefits [36].

Narrow gauge syringes (such as Hamilton model 7000.5 with total volume 0.5 μL) enable hand-application of sample volumes as low as 10 nL [36,37], however precise manual placement of repeatable spots may require customized apparatus [62] (see **3.3.3 Calibrated syringe**). The CAMAG Automatic TLC Sampler 4 is the state-of-the-art tool in HPTLC spot application. Although an exceptionally powerful spotting robot, modifications to its hardware and firmware settings are required to achieve < 25 nL volumes [52,63]. The Office Chromatography approach uses inkjet printers to perform rapid and precise application of sharp ~ 10 nL aqueous sample bands [21,60]. However, the plastic components in current inkjet printers preclude samples dissolved in some organic solvents.

Development chambers

Successful ascending (upright) UTLC separations have been achieved within custom sealed glass containers [49–52,64] and existing HPTLC chambers (for example, CAMAG Twin Trough chamber designed for 10 cm x 10 cm plates [55]). Other separations have been performed in small modified horizontal development chambers such as the 50 mm x 50 mm Desaga H-chamber [63] (**Figure 3-6**). Nonetheless, these chambers are generally grossly oversized for miniaturized UTLC plates. In addition to excessive reagent requirements, large reservoirs and dead volumes adjacent to the stationary phases can affect mobile phase composition, flow uniformity, and reproducibility [3]. Details about these effects are discussed further in **3.4.3 Ultrathin-layer chromatography development** and in **8 Customized GLAD UTLC chamber**.

Documentation

Adequate recording of the short separation patterns on miniature planar chromatography plates requires higher imaging resolution than most conventional TLC and HPTLC instruments can produce. Office Chromatography employs consumer reflection-mode flatbed scanners to digitize developed UTLC plates for subsequent chromatogram extraction [21]. Meanwhile, flatbed film scanners can be used to image transparent UTLC media in transmission mode [27,63,65].

Consumer digital cameras capable of high image resolutions are often effective in capturing separation patterns illuminated by visible [60] and UV light [51,56]. Time-resolved UTLC exploits the high-definition video recording capabilities of modern digital cameras to record developments of visible analytes [19] (see also **6 Time-resolved UTLC**). Extracted video frames are processed to quantify separation performance at different times throughout the development. Chromatograms were documented in this work using both transmission mode scanning and time-resolved UTLC methods.

Hyphenation with mass spectroscopy

Ultrathin stationary phases can increase the sensitivity of mass spectroscopy characterization performed on separated analytes. Benefits have been observed for several sampling mechanisms including matrix assisted laser desorption ionization (MALDI) [45,66], atmospheric pressure MALDI (AP-MALDI) [67,68], desorption electrospray ionization (DESI) [69], and electrospray ionization (ESI) [52,60,70]. The significant sensitivity improvements (as high as 10-100 times better than for HPTLC plates [67]) are attributed to the thinness of UTLC stationary phases. Reduced layer thickness produces higher analyte surface densities (molecules per unit area) and increases extraction from the layer interior (ions are closer to the surface) in AP-MALDI performed on UTLC layers [67]. These monolithic layers are also especially compatible with DESI since incident sprayed solvent tends to erode them less than the granular HPTLC layers composed of binded silica gel particles [69].

Table 2-2 Comparison of ultrathin and nanostructured stationary phase properties and performance. (**Table 9-4** is a version of this table modified to include GLAD UTLC data.)

	Monolithic Silica Gel [5]	Monolithic Polymer	Electrospun Polymer	Carbon Nanotube-Templated Silica
Stationary Phase Material	Silica sol-gel [35–37,39,41,42]	Photopolymerized poly(butyl methacrylate-*co*-ethylene dimethacrylate) [43,44]; poly(glycidyl methacrylate-*co*-ethylene dimethacrylate) [45]	Polyacrylonitrile [49–52]; Glassy carbon [50]; Polyvinyl alcohol [53]; Cellulose acetate [54]	SiO_2 nanowire hedges [55,57]; (also functionalized with 3-aminopropyltriethoxysilane (APTES) [56,58])
Thickness	10-12 μm [35–37,41]; ~ 100 μm [39]	50-200 μm [43–45]	5-25 μm [49–54]	~50 μm [55–58]
Morphology[6]	Isotropic monolith; macroporous and mesoporous [35,39,42]; SSA ~ 350 m^2g^{-1} [35]	Isotropic monolith; macroporous and mesoporous [43–45]	Isotropic [49–54] or anisotropic [51]; mat composed of nanofibres (width 150-600 nm [49–54]); SSA 21.7 m^2g^{-1} [49]	Anisotropic; herring-bone (zig-zag) pattern [55–58]; composed of 3-4 μm wide hedges spaced 4-6 μm apart [56–58]; with 100-120 nm diameter SiO_2 nanowires [58]; SSA 19-27 m^2g^{-1} for oxidized SiCNTs [57]

[5] The monolithic silica gel properties listed here include those of Merck UTLC plates and others. **Table 2-1** includes only Merck UTLC plate data.
[6] The reported specific surface areas (SSA) were measured using the Brunauer, Emmett and Teller (BET) method [113], where available.

Table 2-2 Comparison of ultrathin and nanostructured stationary phase properties and performance. (**Table 9-4** is a version of this table modified to include GLAD UTLC data.) (Continued.)

	Monolithic Silica Gel [5]	Monolithic Polymer	Electrospun Polymer	Carbon Nanotube-Templated Silica
Substrate	Glass [35–37,39,41,42]	Glass [43–45]	Aluminum [49,52–54]; Stainless steel [50,51]	Si wafer [55–58]
Substrate Size	25-40 mm x 30-100 mm [35–37,39,41,42]	26-30 mm x 33-76 mm [43–45]	20-40 mm x 40-85 mm [49–54]	Limited by 100 mm circular wafer [55–58]
Development Distance and Time	10-30 mm in 1-8 min [35–37,39,42,67]	30-60 mm in < 6 min [43,45]	25-35 mm in 3-12 min [49–53] or 70 mm in 30-45 min [54]; 25 mm in 1-1.5 min for aligned nanofibres [51]	25-45 mm in 1-4.5 min [55–58]
Tested Analytes	Dyes [36,39,42]; Pharmaceutically active ingredients [35,37,67–69]; Phenols and plasticizers [35,37]; Amino acids and pesticides [35]; Steroids [37]; Triazoles [67]	Proteins and peptides [43–45]; Dyes [43]	UV fluorescent laser dyes [49–51]; Steroids [49,51,54]; Amino acids [50,53]; β-blockers [51]; Beverage preservatives [52]; Aspartame hydrolysis products (aspartic acid, phenylalanine) [53]	Dyes [55–58]; Analgesics [57]

2.4 Glancing angle deposition

Porous thin films with intricate columnar geometries can be fabricated using an approach called glancing angle deposition (GLAD)[7] [71–73]. This single-step physical vapour deposition (PVD)[8] method combines the inclined columnar features attained through oblique angle deposition with complex substrate manipulation to produce microstructures unachievable through other techniques. The method has progressed significantly since its inception by K. Robbie, M.J. Brett, and colleagues in the mid-1990s [71,74–76] and eventual patenting in 1999 [77]. Many research groups around the world actively pursue improved understanding, fabrication, and application of nanostructured GLAD thin films. An exhaustive review of the expanding field cannot fit within this thesis. Readers interested in a more comprehensive summary are directed to several excellent sources [78–80].

2.4.1 Theory and implementation

Specific criteria must be met in order to deposit nanostructured GLAD thin films. The properties of the evaporated material, substrate, vacuum deposition system, and other parameters affect the resultant film morphology. Appropriate GLAD materials have low adatom mobility, nucleate according to the Volmer-Webber "island" mode [81], and have relatively high melting temperatures [72,79]. These properties enable columnar film growth characteristic of zone 1 (low deposition to melting temperature ratio, typically < 0.3) in Movchan and Demchishin's structure zone model [82]. Processing should occur in a vacuum chamber with the sufficiently large source-to-substrate throw distances and low gas pressures required to produce highly uniform and directional (ideally collimated) evaporant flux [79]. Assuming these conditions are met, GLAD thin films can be fabricated in a system equipped with biaxial substrate motion control (**Figure 2-7a**).

[7] GLAD films are sometimes called sculpted thin films (STFs).
[8] Electron beam evaporation is the most common type of PVD used for GLAD. However, other techniques such as sputtering have also been used.

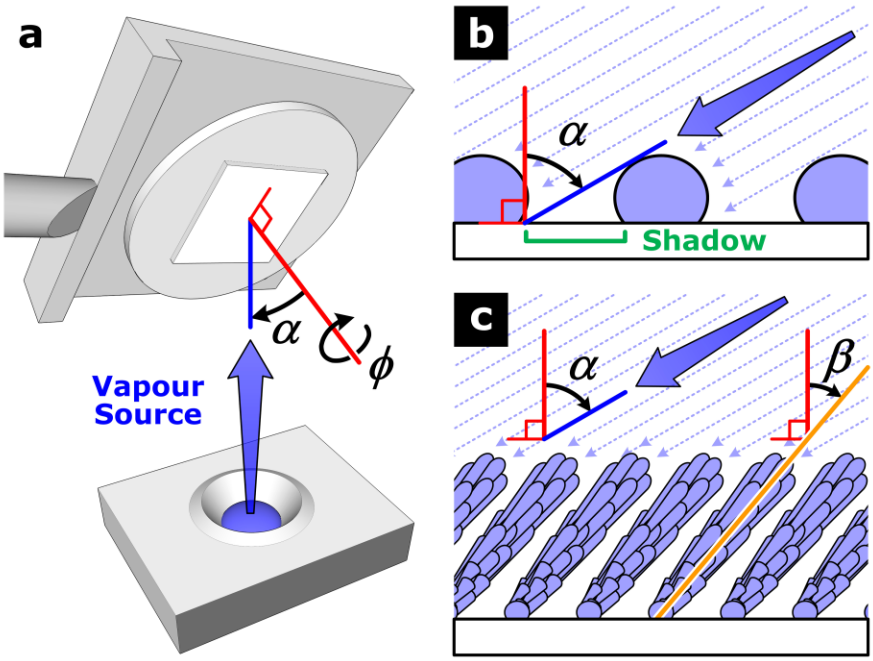

Figure 2-7 Schematic representation of the GLAD thin film physical vapour deposition technique and growth mechanisms. (a) Directional source material evaporant reaches the substrate at a given oblique angle α and azimuthal angle ϕ. (b) When evaporant is incident at large α, growing nuclei cast shadows across the substrate into which additional material cannot be deposited. (c) These nuclei grow into columns inclined towards the apparent vapour source by an angle β.

Geometric self-shadowing mechanisms occur when the evaporated atomic flux is incident on the substrate at an oblique deposition angle (α, measured from the substrate normal; $0° \leq \alpha \leq 90°$). Nuclei "islands" that form early in the deposition cast ballistic shadows across the substrate into which further evaporant cannot arrive (**Figure 2-7b**). As the deposition continues, these nuclei grow into columnar microstructures with a preferred inclination towards the apparent evaporant source (**Figure 2-7c**). Several formulae have been derived to relate the column inclination angle β to the deposition angle α. The "tangent rule" for obliquely deposited films was determined experimentally by Nieuwenhuizen and Haanstra [83]:

$$\tan\alpha = 2\tan\beta \qquad \textbf{(2-10)}$$

While Tait *et al.* performed a geometrical treatment [84]:

$$\beta = \alpha - \arcsin\left(\frac{1-\cos\alpha}{2}\right) \quad \textbf{(2-11)}$$

In the same report [84], Tait *et al.* also derived a relationship between the film density (ρ) at a given α and that at $\alpha = 0°$ (normal incidence, ρ_0):

$$\rho = \rho_0 \frac{2\cos\alpha}{1+\cos\alpha} \quad \textbf{(2-12)}$$

It is important to note that **Equations (2-10)**, **(2-11)**, and **(2-12)** should be considered only approximate relationships [79] since specific behaviours depend upon film material properties, deposition behaviours, GLAD system geometry, and other factors. However, these formulae describe the observed increase in β and decrease in ρ for films deposited at higher α. These effects are especially significant for films deposited at the high α (approaching 90°) such as those studied in this thesis.

GLAD distinguishes itself from traditional oblique angle deposition by introducing an azimuthal ordinate ϕ [72,79]. Manipulating this angle changes the apparent location of the evaporant source (from the perspective of the inclined growing column) and therefore the direction towards which the column grows. Modulation of α and ϕ during deposition enables many unique architectures achievable only by GLAD (typical types are discussed **below**). As α and ϕ are typically specified as functions of film thickness [79], accurate deposition rate monitoring and real-time computer control are necessary. The local deposition rate (at the substrate) is dependent upon α and can be related to that measured by a quartz crystal microbalance rate monitor located within the GLAD system after considering deposition chamber geometry. Finite evaporant source size, deposition protocol, and chamber geometry also have a tangible impact on film uniformity. A theoretical treatment of these effects was performed by Wakefield and Sit [85].

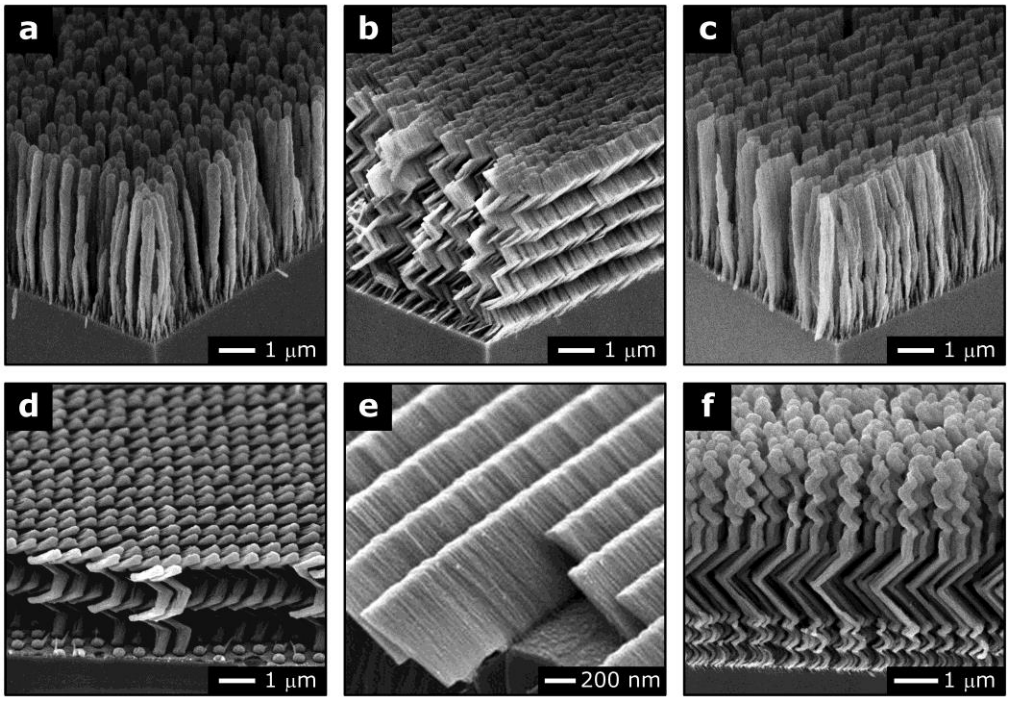

Figure 2-8 Scanning electron micrographs of typical GLAD thin film morphologies. (a) Vertical posts, (b) chevrons, (c) serial bideposition (SBD) blades, (d) square helices on patterned seed dots, (e) nanoribbons (inclined columns deposited on patterned seed lines), and (f) hybrid nanocolumns. Images reproduced with permission from (a-c) reference [63], copyright (2010) American Chemical Society; (d) reference [86], copyright (2005) SPIE; (e) reference [87], copyright (2005) SPIE; and (f) reference [88], copyright (2004) SPIE.

2.4.2 Representative architectures

Numerous architectures can be produced by holding α constant and manipulating ϕ alone. Continuous slow azimuthal rotation sculpts the inclined columns into helices (not shown). Rapid rotation causes the flux to effectively arrive from all directions and the helices to degenerate into vertical posts (**Figure 2-8a**). Periodically changing ϕ in multiples of $\Delta\phi = 180°$ produces chevrons composed of alternating inclined column segments (**Figure 2-8b**). The degenerate case of chevrons with short period (deposited thickness comparable to column width) produces serial bideposition (SBD) media (**Figure 2-8c**) consisting of blade-like fins. Polygonal helices (square, hexagonal, and others) are also possible by discretely changing ϕ ($\Delta\phi < 180°$) during the deposition (**Figure 2-8d**). Other

motion algorithms produce inclined columns (constant α and ϕ, **Figure 2-8e**) and complex hybrid nanostructures (**Figure 2-8f**). Concurrent modulation of α (and film density) enables fabrication of Bragg stacks (discrete changes in α; abrupt high-low-high-… density layers) and Rugate films (gradual changes in α; smooth high-medium-low-medium-high-… density layers) useful in optics [72,79]. The GLAD UTLC investigations described in this thesis considered vertical post, chevron, and SBD media (see **3.1.3 Studied GLAD UTLC morphologies** and **4 Anisotropic UTLC microstructures** for details).

Visual similarities between GLAD nanostructures and pasta noodles (spaghetti, fusilli, linguini, fettuccine, lasagne, and others) prompted proposals for ultra-fast cooking nano-pastas [89]. Regrettably, initial industrial interest in this potentially revolutionary research field dwindled due to the impractical and cost-prohibitive mass manufacturing scaling required for human consumption.

2.4.3 Advanced GLAD methods

Research into modified GLAD techniques continues to be very active [79,80]. These enhancements may be broadly classified as taking place before, during, or after deposition. Although only post-deposition methods were employed in this thesis, examples of all three classes are listed below for completeness.

Pre-deposition

Substrates patterned with carefully designed topologies can affect the morphology of the resultant GLAD film [87,90–92]. Electron beam lithography (EBL) and other methods can be used to produce layers of seeds with dimensions comparable to nuclei that form early into deposition [79] (**Figure 2-8d**). Through simple geometric shadowing, seeds can force columnar structures to grow at specific locations rather than randomly across the substrate. (Lines patterned prior to GLAD produced the nanoribbons shown in **Figure 2-8e**.) Self-sealed chambers have also been produced by performing GLAD on substrates patterned with larger lines and mesas using conventional photolithography [92]. Even larger

mechanically-machined blocks placed adjacent to substrates during deposition can introduce macroscopic shadows that produce spatially-graded GLAD films with thickness and morphology varied over several centimetres [93].

During deposition

Numerous parameters may be manipulated during GLAD film deposition. The PhiSweep motion algorithm oscillates the ϕ ordinate to supress column broadening typical in GLAD films by introducing shadowing perpendicular to the deposition plane [94]. Capping layers may be deposited onto GLAD columns by appropriately reducing α near the end of the deposition [79,90]. Substrate heating and cooling modifies surface diffusion (adatom mobility) to extend the selection of compatible materials and variety of microstructures [79]. Heating can also enable simultaneous vapour-liquid-solid (VLS) nanowire growth [95]. Ion-assisted GLAD utilizes an incident Ar beam to increase column inclination and film density [96,97].

Post-deposition [9]

Additional processing can modify the morphology and surface chemistry of deposited GLAD films. Their long pores open from above make GLAD films especially amenable to etching and coating techniques. Annealing and thermal oxidation treatments may be used to modify the crystallinity and stoichiometry of the thin films [72,79]. The columnar films may also be filled and used as sacrificial templates in creation of inverse structures and nanotubes [72,79,98]. Ion milling can be used to sharpen and smooth the broad rough columns typical in GLAD films [99]. More extensive column thinning and rarefaction are possible using reactive ion etching (RIE) [27,100]. Vapour phase hydrophobic silane functionalization of GLAD films is also possible [101,102]. Coupling GLAD with atomic layer deposition (ALD) enables interesting core-shell nanostructures

[9] Post-deposition treatments were used in GLAD UTLC investigations. Ion milling was found to produce only small changes in GLAD UTLC layers however, the RIE and ALD significantly affected UTLC layer properties and are discussed further. See **5 Modified morphology and development** and **7 Surfaces modified by atomic layer deposition** for details.

[62,103,104]. The significant changes to morphology and surface chemistry possible through combinations of these post-deposition techniques make them particularly appealing in applications of GLAD to UTLC.

2.4.4 Example applications

GLAD enables dynamic control of porosity, surface area enhancement, and morphology throughout the film's thickness [72,79]. These capabilities make nanostructured thin films useful in many applications. The ability to control film density permits fabrication of photonic crystals, filters, polarizers, and other optical layers [72,79]. While typical multilayer optical filters are composed of two materials of different index of refraction, GLAD structures can produce high and low index layers simply by modulating α (and resultant density). High GLAD film surface areas (for example, ~ 1,000 times the footprint area [105]) are appealing in sensing applications. Large surface areas and pores easily accessible from above make them suitable in highly-responsive humidity sensors [106]. Large interfacial areas also make GLAD films interesting in organic photovoltaics, catalysis, and fuel cells [79,107,108]. Nanostructured thin films have also found application in microfluidics [90,109,110] and matrix-assisted laser desorption ionization mass spectroscopy (MALDI-MS) [111].

2.4.5 Applications of GLAD to UTLC[10]

GLAD thin films were first used in UTLC by Bezuidenhout and Brett in 2007-2008 [64]. This preliminary investigation explored nanostructured SiO_2 thin films of varied porosity (achieved by varying α over 45° - 86°) and thickness (1 μm - 7 μm). Separations performed on isotropic helical stationary phase layers indicated that deposition angles $\alpha > 80°$ were required for analyte migration and that only incremental performance improvements were achieved by increasing layer thickness beyond ~ 5 μm. The study was also the first to describe anisotropic

[10] Portions of this section were reproduced with permission from S.R. Jim, M.T. Taschuk, G.E. Morlock, L.W. Bezuidenhout, W. Schwack, M.J. Brett, Engineered anisotropic microstructures for ultrathin-layer chromatography, Analytical Chemistry. 82 (2010) 5349–5356. Copyright (2010) American Chemical Society.

stationary phases that possessed 5 μm thick chevron ("zig-zag") architectures and channel-like features. Analyte migration along the anisotropic channel-like features was more rapid than across them. The intriguing behaviours of the anisotropic GLAD UTLC layers motivated the follow-up studies described in references [63,65] and in **4 Anisotropic UTLC microstructures**. The second GLAD UTLC publication described advantages achieved by combining these media with the Office Chromatography framework [21]. This work demonstrated that inkjet printers and flatbed scanners enabled higher GLAD UTLC separation performance than standard HPTLC instrumentation. (See also **2.3.5 Advanced instrumentation and techniques**.) These two reports served as the foundations for the research described in this dissertation.

S.R. Jim was not closely involved with two other GLAD UTLC papers published during his studies. These are briefly described below as they are relevant to the GLAD UTLC field. Hall *et al.* studied SiO_2 GLAD UTLC layers functionalized using hydrophobic silane chemistries and used in reversed-phase separations [102]. Treating functionalized layers with oxygen plasma enabled tuning of surface hydrophobicity and resultant separation performance. Similar tuning was not possible on commercial reversed-phase HPTLC layers that lacked GLAD's characteristic open pore morphologies. In another paper, Y.-P. Zhao's research group reported Ag inclined column (nanorod) films fabricated using oblique angle deposition [112]. Dyes separated on these Ag UTLC media were successfully detected using scanning surface-enhanced Raman spectroscopy (SERS).

References

[1] N.A. Izmailov, U.M.S. Shraiber, Spot Chromatographic Adsorption Analysis and its Application in Pharmacy Communication, Farmatsiya. (1938) 1–7.

[2] A.-M. Siouffi, From Paper to Planar: 60 Years of Thin Layer Chromatography, Sep. Purif. Rev. 34 (2005) 155–180.

[3] B. Spangenberg, C.F. Poole, C. Weins, Quantitative Thin-Layer Chromatography, Springer Berlin Heidelberg, Berlin, Heidelberg, 2011.

[4] S.K. Poole, C.F. Poole, High performance stationary phases for planar chromatography, J. Chromatogr. A. 1218 (2011) 2648–2660.

[5] J. Sherma, Review of advances in the thin layer chromatography of pesticides: 2006-2008, J. Environ. Sci. Heal. B. 44 (2009) 193–203.

[6] E. Reich, A. Schibli, High-Performance Thin Layer Chromatography for the Analysis of Medicinal Plants, Thieme Medical Publishers, New York, 2007.

[7] J. Sherma, Review of HPTLC in drug analysis: 1996-2009, J. AOAC Int. 93 (2010) 754–764.

[8] G.E. Morlock, W. Schwack, The contribution of planar chromatography to food analysis, J. Planar Chromatogr. 20 (2007) 399–406.

[9] B. Fried, J. Sherma, Thin-Layer Chromatography, Revised And Expanded, CRC Press, 1999.

[10] P.E. Wall, Thin-Layer Chromatography: A modern practical approach, Royal Society of Chemistry, Cambridge, 2005.

[11] G.E. Morlock, W. Schwack, Hyphenations in planar chromatography, J. Chromatogr. A. 1217 (2010) 6600–6609.

[12] J. Sherma, Biennial Review of Planar Chromatography: 2009–2011, J. AOAC Int. 95 (2012) 992–1009.

[13] G.E. Morlock, E.S. Chernetsova, Coupling of planar chromatography with Direct Analysis in Real Time mass spectrometry, Cent. Eur. J. Chem. 10 (2012) 703–710.

[14] T.H. Dzido, P.W. Płocharz, P. Slazak, A. Hałka, Progress in planar electrochromatography., Anal. Bioanal. Chem. 391 (2008) 2111–8.

[15] E. Washburn, The dynamics of capillary flow, Phys. Rev. 17 (1921) 273–283.

[16] I. Vovk, M. Prosek, Quantitative evaluation of chromatograms from totally illuminated thin-layer chromatographic plates, J. Chromatogr. A. 768 (1997) 329–333.

[17] M. Lancaster, D.M. Goodall, E.T. Bergström, S. Mccrossen, P. Myers, Quantitative measurements on wetted thin layer chromatography plates using a charge coupled device camera, J. Chromatogr. A. 1090 (2005) 165–171.

[18] B. Hemmateenejad, N. Mobaraki, F. Shakerizadeh-Shirazi, R. Miri, Multivariate image analysis-thin layer chromatography (MIA-TLC) for simultaneous determination of co-eluting components., Analyst. 135 (2010) 1747–58.

[19] A.J. Oko, S.R. Jim, M.T. Taschuk, M.J. Brett, Time resolved chromatograms in ultra-thin layer chromatography, J. Chromatogr. A. 1249 (2012) 226–232.

[20] S. Mustoe, S. McCrossen, TLC image capture and analysis by use of a prototype device for visualizing fluorescence, J. Planar Chromatogr. 14 (2001) 252–255.

[21] G.E. Morlock, C. Oellig, L.W. Bezuidenhout, M.J. Brett, W. Schwack, Miniaturized planar chromatography using office peripherals, Anal. Chem. 82 (2010) 2940–2946.

[22] J. Sherma, B. Fried, Handbook of Thin-Layer Chromatography, 3rd ed., Marcel Dekker [Taylor and Francis], New York, 2003.

[23] R. Delley, The peak width of nearly Gaussian peaks, Chromatographia. 18 (1984) 374–382.

[24] V.B. Di Marco, G.G. Bombi, Mathematical functions for the representation of chromatographic peaks, J. Chromatogr. A. 931 (2001) 1–30.

[25] A.-M. Siouffi, F. Bressolle, G. Guiochon, Optimization in thin-layer chromatography, J. Chromatogr. 209 (1981) 129–147.

[26] T.H. Jupille, J.A. Perry, Programmed multiple development in thin-layer chromatography, Science (80-.). 194 (1976) 288–293.

[27] S.R. Jim, A.J. Oko, M.T. Taschuk, M.J. Brett, Morphological modification of nanostructured ultrathin-layer chromatography stationary phases, J. Chromatogr. A. 1218 (2011) 7203–7210.

[28] D.C. Abbott, J. Thomson, Preparation and Uses of Multi-band Chromatoplates, Chem. Ind. (1965) 310.

[29] A. Musgrave, Sample application to silica gel layers via kieselguhr layers, J. Chromatogr. 41 (1969) 470–472.

[30] T.E. Beesley, A new dimension for an established technique, Am. Lab. 4 (1972) 25–32.

[31] H. Halpaap, K.-F. Krebs, Thin-layer chromatographic and high-performance thin-layer chromatographic ready-for-use preparations with concentrating zones, J. Chromatogr. 142 (1977) 823–853.

[32] J.J. van Deemter, F.J. Zuiderweg, A. Klinkenberg, Longitudinal diffusion and resistance to mass transfer as causes of nonideality in chromatography, Chem. Eng. Sci. 5 (1956) 271–289.

[33] F.M. Rabel, Sorbents and Precoated Layers in Thin-Layer Chromatography, in: J. Sherma, B. Fried (Eds.), Handbook of Thin Layer Chromatography, 3rd ed., Marcel Dekker [Taylor and Francis], New York, 2003: pp. 129–176.

[34] Merck KGaA ChromBook 2008|09, (2008).

[35] H.E. Hauck, M. Schulz, Ultrathin-layer chromatography, J. Chromatogr. Sci. 40 (2002) 550–552.

[36] H.E. Hauck, O. Bund, W. Fischer, M. Schulz, Ultra-thin layer chromatography (UTLC) — A new dimension in thin-layer chromatography, J. Planar Chromatogr. 14 (2001) 234–236.

[37] H.E. Hauck, M. Schulz, Ultra thin-layer chromatography, Chromatographia. 57 (2003) S313–S315.

[38] R.B. Patel, M.C. Gopani, M.R. Patel, UTLC: An Advanced Technique in Planar Chromatography, Chromatographia. (2013).

[39] A.M. Frolova, O.Y. Konovalova, L.P. Loginova, A. V Bulgakova, A.P. Boichenko, Thin-layer chromatographic plates with monolithic layer of silica: Production, physical-chemical characteristics, separation capabilities, J. Sep. Sci. 34 (2011) 2352–2361.

[40] J. Rouquerol, D. Avnir, C.W. Fairbridge, D.H. Everett, J.M. Haynes, N. Pernicone, et al., Recommendations for the characterization of porous solids (Technical Report), Pure Appl. Chem. 66 (1994) 1739–1758.

[41] M. Tsionsky, A. Vanger, O. Lev, Macroporous thin films for planar chromatography, J. Sol-Gel Sci. Technol. 2 (1994) 595–599.

[42] A.M. Frolova, M.A. Chukhlieb, A. V. Drobot, A.P. Kryshtal, L.P. Loginova, A.P. Boichenko, Producing of Monolithic Layers of Silica for Thin-Layer Chromatography by Sol-Gel Synthesis, Open Surf. Sci. J. 1 (2009) 40–45.

[43] R. Bakry, G.K. Bonn, D. Mair, F. Svec, Monolithic porous polymer layer for the separation of peptides and proteins using thin-layer chromatography coupled with MALDI-TOF-MS, Anal. Chem. 79 (2007) 486–493.

[44] Y. Han, P. Levkin, I. Abarientos, H. Liu, F. Svec, J.M.J. Fréchet, Monolithic superhydrophobic polymer layer with photopatterned virtual channel for the separation of peptides using two-dimensional thin layer chromatography-desorption electrospray ionization mass spectrometry, Anal. Chem. 82 (2010) 2520–2528.

[45] I. Urbanova, F. Svec, Monolithic polymer layer with gradient of hydrophobicity for separation of peptides using two-dimensional thin layer chromatography and MALDI-TOF-MS detection, J. Sep. Sci. 34 (2011) 2345–2351.

[46] S.D. Woodward, I. Urbanova, D. Nurok, F. Svec, Separation of peptides and oligonucleotides using a monolithic polymer layer and pressurized planar electrophoresis and electrochromatography, Anal. Chem. 82 (2010) 3445–3448.

[47] Y. Lv, Z. Lin, T. Tan, F. Svec, Preparation of porous styrenics-based monolithic layers for thin layer chromatography coupled with matrix-assisted laser-desorption/ionization time-of-flight mass spectrometric detection., J. Chromatogr. A. 1316 (2013) 154–9.

[48] M. Ma, G.C. Rutledge, 7.10 Nanostructured Electrospun Fibers, in: K. Matyjaszewski, M. Möller (Eds.), Polym. Sci. A Compr. Ref., Elsevier, Amsterdam, 2012: pp. 187–210.

[49] J.E. Clark, S. V Olesik, Technique for ultrathin layer chromatography using an electrospun, nanofibrous stationary phase, Anal. Chem. 81 (2009) 4121–4129.

[50] J.E. Clark, S. V Olesik, Electrospun glassy carbon ultra-thin layer chromatography devices, J. Chromatogr. A. 1217 (2010) 4655–4662.

[51] M.C. Beilke, J.W. Zewe, J.E. Clark, S. V Olesik, Aligned electrospun nanofibers for ultra-thin layer chromatography., Anal. Chim. Acta. 761 (2013) 201–208.

[52] P. Kampalanonwat, P. Supaphol, G.E. Morlock, Electrospun nanofiber layers with incorporated photoluminescence indicator for chromatography and detection of ultraviolet-active compounds, J. Chromatogr. A. 1299 (2013) 110–117.

[53] T. Lu, S. V Olesik, Electrospun polyvinyl alcohol ultra-thin layer chromatography of amino acids, J. Chromatogr. B. 912 (2013) 98–104.

[54] T. Rojanarata, S. Plianwong, K. Su-uta, P. Opanasopit, T. Ngawhirunpat, Electrospun cellulose acetate nanofibers as thin layer chromatographic media for eco-friendly screening of steroids adulterated in traditional medicine and nutraceutical products, Talanta. 115 (2013) 208–213.

[55] J. Song, D.S. Jensen, D.N. Hutchison, B. Turner, T. Wood, A.E. Dadson, et al., Carbon-Nanotube-Templated Microfabrication of Porous Silicon-Carbon Materials with Application to Chemical Separations, Adv. Funct. Mater. 21 (2011) 1132–1139.

[56] D.S. Jensen, S.S. Kanyal, V. Gupta, M.A. Vail, A.E. Dadson, M. Engelhard, et al., Stable, microfabricated thin layer chromatography plates without volume distortion on patterned, carbon and Al(2)O(3)-primed carbon nanotube forests., J. Chromatogr. A. 1257 (2012) 195–203.

[57] S.S. Kanyal, D.S. Jensen, A.J. Miles, A.E. Dadson, M.A. Vail, R. Olsen, et al., Effects of catalyst thickness on the fabrication and performance of carbon nanotube-templated thin layer chromatography plates, J. Vac. Sci. Technol. B. 31 (2013) 031203.

[58] D.S. Jensen, S.S. Kanyal, N. Madaan, A.J. Miles, R.C. Davis, R. Vanfleet, et al., Ozone priming of patterned carbon nanotube forests for subsequent atomic layer deposition-like deposition of SiO2 for the preparation of microfabricated thin layer chromatography plates, J. Vac. Sci. Technol. B. 31 (2013) 031803.

[59] M.R. Linford, Fabrication and Chromatographic Separations on Binder-Free, Carbon Nanotube-Fabricated TLC Plates, in: Int. Symp. Thin-Layer Chromatogr. (July 6-8), Basel, Switzerland, 2011.

[60] S. Kirchert, Z. Wang, M.T. Taschuk, S.R. Jim, M.J. Brett, G.E. Morlock, Inkjet application, chromatography, and mass spectrometry of sugars on nanostructured thin films, Anal. Bioanal. Chem. (2013).

[61] J. Wannenmacher, S.R. Jim, M.T. Taschuk, M.J. Brett, G.E. Morlock, Ultrathin-layer chromatography on SiO2, Al2O3, TiO2, and ZrO2 nanostructured thin films, J. Chromatogr. A. 1318 (2013) 234–243.

[62] S.R. Jim, A. Foroughi-Abari, K.M. Krause, P. Li, M.R. Kupsta, M.T. Taschuk, et al., Ultrathin-layer chromatography nanostructures modified by atomic layer deposition, J. Chromatogr. A. 1299 (2013) 118–125.

[63] S.R. Jim, M.T. Taschuk, G.E. Morlock, L.W. Bezuidenhout, W. Schwack, M.J. Brett, Engineered anisotropic microstructures for ultrathin-layer chromatography, Anal. Chem. 82 (2010) 5349–5356.

[64] L.W. Bezuidenhout, M.J. Brett, Ultrathin layer chromatography on nanostructured thin films, J. Chromatogr. A. 1183 (2008) 179–185.

[65] A.J. Oko, S.R. Jim, M.T. Taschuk, M.J. Brett, Analyte migration in anisotropic nanostructured ultrathin-layer chromatography media, J. Chromatogr. A. 1218 (2011) 2661–2667.

[66] Z. Zhang, S.N. Ratnayaka, M.J. Wirth, Protein UTLC-MALDI-MS using thin films of submicrometer silica particles, J. Chromatogr. A. 1218 (2011) 7196–202.

[67] P.K. Salo, H. Salomies, K. Harju, R.A. Ketola, T. Kotiaho, J. Yli-Kauhaluoma, et al., Analysis of small molecules by ultra thin-layer chromatography-atmospheric pressure matrix-assisted laser desorption/ionization mass spectrometry., J. Am. Soc. Mass Spectrom. 16 (2005) 906–915.

[68] P.K. Salo, S. Vilmunen, H. Salomies, R.A. Ketola, R. Kostiainen, Two-dimensional ultra-thin-layer chromatography and atmospheric pressure matrix-assisted laser desorption/ionization mass spectrometry in bioanalysis, Anal. Chem. 79 (2007) 2101–2108.

[69] T.J. Kauppila, N. Talaty, P.K. Salo, T. Kotiaho, R. Kostiainen, R.G. Cooks, New surfaces for desorption electrospray ionization mass spectrometry: porous silicon and ultra-thin layer chromatography plates, Rapid Commun. Mass Spectrom. 20 (2006) 2143–2150.

[70] I. Vovk, G. Popović, B. Simonovska, A. Albreht, D. Agbaba, Ultra-thin-layer chromatography mass spectrometry and thin-layer chromatography mass spectrometry of single peptides of angiotensin-converting enzyme inhibitors., J. Chromatogr. A. 1218 (2011) 3089–3094.

[71] K. Robbie, Sculptured thin films and glancing angle deposition: Growth mechanics and applications, J. Vac. Sci. Technol. A. 15 (1997) 1460.

[72] M.M. Hawkeye, M.J. Brett, Glancing angle deposition: Fabrication, properties, and applications of micro- and nanostructured thin films, J. Vac. Sci. Technol. A. 25 (2007) 1317–1335.

[73] M.J. Brett, M.M. Hawkeye, New materials at a glance, Science (80-.). 319 (2008) 1192–3.

[74] K. Robbie, L. Friedrich, S.K. Dew, T. Smy, M.J. Brett, Fabrication of thin films with highly porous microstructures, J. Vac. Sci. Technol. A. 13 (1995) 1032–1035.

[75] K. Robbie, M.J. Brett, A. Lakhtakia, First thin film realization of a helicoidal bianisotropic medium, J. Vac. Sci. Technol. A. 13 (1995) 2991–2993.

[76] K. Robbie, J.C. Sit, M.J. Brett, Advanced techniques for glancing angle deposition, J. Vac. Sci. Technol. B. 16 (1998) 1115–1122.

[77] K. Robbie, M.J. Brett, Method of depositing shadow sculpted thin films, U.S. Patent 5,866,204, 1999.

[78] A. Lakhtakia, R. Messier, Sculptured Thin Films: Nanoengineered Morphology and Optics, SPIE, 1000 20th Street, Bellingham, WA 98227-0010 USA, 2005.

[79] M.T. Taschuk, M.M. Hawkeye, M.J. Brett, Glancing Angle Deposition, in: P. Martin (Ed.), Handbook of Deposition Technologies for Films and Coatings: Science, Applications and Technology, 3rd ed., William Andrew (Elsevier), Oxford, United Kingdom, 2010: pp. 621–678.

[80] M.M. Hawkeye, M.T. Taschuk, M.J. Brett, Glancing Angle Deposition: Engineering the Nanoscale (in-press), Wiley, 2014.

[81] M. Ohring, Materials Science of Thin Films: Deposition and Structure, 2nd ed., Academic Press (Elsevier), San Diego, USA, 2002.

[82] B. Movchan, A. Demchishin, Structure and properties of thick vacuum-condensates of nickel, titanium, tungsten, aluminum oxide, and zirconium dioxide (in Russian), Fiz. Met. I Metalloved. 28 (1969) 653.

[83] J. Nieuwenhuizen, H. Haanstra, Microfractography of thin films, Philips Tech. Rev. 27 (1966) 87–91.

[84] R.N. Tait, T.J. Smy, M.J. Brett, Modelling and characterization of columnar growth in evaporated films, Thin Solid Films. 226 (1993) 196–201.

[85] N.G. Wakefield, J.C. Sit, On the uniformity of films fabricated by glancing angle deposition, J. Appl. Phys. 109 (2011) 084332.

[86] P.C.P. Hrudey, A.C. van Popta, J.C. Sit, M.J. Brett, Photonic device applications of nano-engineered thin film materials, Proc. SPIE. 5931 (2005) 593113–593113–13.

[87] M.A. Summers, B. Djurfors, M.J. Brett, Fabrication of silicon submicrometer ribbons by glancing angle deposition, J. Microlithogr. Microfabr. Microsystems. 4 (2005) 033012.

[88] A.C. van Popta, J.C. Sit, M.J. Brett, Optical properties of porous helical thin films and the effects of post-deposition annealing, Proc. SPIE. 5464 (2004) 198–208.

[89] W.M.J. Green, K. Westra, K. Robbie, M.J. Brett, Nano-Pasta--Thin Film Realization of Ultra-Fast Cooking Pasta Using Glancing Angle Deposition, Ann. Improbable Res. 6 (2000) 25–29.

[90] G.K. Kiema, M.O. Jensen, M.J. Brett, Glancing Angle Deposition Thin Film Microstructures for Microfluidic Applications, Chem. Mater. 17 (2005) 4046–4048.

[91] D. Gish, M.A. Summers, M.J. Brett, Morphology of periodic nanostructures for photonic crystals grown by glancing angle deposition, Photonics Nanostructures - Fundam. Appl. 4 (2006) 23–29.

[92] M. Seto, K. Westra, M.J. Brett, Arrays of self-sealed microchambers and channels, J. Mater. Chem. 12 (2002) 2348–2351.

[93] K.M. Krause, M.J. Brett, Spatially Graded Nanostructured Chiral Films as Tunable Circular Polarizers, Adv. Funct. Mater. 18 (2008) 3111–3118.

[94] M.O. Jensen, M.J. Brett, Porosity engineering in glancing angle deposition thin films, Appl. Phys. A. 80 (2005) 763–768.

[95] A.L. Beaudry, R.T. Tucker, J.M. Laforge, M.T. Taschuk, M.J. Brett, Indium tin oxide nanowhisker morphology control by vapour-liquid-solid glancing angle deposition., Nanotechnology. 23 (2012) 105608.

[96] J.B. Sorge, M.J. Brett, Film morphology modification in ion-assisted glancing angle deposition, Thin Solid Films. 519 (2010) 1356–1360.

[97] J.B. Sorge, M.T. Taschuk, N.G. Wakefield, J.C. Sit, M.J. Brett, Metal oxide morphology in argon-assisted glancing angle deposition, J. Vac. Sci. Technol. A. 30 (2012) 021507.

[98] Z. Huang, K.D. Harris, M.J. Brett, Morphology Control of Nanotube Arrays, Adv. Mater. 21 (2009) 2983–2987.

[99] J.K. Kwan, J.C. Sit, The use of ion-milling to control clustering of nanostructured, columnar thin films., Nanotechnology. 21 (2010) 295301.

[100] M.R. Kupsta, M.T. Taschuk, M.J. Brett, J.C. Sit, Reactive Ion Etching of Columnar Nanostructured TiO2 Thin Films for Modified Relative Humidity Sensor Response Time, IEEE Sens. J. 9 (2009) 1979–1986.

[101] S. Tsoi, E. Fok, J.C. Sit, J.G.C. Veinot, Surface Functionalization of Porous Nanostructured Metal Oxide Thin Films Fabricated by Glancing Angle Deposition, Chem. Mater. 18 (2006) 5260–5266.

[102] J.Z. Hall, M.T. Taschuk, M.J. Brett, Polarity-adjustable reversed phase ultrathin-layer chromatography., J. Chromatogr. A. 1266 (2012) 168–174.

[103] O. Albrecht, R. Zierold, C. Patzig, J. Bachmann, C. Sturm, B. Rheinländer, et al., Tubular magnetic nanostructures based on glancing angle deposited templates and atomic layer deposition, Phys. Status Solidi B. 247 (2010) 1365–1371.

[104] M.T. Taschuk, K.D. Harris, D.P. Smetaniuk, M.J. Brett, Decoupling sensor morphology and material: Atomic layer deposition onto nanocolumn scaffolds, Sensors Actuators B Chem. 162 (2012) 1–6.

[105] K.M. Krause, M.T. Taschuk, K.D. Harris, D.A. Rider, N.G. Wakefield, J.C. Sit, et al., Surface area characterization of obliquely deposited metal oxide nanostructured thin films., Langmuir. 26 (2010) 4368–4376.

[106] J.J. Steele, M.T. Taschuk, M.J. Brett, Nanostructured Metal Oxide Thin Films for Humidity Sensors, IEEE Sens. J. 8 (2008) 1422–1429.

[107] J.G. Van Dijken, M.D. Fleischauer, M.J. Brett, Controlled nanostructuring of CuPc thin films via glancing angle deposition for idealized organic photovoltaic architectures, J. Mater. Chem. 21 (2011) 1013–1019.

[108] M. Thomas, W. Li, Z.S. Bo, M.J. Brett, Inverted photovoltaic cells of nanocolumnar C60 filled with solution processed small molecule 3-Q, Org. Electron. 13 (2012) 2647–2652.

[109] K.D. Harris, M.J. Brett, T.J. Smy, C. Backhouse, Microchannel Surface Area Enhancement Using Porous Thin Films, J. Electrochem. Soc. 147 (2000) 2002.

[110] L.W. Bezuidenhout, E. Flaim, A.L. Elias, M.J. Brett, PDMS microchannels with embedded silicon dioxide nanostructures, in: Proc. microTAS 2009 13th Int. Conf. Miniaturized Syst. Chem. Life Sci., Jeju, Korea, 2009.

[111] A.B. Jemere, L.W. Bezuidenhout, M.J. Brett, D.J. Harrison, Matrix-free laser desorption/ionization mass spectrometry using silicon glancing angle deposition (GLAD) films., Rapid Commun. Mass Spectrom. 24 (2010) 2305–11.

[112] J. Chen, P. Abgrall, Y.-W. Huang, Y.-P. Zhao, On-chip ultra-thin layer chromatography and surface enhanced Raman spectroscopy., Lab Chip. 12 (2012) 3096–3102.

[113] S. Brunauer, P. Emmett, E. Teller, Adsorption of gases in multimolecular layers, J. Am. Chem. Soc. 60 (1938) 309–319.

3 GLAD UTLC methods

Investigation of nanostructured planar chromatography media involves several steps. This chapter presents experimental techniques customized for GLAD UTLC. Specific methods of preparing and modifying GLAD media are detailed. Considerations and approaches to utilizing these media in UTLC dye separations are also outlined. The chapter concludes with a summary of methods for digitizing resultant separation patterns and producing chromatograms. Some of the described techniques were performed in collaboration with Anthony Oko, Jane Hall, Ali Foroughi-Abari, and Mike Taschuk from the GLAD Laboratory (University of Alberta, Edmonton, Canada). Ali Foroughi-Abari performed atomic layer deposition (ALD) processing using one of the reactors in Professor Ken Cadien's laboratory (Cadien Nanofabrication Group, University of Alberta, Edmonton, Canada). Other work involved Julia Wannenmacher, Simone Kirchert, and Gerda Morlock (Universität Hohenheim, Stuttgart, Germany and Justus Liebig University of Gießen, Gießen, Germany).

3.1 GLAD thin film fabrication

3.1.1 Substrate preparation

GLAD thin films were generally deposited onto optically smooth glass substrates (25.4 mm squares, 25 mm x 50 mm pieces, or 25.4 mm x 50.8 mm pieces; 1.00 mm thick; Schott B270, S. I. Howard Glass, Worchester, Massachusetts, USA). These substrates were labelled on their underside with a diamond scribe. A substrate number was written in the corner (using mirror writing) so that it could be read from the top side; arrows were used to indicate approximate channel orientations on anisotropic UTLC media. This practice enabled accurate substrate tracking.

Substrates were cleaned with an aqueous detergent solution (Citranox, Alconox, White Plains, New York, USA) to ensure that fingerprints, machining oils, and other contaminants were removed prior to film deposition. Manual scrubbing with the detergent using gloved finger tips took considerable time but was generally more reliable than other tested cleaning protocols including acetone-IPA (isopropyl alcohol) rinses and hot "piranha" (concentrated H_2SO_4 and H_2O_2 solution). The substrates were considered sufficiently clean when their surfaces could be uniformly wet with deionized water. The substrates were rinsed thoroughly and soaked in deionized water. They were dried serially using a N_2 gun immediately upon removal from the water. Silicon <100> wafer "witness" substrates were similarly cleaned and dried. Silicon test wafers (p-type) were sufficient because electrical testing was not required.

The cleaned substrates were mounted to a flat metal deposition chuck with a layout carefully marked onto the chuck using permanent marker. These pieces were attached using double-sided polyimide (Kapton™) tape with silicone adhesive (CAPLINQ, Ottawa, Ontario, Canada). This type of adhesive tape was used in the high-vacuum processing steps (GLAD film fabrication and reactive ion etch processing) because the adhesive does not outgas. (The adhesive in Scotch tape, for instance, will outgas from the tape and contaminate vacuum

systems.) Double-sided tape was critical to production of large batches (up to ~ 28 squares or ~ 14 rectangular pieces) of GLAD UTLC plates required in these experiments (**Figure 3-1**). It allowed the glass substrates to be mounted directly next to each other to maximize the number of plates in a given deposition set. As the tape only contacted the underside of the GLAD UTLC plates, it did not mask off portions of the edges and introduce mobile phase flow non-uniformities. Since the substrates were in direct contact with each other, it was important that they all be pressed very flat against the chuck to minimize deposition shadows cast across each substrate by adjacent substrates. Note that the 0.5 mm thick silicon substrates could not be placed in direct contact with 1.00 mm thick glass substrates for this reason. The silicon substrates were typically backed by another piece of silicon (to ~ 1.00 mm total thickness) and mounted in the centre of the chuck > 5 mm away from other glass substrates.

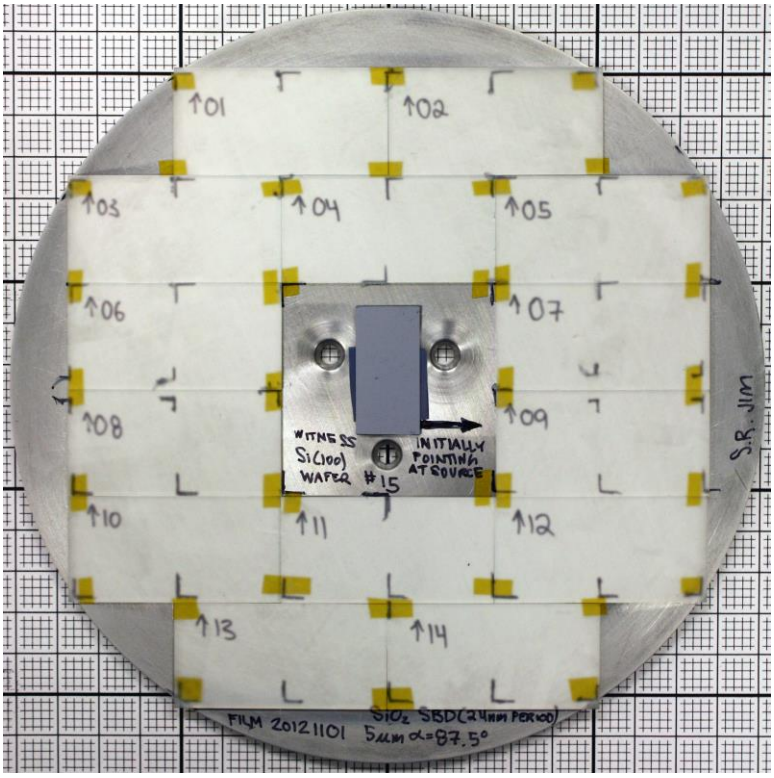

Figure 3-1 GLAD UTLC films deposited onto substrates mounted to a metal deposition chuck. 1 in. x 2 in. glass pieces are mounted in direct contact using double-sided polyimide tape. A witness Si(100) wafer piece is mounted in the centre of the chuck.

3.1.2 Electron beam evaporation

GLAD film fabrication was performed within a custom ultra high vacuum electron beam evaporation chamber (AXXIS, Kurt J. Lesker Co., Clairton, Pennsylvania, USA) [1,2] (**Figure 3-2**). This chamber was lined with ultra high vacuum aluminum foil (All-Foils, Strongsville, Ohio, USA) that was removed between deposition runs to reduce contamination. Evaporant materials such as SiO_2 (99.99% pure SiO_2, Materion, Milwaukee, Wisconsin, USA), TiO_2 (99.9 %, rutile form, Materion), or Al_2O_3 (99.99% pure Al_2O_3, Materion) source pellets were loaded into carbon or copper crucible liners (Kurt J. Lesker Co.) placed into the electron beam hearth. Disposable quartz crystal thickness monitors (Infinicon, East Syracuse, New York, USA) were loaded to enable real-time deposition rate monitoring.

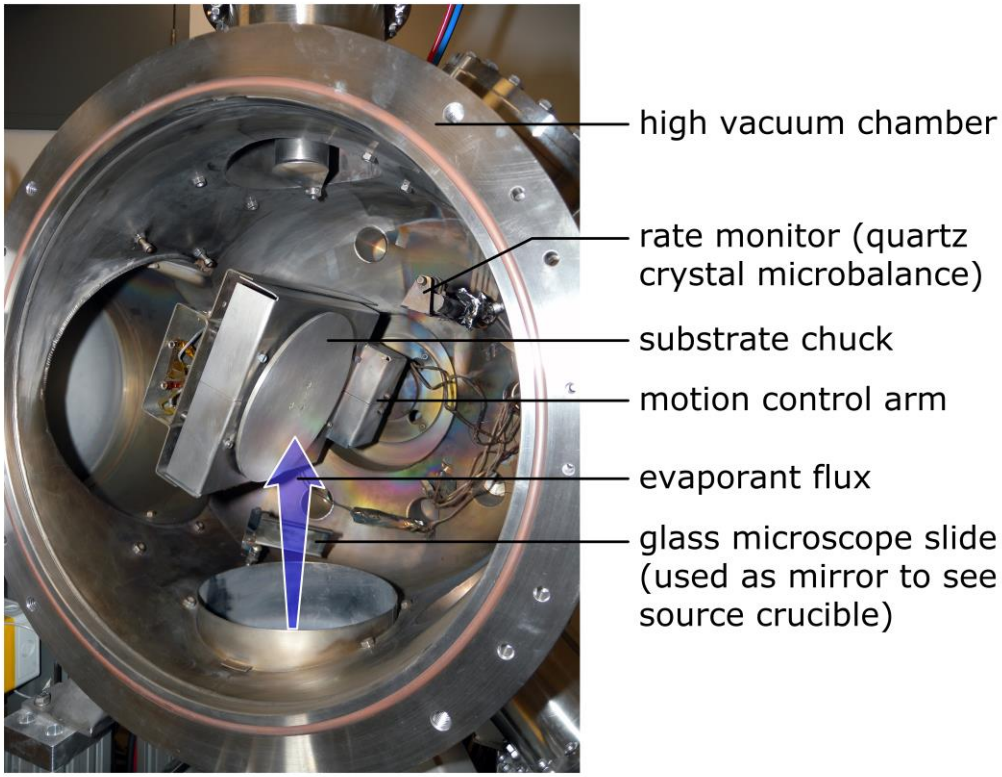

Figure 3-2 AXXIS system customized for GLAD thin film deposition.

The motion control assembly used to manipulate the deposition chuck was calibrated prior to evaporation. A simple gravimetric method was used since the deposition system was assumed levelled such that the evaporant crucible was located directly beneath the centre of the deposition chuck. This allowed the discrepancy in the deposition angle to be measured using a digital level placed against a flat chuck mounted to the control assembly and set to a nominal $\alpha = 90°$. Small adjustments to the α-offset value were used to correct α when the discrepancy was greater than ~ 0.2°.

The deposition chuck with attached substrates was loaded into the prepared deposition chamber and evacuated for > 1 hour (often overnight) using a cryogenic high vacuum pump (CTI Cryogenics, Helix Technology Corporation, Mansfield, Massachusetts, USA). Typical chamber base pressures were < $1x10^{-6}$ Torr. A low chamber base pressure was required to minimize evaporant scattering during deposition as a highly-directional evaporant flux is required for GLAD. Lower base pressures may be required for other (non-oxide) GLAD films since residual chamber gases (namely H_2O, N_2, and O_2) can introduce contaminants into GLAD films.

An incident high-energy (5-6 keV) electron beam was used to heat the crucible of deposition material until evaporation. SiO_2 and ZrO_2 sublimated during deposition, Al_2O_3 melted locally before evaporation, and TiO_2 melted into a pool before evaporation. (See **Table 3-1** for typical SiO_2 deposition parameters.) These four materials were studied in collaboration with J. Wannenmacher [3] and A. Foroughi-Abari [4].

J. Wannenmacher performed food dye separations on SiO_2, TiO_2, and ZrO_2 GLAD UTLC films that she had deposited and post-processed. S.R. Jim analyzed her separation videos using time-resolved UTLC. These experiments indicated that heat treatments (**3.2.1 Heat treatments**) and UV irradiation change analyte retention significantly [3]. A subset of the collected data is presented in **6.4 Application of TR-UTLC to alternative GLAD UTLC metal oxides**.

A. Foroughi-Abari performed lipophilic dye separations on GLAD SiO_2, GLAD Al_2O_3, and films ALD coated with Al_2O_3, ZrO_2, and ZnO. He deposited these films, coated them (**3.2.3 Atomic layer deposition (ALD)**), and performed the developments. S.R. Jim studied dye separation data A. Foroughi-Abari had collected to characterize changes in separation performance upon coating [4] (**7 Surfaces modified by atomic layer deposition**).

Table 3-1 Typical SiO_2 GLAD UTLC plate deposition parameters.

Deposition Angle (α)	84.0 - 88.5°
Electron Beam Current	50 - 240 mA
Accelerating Voltage	5.35 - 6.50 kV
Base Pressure	$< 10^{-6}$ Torr
Deposition Pressure	1 - 6 x 10^{-6} Torr
Deposition Rate	1.0 - 1.4 nm s^{-1}

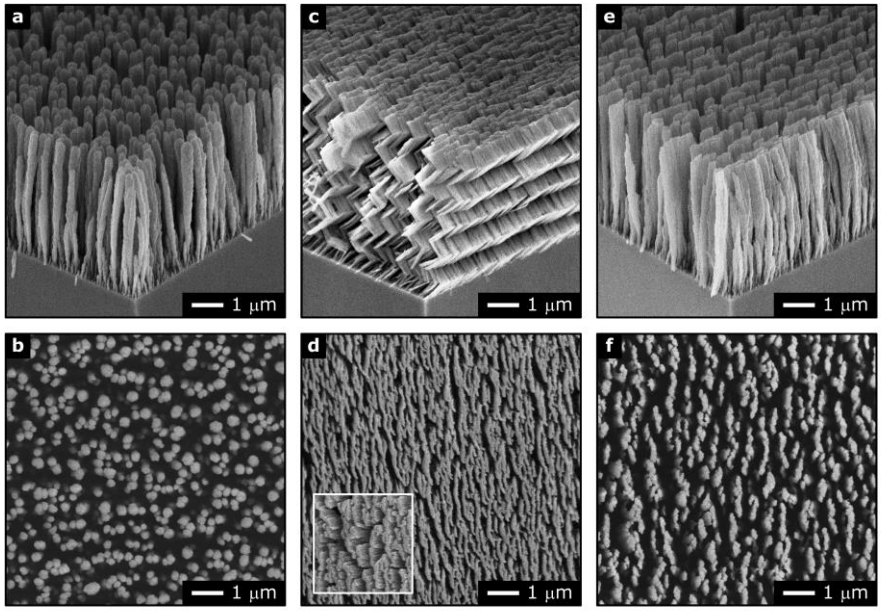

Figure 3-3 SEM micrographs of macroporous SiO_2 GLAD thin film separation media. Micrographs of (a, b) isotropic vertical posts as well as anisotropic (c, d) chevron and (e, f) serial bideposition (SBD) media when viewed from an oblique angle and from above, respectively. Pores within the top layer of the chevron film are apparent only when the film is viewed along the angled segments in this layer (~ 53° to the substrate normal) (d). The inset in (d) shows the film when viewed normal to the substrate. Reproduced with permission from [5]. Copyright (2010) American Chemical Society.

3.1.3 Studied GLAD UTLC morphologies

Vertical post SiO_2 (**Figure 3-3a, b**) were designed to be isotropic in the plane of the substrate. Continuous rapid substrate ϕ-rotation (20 nm of film growth per rotation) caused the oblique evaporant flux to effectively arrive from all azimuthal directions rather than from a localized source. This morphology can be considered the limiting case of a helical film in which the helix pitch is small enough to be comparable to the column diameter [6]. The vertical post films in these studies had 4.5 – 5 μm nominal thickness and columnar structures normal to the substrate surface. The SiO_2 and Al_2O_3 films deposited by A. Foroughi-Abari had ~ 5 μm nominal thickness and 20 nm of nominal film growth per rotation.

Anisotropic chevron ("zig-zag") SiO_2 films (**Figure 3-3c, d**) were composed of layers of slanted columnar segments. The columns in each layer were produced with constant ϕ (no substrate rotation) and inclined towards the apparent source position. Rapid $\Delta\phi = 180°$ rotations (over ~ 10 nm of film growth) were conducted periodically during fabrication. After depositing a ~ 500 nm thick layer of columns inclined in the $\phi = 0°$ direction (a "zig" segment), a second ~ 500 nm thick layer of columns inclined in the $\phi = 180°$ direction (a "zag" segment) was deposited to complete one period of the chevron. Subsequent repetitions of this sequence produced chevron films with ~ 5 μm nominal thickness and a ~ 1 μm nominal period.

In the limit of a small period, chevron films degenerate into serial bideposition (SBD) films (**Figure 3-3e, f**). Although deposited with a similar sequence of step-wise $\Delta\phi = 180°$ rotations (over ~ 2 nm of film growth), the short "zig" and "zag" layers in the SBD film (each ~ 12 nm thick) merged to form dense vertical blade-like structures. These SiO_2 films had ~ 4.5 – 5 μm nominal thickness and a 24 nm nominal period. The SiO_2, TiO_2, and ZrO_2 SBD films deposited by J. Wannenmacher had ~ 2.6 μm nominal thickness and a 24 nm nominal period.

3.2 Post-deposition processing

3.2.1 Heat treatments

Although as-deposited GLAD SiO_2 films are approximately stoichiometric, as-deposited TiO_x ($x < 2$), ZrO_x ($x < 2$), and AlO_x ($x < 3/2$) films were generally oxygen-deficient. Heating these media for 24 hours at 200 °C in an annealing furnace (ThermoLyne 48000 Furnace, Barnstead Thermolyne, Dubuque, Iowa, USA) improved the stoichiometry of the column surfaces [7]. As-deposited oxygen-deficient TiO_x, ZrO_x, and AlO_x films appeared black, pink, and yellow in colour, respectively. All were lighter in colour (almost white) after this heat treatment. Heat treatments were also used to desorb the fluorocarbon polymer remaining after reactive ion etch processing (**5.2 Post-etching annealing treatments**) [8].

3.2.2 Reactive ion etching (RIE)

Fluorocarbon RIE was used to selectively modify the morphology of GLAD films. This processing was performed in a dedicated RIE system (Phantom III, Trion Technology, Clearwater, Florida, USA) equipped with O_2, CHF_3, CF_4, and SF_6 feed gases. An oxygen plasma cleaning step (10 min) was used to remove residual contaminants from the chamber before the GLAD thin films were loaded. Standard oxygen plasma cleaning and SiO_2 etching recipes are provided in **Table 3-2**. Further details are provided in **5.1 Method of reactive ion etching GLAD UTLC**. This processing was performed in the University of Alberta NanoFab.

3.2.3 Atomic layer deposition (ALD)[1]

A. Foroughi-Abari performed ALD coating in K.C. Cadien's research laboratory (Department of Chemical and Materials Engineering, University of Alberta). The thin film deposition research system (ALD-150L, Kurt J. Lesker) integrates an

[1] Portions of this section were reproduced with permission from S.R. Jim, A. Foroughi-Abari, K.M. Krause, P. Li, M.R. Kupsta, M.T. Taschuk, K.C. Caiden, M.J. Brett, Ultrathin-layer chromatography nanostructures modified by atomic layer deposition, Journal of Chromatography A. 1299 (2013) 118–125. Copyright (2013) Elsevier.

Table 3-2 RIE system recipes used during the "Clean" and "Etch" processes. This recipe was used by the Trion Phantom III system in the University of Alberta NanoFab.[2]

	"Clean"	"Etch"
Operating Pressure (10^{-3} Torr)	250	40
Radio Frequency (RF) Forward Power (W)	50	125
O_2 flow rate (sccm)	50	5
CHF_3 flow rate (sccm)	-	40

ALD reactor with an *in-situ* spectroscopic ellipsometry characterization unit (J. A. Woollam M-2000DI, Lincoln, Nebraska, USA) [9]. The reactor has both thermal and remote plasma capabilities but only plasma-enhanced ALD was used. The ellipsometer has a wide spectral range (197-1700 nm) and fast acquisition speed (20 spectra per second). This optical method was used for real-time coating thickness monitoring. A vacuum transfer load-lock connects the sample preparation chamber to the ALD reactor.

Trimethylaluminium (TMA) precursor was used with oxygen plasma to deposit Al_2O_3. High purity argon (99.999%) purged excess precursors and reaction by-products between cycles. Each ALD cycle (~ 0.15 nm deposited Al_2O_3 thickness) consisted of a short 20 ms pulse of precursor gas, 5 s purge, 1-2 s oxygen plasma exposure, and 2 s purge. Substrates were heated to 100 ^oC during deposition. The ALD system was also equipped with precursors for similar deposition of other metal oxides including ZrO_2 (tetrakis(dimethylamido)zirconium, TDMAZ), and ZnO (diethylzinc, DEZ). Deposition grade precursors were obtained from Sigma-Aldrich (Oakville, Ontario, Canada). Complete ALD metal oxide process parameters are provided in **Table 3-3**.

[2] O_2 and CHF_3 flow rates are provided in standard cubic centimetres per minute (sccm).

Table 3-3 Plasma ALD processing parameters for alumina, zirconia, and zinc oxide.

	Al_2O_3	ZrO_2	ZnO
Precursor Gas Pulse (ms)	20	40	30
Argon Purge 1 (s)	5	5	5
Oxygen Plasma Exposure (s)	2	2	2
Argon Purge 2 (s)	2	2	2
Operating Pressure[3] (Torr)	~1	~1	~1
Substrate Temperature (°C)	100	250	200
Oxygen Plasma Power[4] (W)	600	600	600
Growth per Cycle (nm cycle^{-1})	~ 0.15	~0.21	~0.15
Number of Cycles for 5 nm Coating	33	24	33

Table 3-4 Representative spot application parameters. Parts a-f correspond to the applied spot images in **Figure 3-4**.

Part	Applied Sample	Instrument and Method	GLAD Film
a	Unknown volume; CAMAG dye; 50 % dilution in toluene	Contact; I&J Fisnar robot; small 32 Ga blunt needle	SiO_2; vertical post; isotropic
b	50 nL spot^{-1}; CAMAG dye; 20 % dilution in toluene	Contact; Hamilton syringe manipulated manually	SiO_2; SBD; anisotropic
c	50 nL spot^{-1}; CAMAG dye; 20 % dilution in *n*-hexane	Contact; Hamilton syringe manipulated manually	SiO_2; SBD; anisotropic
d	10 nL spot^{-1}; CAMAG dye; alternating undiluted and 50 % dilution in toluene	Contact; CAMAG ATS 4; slow 1 nL s^{-1} dispensing rate	TiO_2; SBD; anisotropic
e	10 nL spot^{-1}; CAMAG dye; alternating undiluted and 50 % dilution in toluene	Aerosol; CAMAG ATS 4; rapid 80 nL s^{-1} dispensing rate and low 25 kPa N_2 pressure	TiO_2; SBD; anisotropic
f	9 nL band^{-1}; synthetic food dyes; dissolved in water	Inkjet print; Canon Pixma MG 5320; 2 mm x 0.2 mm bands	SiO_2; SBD; anisotropic

[3] The carrier gas was argon.
[4] Radio frequency inductively-coupled remote plasma source.

3.3 Sample spot application

The manner in which sample spots are applied to planar chromatographic media has a significant effect on overall separation performance. Large and poorly-applied spots are undesirable because they limit the resolution between separated spots [5,10]. These issues motivated efforts to create GLAD UTLC layers with concentration zones (see **5.4 GLAD UTLC-CZ demonstration**). A variety of

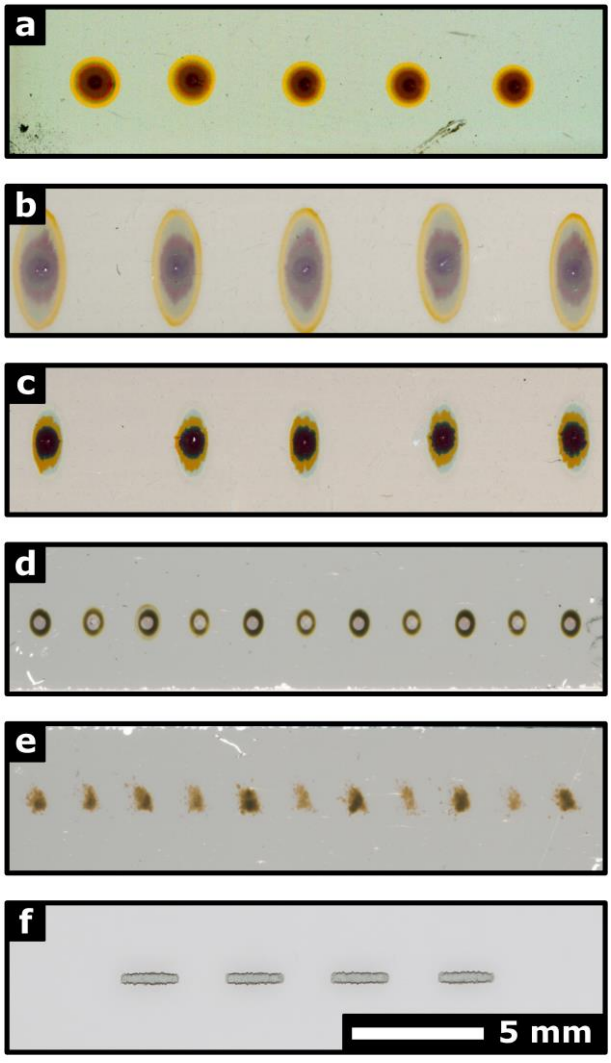

Figure 3-4 Application of dye spots to GLAD UTLC layers in (a-d) contact, (e) aerosol, and (f) inkjet application modes by S.R. Jim. Anisotropic media (b-f) had channel features aligned vertically on page. Specific details provided in **Table 3-4**. All images were enhanced for presentation and dimensions were scaled similarly.

sample spot application techniques were employed in these investigations. The type of sample solvent also affects final spot size [10]. For example, dissolving samples in low elution strength *n*-hexane produced smaller spots than dissolving in high elution strength toluene. Method selection was generally based on the desired spot volumes, available instrumentation, and the competing factors of simplicity and precision (**Table 3-4** and **Figure 3-4**). Spots were typically applied ~ 2.5 - 3.5 mm from the bottom edge of the GLAD UTLC plates [4,5,8].

3.3.1 Hand application

Without question, the simplest method of applying sample spots for planar chromatography research purposes is by hand in contact-mode. Glass capillary tubes of known volume (~ 1 μL or 5 μL, Drummond Microcaps) may be used to draw sample mixture and transfer it onto planar chromatography plates. Holding the loaded capillary tube against the plate allows the sample to wick into the chromatographic layer. The absolute positioning is dependent upon the user and the dispensing rate cannot be controlled. This results in big sample spots of large volume sometimes acceptable in "quick and dirty" TLC but usually unacceptable in HPTLC and UTLC.

3.3.2 Robot application

(**Figure 3-4a**.) A robotic arm (I&J 2200, I&J Fisnar, Wayne, New Jersey, USA) equipped with stainless steel blunt-ended needles offers some improvement over hand application. Needle manipulation is precisely controlled by *x*-, *y*-, and *z*-position stepper motors. Sample mixtures loaded into the blunt needle tip similarly wick into the chromatographic layer when brought into direct contact. The applied volume is controlled by modifying the gauge of the needle (30 gauge for large spots or 32 gauge for small spots, I&J Fisnar) and the duration for which the needle contacts the layer (typically 1 s). Although sample spots may be applied quickly and with reasonable position precision, this method could not be used for quantitative analysis. Spot volumes are assumed to be < 100 nL, but could not be measured absolutely.

3.3.3 Calibrated syringe

(**Figure 3-4b, c**.) Precise spot volumes were achieved using a calibrated syringe (model 7000.5, Hamilton Company, Reno, Nevada, USA). This syringe could produce repeatable 10 nL – 500 nL spot volumes (graduated markings every 5 nL). The tungsten wire plunger of this syringe extends to the tip of the stainless steel needle to ensure as close to zero dead volume as possible. A Chaney adapter (Hamilton) mounted to the top of the syringe ensures that the same sample liquid volume is drawn and dispensed for each spot. Manipulation of this somewhat fragile syringe was performed using a customized spotting system (**Figure 3-5**) built from optical clamps (Thorlabs, Newton, New Jersey, USA). Micrometers enabled precise syringe positioning. Each spot was carefully applied by manually depressing the syringe plunger with the needle tip in contact with the plate. This serial technique produced reasonably precise spots but was often time consuming.

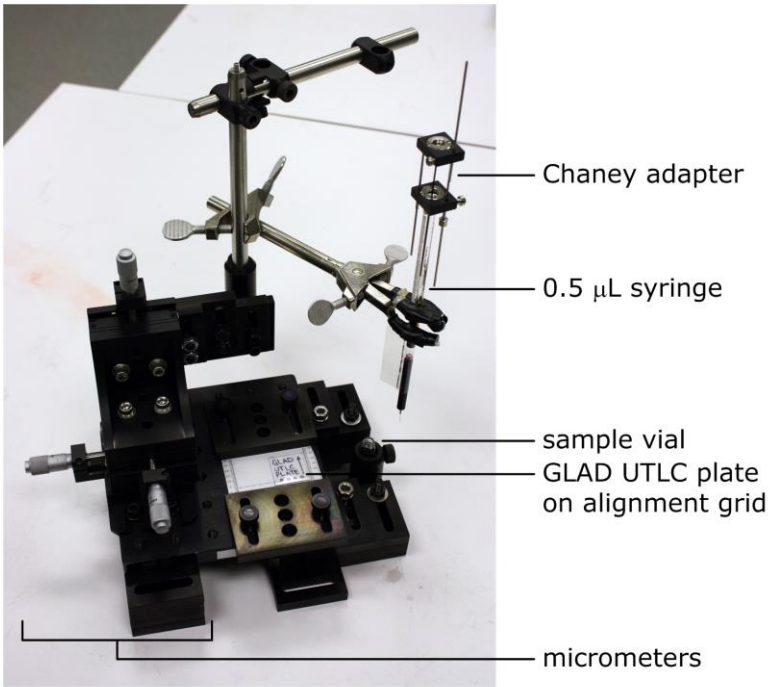

Figure 3-5 Custom apparatus for contact-mode sample spot application onto GLAD UTLC media. Precise *x*-, *y*-, *z*- placement of the 0.5 μL syringe is possible using micrometer screw drives. The Chaney reproducibility adapter ensures repeatable 50 nL spot volumes. Reproduced with permission from [4]. Copyright (2013) Elsevier.

3.3.4 ATS 4 HPTLC spotting system[5]

(**Figure 3-4d, e**.) S.R. Jim was fortunate to have visited G.E. Morlock's HPTLC laboratory (Institut für Lebensmittelchemie, Universität Hohenheim) to perform some of his dissertation research. Her laboratory was equipped with the current state-of-the-art spotting instrument: an Automatic TLC Sampler (ATS 4, controlled by the WinCats 1.4.2 Planar Chromatography Manager, CAMAG) designed specifically for applying spots to HPTLC plates. G.E. Morlock and S.R. Jim together used this computer-controlled system to manipulate a fine Hamilton syringe using a robotic arm. The ATS 4 is programmed to draw samples from autosampler vials held in a tray with addressable locations. The loaded syringe is manipulated above a motorized stage that holds HPTLC plates. Sample spots and bands are typically applied in spray-on mode. In this mode, N_2 gas propels sample liquids dispensed by the syringe located above the plate. The system can also be programmed to touch the syringe needle to the plate and produce contact mode spots. ATS 4 spot volumes and dispensing rates can be adjusted in the winCATS software. The syringe is automatically rinsed with solvent before and after use to reduce contamination. A wide sample volume range is possible by adjusting system firmware and using Hamilton syringes of different total volume.

Although the ATS 4 is a very powerful instrument useful in TLC and HPTLC, several modifications were required before it could be used for GLAD UTLC. Since a standard ATS 4 instrument cannot handle sample volumes less than 100 nL, modifications were necessary to achieve the small volumes desired for the GLAD UTLC plates. The 100 μL syringe in the ATS 4 was replaced with a 25 μL syringe but the system firmware remained set for a 100 μL syringe. The narrower inner diameter of the smaller syringe reduced the instrumental volume limit by a factor of four and permitted the 25 nL sample spots used in these experiments [5]. Under normal operating conditions, ATS 4 spot volume

[5] Portions of this section were reproduced with permission from S.R. Jim, M.T. Taschuk, G.E. Morlock, L.W. Bezuidenhout, W. Schwack, M.J. Brett, Engineered anisotropic microstructures for ultrathin-layer chromatography, Analytical Chemistry. 82 (2010) 5349–5356. Copyright (2010) American Chemical Society. CAMAG (Muttenz, Switzerland) graciously supplied the ATS 4.

precision inclusive of chromatography and evaluation is better than 1.8% RSD. However, the 25 nL spot precision was likely worse due to these instrument modifications. Sample spots were sprayed at twice the typical dosage speed (300 nL s^{-1} [5]) in order to prevent drying of the tiny sample volumes at the end of the stainless steel needle. Spotwise application was started and ended with one spot placed outside the plate to ensure homogeneously applied spots on the plate. The standard N_2 gas pressure used in spray-on mode was found to damage the fragile GLAD UTLC plates, however reducing this pressure worsened the spot size and shape. Contact mode application was sometimes preferred for this reason.

3.3.5 Inkjet printing

(**Figure 3-4f**.) The Office Chromatography concept involves the use of consumer inkjet printers in the application of bands to UTLC plates [11]. Continuous improvements in photo printer resolution have produced impressive ink spot precision. The inkjet printer used in this work (Pixma MG 5350, Canon, Montréal, Canada) claims to have 1200 dpi (dots per inch) resolution and 1-5 pL dots. Empty inkjet cartridges (InkXPro.com, Flushing, New York, USA) were purchased and cut open to remove sponges used to modulate ink flow to the print heads. These cartridges were installed into the printer then filled with a small volume of sample solution. The plastic parts of the printer restricted its use to aqueous solutions; organic solvents would have corroded the printer. J. Wannenmacher and S. Kirchert used published methods to calibrate the printer [11,12]. By printing a sugar solution of known concentration over a large area of paper and measuring the applied mass, they determined the volume per unit area for this printer to be 23 ± 2 nL mm^{-2} [12].

Bands were printed onto GLAD UTLC plates that were mounted into the cassette used to hold printable compact disks (of similar ~ 1 mm thickness). Modifications to the printer's rollers prevented direct contact between the printer and UTLC plates. J. Wannenmacher and S. Kirchert found that although sharp bands could be produced, clogged print heads sometimes made printing these

bands inconsistent. Later work by S.R. Jim found that sharper bands could be achieved by printing large bands beside the plate at the same time as on the plate. (Printing into the large bands seemed to prime the print heads and make printing onto the UTLC plate more consistent.) Overall, the Office Chromatography inkjet approach was effective in printing onto GLAD UTLC plates [11,12] however clogged print heads and sample solvent limitations remain challenges.

3.4 Separation methodologies[6]

3.4.1 Model dye system

UTLC experiments used separations of lipophilic Test Dye Mixture III (CAMAG, Muttenz, Switzerland). The undiluted mixture contained 3 mg of Dimethyl Yellow, 0.5 mg of Oracet Red G, 2 mg of Sudan Blue II, 1.5 mg of Ariabel Red, 2 mg of Oracet Violet 2R, and 4 mg of Indophenol per mL of toluene (listed according to typical descending hR_F values) [5]. The undiluted CAMAG dye mixture was diluted in toluene or *n*-hexane as required; *n*-hexane dilution produced smaller spots (see for example **Figure 3-4b** versus **Figure 3-4c**.). Dilution to 10-50 % relative concentrations were typical. In general, the Dimethyl Yellow (DY), Sudan Blue II (SB), and Ariabel Red (AR) dyes were best resolved. The other dyes tended to be too faint for reliable detection.

This test system was used throughout the GLAD UTLC investigations for a variety of reasons. It is a commercially available dye mixture with numerous coloured components that requires a relatively simple mobile phase. The dye mixture provides some insight into how normal-phase separations of other lipophilic analytes would occur. Furthermore, consistent use of this system allowed comparisons between UTLC experiments in the GLAD research group [4,5,8,13,14] and with other planar chromatography research [15,16].

[6] Portions of this section were reproduced with permission from A.J. Oko, S.R. Jim, M.T. Taschuk, M.J. Brett, Analyte migration in anisotropic nanostructured ultrathin-layer chromatography media, Journal of Chromatography A. 1218 (2011) 2661–2667. Copyright (2011) Elsevier.

3.4.2 Mobile phase optimization

G.E. Morlock optimized the mobile phase for normal-phase separations of CAMAG test dye mixture on GLAD UTLC layers [5]. Initial attempts at using the 100% toluene mobile phase typically used on HPTLC and UTLC layers resulted in analyte front migration. (The dyes migrated rapidly with the mobile phase front and did not separate.) The reduced dye component retention was attributed to the lower surface activity (specific surface area and thickness) of the GLAD UTLC layers [5]. Improved CAMAG dye separations were achieved by adding non-polar *n*-hexane to the moderately polar toluene. The reduced elution strength of the 4:3 toluene:*n*-hexane (v/v) binary mobile phase prevented front migration while enabling rapid separations. This relatively simple mobile phase was used throughout the GLAD UTLC investigations.

The low evaporation temperatures of the organic solvents, 111 °C (toluene) and 69 °C (*n*-hexane), introduce a couple of complications. (Boiling points reported for 101.325 kPa [17].) In the absence of a well-saturated solvent vapour, these solvents will rapidly evaporate from the ultrathin GLAD UTLC layers and reduce migration velocities and flow uniformity. Differences in evaporation rate can cause the mobile phase composition to change during an experiment or even during a single development when the vapour is unsaturated. In this case, the *n*-hexane evaporates faster and causes the mobile phase to increase in elution strength over time. A quasi-saturated mobile phase vapour ("vapour phase") produced beneath the GLAD UTLC plates in all CAMAG dye separation experiments (see **below**) counters these problems but introduces another. Vapour molecules adsorbed to the UTLC layer surface prior to development may be pushed together and forced to condense ahead of the mobile phase front. This produces an "observed" front in advance of the "real" mobile phase front. Mistaking the observed for the real mobile phase front position can affect hR_F measurements.

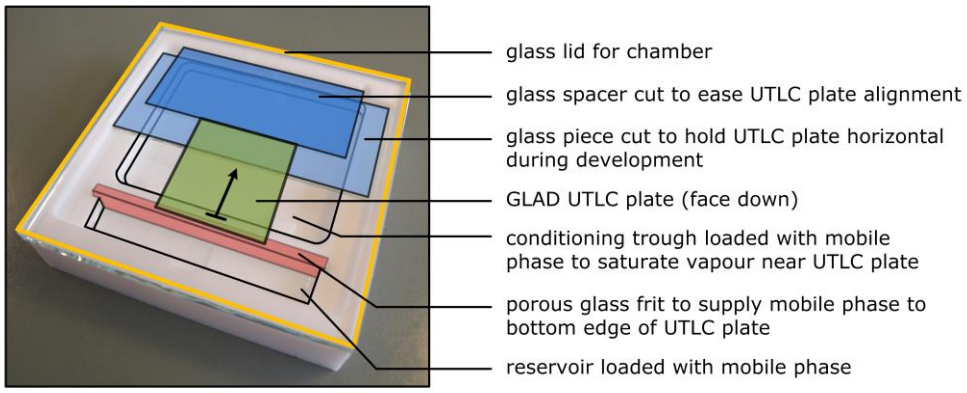

Figure 3-6 Horizontal Desaga separation chamber configured for miniaturized GLAD UTLC plate formats. Reproduced with permission from [5]. Copyright (2010) American Chemical Society.

In spite of these issues, the 4:3 toluene:*n*-hexane (v/v) binary mixture used in the CAMAG dye separations is an easier mobile phase to use than many others. Other samples may require complex mobile phases containing precise mixtures of multiple solvents and additives. Snyder's selectivity triangle [18] and Nyiredy's PRISMA model [19,20] are common tools in mobile phase optimization for more difficult samples. Detailed descriptions of these and other mobile phase considerations are thoroughly discussed in literature [10,21–23].

3.4.3 Ultrathin-layer chromatography development[7]

Spotted plates were generally developed face-down in a modified horizontal separation chamber (Desaga H-Chamber, 50 mm x 50 mm, Sarstedt, Nümbrecht, Germany; **Figure 3-6**). Although this chamber is one of the smallest commercially available chambers, two glass spacers were required to position the ~ 25 mm long GLAD UTLC plates. Porous glass frits supplied the mobile phase loaded into the reservoir (~1 mL) to the stationary phase layer. Glass capillary tubes were placed beneath frits to position them ~ 1 mm higher and into direct

[7] Portions of this section were reproduced with permission from S.R. Jim, M.T. Taschuk, G.E. Morlock, L.W. Bezuidenhout, W. Schwack, M.J. Brett, Engineered anisotropic microstructures for ultrathin-layer chromatography, Analytical Chemistry. 82 (2010) 5349–5356. Copyright (2010) American Chemical Society.

contact with the UTLC plate. Additional mobile phase (~ 1 mL) was added to the conditioning trough beneath the GLAD UTLC plate to produce the quasi-saturated vapour phase (mobile phase vapour) described **above**. Immediately upon removal from the chamber, the developed plates were rapidly dried under the warm air stream from a hair drier. This procedure is commonly used for TLC and HPTLC plates however drying occurred much more quickly (only a few seconds) on the GLAD UTLC layers. Additional experiments were performed using a customized chamber designed for GLAD UTLC media (**8 Customized GLAD UTLC chamber**).

3.5 Imaging

3.5.1 Flatbed film scanner

The second major component of the Office Chromatography concept involves the use of consumer flatbed scanners to image developed planar chromatography media. Flatbed scanners offer high image resolution (> 600 pixels per inch) and are less expensive than dedicated scanning slit densitometers. Coloured images of the separated spot patterns may then be processed using a variety of video densitometry software packages to produce chromatogram intensity curves.

The translucence of GLAD UTLC layers make them amenable to high-resolution imaging by flatbed scanners in both reflection and transmission imaging modes. (Increased light scattering in the thicker HPTLC layers permits only reflection mode imaging.) Some consumer flatbed scanners have light sources built into their lid that transmit light through photographic film negatives into the detector. This feature of the CanoScan CS 5600F and CanoScan 9000F scanners (Canon, Mississauga, Ontario, Canada) was used in several GLAD UTLC investigations [5,8,13] to collect high-resolution images (1200 dpi, rgb mode, 8-bits per channel) of GLAD UTLC media before and after development (**Figure 3-7**). Although generally limited to visible spots, other planar chromatography users have considered UV light sources compatible with fluorescent HPTLC media [24].

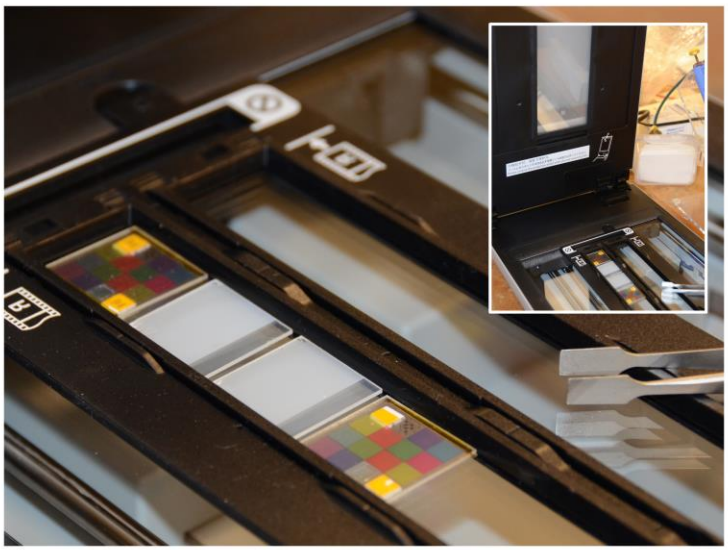

Figure 3-7 Consumer flatbed film scanner (Canon 9000F) used to image GLAD UTLC media before and after development. A light source built into the scanner lid transmits light through the translucent plates into the detector below (inset).

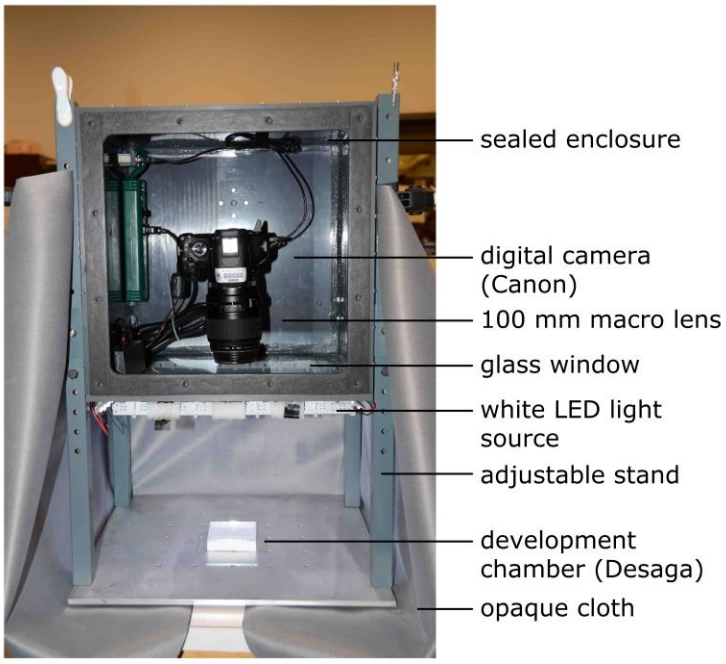

Figure 3-8 Time-resolved UTLC digital camera imaging booth. Chromatographic separations are illuminated by white LEDs and imaged from above. The opaque cloth prevents stray ambient light from affecting videos and the sealed enclosure protects the camera from solvent vapours. Figure modified with permission from [14]. Copyright (2012) Elsevier.

3.5.2 Time-resolved UTLC

Recent work used a high-definition camera to record videos during separations on UTLC [14] and GLAD UTLC media. The Canon EOS Rebel T2i digital single-lens reflex (DSLR) camera had a macro lens (Canon EF 100 mm f/2.8 USM) and could capture 1920 pixel × 1080 pixel frames at up to 30 frames per second (**Figure 3-8**). This approach was only used with visible analytes, but provided a wealth of information about separation quality. Semi-automatic analysis of a series of frame images extracted from a separation video produces a series of chromatogram curves, Gaussian peak fits, and calculated figures of merit. Details about this technique are described separately in **6 Time-resolved UTLC**.

3.5.3 Colour calibration

A commercially-available reflective colour standard (Munsell ColorChecker Chart, ColorAccuracy.com) was used to validate the imaging systems. This card contained coloured swatches with certified red-green-blue (*r*,*g*,*b*) and hue-saturation-lightness (*h*,*s*,*l*) values. Colour fidelity was evaluated by comparing the certified values against those measured from corresponding regions cropped from video frames. The time-resolved UTLC system provided excellent agreement between measured and certified colour swatch hue values [14]. Flatbed scanner colour fidelity was similarly evaluated in reflection mode [8] but not in transmission mode. Separate transparent colour standards would be required for such transmission mode calibration.

3.6 Chromatogram extraction and analysis

3.6.1 Colour models and transformation

The red-green-blue (rgb) model describes a pixel colour as a point in rectangular coordinates (**Figure 3-9a**). Each of the normalized *r*, *g*, and *b* values lies within the range 0-1; (*r*,*g*,*b*) = (1,0,0) describes a perfectly red pixel while (*r*,*g*,*b*) =

(1,1,0) describes a yellow pixel composed of full red and green signals. An 8-bit rgb image discretizes each of the red, green, and blue channel levels as integers over the range 0-255 so that (*r*,*g*,*b*) = (255,0,0) describes a perfectly red pixel. GLAD UTLC separation images (scans) and video frames were collected in this 8-bit rgb image format.

The hue-saturation-lightness (hsl) model is more intuitive and uses cylindrical coordinates to represent colours within a double hexicone (**Figure 3-9b**) [25]. The azimuthal ordinate (hue, h, $0 \leq h < 360$) indicates the colour of the pixel (in degrees); red pixels have $h = 0$ while yellow pixels have $h = 60$. (Neutral colours have undefined hue.) The radial ordinate (saturation, s, $0 \leq s \leq 1$) describes the intensity of the colour; neutral colours have $s = 0$ and intense colours have $s = 1$. The axial ordinate (lightness, l, $0 \leq l \leq 1$) represents tendencies towards black ($l = 0$) and white ($l = 1$). In the hsl model, pure colours have $s = 1$ and $l = 0.5$.

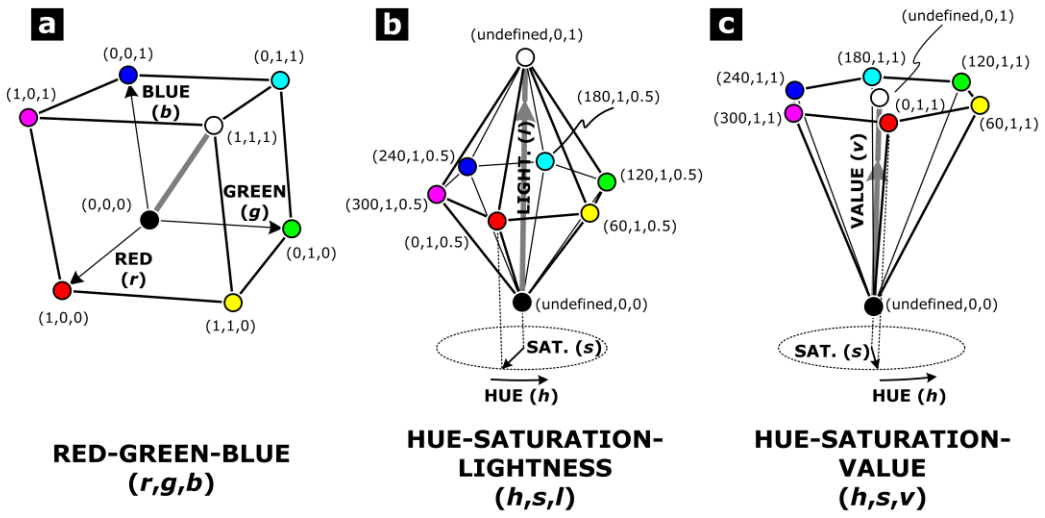

Figure 3-9 Standard colour models for digital images. Representations of pure colours in (a) red-green-blue (*r*,*g*,*b*), (b) hue-saturation-lightness (*h*,*s*,*l*), and hue-saturation-value (*h*,*s*,*v*) spaces. The pure colour vertices (red, yellow, green, cyan, blue, magenta, black, white) of each geometric solid are shown. Thick grey line between black and white vertices represents axis of neutral (grey) colours.

The hue-saturation-value (hsv) model is very similar to the hsl model (**Figure 3-9c**) [25]. In this variation, hue and saturation are similarly defined but value replaces the lightness. This axial component (value, v, $0 \leq v \leq 1$) again describes tendencies towards black ($v = 0$) and white ($v = 1$). The main difference is that pure colours have $v = 1$ in the hsv model. This difference was irrelevant in the GLAD UTLC colour-filtered chromatogram implementations since the v was not used in any intensity calculations [3,4,8,12,14,26].

3.6.2 Darkness signal [7]

Early analysis of GLAD UTLC separations employed a colour-independent darkness signal (d). A custom MATLAB script calculated pixel lightness values by transforming 8-bit rgb images into hsl space according to the equation [25] (**B.1 ExtractChromaSJ20100128.m**):

$$l = \frac{1}{2}[\max(r, g, b) + \min(r, g, b)] \quad \textbf{(3-1)}$$

where r, g, and b are the normalized red, green, and blue channel values (defined over 0-1). Darkness (d) was then defined as:

$$d = 1 - l \quad \textbf{(3-2)}$$

Chromatograms were produced by averaging these darkness values across the rows contained within the separation track at every position along the development direction. This approach was only used in a couple of early GLAD UTLC studies [5,13].

3.6.3 Hue-filtered summed saturation signal

Densitogram specificity was improved significantly by incorporating pixel hue; especially in cases of closely spaced spots with different colours (hues). Collected 8-bit rgb GLAD UTLC separation images or video frames were converted into *hsv* space so that pixel h and s could be used. (The hsl model could have equivalently been used but the built-in MATLAB rgb-hsv conversion

function was easier to implement.) The calculated densitogram signal sums the *s* values of only those pixels with *h* inside of the given hue filter. In this way, cyan pixels ($h \sim 180$) are excluded from a red ($h \sim 0$) signal, for example. This method was applied to individual separation images [4,8] and in TR-UTLC video analysis [3,12,14]. Details about this method are discussed in in **6 Time-resolved UTLC**.

3.6.4 Chromatogram analysis

Standard planar chromatography figures of merit were calculated from the chromatograms. The locations of the applied spot and migration front were generally identified manually except in TR-UTLC analysis (see **6.3.2 Define processing parameters**). Positions and widths of peaks corresponding to separated spots were manually measured directly from extracted signals or taken from Gaussian peak fits. These values enabled calculations of spot migration distance *Z*, retention factor hR_F (**Equation (2-4)**), plate number *N* (**Equation (2-6)**), and plate height *H* (**Equation (2-7)**). Chromatogram extraction and analysis was typically performed using MATLAB, however M.T. Taschuk used some of his custom Python [27] scripts to fit peaks in two investigations [8,13].

Although chromatogram extraction was typically performed on unenhanced separation track images, developed GLAD UTLC plate scans in investigations of RIE-modified morphologies (**5 Modified morphology and development**) underwent a minor Photoshop (Photoshop CS3 Extended, version 10.0.1, Adobe Systems, San Jose, USA) "Auto Levels" adjustment prior to analysis. This improved the GLAD UTLC image background and the resultant chromatograms.

3.6.5 Limitations

These approaches to extracting and analyzing chromatograms from GLAD UTLC separation images and video frames require further validation. The mass-range over which the signal (typically integrated peak area) remains linear has not been thoroughly characterized. Although the response is assumed linear for the small analyte masses in these investigations, the mass above which the signal ceases to

be (sufficiently) linear has not been identified. Sources of noise within the chromatograms should also be studied in order to accurately calculate total method sensitivity (limits of detection). Possible sources include instrument limitations, signal discretization (into 8-bit rgb images), and data compression [14].

References

[1] M.M. Hawkeye, M.J. Brett, Glancing angle deposition: Fabrication, properties, and applications of micro- and nanostructured thin films, J. Vac. Sci. Technol. A. 25 (2007) 1317–1335.

[2] M.T. Taschuk, M.M. Hawkeye, M.J. Brett, Glancing Angle Deposition, in: P. Martin (Ed.), Handbook of Deposition Technologies for Films and Coatings: Science, Applications and Technology, 3rd ed., William Andrew (Elsevier), Oxford, United Kingdom, 2010: pp. 621–678.

[3] J. Wannenmacher, S.R. Jim, M.T. Taschuk, M.J. Brett, G.E. Morlock, Ultrathin-layer chromatography on SiO2, Al2O3, TiO2, and ZrO2 nanostructured thin films, J. Chromatogr. A. 1318 (2013) 234–243.

[4] S.R. Jim, A. Foroughi-Abari, K.M. Krause, P. Li, M.R. Kupsta, M.T. Taschuk, et al., Ultrathin-layer chromatography nanostructures modified by atomic layer deposition, J. Chromatogr. A. 1299 (2013) 118–125.

[5] S.R. Jim, M.T. Taschuk, G.E. Morlock, L.W. Bezuidenhout, W. Schwack, M.J. Brett, Engineered anisotropic microstructures for ultrathin-layer chromatography, Anal. Chem. 82 (2010) 5349–5356.

[6] B. Dick, M.J. Brett, T.J. Smy, Investigation of substrate rotation at glancing incidence on thin-film morphology, J. Vac. Sci. Technol. B. 21 (2003) 2569–2575.

[7] J.B. Sorge, M.T. Taschuk, N.G. Wakefield, J.C. Sit, M.J. Brett, Metal oxide morphology in argon-assisted glancing angle deposition, J. Vac. Sci. Technol. A. 30 (2012) 021507.

[8] S.R. Jim, A.J. Oko, M.T. Taschuk, M.J. Brett, Morphological modification of nanostructured ultrathin-layer chromatography stationary phases, J. Chromatogr. A. 1218 (2011) 7203–7210.

[9] A. Foroughi-Abari, K.C. Cadien, In Situ Spectroscopic Ellipsometry Study of Plasma-Enhanced ALD of Al2O3 on Chromium Substrates, J. Electrochem. Soc. 159 (2012) D59–D64.

[10] P.E. Wall, Thin-Layer Chromatography: A modern practical approach, Royal Society of Chemistry, Cambridge, 2005.

[11] G.E. Morlock, C. Oellig, L.W. Bezuidenhout, M.J. Brett, W. Schwack, Miniaturized planar chromatography using office peripherals, Anal. Chem. 82 (2010) 2940–2946.

[12] S. Kirchert, Z. Wang, M.T. Taschuk, S.R. Jim, M.J. Brett, G.E. Morlock, Inkjet application, chromatography, and mass spectrometry of sugars on nanostructured thin films, Anal. Bioanal. Chem. (2013).

[13] A.J. Oko, S.R. Jim, M.T. Taschuk, M.J. Brett, Analyte migration in anisotropic nanostructured ultrathin-layer chromatography media, J. Chromatogr. A. 1218 (2011) 2661–2667.

[14] A.J. Oko, S.R. Jim, M.T. Taschuk, M.J. Brett, Time resolved chromatograms in ultra-thin layer chromatography, J. Chromatogr. A. 1249 (2012) 226–232.

[15] V.G. Berezkln, A. V. Chausov, Quasi-continuous videodensitometric recording of chromatograms in circular TLC, J. Planar Chromatogr. 24 (2011) 188–195.

[16] D.S. Jensen, S.S. Kanyal, V. Gupta, M.A. Vail, A.E. Dadson, M. Engelhard, et al., Stable, microfabricated thin layer chromatography plates without volume distortion on patterned, carbon and Al(2)O(3)-primed carbon nanotube forests., J. Chromatogr. A. 1257 (2012) 195–203.

[17] W. Haynes, ed., Physical Constants of Organic Compounds, in: CRC Handb. Chem. Phys. (Internet Version 2014), 94th ed., CRC Press [Taylor and Francis], Boca Raton, FL, 2014.

[18] L.R. Snyder, Classification of the solvent properties of common liquids, J. Chromatogr. A. 92 (1974) 223–230.

[19] S. Nyiredy, K. Dallenbach-Tölke, O. Sticher, The PRISMA optimization system in planar chromatography, J. Planar Chromatogr. 1 (1988) 336–342.

[20] S. Nyiredy, Planar chromatographic method development using the PRISMA optimization system and flow charts., J. Chromatogr. Sci. 40 (2011) 553–63.

[21] J. Sherma, B. Fried, Handbook of Thin-Layer Chromatography, 3rd ed., Marcel Dekker [Taylor and Francis], New York, 2003.

[22] E. Reich, A. Schibli, High-Performance Thin Layer Chromatography for the Analysis of Medicinal Plants, Thieme Medical Publishers, New York, 2007.

[23] B. Spangenberg, C.F. Poole, C. Weins, Quantitative Thin-Layer Chromatography, Springer Berlin Heidelberg, Berlin, Heidelberg, 2011.

[24] T. Halkina, J. Sherma, Use of the Chromimage flatbed scanner for quantification of high-performance thin layer chromatograms in the visible and fluorescence-quenching modes, Acta Chromatogr. 17 (2006) 250–260.

[25] J.D. Foley, A. Van Dam, Fundamentals of Interactive Computer Graphics, Addison-Wesley, Reading, Massachusetts, 1984.

[26] J.Z. Hall, M.T. Taschuk, M.J. Brett, Polarity-adjustable reversed phase ultrathin-layer chromatography., J. Chromatogr. A. 1266 (2012) 168–174.

[27] Python Reference Manual, http://docs.python.org/ref/ref.html [online], (n.d.).

4 Anisotropic UTLC microstructures[1]

The GLAD platform for engineering nanostructured thin films was used to fabricate and explore the chromatographic properties of ~ 4.5 - 5 μm thick normal-phase SiO_2 UTLC stationary phases with several types of in-plane macropore anisotropies [1,2]. The separation behaviours of two new UTLC media, isotropic vertical posts and anisotropic SBD blade-like films, were assessed using separations of CAMAG dye mixture. These morphologies were compared to that of anisotropic chevron media first studied by L.W.

[1] Portions of this chapter were published in:

- S.R. Jim, M.T. Taschuk, G.E. Morlock, L.W. Bezuidenhout, W. Schwack, M.J. Brett, Engineered anisotropic microstructures for ultrathin-layer chromatography, Analytical Chemistry. 82 (2010) 5349–5356. Reproduced with permission from [1]. Copyright (2010) American Chemical Society.
- A.J. Oko, S.R. Jim, M.T. Taschuk, M.J. Brett, Analyte migration in anisotropic nanostructured ultrathin-layer chromatography media, Journal of Chromatography A. 1218 (2011) 2661–2667. Reproduced with permission from [2]. Copyright (2011) Elsevier. S.R. Jim's contributions to this work include the methods for diagonal chromatogram extraction, measurement of initial channel feature orientation, derivation of analytical $\Delta\theta$ versus θ_C model, and editing of manuscript. Only SEM micrographs of UTLC layers and the $\Delta\theta$ versus θ_C model from this work are reproduced in this chapter.

Bezuidenhout and M.J. Brett [3]. The effects of macropore anisotropies and methods developed to characterize the unique separation behaviours on these media were investigated. Channel-like structures within the anisotropic media introduced preferential mobile phase flow directions that could be exploited to give separation tracks diagonal to the development direction. Extraction of chromatograms from angled tracks required creation of a new analytical approach that involved a commercial flatbed film scanner and custom numerical image analysis software. The chromatograms were used to calculate LODs and separation efficiencies for the Dimethyl Yellow dye component in the dye mixture. Separations rapidly performed over relatively short distances (~ 10 mm) produced unoptimized separation performance comparable to that of other planar chromatography media. These early investigations motivated subsequent efforts to improve GLAD UTLC layer morphology, instrumentation, and overall capability.

4.1 GLAD UTLC morphologies and development

Normal-phase silica GLAD UTLC plates were grown in three different morphologies: isotropic vertical posts, anisotropic chevrons, and anisotropic serial bideposition (SBD) blades (see **3.1.3 Studied GLAD UTLC morphologies**). SEM characterization revealed macroporous structures (> 50 nm pore size [4]) dictated by each material's deposition protocol (**Figure 4-1**). The exact composition and surface chemistry of the evaporated GLAD films is difficult to assess but hydrophilicity measurements (water contact angles) suggest consistency with thermally grown SiO_2 [5]. Lipophilic CAMAG dye mixture separations used to evaluate these media indicated that chromatographic behaviours varied with structure and development direction (**Figure 4-2**).

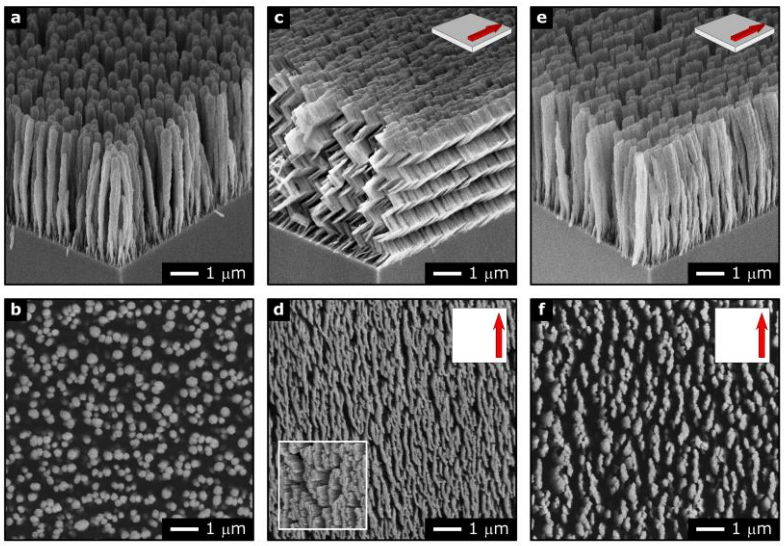

Figure 4-1 SEM micrographs of (a, b) isotropic vertical posts as well as anisotropic (c, d) chevron and (e, f) SBD media when viewed from an oblique angle and from above, respectively. Arrow indicates along-channel vector in anisotropic films. (b) vertical post and (f) SBD films imaged normal to substrate surface. Pores within top layer of chevron film apparent only when viewed along angled segments in this layer (~ 53° to the substrate normal) (d). Inset in (d) shows film as viewed normal to substrate. Reproduced with permission from [1]. Copyright (2010) American Chemical Society.

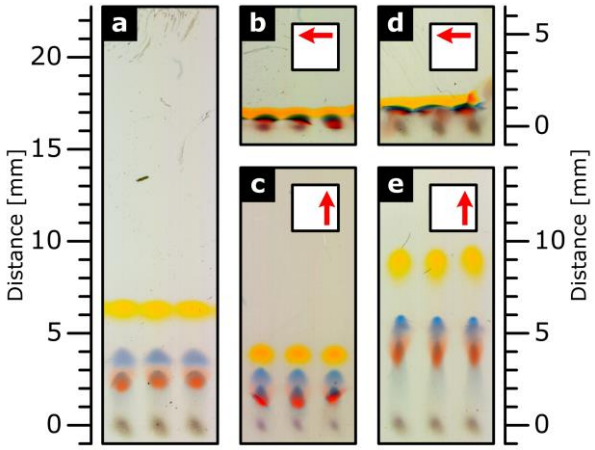

Figure 4-2 Scans of developed GLAD UTLC plates. Undiluted dyes separated on (a) vertical post, (b, c) chevron, and (d, e) SBD films. Dyes moved faster in along-channel direction (c, e) than in across-channel direction (b, d). *MA*s of ~ 4.5 and ~ 6.5 measured for the chevron and SBD films, respectively (see **below**). Plates developed upwards. Arrow indicates along-channel vector in anisotropic films. Images enhanced for presentation. Reproduced with permission from [1]. Copyright (2010) American Chemical Society.

4.1.1 Isotropic vertical posts

Isotropic GLAD vertical post films were fabricated with a deposition angle of α = 84°. These columnar media were 4.6 μm thick (4.5 μm nominal) and composed of ~ 200 nm diameter columns with ~ 200 nm spacing, randomly distributed over the substrate surface (**Figure 4-1a and b**). Surface area enhancement for these films is estimated to be ~ 1000 m^2 m^{-2} (film surface area to footprint area) [6].

4.1.2 Anisotropic chevrons

Anisotropic chevron ("zig-zag") films were deposited at α = 84° and were 5.4 μm thick (5.0 μm nominal) with a 1 μm nominal spatial period (**Figure 4-1c and d**). This film was designed to be similar to those described by Bezuidenhout and Brett [3]. Porous channel-like structures ran in a direction normal to the plane of the chevrons. Perpendicular to this "along-channel" direction, the film appeared less permeable.

4.1.3 Anisotropic serial bideposition blades

Anisotropic SBD blade-like films were fabricated at α = 84° had a 4.6 μm thickness (4.5 μm nominal) and 24 nm nominal period (**Figure 4-1e and f**). Similar channel-like structures were also observed within the anisotropic SBD film. However, the columnar blade-like features in this film were approximately 200 nm thick, twice the thickness of the chevron film. The spacing between these blade-like structures in the SBD films was also wider than that between the features in the chevron film (~ 300 nm versus ~ 100 nm).

Follow-up investigations into the blade-like SBD UTLC media were performed by Oko *et al.* [2] and considered variation of the deposition angle over α = 82.5°, 84.0°, 85.5°, and 87.0° (**Figure 4-3**). The resultant GLAD UTLC media had channel widths that varied from 400 ± 20 nm (α = 82.5°) to 840 ± 20 nm (α = 87.0°). Faster migration was observed in films with wider channels. GLAD UTLC films deposited at greater α also exhibited lower analyte retention

(higher retention factors, hR_F) [2]. This result is likely due to the observed decreases in film surface area enhancement (and total surface area) as α approaches 90° [6].

4.1.4 Macroporosity and development

Although separations of the lipophilic dye mixture on TLC and HPTLC layers are typically performed using toluene, this high elution strength mobile phase was inappropriate for the GLAD UTLC layers. The reduced thickness and specific surface areas of these layers caused them to have lower total surface area (and surface activity) than TLC and HPTLC layers. In order to achieve comparable separations on the less active GLAD UTLC media, a mobile phase with weaker elution strength (4:3 toluene:*n*-hexane (v/v)) was required. (See also **3.4.2 Mobile phase optimization**.)

The development distances for rapid developments (~ 90 s) performed on the α = 84° vertical post (~ 7 mm; **Figure 4-2a**), chevron (~ 5 mm, along channel; **Figure 4-2c**), and SBD (~ 12 mm, along-channel; **Figure 4-2e**) media were consistent with the previous [3] and subsequent [2] finding that migration occurs most rapidly through GLAD UTLC media with the largest macropores. For this reason, separation quality on anisotropic GLAD UTLC layers was best when developments were performed in the along-channel direction [2]. The reduced permeability limited mobile phase migration and separation quality achieved in the across-channel direction of the chevron (**Figure 4-2b**) and SBD films (**Figure 4-2d**).

4.1.5 Mobile phase migration front identification

The morphology of macroporous columnar GLAD thin films is known to change following the introduction and evaporation of liquids [7–9]. As the liquid evaporates, capillary forces cause the columns to bend into each other and "clump" together. Surface forces between adjacent columns cause them to remain clumped together long after the film has dried. Although the resultant clumps can

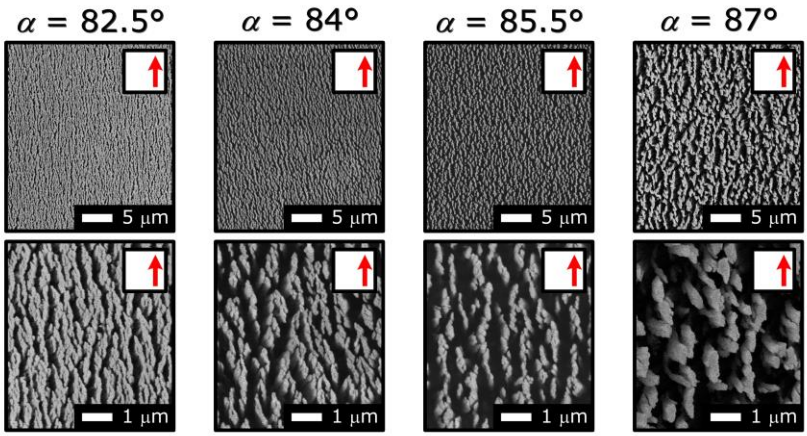

Figure 4-3 Top-down view of serial bideposition blade-like GLAD UTLC layers fabricated at different deposition angles (α). Larger α produce thicker blade features separated further apart. Films deposited and imaged by A.J. Oko. Modified with permission from [2]. Copyright (2011) Elsevier.

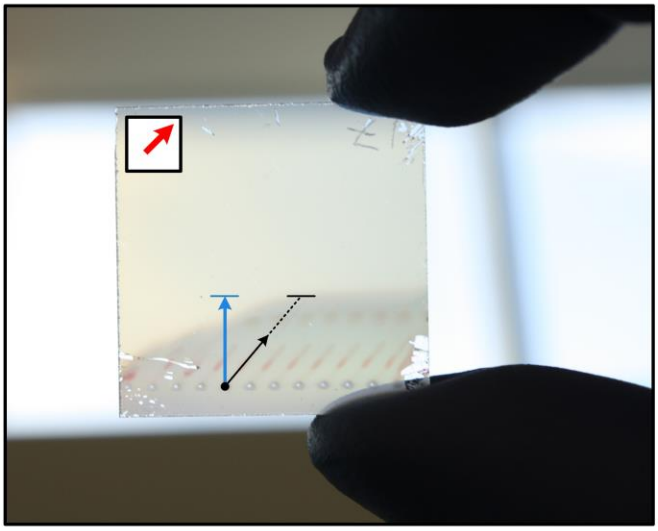

Figure 4-4 Photograph of the migration front intrinsically preserved on a GLAD UTLC plate developed and dried five months earlier. Clumping of columnar grains within the wetted region (bottom) causes the optical properties to change from those of the unperturbed film (top). The interface between these regions is visible to the naked eye when lit from behind by ambient light. The migration front curvature on the anisotropic SBD film is due to the diagonal orientation of the channel-like features and the resultant preferential mobile phase flow to the right. The blue arrow marks the development direction and the horizontal black line marks the migration front position. Reproduced with permission from [1]. Copyright (2010) American Chemical Society.

only be viewed with a microscope, the change in the GLAD thin film optical properties due to clumping can be seen by the unaided eye (**Figure 4-4**). The migration front of a developed GLAD UTLC plate is assumed to be the boundary of the clumped region on the plate and remains visible several months after the separation was performed. The clumping phenomenon therefore offers an intrinsic means of permanently archiving the migration front position on developed GLAD UTLC plates without manual marking. Investigation and modification of the clumping phenomenon through post-deposition processing remain active areas of research in the GLAD research group and others [10].

4.2 Extent of macropore anisotropy

GLAD's ability to easily produce anisotropic microstructures is appealing in UTLC. The unique channel-like features can improve separation performance and throughput. Deposition protocol modification can tune channel spacing and resultant analyte migration velocities. Lower permeability perpendicular to the channel features also reduces transverse broadening and may allow more closely-spaced parallel separation tracks on an anisotropic plate developed in the along-channel direction than on an isotropic plate of the same size. In order to characterize the extent of GLAD UTLC macropore anisotropy, two new metrics were defined: migration anisotropy and separation track deviation angle.

4.2.1 Migration anisotropy

The migration anisotropy (*MA*) describes the extent of anisotropy in terms of the along and across-channel migration distances obtained for the same development time (for example, ~ 90 s):

$$MA_i = \frac{Z_{i,\,along}}{Z_{i,\,across}} \qquad \textbf{(4-1)}$$

Where $Z_{i,along}$ and $Z_{i,across}$ are the migration distances for the i^{th} component in the dye mixture separated in the along-channel and across-channel directions on separate plates with the same anisotropic stationary phase. As the migration

distance in a particular direction depends on the layer permeability in that direction, media with macropore anisotropies exhibit a $MA > 1$. Therefore, the isotropic vertical post film has a *MA* of 1, and a perfectly anisotropic medium would have an infinite *MA*. Dimethyl Yellow migration anisotropies were ~ 4.5 (migration distance in **Figure 4-2c** versus that in **Figure 4-2b**) and ~ 6.5 (migration distance in **Figure 4-2e** versus that in **Figure 4-2d**) for the $\alpha = 84°$ chevron and SBD films, respectively. This measurement therefore indicates that the SBD media are "more anisotropic" than chevron media.

4.2.2 Separation track deviation angle

The anisotropic GLAD UTLC media exhibited particularly interesting behaviours when their channel features were oriented diagonal to the development direction (**Figure 4-5**). Resultant dye separation tracks were found to incline towards the along-channel direction but did not become fully aligned with it, in agreement with L.W. Bezuidenhout and M.J. Brett [3]. In order to characterize this effect, it was convenient to define a separation track deviation angle ($\Delta\theta$):

$$\Delta\theta = \theta_C - \theta_T \qquad \textbf{(4-2)}$$

Where θ_C and θ_T are the orientations of the anisotropic film's along-channel vector and resultant development track. These track angle deviations serve as additional measures of the extent of macropore anisotropy; lower $\Delta\theta$ values suggest that a medium is "more anisotropic." Separation tracks in the $\alpha = 84°$ chevron and SBD films deviated from the along-channel direction ($\theta_C = 45°$ with respect to the development direction) by angles of $\Delta\theta = 10° \pm 2°$ and $\Delta\theta = 5° \pm 2°$, respectively (as defined in **Figure 4-5**). (The 2° estimated orientation error was associated with substrate alignment during film deposition and insertion into the chromatographic development chamber.) A higher *MA* and a smaller $\Delta\theta$ both indicate that the $\alpha = 84°$ SBD media exhibits stronger macropore anisotropy than the chevron media. This finding is consistent with the micrographs collected for the SBD and chevron films (**Figure 4-1**).

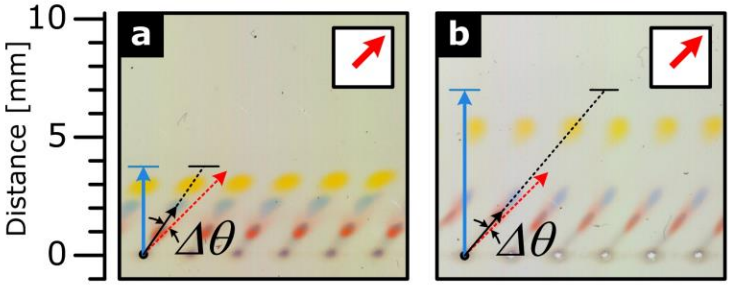

Figure 4-5 Scanned images of diagonally-developed GLAD UTLC plates. Dye separation tracks (dotted black line) on (a) chevron and (b) SBD media deviated from the along-channel direction (red arrow) by angles of $\Delta\theta$ = 10° ± 2° and $\Delta\theta$ = 5° ± 2° when the channel-like structures were oriented at θ_C = 45° with respect to the development direction (blue arrow). Horizontal black line marks migration front position. Diluted dyes (50%) were separated. Images enhanced for presentation only. Reproduced with permission from [1]. Copyright (2010) American Chemical Society.

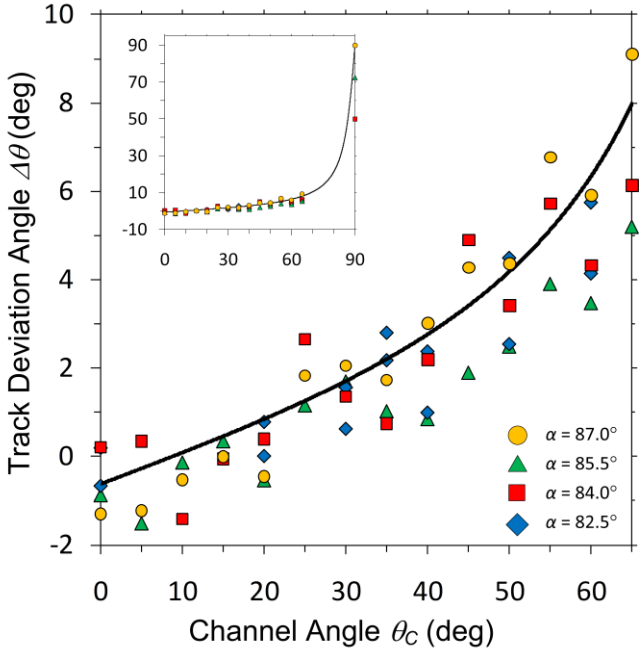

Figure 4-6 Separation track deviation angle ($\Delta\theta$) as a function of channel angle (θ_C) for films grown at different deposition angles (α). $\Delta\theta$ is independent of deposition angle α. The solid line is a best fit of **Equation (4-4)** to the entire data set. Inset shows good agreement between model and experimental data at very high channel angles. Measurements performed by A.J. Oko, theoretical model proposed by S.R. Jim, fitting performed by M.T. Taschuk. Reproduced with permission from [2]. Copyright (2011) Elsevier.

A geometric relationship between the deviation angle and the migration anisotropy may exist. If the separation track vector corresponding to the θ_C = 45° channel features is decomposed into projections in the along- and across-channel directions, then:

$$\tan \Delta\theta = \frac{Z_{i,\,across}}{Z_{i,\,along}} = MA_i^{-1} \qquad \textbf{(4-3)}$$

From the Dimethyl Yellow migration anisotropies reported above, **Equation (4-3)** predicts separation track deviation angles for the chevron and SBD films of $\Delta\theta$ = 12.5° and $\Delta\theta$ = 8.7°, respectively. While the predicted deviation angles are different from the measured values, this simple treatment captured most of the behaviour observed on anisotropic GLAD UTLC media with channel-like features oriented at 45° to the development direction. However, this geometric argument cannot describe media with their channel-like features oriented in different directions. For instance, if the along-channel and development directions are parallel, the track deviation should be $\Delta\theta$ = 0°; if they are perpendicular, the track deviation should be $\Delta\theta$ = 90°.

Our further study of anisotropic blade-like SBD GLAD UTLC plates (α = 82.5°-87.0°) produced an improved generalized model for arbitrarily-oriented channel features [2]. By projecting the development direction onto the channel and separation track vectors, the track deviation angle can be shown to be:

$$\Delta\theta = \theta_C - \theta_T = arctan\left(\frac{1}{\sqrt{d}}\tan\theta_C\right) \qquad \textbf{(4-4)}$$

where d is the diffusivity ratio between the along and across channel directions, respectively. The collected data showed no dependence on deposition angle α (**Figure 4-6**). A fit of the above model to all $\Delta\theta$ data yields a value for d of ~ 200. Applying **Equation (4-4)** to the α = 84° SBD media described earlier ($\Delta\theta$ = 5° ± 2° for θ_C = 45°) [1] produces a calculated value of d ~ 130 that is of similar order to the fitted value. While it is difficult to obtain precise data for the higher

channel angles due to the short migration distances, the inset in **Figure 4-6** shows good agreement between the model and the track deviations observed at higher θ_C angles. For additional model verification, testing very porous films at $\theta_C > 60°$ or increasing development time would be required.

4.3 Effects of film morphology on chromatograms

4.3.1 Chromatogram extraction

Developed GLAD UTLC plates were imaged in transmission mode using the CanoScan 5600F flatbed film scanner. The angled separation tracks on the anisotropic media required a customized chromatogram extraction approach. Individual separation tracks were isolated from the scanned images of the developed UTLC plates using Photoshop (CS3 Extended, version 10.0.1, Adobe Systems, San Jose, USA). In cases where the separation track was diagonal to the development direction, a diagonal track region was defined within the image (**Figure 4-7a**). Pixels outside of this region were masked and excluded from subsequent analysis. Track widths were constant along their lengths and visually selected to include the full width of the largest spot (typically the Dimethyl Yellow spot). A custom MATLAB script (**B.1 ExtractChromaSJ20100128.m**) was used to calculate pixel darkness (*d*) (see **3.6.2 Darkness signal**). Output chromatograms plotted the pixel darkness (row-averaged perpendicular to the plate edges) along the development direction (**Figure 4-7b**).

4.3.2 Effects of film morphology on separation behaviour

The resultant chromatograms reflect the strong dependence of separation behaviour on film microstructure (**Figure 4-8**). Along-channel separations on the $\alpha = 84°$ chevron and SBD media are comparable to those on the vertical post media. While the Dimethyl Yellow peak ($hR_F \sim 60$) appeared well-resolved, the peaks corresponding to the Sudan Blue II ($hR_F \sim 25$) and Ariabel Red ($hR_F \sim 15$)

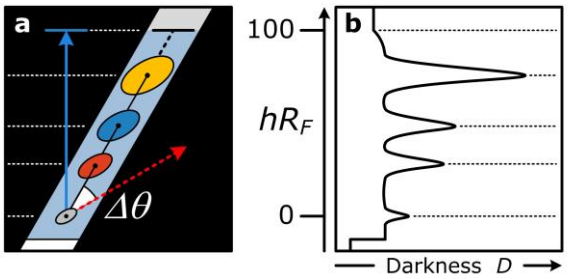

Figure 4-7 Schematic representation of chromatogram extraction from a diagonal separation track. (a) As the separation track was not parallel to the development direction (blue arrow), it had to be isolated from the scan of the developed UTLC plate using an angled mask (black). This track (dotted black line) also deviated from the along-channel direction (red arrow) by an angle $\Delta\theta$. The horizontal black line marks the migration front position. Row-averaging the pixel darkness values across the width of the track for every position along the development direction enabled chromatogram extraction (b). Reproduced with permission from [1]. Copyright (2010) American Chemical Society.

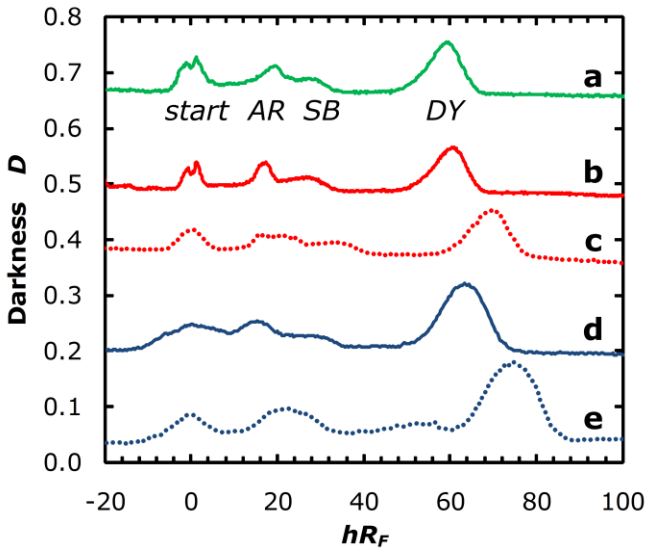

Figure 4-8 Chromatograms from dye separations on isotropic and anisotropic GLAD UTLC media. Vertical post (a, solid green), along-channel SBD (b, solid red), diagonal channel SBD (c, dotted red), along-channel chevron (d, solid blue), and diagonal channel chevron (e, dotted blue) media. Peaks corresponding to the start zone (*start*), Ariabel Red (*AR*), Sudan Blue II (*SB*), and Dimethyl Yellow (*DY*) are identified. Double peaks observed at the starting point in some of the curves are associated with ring-shaped spots. Darkness curves offset for clarity. Reproduced with permission from [1]. Copyright (2010) American Chemical Society.

dye components were only partially resolved. The other dye components were too faint to produce identifiable peaks. The low resolution of all components is attributed to the relatively large initial spot size. The limitations of the colour-independent darkness signal motivated development of the hue-filtered chromatogram extraction approach (see **3.6.3 Hue-filtered summed saturation signal**).

Rapid spot migration in the along-channel direction on the SBD media compensates for increased spot elongation and results in separation performance similar to that of the vertical post media. Increased peak broadening observed in the along-channel direction on the chevron media (~ 40% compared to the vertical post and SBD media) is believed to be related to the increased structure tortuosity relative to the vertical post and SBD media. Non-uniform mobile phase flow around the angled segments in the chevron film may enhance eddy diffusion of the analytes. (See also **Equation (2-8)**.)

Chromatograms corresponding to the diagonal developments conducted on the chevron and SBD media exhibit some interesting trends. Despite increased peak broadening, the chromatograms show increased peak separation and suggest reduced analyte retention on the plate. Although the separation track vector is different from the along-channel direction, spot elongation may have occurred preferentially in the highly-permeable along-channel direction. This effect is most obvious in the diagonally-developed chevron plate (**Figure 4-5a**) as it has the greatest separation track deviation from the along-channel direction. Changes in the observed spot broadening geometry combined with the pixel row averaging technique developed for diagonal separations may account for some of these chromatogram features.

4.4 Performance quantification

Darkness signals associated with the Dimethyl Yellow dye component in the dye mixture were used to calculate the limits of detection (LOD) and estimate separation efficiency of the α = 84° vertical post, chevron, and SBD thin film

separation media (**Table 4-1**). These calculations were performed on chromatograms from early unoptimized separations. Later improvements in sample spot application, UTLC plate imaging, and automated colour-filtered chromatogram extraction contributed to overall performance improvements.

4.4.1 Separation efficiency

The position and width of the chromatogram peak corresponding to the separated Dimethyl Yellow spot were used to calculate standard chromatographic performance metrics (**Table 4-1**). Plate numbers (N) and heights (H) were calculated using **Equation (2-6)** and **Equation (2-7)**, respectively. The plate heights (H = 12 μm - 28 μm) are comparable or better than those of normal-phase TLC, HPTLC, and early monolithic silica gel UTLC plates [11–13] (**Table 2-1**). However, the obviously low plate numbers calculated for the GLAD UTLC media (N = 150 - 540) resulted from the very short migration distances (Z = 3 mm - 10 mm) and poorly applied spots.

Improved sample application methods could have increased separation efficiency (see also **3.3 Sample spot application**). The commercially-available CAMAG dye mixture employs toluene as a solvent. In these experiments, this high elution strength solvent caused the dye spots to expand substantially before they dried. Further diluting the dye mixture in toluene may have enhanced this effect and resulted in the lower observed performance for the 50% relative concentration separations (**Table 4-1**). Subsequent work demonstrated that smaller spots result when the CAMAG dye mixture is diluted instead in low elution strength *n*-hexane. The ATS 4 aerosol application mode might have also hindered these experiments. Rapid spray-on application allowed the dye spots to grow larger before drying. Spraying using the high pressure N_2 jet also damaged the GLAD UTLC layer and could have introduced mobile phase flow non-uniformities. Contact mode application reduced these problems in later experiments.

Table 4-1 GLAD UTLC stationary phase figures of merit based upon the Dimethyl Yellow component separated from undiluted (100%) and diluted (50% in toluene) lipophillic dye mixtures. Migration distance (*Z*), plate number (*N*), and plate height (*H*) are reported. The development direction is listed only for the anisotropic GLAD UTLC layers. Reproduced with permission from [1]. Copyright (2010) American Chemical Society.

Microstructure (direction)	Relative Concentration	*Z* (mm)	*N*	*H* (μm)
Vertical Posts	100	6.3 ± 0.1	540 ± 50	12 ± 1
Vertical Posts	50	5.64 ± 0.07	270 ± 25	21 ± 2
Chevron (along)	100	3.8	170	22
Chevron (along)	50	3.50 ± 0.07	150 ± 5	23.5 ± 0.5
Chevron (diagonal)	50	3.02 ± 0.06	167 ± 6	18 ± 1
SBD (along)	100	9.6 ± 0.6	480 ± 140	21 ± 6
SBD (along)	50	7.2 ± 0.1	260 ± 25	28 ± 2
SBD (diagonal)	100	5.27 ± 0.05	340 ± 20	16 ± 1
SBD (diagonal)	50	5.33 ± 0.05	330 ± 50	17 ± 2

4.4.2 Limits of detection estimates

Limits of detection (LOD) are dependent upon the analyte type, separation medium, detector, and other factors. Separations of dye spots with decreasing concentrations of CAMAG dye mixture were used to estimate the LOD for Dimethyl Yellow separated on GLAD UTLC layers and detected using the visible light flatbed film scanner. M.T. Taschuk calculated signal-to-noise ratios (SNRs) for this dye component numerically using a variant of the "Total Peak Area" method [14] for S.R. Jim's darkness signals described above. Regions adjacent to the corresponding chromatogram peak were identified by eye; linear fits to these regions were used to evaluate background levels and single pixel row noise (*noise*). Chromatogram peak area (*A*) was numerically integrated. After scaling the noise to the full peak width (*w*) using $\sqrt{w}$, the signal-to-noise ratio becomes:

$$SNR = \frac{A}{noise\sqrt{w}} \quad \textbf{(4-5)}$$

The reported limits of detection (LOD) use 99% confidence intervals (*SNR* = 3). The unoptimized LODs were found to be 10 ng ± 4 ng and 11 ng ± 3 ng for the vertical post and SBD media, respectively (**Figure 4-9**). Consideration of alternative analytes and detection modes may further improve these measurements by an order of magnitude towards or beyond the 1 ng LOD reported for caffeine separated on monolithic UTLC layers and detected using UV light (200 nm) [12].

4.5 Conclusions

Thin film morphology has a large effect on GLAD UTLC development characteristics. Separations performed on ~ 5 μm thick isotropic vertical post, anisotropic chevron, and anisotropic SBD blade-like plates determined that capillary-driven mobile phase migration occurs most rapidly in media with larger macropores. Developments performed along the channel-like features in anisotropic media occurred much faster than in a direction perpendicular to these features. Developments performed diagonal to the channels indicated that the

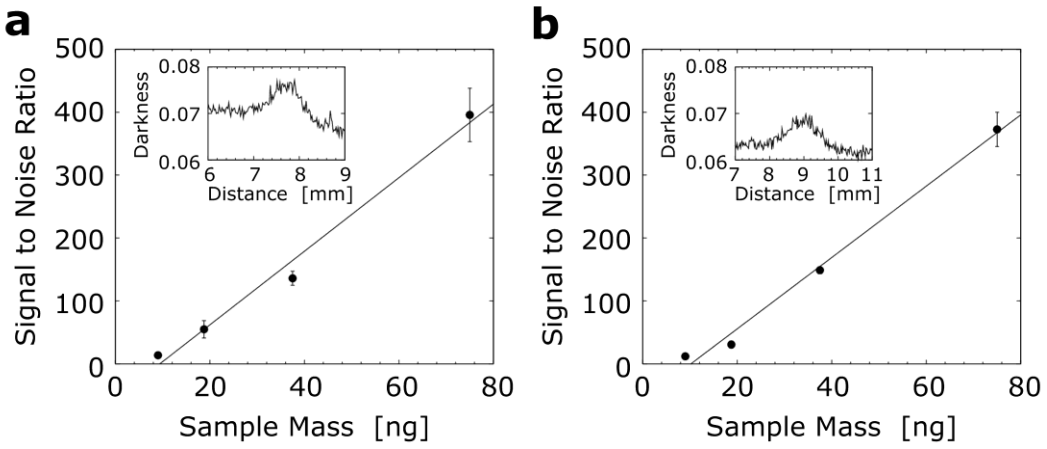

Figure 4-9 Limits of detection for the Dimethyl Yellow dye spots on the (a) vertical post and (b) SBD films. Insets show the measurable peak associated with the 9.4 ng Dimethyl Yellow peak. The limits of detection for the dye on these films were 10 ng ± 4 ng and 11 ng ± 3 ng, respectively, with a 3σ criterion used. Modified with permission from [1]. Copyright (2010) American Chemical Society.

channels strongly influenced but did not entirely dictate the separation track direction. This effect was greatest on media with the highest macropore anisotropy. The extent of macropore anisotropy was characterized using new migration anisotropy (*MA*) and separation track deviation angle ($\Delta\theta$) metrics. Both values suggested that the studied SBD films were "more anisotropic" than the chevron media. Chromatograms generated from colour-independent darkness signals were used to quantify unoptimized GLAD UTLC separation performance. Unoptimized Dimethyl Yellow LOD estimates (~10 ng) are expected to improve upon further optimization of layer microstructure and instrumentation. Although plate heights (*H*) were reasonable, short migration distances resulted in low absolute plate numbers (*N*). Overall separation performance was limited by the available HPTLC instrumentation; especially by the relatively large applied sample spots.

In spite of these challenges, this exploratory work suggested that engineered high surface area isotropic and anisotropic nanostructured GLAD columnar thin films can enhance UTLC capabilities. The GLAD approach is especially powerful in fabricating media with different porosities and unique anisotropic structures impossible or impractical through other methods. Increased permeability in the along-channel direction of these media improves migration velocities and separation distances. Meanwhile, decreased permeability perpendicular to the channel features reduces transverse spot broadening and may allow closer spacing of adjacent separation tracks. This would permit more samples to be analyzed in parallel on a given chromatographic plate. The investigated benefits of GLAD in UTLC motivated subsequent concurrent research into new GLAD UTLC morphologies, methods of modification, and instrumentation optimized for these media.

References

[1] S.R. Jim, M.T. Taschuk, G.E. Morlock, L.W. Bezuidenhout, W. Schwack, M.J. Brett, Engineered anisotropic microstructures for ultrathin-layer chromatography, Anal. Chem. 82 (2010) 5349–5356.

[2] A.J. Oko, S.R. Jim, M.T. Taschuk, M.J. Brett, Analyte migration in anisotropic nanostructured ultrathin-layer chromatography media, J. Chromatogr. A. 1218 (2011) 2661–2667.

[3] L.W. Bezuidenhout, M.J. Brett, Ultrathin layer chromatography on nanostructured thin films, J. Chromatogr. A. 1183 (2008) 179–185.

[4] J. Rouquerol, D. Avnir, C.W. Fairbridge, D.H. Everett, J.M. Haynes, N. Pernicone, et al., Recommendations for the characterization of porous solids (Technical Report), Pure Appl. Chem. 66 (1994) 1739–1758.

[5] R.G. Frieser, Characterization of Thermally Grown SiO2 Surfaces by Contact Angle Measurements, J. Electrochem. Soc. 121 (1974) 669.

[6] K.M. Krause, M.T. Taschuk, K.D. Harris, D.A. Rider, N.G. Wakefield, J.C. Sit, et al., Surface area characterization of obliquely deposited metal oxide nanostructured thin films., Langmuir. 26 (2010) 4368–4376.

[7] J.-G. Fan, D. Dyer, G. Zhang, Y.-P. Zhao, Nanocarpet Effect: Pattern Formation during the Wetting of Vertically Aligned Nanorod Arrays, Nano Lett. 4 (2004) 2133–2138.

[8] J.-G. Fan, Y.-P. Zhao, Spreading of a water droplet on a vertically aligned Si nanorod array surface, Appl. Phys. Lett. 90 (2007) 013102.

[9] J.-G. Fan, J.-X. Fu, A. Collins, Y.-P. Zhao, The effect of the shape of nanorod arrays on the nanocarpet effect, Nanotechnology. 19 (2008) 045713.

[10] J.K. Kwan, J.C. Sit, The use of ion-milling to control clustering of nanostructured, columnar thin films., Nanotechnology. 21 (2010) 295301.

[11] C.F. Poole, Thin-layer chromatography: challenges and opportunities, J. Chromatogr. A. 1000 (2003) 963–984.

[12] H.E. Hauck, M. Schulz, Ultrathin-layer chromatography, J. Chromatogr. Sci. 40 (2002) 550–552.

[13] B. Fried, J. Sherma, Thin-Layer Chromatography, Revised And Expanded, CRC Press, 1999.

[14] P.A. Baedecker, Digital methods of photopeak integration in activation analysis, Anal. Chem. 43 (1971) 405–410.

5 Modified morphology and development[1]

GLAD thin films are compatible with several post-deposition microprocessing techniques. The open pore structure of the columnar films enables morphological change throughout the thickness of the film; not simply at the top surface. Ion milling can yield subtle changes in columnar morphologies [1,2]. In this physical etching technique, an incident Ar^+ ion flux sputters material from the column surfaces. The resultant milled posts exhibit sharpened tips and smoothed vertical surfaces [1,2]. Reactive ion etch (RIE) processing [3–7] is an alternative microfabrication technique that utilizes physical and chemical etching mechanisms to achieve rapid anisotropic (downwards) etching (**Figure 5-1**). The controlled increases in GLAD film macroporosity possible using this method [8,9] motivated investigations into enhanced GLAD UTLC microstructures [9].

[1] A version of this chapter was published in: S.R. Jim, A.J. Oko, M.T. Taschuk, M.J. Brett, Morphological modification of nanostructured ultrathin-layer chromatography stationary phases, Journal of Chromatography A. 1218 (2011) 7203–7210. Adapted with permission from [9]. Copyright (2011) Elsevier.

This chapter describes a post-deposition process that extends the range of possible stationary phase porosities and chromatographic properties [9] beyond those that can be realized by GLAD alone. The method modified the separation performance of ~ 5 μm thick isotropic $\alpha = 85.5°$ SiO_2 vertical post GLAD UTLC plates using fluorocarbon RIE (**Figure 5-2**). These effects were characterized using figures of merit calculated from hue-filtered chromatograms extracted from transmission-mode scans of developed GLAD UTLC plates (**3.5.1 Flatbed film scanner**). Minor colour corrections were performed in Adobe Photoshop before the separation tracks were cropped and processed by a single-track MATLAB analysis script (**B.2 ExtractChroma20101012.m**). Dimethyl Yellow, Sudan Blue II, and Ariabel Red in the CAMAG lipophilic dye mixture were isolated using "yellow" ($30° \le h \le 90°$), "cyan" ($150° \le h \le 210°$), and "red" ($330° \le h \le 30°$) hue filters, respectively. (The hue measurement tools described in **C.13 sampleSpots.m** were not available during these investigations.)

Experimental results indicate that the etching and post-etch annealing treatments permit tuning of analyte retention and migration velocity. When coupled with a simple shadow mask technique, RIE enabled fabrication of adjacent stationary phase regions with different morphologies and development behaviours, thus producing a UTLC concentration zone (UTLC-CZ) plate. Dye

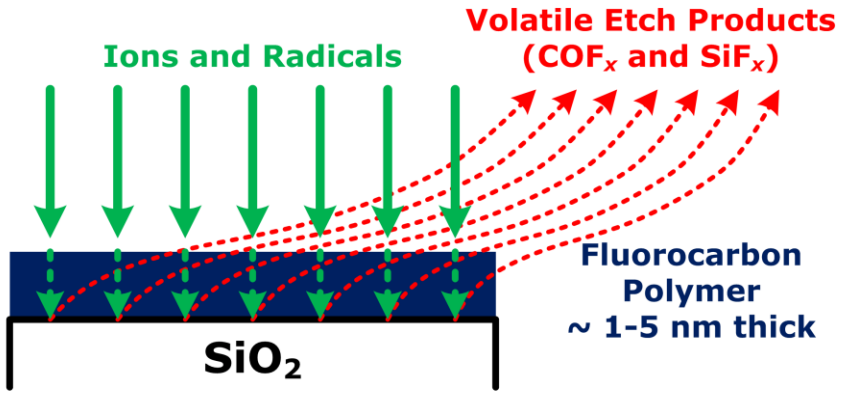

Figure 5-1 Schematic representation of processes involved in RIE. Incident ions and radicals activate etching reactions between a SiO_2 surface and the fluorocarbon film deposited onto it. These reactions produce volatile etch products that are pumped from the RIE reactor.

separations demonstrated that concentration zones defined on GLAD UTLC plates improve utility by enabling high-quality separations of large volume, low concentration applied sample spots. Although produced using an entirely new approach, GLAD UTLC concentration zone media behaved in a manner consistent with traditional TLC and HPTLC concentration zone plates (see also **2.2.1 Concentration zones for improved starting spots**).

5.1 Method of reactive ion etching GLAD UTLC

5.1.1 Full-plate processing

The porosity and morphology of selected regions on as-deposited SiO_2 vertical post GLAD thin films (nominal ~ 5 μm thickness and α = 87°) were modified using the RIE anisotropic plasma etching technique. Similar dramatic increases in porosity could not be realized simply by arbitrarily selecting a larger α for the deposition process since the film deposition rate becomes impractically low as α approaches 90°. Moreover, selective and simultaneous patterning of different

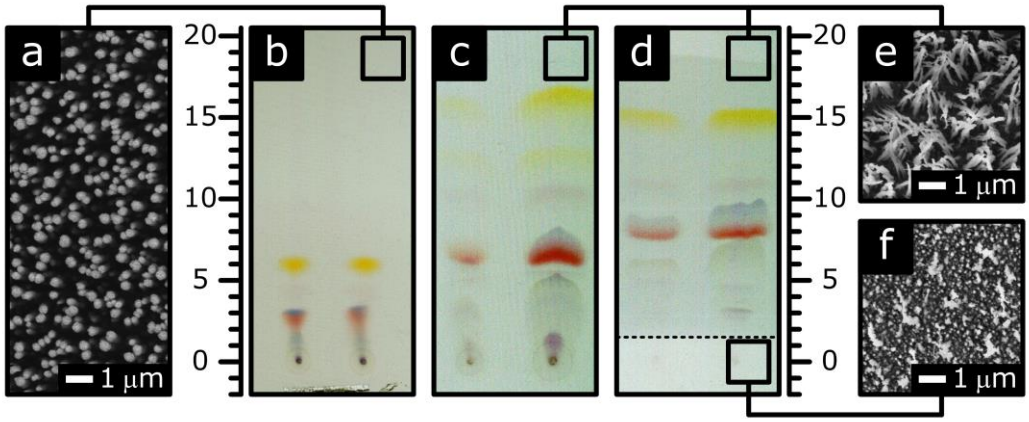

Figure 5-2 Reactive ion etching GLAD UTLC plates. (a) Top view SEM image and (b) dye separation chromatogram for an as-deposited GLAD SiO_2 vertical post plate. (c) Chromatogram obtained on an etched plate. (d) Chromatogram obtained on a plate with etched separation and concentration zones. (e, f) SEM images of film regions etched for 7 min and 22 min, respectively. Development distances shown in millimetres. Scanned chromatograms were digitally enhanced and had several dust and surface defects digitally removed for clarity.

regions on the same substrate with different morphologies cannot be achieved with the GLAD technique. Although ion milling may also be used to pattern regions onto GLAD media, initial experiments indicated that this method produced comparatively small changes to the morphology and UTLC development behaviours (even after long 10 min milling durations). For this reason, it was not as practical a method for producing large changes in GLAD UTLC stationary phase porosity desired in this work.

Fluorocarbon (CHF_3) reactive ion etching of SiO_2 [3–6] was performed within a dedicated RIE chamber (see **3.2.2 Reactive ion etching (RIE)** for details). The GLAD thin film plates were mounted to a modified Si carrier wafer during the SiO_2 etch process (**Figure 5-3**). Although the duration of the full-plate (no concentration zone) RIE-processing was varied from 0 min to 10 min, 5 min and 7 min processing times were typical.

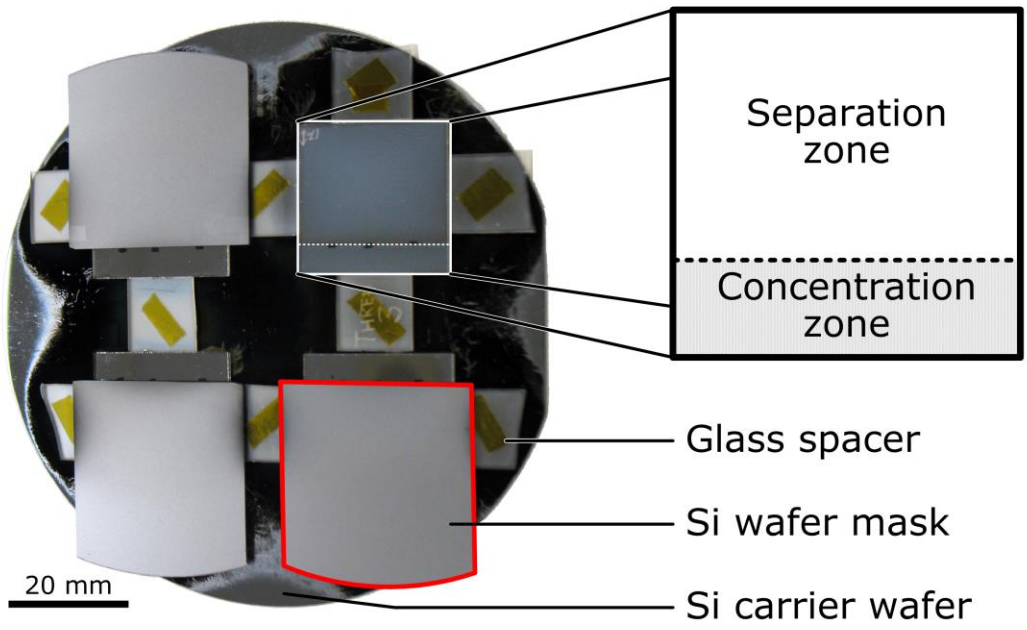

Figure 5-3 100 mm silicon carrier wafer used during GLAD UTLC and UTLC-CZ reactive ion etching. Glass pieces hold 25.4 mm square chromatography plates during etching. Cleaved silicon wafer shadow masks cover separation zones during concentration zone etching.

5.1.2 Concentration zone processing

GLAD UTLC-CZ plates were fabricated using two sequential reactive ion etching steps: (1) concentration zone patterning and (2) full-plate processing. The first step restricted morphological modification to the concentration zone. Pieces of a ~ 500 μm thick Si(100) wafer were cleaved by hand and used as shadow masks during this step. These masks were mounted onto the carrier wafer using double-sided polyimide tape (CAPLINQ, Ottawa, Ontario, Canada) to cover the separation zones on each plate without directly contacting them (**Figure 5-3**). The gap between the film and these Si masks was estimated to be ~ 0.3 mm. The remaining exposed 5 mm wide concentration zone on each 25.4 mm square plate's bottom edge was patterned by a 15 min reactive ion etch. In the second step, film morphologies in both of the concentration and separation zones were further modified using an additional full-plate 7 min RIE treatment without any masks. Total etching times for the concentration and separation zones were 22 min and 7 min, respectively.

5.2 Post-etching annealing treatments

Fluorocarbon RIE produced the desired changes in columnar SiO_2 GLAD thin film morphology (**5.3 Modified full-plate morphology and development**). However, as-etched plates exhibited poor chromatographic performance. The ~ 1 – 5 nm thick polymer residue that forms on the SiO_2 during fluorocarbon RIE [3–7] was believed primarily responsible (**Figure 5-1**). This fluorocarbon layer is plasma-deposited during the RIE process and serves two purposes [6,7]. It regulates delivery of reactants to the polymer-oxide interface and the activation energy provided by incident ions. When activated by ion bombardment, the polymer itself also reacts with the underlying SiO_2 to produce the volatile etch products COF_x and SiF_x. This reaction consumes the polymer and removes the SiO_2. Etch rate is inversely proportional to steady-state polymer thickness; thinner layers enable higher reactant delivery and incident energies [5].

Several post-RIE treatments were considered. Oxygen plasmas typically used to remove ("ash") polymer residues in microfabrication [6] and ultraviolet ozone cleaning techniques [4] were found insufficient. However, a simple annealing treatment in air (similar to the 30 min 400 °C dry oxygen heat treatment used by Oehrlein *et al*. [3]) desorbed the fluorocarbon residue [3] and restored GLAD UTLC plate performance.

The effects of annealing temperature on the microstructure and development behaviours of RIE-processed GLAD UTLC plates were studied. Scanning electron micrographs and developed plate images for films annealed for 24 hours at varied temperatures (T: not annealed and 100 °C $\leq T \leq$ 500 °C) are provided in **Figure 5-4**. Small spots of CAMAG dye (diluted to 50% in toluene) were applied using 32 gauge blunt-end needles. The corresponding dye component migration distances (Z), retention factors (hR_F), and plate numbers (N) were calculated and plotted in **Figure 5-5**. (See also **Equations (2-4)** and **(2-6)**.) Annealing improved plate performance significantly for T = 100 °C and T = 200 °C. Further increases in temperature (T > 200 °C) showed a monotonic decrease in retention (increase in hR_F) for all analytes. Annealing therefore offered a means of fine-tuning analyte retention on the etched GLAD UTLC stationary phases. The T = 200 °C annealing temperature was selected for all subsequent processing because it provided large plate numbers while still clearly resolving the Oracet Red G dye between the Dimethyl Yellow and Sudan Blue II dye spots.

Observed changes in analyte retention with annealing temperature may be associated with a reduction in specific surface area. It is speculated that each GLAD column's constituent 'fibres' (see for example transmission electron micrographs in Steele *et al*. [10]) soften and merge together, decreasing nanometre-scale surface roughness. Alternatively, there are some reports of silica dehydroxylation at higher temperatures, which may also affect separation behaviour [11]. Further investigation of these effects may yield additional control over GLAD UTLC media.

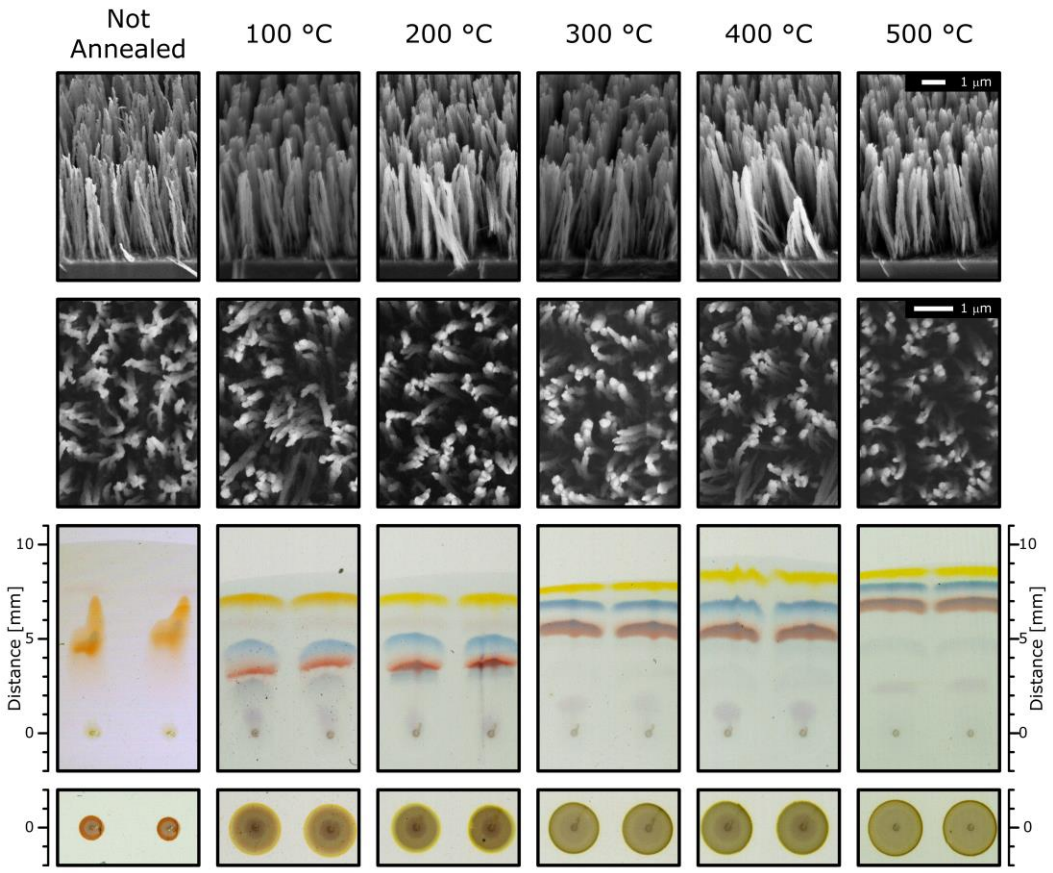

Figure 5-4 Annealing of RIE-processed GLAD UTLC media. Oblique (first row) and top-down (second row) view SEM images as well as corresponding scanned images of applied spots (fourth row) and developed plates (third row). GLAD UTLC plates were etched for 5 min then annealed for 24 hours at various temperatures (not annealed; *T* = 100 °C – 500 °C). Annealed plates were developed for 25 s (21 °C, 46% relative humidity). The processed plate that had not been annealed was developed for 25 s on a different day (20 °C, 39% relative humidity). Scanned images enhanced for presentation. Reproduced with permission from [9]. Copyright (2011) Elsevier.

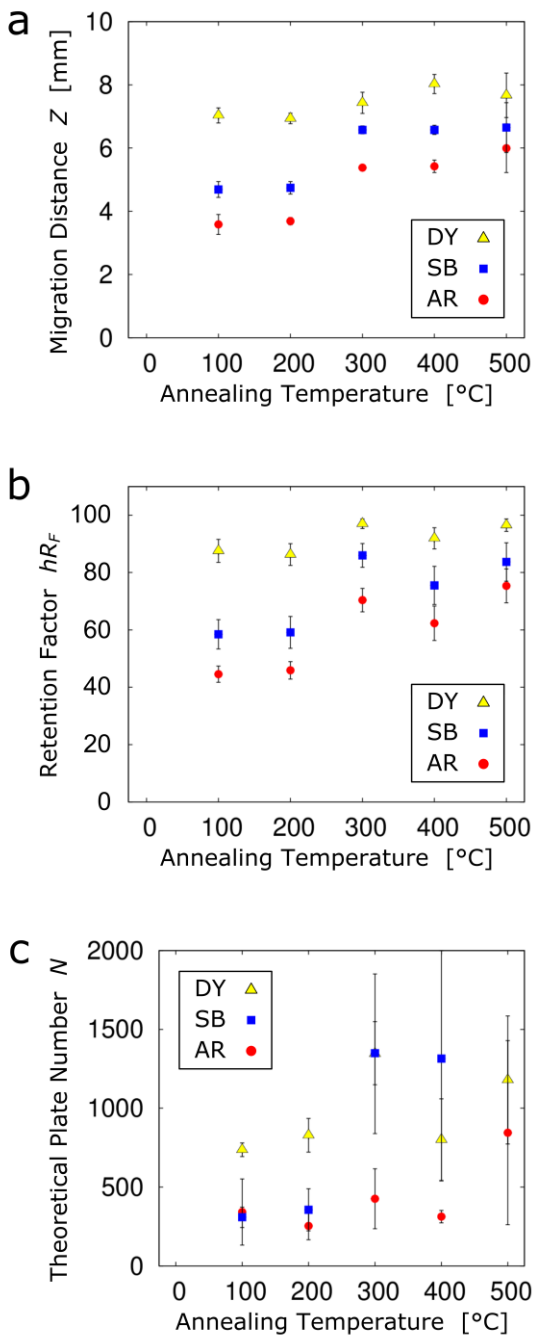

Figure 5-5 (a) Migration distance, (b) retention factor, and (c) plate number as functions of 24 hour anneal temperature on RIE-processed (5 min) GLAD UTLC plates. Dimethyl Yellow (DY, yellow triangles), Sudan Blue II (SB, blue squares), and Ariabel Red (AR, red circles) dye components considered. Temperatures > 200 °C are believed to reduce post surface roughness (surface area) and analyte retention. Plates were developed for 25 s (21 °C, 46% relative humidity). Errors bars reflect variation across 5 separation tracks on the same processed GLAD UTLC plate. Reproduced with permission from [9]. Copyright (2011) Elsevier.

5.3 Modified full-plate morphology and development

Given an effective post-etching annealing treatment (**above**), the impact of RIE duration on GLAD UTLC stationary phase morphology and development behaviour could be studied (**Figure 5-6**). Small spots of 50% diluted dye were again applied using 32 gauge blunt-tip needles to uniformly RIE-processed plates (without concentration zones). Migration distance (Z), retention factor (hR_F), and plate number (N) as functions of etch time (t) are provided in **Figure 5-7**. A smooth transition through approximately three morphological regimes occurred as the full-plate etch time was varied over 0 min $\leq t \leq$ 10 min.

In Regime 1, short etch times (t < 4 min) produced thinned and smoothed GLAD columnar grains. Wider pores within this regime resulted in greater migration velocities. Increases in migration distance enabled corresponding increases in observed plate numbers.

In Regime 2, intermediate etch times (4 min $\leq t \leq$ 8 min) caused a partial collapse of the thinned columnar grains into small clumps. This morphology is similar to that reported for TiO_2 GLAD vertical post films subjected to reactive ion etching [8]. Wide pores between the clumps continued to permit rapid migration while lower specific surface areas caused reduced overall analyte retention (higher hR_F values). Migration distances, retention factors, and plate numbers all increased with etch time within this regime.

In Regime 3, long etch times ($t \geq$ 8 min) caused significant decreases in film thickness and column density. These regions exhibited exceptionally high porosity, low surface area, and low analyte retention. Migration velocities may diminish since the rarefied stationary phase cannot support capillary-driven flow as effectively. Measured plate numbers are artificially high due to analyte front migration. The morphologies and development behaviours achieved by Regime 3 etch times appear well-suited for concentration zones (**below**).

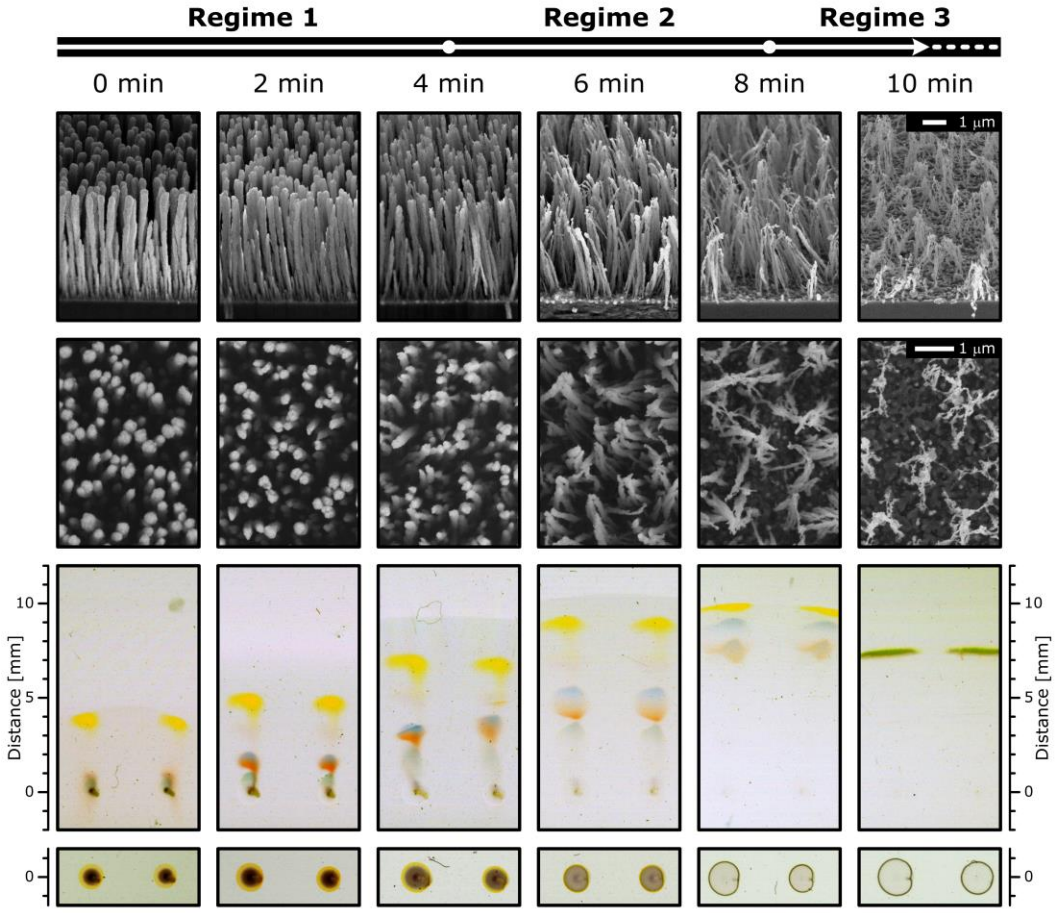

Figure 5-6 Full-plate reactive ion etching to modify GLAD morphology and UTLC performance. Oblique view (first row) and top-down view (second row) SEM images as well as corresponding scanned images of applied spots (fourth row) and developed plates (third row). GLAD UTLC plates without concentration zones were etched for varied durations (t = 0 min – 10 min) then annealed for 24 hours at 200 °C. Plates were developed for 45 s (20 °C, 39% relative humidity). Scanned images enhanced for presentation. Reproduced with permission from [9]. Copyright (2011) Elsevier.

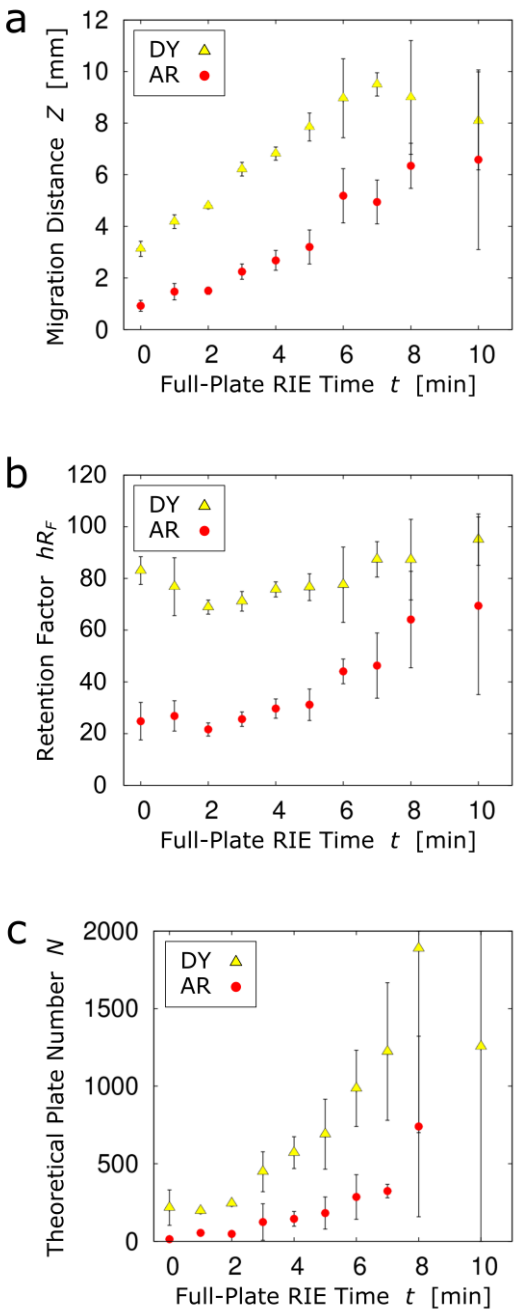

Figure 5-7 (a) Migration distance, (b) retention factor, and (c) plate number for the Dimethyl Yellow (DY, yellow triangles) and Ariabel Red (AR, red circles) dyes as functions of full-plate etch time. Plotted data incorporate results from two different days with development times chosen for good performance; no significant differences between results. Development conditions: 90 s, 21 °C, 49% relative humidity; 45 s, 20 °C, 39% relative humidity. All plates annealed for 24 hours at 200 °C after RIE. Error bars reflect variation across all 9 available separation tracks (5 from day 1 and 4 from day 2). Reproduced with permission from [9]. Copyright (2011) Elsevier.

Reactive ion etch time variation therefore allowed tuning of both migration velocity and analyte retention. Etching the full GLAD UTLC plate for t = 7 min (Regime 2) gave the best analyte retention factor distribution for the given dye sample mixture and mobile phase. It also produced theoretical plates numbers (and migration distances) of N_{DY} = 1200 ± 400 (Z_{DY} = 9.5 ± 0.4 mm) for Dimethyl Yellow and N_{AR} = 320 ± 40 (Z_{AR} = 5.0 ± 0.9 mm) for Ariabel Red. This etch time was selected for the separation zones of the GLAD UTLC concentration zone plates.

Water contact angle measurements were attempted on as-deposited and RIE-processed GLAD SiO_2 films. The hydrophilicity and high porosity of the media caused water droplets to wick into the films and give measured contact angles of ~ 0 ° regardless of their RIE-processing. Therefore this technique did not offer a means of assessing changes in the surface polarity of GLAD UTLC media etched for different durations.

5.4 GLAD UTLC-CZ demonstration

GLAD UTLC concentration zone plates were fabricated using the shadow mask reactive ion etch method described in **5.1.2 Concentration zone processing** and shown schematically in **Figure 5-8**. The morphological and thickness gradients between the resultant concentration and separation zones were characterized by SEM (**Figure 5-9**). These zones had morphologies consistent with RIE Regimes 3 and 2, respectively. Thickness measurements were obtained from edge view SEM images captured at different positions along the cross-section of an etched GLAD UTLC plate. The layer thickness increased from ~ 1.5 μm (concentration zone) to ~ 3.2 μm (separation zone). The width of the interface between these zones was estimated to be ~ 420 μm by fitting a sigmoidal mathematical function [12] to film thickness.

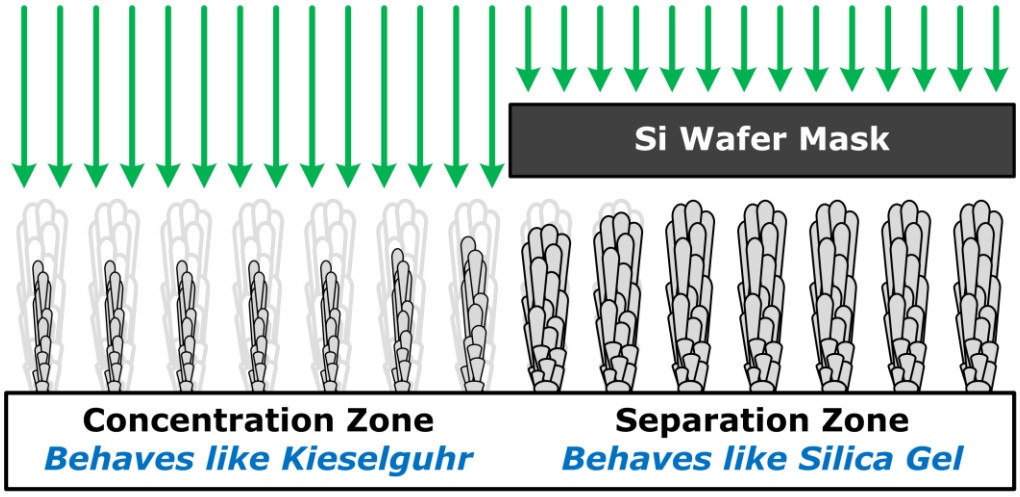

Figure 5-8 Schematic representation of UTLC-CZ fabrication using a Si wafer shadow mask during RIE. The resultant concentration zone has significantly higher porosity and lower surface area.

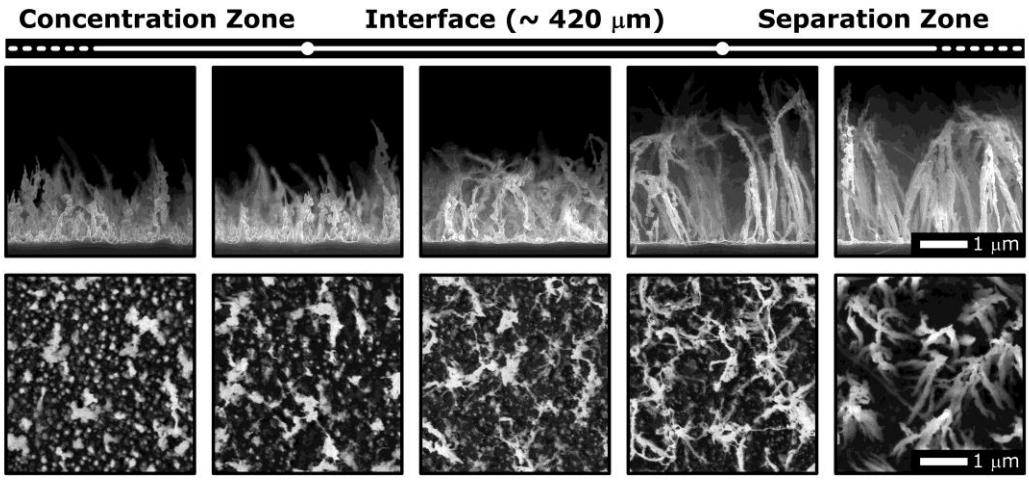

Figure 5-9 SEM images at different positions along a UTLC-CZ interface. Edge and top view micrographs are presented on the top and bottom rows, respectively. Micrographs collected with assistance from J.M.A. Siewert (Glancing Angle Deposition Laboratory, University of Alberta). Bottom right micrograph had its contrast and brightness manually corrected.

The focussing effectiveness of the GLAD UTLC media was evaluated through separations of large volume, low concentration CAMAG dye spots (**Figure 5-10**). Dilute 10% relative dye concentration sample spots were applied by hand using glass capillary tubes (1.0 μL Drummond Microcap; < 1 μL applied volumes). Developments performed on GLAD UTLC plates (with layers etched for 7 min) produced faint arc-shaped dye bands. On the other hand, the GLAD UTLC concentration zone media produced well-defined bands that were darker and straighter. The chromatogram signals for the yellow and red channels are included along with the scanned plate images in **Figure 5-10**. Qualitatively, peak height and width were improved for the GLAD UTLC concentration zone plates. However, limited control over capillary tube spot volumes prevented quantification of this improvement in this initial demonstration.

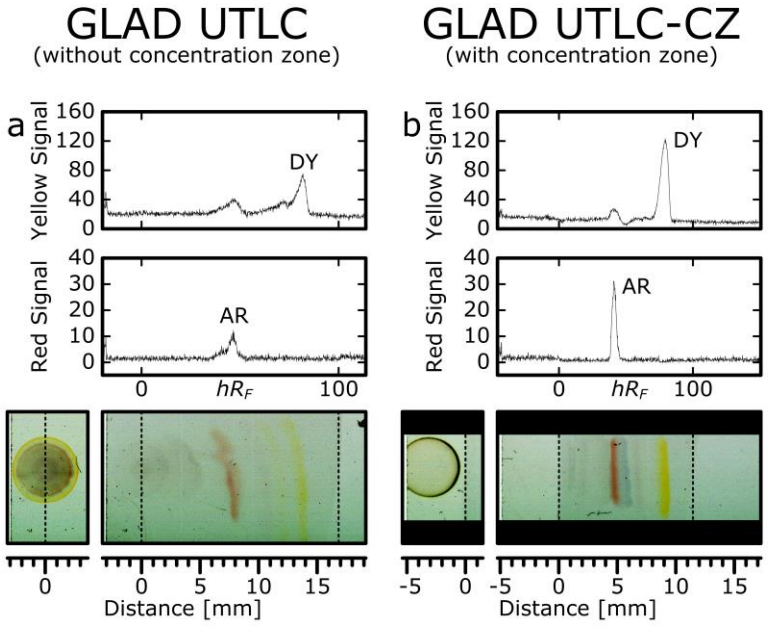

Figure 5-10 Large volume dye spots applied with a glass capillary tube separated on (a) GLAD UTLC plates and (b) GLAD UTLC-CZ plates. The applied dye mixture was diluted to 10%. Chromatograms produced using the colour-filtered yellow and red signals are provided above their respective scanned images. Developments were performed for ~ 60 s (22 °C, 14% relative humidity ambient). Images enhanced for presentation. Reproduced with permission from [9]. Copyright (2011) Elsevier.

5.5 Conclusions

Reactive ion etching and a subsequent annealing treatment modified thin film stationary phase morphology, tuning GLAD UTLC development behaviours. Widened pores and reduced specific surface areas increased migration velocity and decreased analyte retention on etched ultrathin-layer chromatography media. Variation of RIE duration enabled increases in migration distance by up to a factor of three for Dimethyl Yellow (~ 3 - 9 mm) and up to a factor of six for Ariabel Red (~ 1 - 6 mm). The treatments further permitted modulation of the retention factors within hR_F ~ 65 - 90 for Dimethyl Yellow and hR_F ~ 20 - 70 for Ariabel Red. Plate numbers were found to increase monotonically with etch duration to values in excess of 1000. In this study, the partially collapsed etched column morphology (Regime 2, 7 min etch duration) produced high separation efficiencies and the best analyte retention factor distribution.

The RIE technique also enabled patterning of adjacent concentration and separation zones with vastly different development behaviours to produce GLAD UTLC concentration zone plates. These GLAD UTLC-CZ plates had concentration zones etched for 22 min (Regime 3) and separation zones etched for 7 min (Regime 2). The concentration zones focussed applied spots into narrow bands at their interface, facilitating high-quality separations of hand-spotted large volume dilute sample mixtures. Similar GLAD UTLC-CZ plates with optimized separation and concentration zones may prove practical in analytical or organic laboratories where precise low volume sample spotting is unavailable. Further improvements may be achieved in the future by incorporating the rapid migration velocities and reduced transverse broadening capabilities of anisotropic GLAD UTLC layers (**4 Anisotropic UTLC microstructures**).

References

[1] Z. Huang, K.D. Harris, M.J. Brett, Morphology Control of Nanotube Arrays, Adv. Mater. 21 (2009) 2983–2987.

[2] J.K. Kwan, J.C. Sit, The use of ion-milling to control clustering of nanostructured, columnar thin films., Nanotechnology. 21 (2010) 295301.

[3] G.S. Oehrlein, J.G. Clabes, P. Spirito, Investigation of Reactive-Ion-Etching-Related Fluorocarbon Film Deposition onto Silicon and a New Method for Surface Residue Removal, J. Electrochem. Soc. 133 (1986) 1002.

[4] R. Jackson, A. Pidduck, M. Green, Removal of surface contamination after reactive ion etching of silicon dioxide, Vacuum. 45 (1994) 519–524.

[5] M. Schaepkens, T.E.F.M. Standaert, N.R. Rueger, P.G.M. Sebel, G.S. Oehrlein, J.M. Cook, Study of the SiO2-to-Si3N4 etch selectivity mechanism in inductively coupled fluorocarbon plasmas and a comparison with the SiO2-to-Si mechanism, J. Vac. Sci. Technol. A. 17 (1999) 26–37.

[6] A. Sankaran, M.J. Kushner, Integrated feature scale modeling of plasma processing of porous and solid SiO2. I. Fluorocarbon etching, J. Vac. Sci. Technol. A. 22 (2004) 1242–1259.

[7] A. Sankaran, M.J. Kushner, Integrated feature scale modeling of plasma processing of porous and solid SiO2. II. Residual fluorocarbon polymer stripping and barrier layer deposition, J. Vac. Sci. Technol. A. 22 (2004) 1260–1274.

[8] M.R. Kupsta, M.T. Taschuk, M.J. Brett, J.C. Sit, Reactive Ion Etching of Columnar Nanostructured TiO2 Thin Films for Modified Relative Humidity Sensor Response Time, IEEE Sens. J. 9 (2009) 1979–1986.

[9] S.R. Jim, A.J. Oko, M.T. Taschuk, M.J. Brett, Morphological modification of nanostructured ultrathin-layer chromatography stationary phases, J. Chromatogr. A. 1218 (2011) 7203–7210.

[10] J.J. Steele, M.T. Taschuk, M.J. Brett, Nanostructured Metal Oxide Thin Films for Humidity Sensors, IEEE Sens. J. 8 (2008) 1422–1429.

[11] K.K. Unger, Porous silica, its properties and use as suport in column liquid chromatography, Elsevier, Amsterdam, 1979.

[12] D.H. von Seggern, CRC Standard Curves and Surfaces with Mathematica, 2nd ed., CRC Press [Taylor and Francis], Boca Raton, 2007.

6 Time-resolved UTLC

The quality of a planar chromatography separation depends on more than just the properties of the stationary phase. Overall performance depends on the sample analytes, mobile phase selection, development technique, instrumentation, and many other factors. The absence of appropriate spotting, imaging, and development instrumentation can severely hinder separations on UTLC layers [1,2]. Some of these factors are pronounced on nanostructured GLAD UTLC layers. For example, rapid migration across these layers enables extremely fast separations but can also distort separation patterns when the GLAD UTLC plate is removed from the development chamber and dried. This chapter focuses on improved methods of imaging and analyzing separations performed on GLAD UTLC layers. Time-resolved UTLC (TR-UTLC) methods collect data throughout planar chromatography developments and negate distortions that can occur when the plate is removed. The technique improves performance and provides rich insight into how chromatographic figures of merit change with development time [3].

6.1 Overview of enhanced approach

This work builds upon the previously published TR-UTLC proof-of-concept developed in partnership with A.J. Oko[1] [3]. Videos of UTLC separations performed in a horizontal development chamber are recorded using a high definition video camera (EOS Rebel T2i digital single lens reflex, Canon) equipped with a dedicated macro lens (EF 100 mm f/2.8 USM, Canon). Frames extracted from each video are analyzed using custom programming scripts prepared for MATLAB. These algorithms generate and fit hue (colour) filtered chromatograms from each separation track in each extracted frame. This method enables automated calculation of chromatographic figures of merit at different instants in time during the development. The potential advantages of TR-UTLC were demonstrated in the initial report using optimized separations of undiluted dyes separated on monolithic silica gel UTLC plates [3]. This chapter describes implementation and demonstration of the enhancements required to extend TR-UTLC to unoptimized separations of diluted dyes on GLAD UTLC media.

GLAD UTLC's thinner layers introduced several challenges. Applied dye spots need to be of lower concentration and volume since these layers are prone to overloading [1]. The image background was different since GLAD film stationary phases are more translucent than the thicker monolithic UTLC layers. Identification of the mobile phase migration front was also especially difficult. Fitting algorithm reliability was improved to address these problems.

The overall utility of the enhanced TR-UTLC approach was also increased in many different ways. The analysis package was made more user-friendly by incorporating graphical and numerical inputs. (This information doesn't need to

[1] A.J. Oko and S.R. Jim worked closely during this earlier proof-of-concept project [3]. A.J. Oko designed the imaging cabinet, selected and installed the LED light sources, calibrated the camera, performed dye separations on monolithic UTLC plates, implemented the first TR-UTLC code iteration, and drafted the paper. S.R. Jim selected the video camera and lens, assisted in camera calibration, provided original single-image hue-filtered chromatogram MATLAB code (written for use in a preceding work [2]), expanded and verified A.J. Oko's first TR-UTLC code (revised code used in final data analysis), frequently discussed results and interpretation, and revised the paper.

The new enhancements described in this chapter advanced this previously reported proof-of-concept into a practical tool for UTLC.

be coded directly into the programming scripts.) Relevant parameters defined in each UTLC separation video's initialization "recipe file[2]" can now be saved, edited, reviewed, and automatically checked for errors. (See **6.3.2 Define processing parameters**.) This allows even those unfamiliar with the program's inner workings to use the analysis package. New automation capabilities allow high-throughput batch processing of several videos without user intervention. Additional new programming scripts improve interpretation of the results by facilitating intra- and inter-plate comparisons.

6.2 Recording GLAD UTLC separation videos

GLAD UTLC dye separation videos were recorded in a similar manner to that reported previously [3,4]. Developments were performed in a horizontal development chamber (see modified Desaga chamber in **Figure 3-6** and customized GLAD UTLC chamber in **Figure 8-1**) illuminated by white light emitting diodes (LEDs) within a covered booth (**Figure 3-8**). A pulse width modulator controller was purchased so that the intensity of the white LEDs could be reduced. Although using this controller to manipulate the duty cycle reduced the apparent brightness, the frequency of the on-off switching was of similar magnitude to that of the video camera frame rate. This introduced a flicker to the recorded videos. Therefore, the dimming feature could not be used in this work. The DSLR camera was operated in full 1080p high definition video mode (1920 pixels x 1080 pixels per frame; 30 fps). Its exposure settings were manually set and ensured constant throughout the development (ISO 400, shutter speed 1/100 s, lens aperture f/3.2) and its white point was set using a calibrated colour standard (Munsell ColorChecker Chart, ColorAccuracy.com, Lincroft, NJ, USA). The camera settings had been selected to achieve adequate agreement between the measured and certified rgb values of the colour swatches.

[2] A.J. Oko employed recipe (initialization) files in the first TR-UTLC implementation. These are very effective in storing parameter definitions required for subsequent analysis. Without such recipe files, the user would need to set the parameters at runtime for each data set. This approach was extended to the enhanced TR-UTLC algorithms.

Each video was used to produce a directory of sequentially numbered frame images. Video frames could be extracted from the recorded *.MOV video files using any appropriate method since the enhanced TR-UTLC suite enabled either JPEG or TIFF image formats. The ZoomBrowser EX software (version 6.5.1.15, Canon) was used to export frames at typically 2 fps (every 15th frame) as JPEG images (8 bits per rgb channel) [3]. M.T. Taschuk also used Python [5] to export frames as TIFF images (8 bits per rgb channel) at the same rate. Extracting frames at higher rates is possible but was generally of little benefit to GLAD UTLC separation analysis. Extraneous frames from before or after the

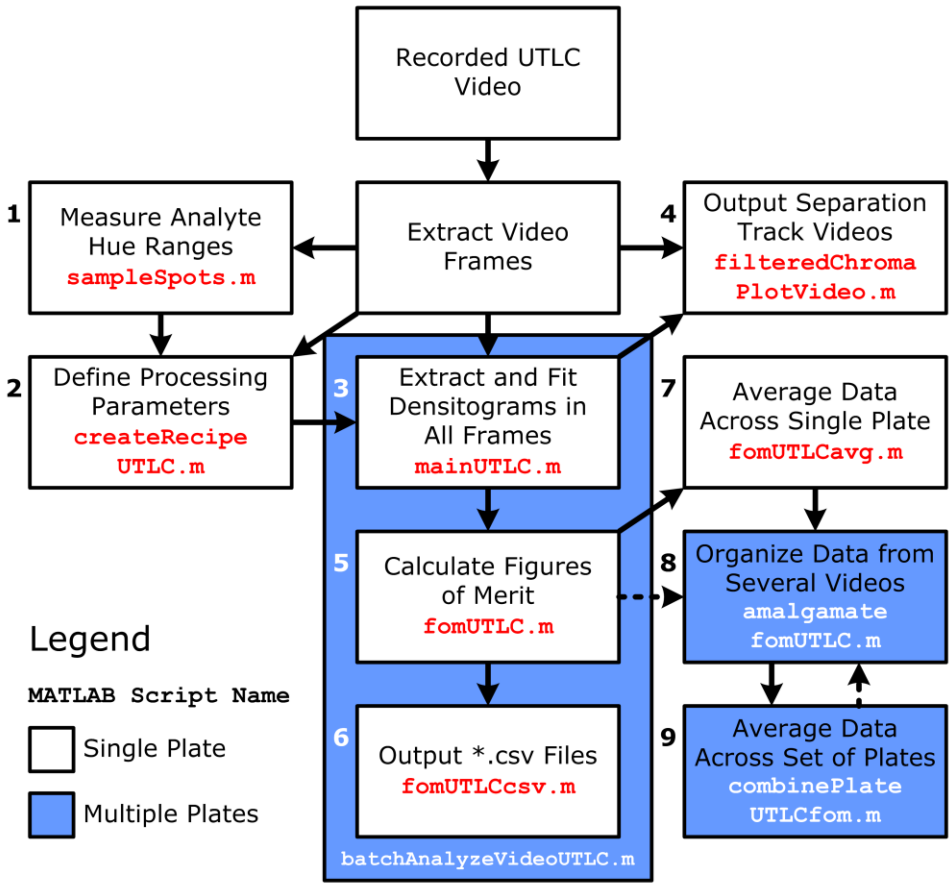

Figure 6-1 Overview of enhanced time-resolved UTLC process flow. Some MATLAB programming scripts operate on individual data sets (white). Others are used to process or collect several data sets together (blue). The initial TR-UTLC approach [3] employed scripts analogous to those in steps 1-3, 5, and 6.

development were removed prior to image processing. The first video frame in the directory was considered to be the start of the development.

6.3 Implementation

The enhanced TR-UTLC process flow is outlined in **Figure 6-1**. The series of MATLAB scripts enabled each set of extracted GLAD UTLC separation video frames to be analyzed and interpreted in numerous ways. Key aspects about each of these steps are provided below. Further details about and excerpts from the final MATLAB *.m scripts are provided in **C Time-resolved UTLC scripts**. Representative figures outlining this process (**Figure 6-2** through **Figure 6-6**) correspond to a data set collected when processing videos of separations in the modified Desaga development chamber. Note that this data is also compared to that of the customized GLAD UTLC chamber in **8.3 Chamber testing**.

A modified script modelled on the TR-UTLC package was also created for use on single video frames. This **`singleImageUTLC.m`** script incorporates steps 1-3, 5, and 6 in **Figure 6-1** and is also provided in the same appendix.

6.3.1 Measure analyte hue ranges

TR-UTLC employs hue (colour) filters to distinguish signals associated with different analytes. Considerable care must therefore be taken to define appropriate filters. **`sampleSpots.m`** enables the user to sample the pixels of different coloured analyte spots in a selected video frame. The script uses a graphical interface that allows the user to select pixels from each analyte spot on each separation track. For each analyte, the script generates a signal $A(j)$ that plots the totalled saturation values at each integer hue value bin number ($\{j \in \mathbb{Z} | 0 \leq j \leq 359\}$) according to the equations:

$$A(j) = \sum_{i=1}^{nPixels} s_i \cdot \delta(h_i', j) \qquad \textbf{(6-1)}$$

$$\text{where } \delta(h_i', j) = \begin{cases} 1 & if \quad h_i' = j \\ 0 & else \end{cases}$$

$$\text{and } nPixels = \sum_{n=1}^{nTracks} W_n \cdot L_n$$

In these equations, s_i and h_i' are the saturation value and rounded hue value of the i^{th} pixel; W_n and L_n are the width and length of the rectangular region sampled from the given analyte's spot on the n^{th} separation track; and *nTracks* is the total number of tracks. Incorporating analyte spot pixels from all tracks ensures that possible variations in the hue values of spots of different analyte mass are considered. (Similar analysis is also performed separately on each sampled region.) This allows the user to measure the range of hues associated with each analyte (**Figure 6-2**). The same script can also be used to assess the background hues in the image. Appropriate hue filters can therefore be determined by performing this process on a frame from each UTLC video in the set.

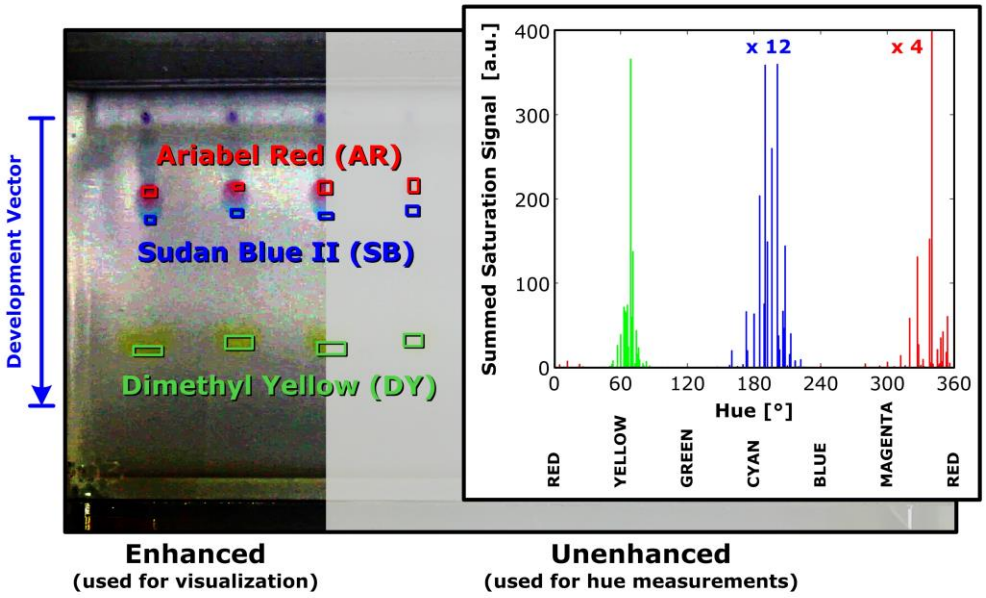

Figure 6-2 Overview of hue measurement process. Pixels selected from analyte spots on each track (left) are used to produce signals (right) from which associated hues may be measured. Although image enhancements ease spot localization, only pixels isolated from the unenhanced image are analyzed.

6.3.2 Define processing parameters

Setting up the analysis for each UTLC separation video requires the majority of the user's effort. **`createRecipeUTLC.m`** is used to create the recipe file (initialization file) for each separation video. This MATLAB *.mat data file stores about a dozen parameters required by subsequent scripts. These parameters are defined through a combination of graphical and numerical input tools. Optional image enhancements may be used to ease visual identification of important features (for example, spot and migration front positions). However, chromatograms are extracted only from the unenhanced images. The parameters may be reviewed, edited, and checked for errors by running this script. This information is saved periodically so that the lengthy process can be interrupted as required.

The script first sets the input and output file directories. It then permits calibration of the frame resolution by locating a rectangle (or line) of known dimension within the video frame. For example, the edge length of a square GLAD UTLC plate was known to be 25.4 mm long. A calibrated rule located in the frame may also be used (see **8.2.9 In-frame size standard**). Typical frame resolutions are within 35-38 pixels mm^{-1}. It then defines the number and initial locations of the applied dye spots and separation tracks (**Figure 6-3**).

Information about the specific analytes is also defined using this script. The user sets the names and hue filters associated with each analyte. The k^{th} analyte's hue range is defined as an inclusive interval $[h_{k,min}, h_{k,max}]$. For example, a yellow analyte could be assigned a filter [30, 90]°. Applied spot volumes, sample concentrations, and analyte masses may be set if desired.

Locating the migration front position at different development times can be particularly challenging. Automatic identification of this feature from video frame images was very difficult to implement. As in the first iteration of the TR-UTLC analysis method [3], the user instead manually identifies the migration front at different times throughout the development using a sub-function

`frontFit.m`. These data points are then used to fit the migration front position (Z_F) according to the equation:

$$Z_F = \sqrt{\chi(t + t_{start})} + Z_{start} \quad \textbf{(6-2)}$$

Using fitting parameters χ (in pixels^2 frame^{-1}), t_{start} (in frames) and Z_{start} (in pixels). This modified version of **Equation (2-1)** contains the additional constants t_{start} and Z_{start} that compensate for developments beginning slightly before the first extracted video frame and for the effective position of the mobile phase source. The **`frontFit.m`** sub-function uses a graphical interface to show enhanced separation track images with adjacent regions and calculated rgb and lightness signals (**Figure 6-4**). The process is still tedious, but the trained eye can use these tools to pick the appropriate migration front positions in frames corresponding to different development times. More of the frames are selected early into the development when migration front velocity is greatest. The user has the option to create a unique migration front fit for each separation track. This

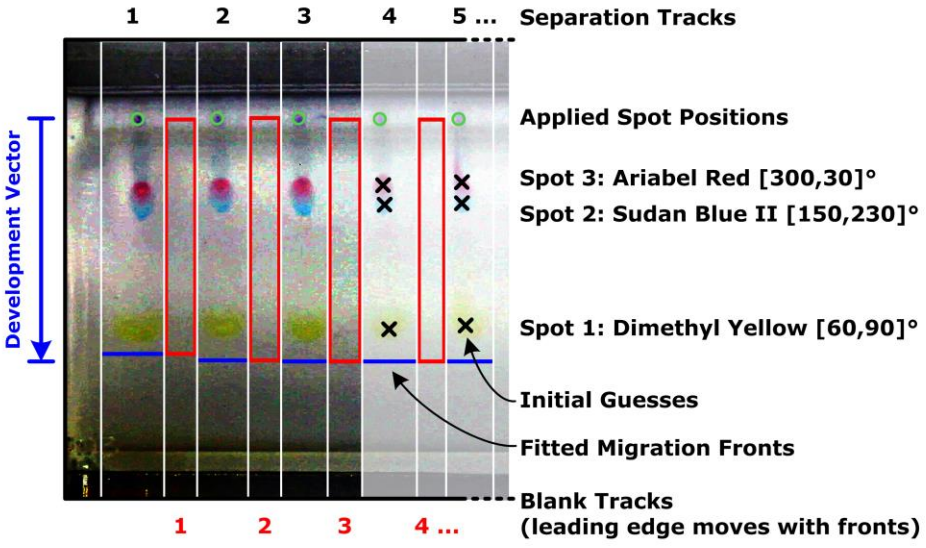

Figure 6-3 Parameters defined prior to TR-UTLC processing. The locations of separation tracks, applied spots, and initial guesses are specified by the user. Analyte names and associated hue filters are recorded. Migration front fits are calculated (see **Figure 6-4**). Blank tracks between separation tracks are automatically defined.

improves accuracy especially in cases where the migration front is bowed due to increased evaporation and slower migration along the plate edges. (See also **8.3.1 Intra-plate variation** for discussion of bowed front implications.)

The user provides initial guesses on the analyte hR_F values using a video frame midway through the development. As the hR_F values are relatively constant through the development, they may be used to define initial regions of interest for Gaussian peak fitting (**below**).

Finally, the **`createRecipeUTLC.m`** automatically defines blank regions between adjacent separation tracks (**Figure 6-3**). The edge of the blank region can be made to advance with the migration front. These regions may be used to estimate noise and limits of detection (LOD) in each video frame.

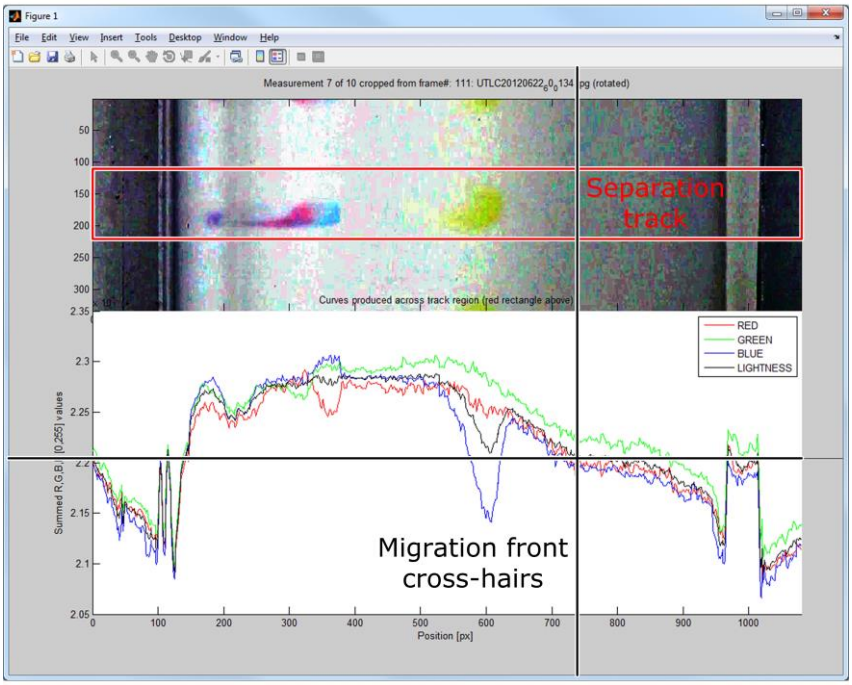

Figure 6-4 Graphical interface for migration front selection. An enhanced image of the separation track (red rectangle) and adjacent regions is shown in the top. Summed red, green, blue, and lightness signals produced by integrating across the width of the unenhanced track are shown below. These images and plots allow the user to identify front position using cursors (black cross-hairs). Clicking records the selected position and loads another video frame. (Overlaid labels and bolded rectangle and cross-hairs added for clarity.)

6.3.3 Extract and fit densitograms in all frames

Hue-filtered densitograms are produced for each analyte spot on each separation track in each video frame using **`mainUTLC.m`**. This script processes the full directory of extracted video frames using parameters defined in the recipe file by **`createRecipeUTLC.m`**.

The sub-function **`filteredDensitogram.m`** generates hue-filtered densitograms by converting pixel rgb values to hsv values (**3.6.1 Colour models and transformation**). It then forces all pixels with hue outside of the given filter to have a saturation value of 0. Remaining saturation values are integrated across the width of the separation track. This method is expressed using the equation [3]:

$$D_k(t,x) = \sum_{y=1}^{W} s(t,x,y) \text{ for } \{h_{k,min} \leq h(t,x,y) \leq h_{k,max}\} \quad \textbf{(6-3)}$$

Where x is the pixel position along the track length, y is the pixel position along the track width (W), k is the analyte hue filter, t is the time into development, $s(t,x,y)$ is the saturation, and $h(t,x,y)$ is the hue. The filtered densitograms may be discarded after processing or saved for use when generating separation track videos (**below**). This sub-function is also used to analyze the saturation values of the blank regions.

Another sub-function **`iterativeGaussFit.m`** is used to fit Gaussian peaks to each extracted hue-filtered densitogram. While other more complicated peak definitions may be implemented [6,7], Gaussian fits were generally adequate in this analysis. The raw data and initial fitting limits, and other fitting criteria are supplied to **`iterativeGaussFit.m`**. Assuming that enough data points exist within the fitting limits, this custom function uses MATLAB's built-in `nlinfit` nonlinear fitting algorithm. Each set of output parameters is automatically used to define new fitting limits for a subsequent iteration. This approach is more tolerant of initial fitting regions that are too large, too small, or slightly misaligned

(**Figure 6-5**). It also excludes raw signal artefacts (for example, the edge of the UTLC plate) far from the chromatogram peak. Whenever `nlinfit` returns a Gaussian fit, residuals are calculated by subtracting this fit from the raw signal. Noise is estimated as the standard deviation in these residuals and used to assess whether two key acceptance criteria are satisfied: (1) the fitted peak amplitude must be at least 6 times greater than the noise; and (2) the fitting region must be wide enough that, with 99% (3 σ) certainty, it contains at least the top half of the peak. Although **`iterativeGaussFit.m`** can return any fit that satisfies these criteria, it uses up to 10 subsequent iterations to improve the fitted parameters when possible. Fit convergence is achieved when the fitted standard deviations differ by less than 1% between subsequent iterations. Therefore, fits returned by the function at least satisfy the acceptance criteria and ideally also satisfy the convergence criteria. The **`mainUTLC.m`** script uses these Gaussian peak fits to calculate analyte peak positions (Z) and widths (standard deviations and FWHM).

6.3.4 Output separation track videos

The hue-filtered densitograms and Gaussian peak fits produced by **`mainUTLC.m`** can be previewed in videos generated by **`filteredChromaPlotVideo.m`**. This optional diagnostic step creates a short video showing the evolution of the separation track, calculated densitograms, and fitted Gaussians over the course of the development (**Figure 6-6**). Such videos are useful in verifying expected execution of the above scripts.

6.3.5 Calculate figures of merit

The Gaussian peak fits are used to calculate standard planar chromatography figures of merit using **`fomUTLC.m`**. This script calculates hR_F, FWHM, N, and H for each analyte peak on all tracks in all video frames. (See relevant formulae in **2.1.2 Chromatograms and performance metrics**.) The script can also be used to calculate the resolution between each pair of analytes, estimate the LOD when sufficient mass ranges exist, and estimate separation number [8] when sufficient numbers of analytes exist.

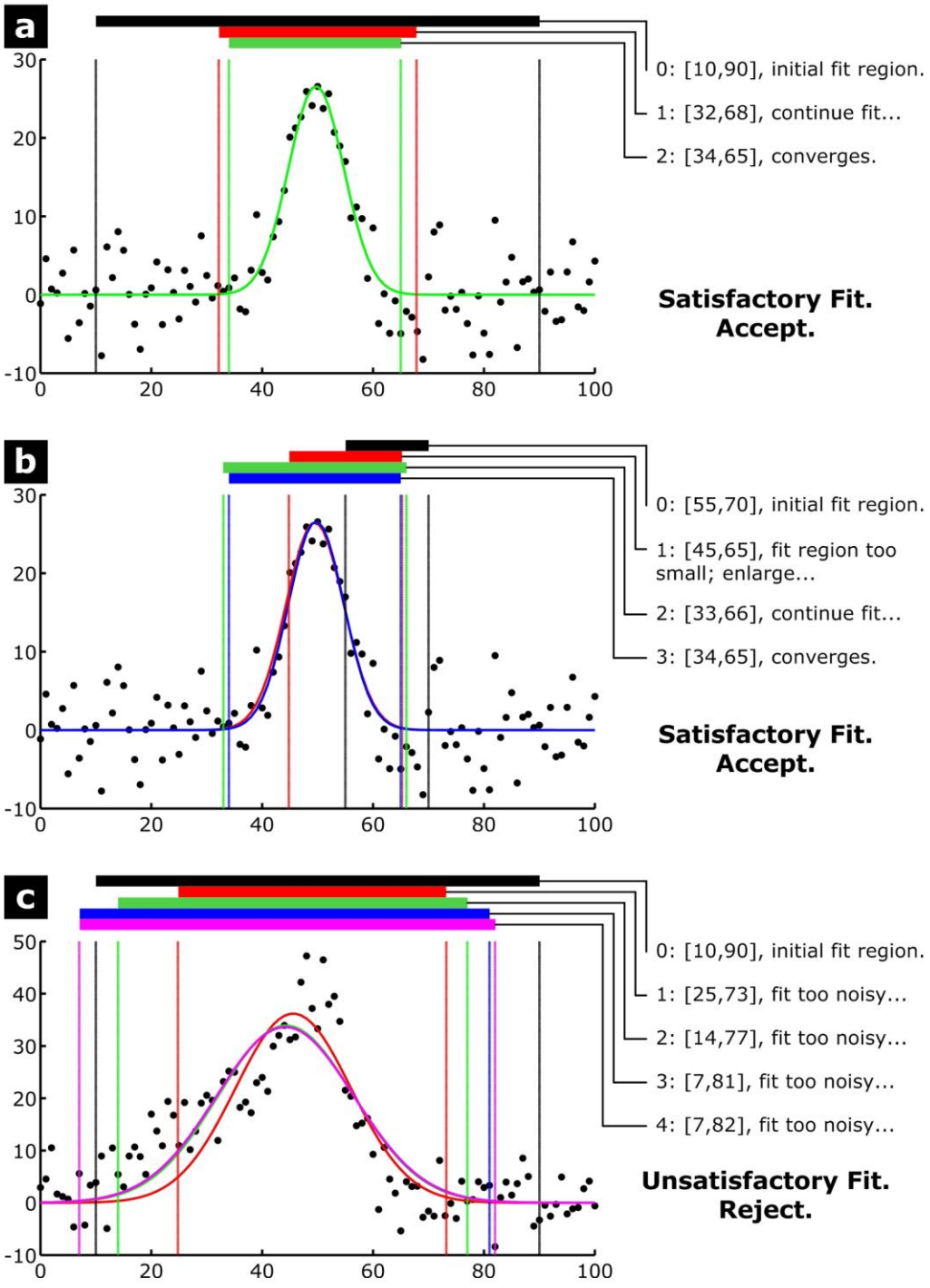

Figure 6-5 Iterative Gaussian fit testing. The algorithm converges even if the initial fitting region is (a) too large or (b) small and slightly misaligned. (c) The algorithm invalidates fits to signals that are too noisy or appear composed of multiple peaks. Coloured bars and limits within the square brackets represent the fitting interval used in each iteration.

6.3.6 Output *.csv files and UTLC video batch processing

The TR-UTLC scripts are designed to handle MATLAB's proprietary *.mat format. **`fomUTLCcsv.m`** is an optional script used to output the calculated figures of merit as *.csv files when platform-independent data formats are preferred. Each figure of merit's data array is output as a separate file and a summary text file (*.txt) provides an overview of the analysis performed.

Although **`mainUTLC.m`**, **`fomUTLC.m`**, and **`fomUTLCcsv.m`** may be run independently, **`batchAnalyzeVideoUTLC.m`** may be more convenient when processing several similar UTLC separation videos. This script enables processing of a series of recipe files without further user intervention.

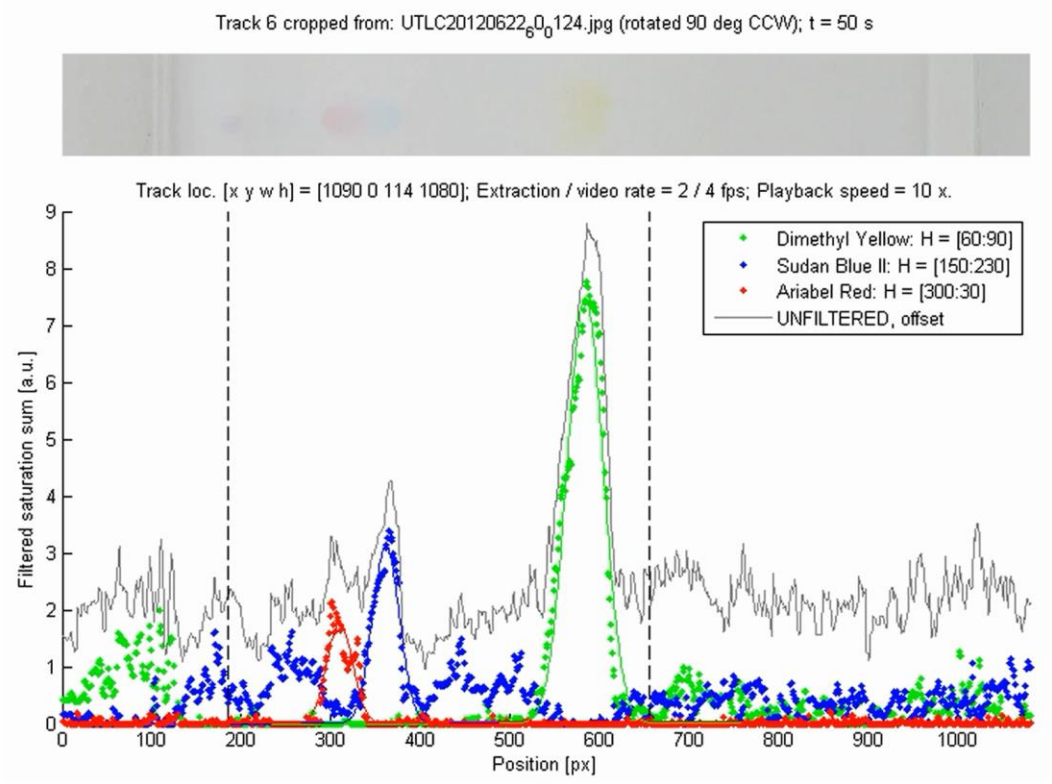

Figure 6-6 Screenshot from GLAD UTLC separation track video. Raw extracted chromatograms and their associated Gaussian peak fits are shown beneath the corresponding separation track image. Dashed vertical lines indicate positions of the applied spot (left) and fitted migration front (right).

6.3.7 Average data across a single UTLC plate

The TR-UTLC scripts generate overwhelming amounts of data. A typical separation video may produce 8 figure of merit arrays for 3 analytes on 9 tracks in 250 frames. One method of increasing the validity and reducing the volume of this data is to average. **`fomUTLCavg.m`** is used to average the calculated figures of merit across (similarly loaded) separation tracks on a given plate. This script can be used to generate an arbitrary number of signals calculated by including any combination of separation tracks together. It calculates averages and standard deviations for each relevant figure of merit at each instant in time (video frame). It can be used when considering averages across all tracks or excluding specific tracks. This is helpful in cases when the outermost tracks should be excluded (due to a bowed migration front) or a GLAD UTLC layer defect (scratch) distorts the chromatogram. This script was used to assess figure of merit variations for tracks on single plates developed in the Desaga and customized GLAD UTLC chambers (**8.3.1 Intra-plate variation)**.

6.3.8 Organize data from several UTLC plates

Processing a single UTLC separation video generates more than a hundred variables. These store parameters from the recipe file, information about the analyses performed, and the calculated data. **`amalgamatefomUTLC.m`** collects and organizes the data from multiple UTLC plates (videos) to enable plate-to-plate comparisons. (*.mat files generated by **`fomUTLCavg.m`** also contain all data produced by **`fomUTLC.m`**; files output by either script may be loaded.) This amalgamation script places data from each video into a 3D virtual array of data structures. Once in this form, the effects of up to three different UTLC development variables can be studied. For instance, a 3 x 2 x 4 array may organize separation data on GLAD UTLC plates processed with combinations of different architectures (vertical post, chevron, SBD), deposition angle (α = 85°, 87°), and RIE etch durations (0, 1, 2, 4 min). Careful organization makes plotting of calculated data and determination of possible trends easier.

The script is also used to organize calculated figures of merit for redundant TR-UTLC videos so that they may be combined together (see **below**). Combined data sets can also themselves be organized using the **`amalgamatefomUTLC.m`** script.

6.3.9 Average data across a set of UTLC plates

The user may combine the figures of merit calculated from similarly loaded separation tracks in redundant GLAD UTLC development videos. **`combinePlateUTLCfom.m`** combines separation video data that was organized into a 1D array using **`amalgamatefomUTLC.m`**. The script generates figure of merit averages and standard deviations across all available tracks at each development time. The script was used to assess run-to-run changes in figures of merit when evaluating the customized GLAD UTLC chamber (**8.3.2 Inter-plate variation**).

6.4 Application of TR-UTLC to alternative GLAD UTLC metal oxides

The TR-UTLC approach was recent applied to a study of GLAD UTLC plates prepared from various metal oxides: SiO_2, Al_2O_3, TiO_2, and ZrO_2 [4]. S.R. Jim used versions of the MATLAB scripts described above to analyze experimental data collected by J. Wannenmacher (diplom thesis student, Universität Hohenheim, Stuttgart, Germany). The TR-UTLC scripts provided insight into the development behaviours of these materials with and without post-deposition treatments. Food dye separations on the ZrO_2 media were particularly interesting and are described below as a practical demonstration of TR-UTLC's utility.

Anisotropic SBD ZrO_2 GLAD thin films (~ 2.6 μm thick, α = 87.5 °) were prepared using protocols similar to those in **3.1 GLAD thin film fabrication**. Post-deposition oxidation heat treatments (in atmosphere for 24 h at 200 °C) and UV irradiation treatments (under an 8 W Hg lamp for 72 h) performed prior to use influenced their chromatographic properties. As per the Office Chromatography

approach [4,9,10], aqueous food dye mixtures were applied using an inkjet printer (Pixma MG 5320, Canon; see also **3.3.5 Inkjet printing**). The undiluted dye mixture contained Green B (GB, ~ 7 ng nL^{-1}), Acid Red 14 (AR, ~ 12 ng nL^{-1}), Tartrazine (T, ~ 12 ng nL^{-1}), and Brilliant Black BN (BB, ~ 7 ng nL^{-1}). Spotted plates were developed in the modified CAMAG horizontal chamber without vapour saturation using ethyl acetate / methanol / water mobile phases[3]. Video frames from food dye separations on the treated ZrO_2 media are shown in **Figure 6-7**. In the cropped separation tracks, undiluted dyes were separated from bands applied using an inkjet printer (~ 14 nL). Although the qualitative comparisons in this figure are informative, improved insight was possible using TR-UTLC.

The collected data analyzed and reported in [4] was reanalyzed after publication using the updated TR-UTLC scripts described in this chapter. (Steps 1-3 and 5-8 in **Figure 6-1** were completed.) Hue-filtered densitograms extracted

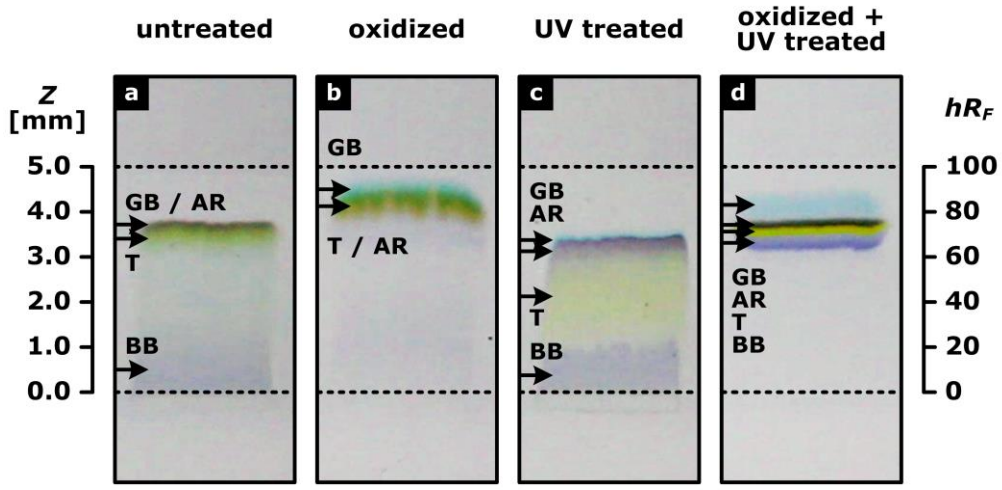

Figure 6-7 Food dye separation chromatograms on ~ 2.6 μm thick α = 87.5° ZrO_2 thin film GLAD UTLC plates that were (a) untreated, (b) oxidized at 200 °C for 24 hr, (c) irradiated with UV for 72 h, and (d) oxidized then irradiated. Green B (GB), Acid Red 14 (AR), Tartrazine (T), and Brilliant Black BN (BB) were separated. Crops were taken from frames selected at different development times so that Z_F = 5 mm. Images enhanced for presentation. Figure modified with permission from [4]. Copyright (2013) Elsevier.

[3] Exact mobile phase compositions optimized for each oxide. A small amount of formic acid was added for separations on TiO_2 layers.

from 3-4 separation tracks in many video frames were fit with Gaussian peaks. Applied undiluted dye bands had volumes between ~ 7-28 nL. This analysis provided further study of the effects of treating ZrO_2 GLAD UTLC layers. Calculated plate-averaged figures of merit are presented in **Figure 6-8** (Z and FWHM), **Figure 6-9** (hR_F), and **Figure 6-10** (H and N). The figures exclude some of the collected data: (1) the Brilliant Black spots were too faint for reliable detection; and (2) the video of the un-oxidized UV-irradiated plate was accidentally started midway through the development. These signals were removed for clarity.

TR-UTLC analysis provides valuable insight into the manner in which each coloured dye spot migrates and broadens when separated on the treated ZrO_2 media. For instance, **Figure 6-8b** suggests that Green S broadening occurred most rapidly over the first ~ 30 s of the development performed on heat treated and UV-irradiated GLAD ZrO_2. Meanwhile, **Figure 6-9** illustrates that it took at least ~ 50 s for the dyes to separate and produce meaningful hR_F measurements. **Figure 6-10** indicates that analyte plate heights stabilized after some time but that plate heights continued to increase. Thus the TR-UTLC approach offers guidance on the minimum development time required for adequate separation and chromatographic figure of merit stabilization.

Although only single plates (videos) for each treatment are considered here, the figures suggest interesting trends. **Figure 6-9** indicates that oxidation heat treatments reduced analyte retention while UV-irradiation increased analyte retention. However, the effects of the heat treatment were dominant on the layer oxidized before UV exposure. **Figure 6-10** shows that good separation efficiency was achieved in many cases. The excellent plate heights (H < 5 μm) are attributed to the sharp dye bands applied using the inkjet printer but the moderate plate numbers (N > 1000) are due to the short migration distances (< 6 mm, **Figure 6-8**). An extended study involving more GLAD UTLC plates would enable improved quantification of these post-processing effects and overall separation performance.

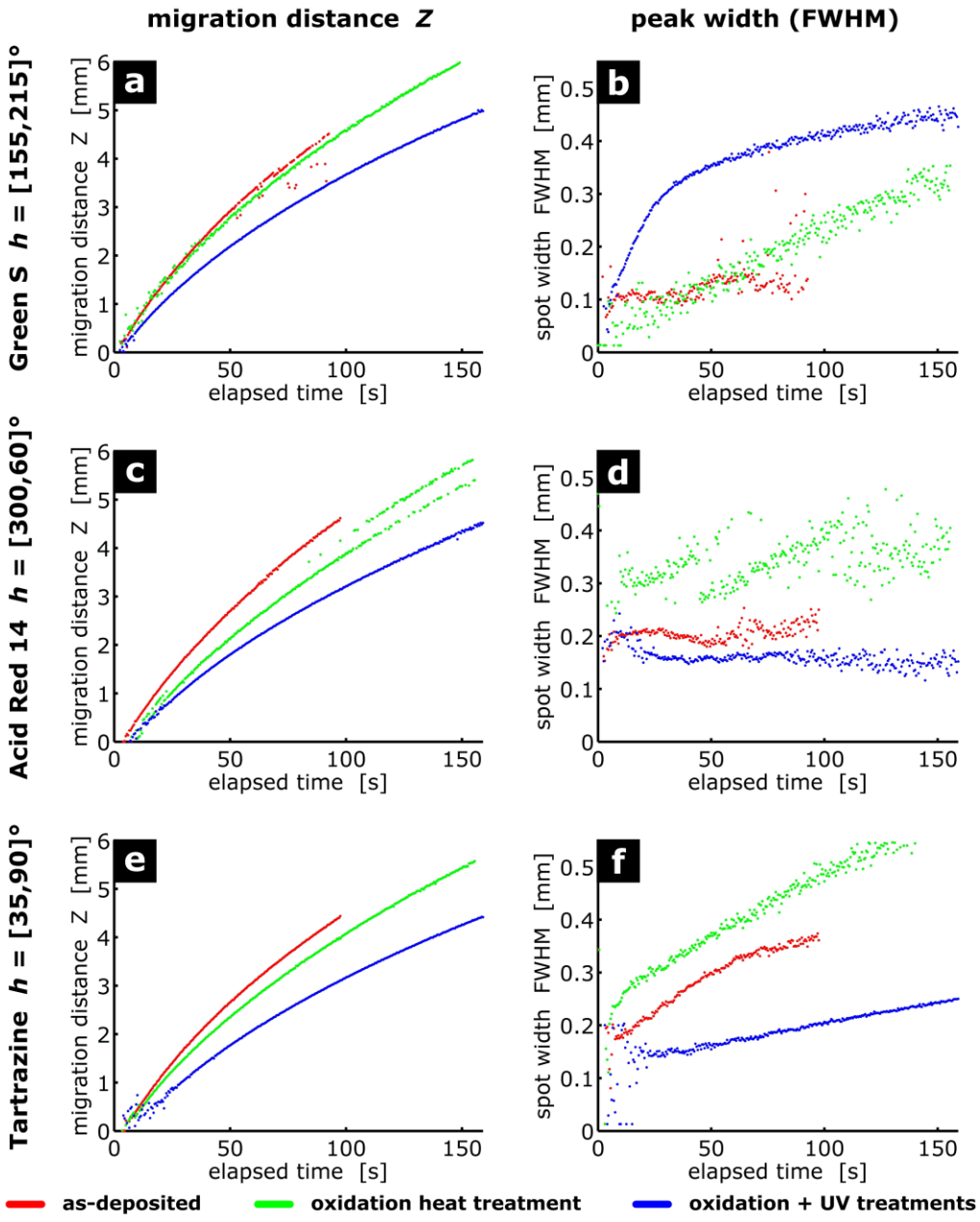

Figure 6-8 Averaged fitted (Gaussian) *Z* and FWHM for (a,b) Green S, (c,d) Acid Red 14, and (e,f) Tartrazine food dyes separated on ZrO_2 GLAD UTLC plates. As-deposited plates (red) were compared to those processed using an oxidation heat treatment (green) and using a combined oxidation then UV irradiation treatment (blue). Data collected by J. Wannenmacher and processed by S.R. Jim.

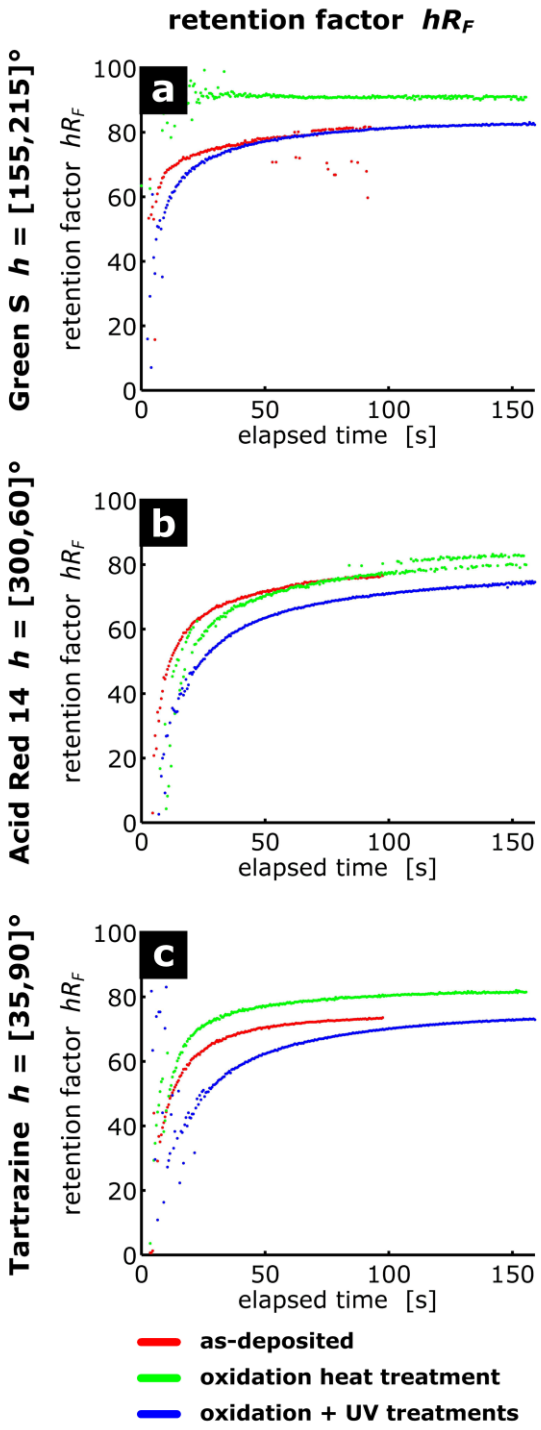

Figure 6-9 Averaged hR_F values for (a) Green S, (b) Acid Red 14, and (c) Tartrazine food dyes separated on treated ZrO_2 GLAD UTLC plates. Calculations performed using fitted (Gaussian) analyte positions and fitted migration fronts. Data collected by J. Wannenmacher and processed by S.R. Jim.

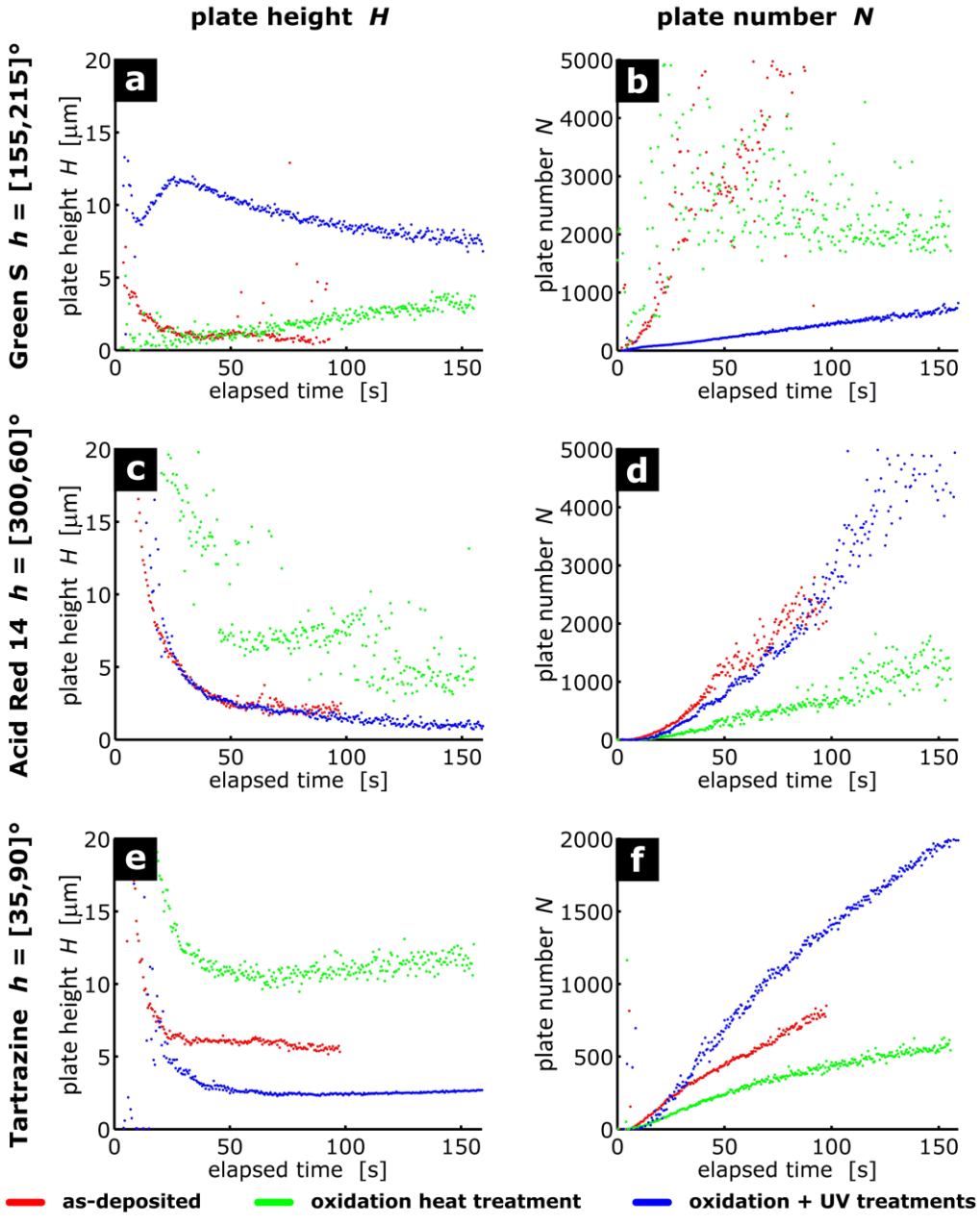

Figure 6-10 Averaged plate heights and plate numbers for (a,b) Green S, (c,d) Acid Red 14, and (e,f) Tartrazine food dyes separated on treated ZrO_2 GLAD UTLC plates. Calculations performed using fitted (Gaussian) analyte positions and widths. Data collected by J. Wannenmacher and processed by S.R. Jim.

6.5 Conclusions

The enhanced approach described in this chapter extends the capabilities of the original TR-UTLC technique [3] to GLAD UTLC. It continues to leverage the excellent frame rates and image resolution of modern digital video cameras to document visible analytes as they separate, and calculate chromatographic figures of merit at different development times. However, the modified approach incorporates key enhancements that significantly increase utility:

- Generalization to unoptimized separations of diluted dyes on GLAD UTLC layers.
- Improved migration front and analyte peak fitting.
- Increased automation (batch processing).
- New tools for data set interpretation (averaging, organization, and comparison).
- Greater user-friendliness (graphical inputs, saved parameters, and error checking).

These features convert the previously reported TR-UTLC proof-of-concept [3] into a powerful and practical tool for GLAD UTLC [4]. The technique is especially useful for the rapid separations over short distances achieved by GLAD UTLC. Many data points are collected without concern of chromatogram distortion (washing) upon removal from the development chamber. It can permit identification of a development time that optimizes figures of merit for each analyte. Coupling TR-UTLC with GLAD UTLC media enables study of the unique chromatographic properties of these materials and potentially increases overall separation performance.

Further development of TR-UTLC techniques may produce new analytical capabilities. Documenting the spots as they separate can be advantageous for environmentally sensitive compounds. For example, carotenoid samples visible during separations on the GLAD UTLC metal oxides faded soon after

development [4]. In principle, TR-UTLC could be extended to UV active analytes that cannot be detected with visible light. Compounds that fluoresce when illuminated by UV light could be imaged directly while UV absorbing compounds could be detected as dark spots on future chromatography plates that incorporate fluorescence indicators similar to those in some commercially-available TLC and HPTLC layers. Illuminating the underside of translucent GLAD UTLC media may also permit transmission mode imaging and improve quantitation for visible and UV active analytes.

References

[1] S.R. Jim, M.T. Taschuk, G.E. Morlock, L.W. Bezuidenhout, W. Schwack, M.J. Brett, Engineered anisotropic microstructures for ultrathin-layer chromatography, Anal. Chem. 82 (2010) 5349–5356.

[2] S.R. Jim, A.J. Oko, M.T. Taschuk, M.J. Brett, Morphological modification of nanostructured ultrathin-layer chromatography stationary phases, J. Chromatogr. A. 1218 (2011) 7203–7210.

[3] A.J. Oko, S.R. Jim, M.T. Taschuk, M.J. Brett, Time resolved chromatograms in ultra-thin layer chromatography, J. Chromatogr. A. 1249 (2012) 226–232.

[4] J. Wannenmacher, S.R. Jim, M.T. Taschuk, M.J. Brett, G.E. Morlock, Ultrathin-layer chromatography on SiO2, Al2O3, TiO2, and ZrO2 nanostructured thin films, J. Chromatogr. A. 1318 (2013) 234–243.

[5] Python Reference Manual, http://docs.python.org/ref/ref.html [online], (n.d.).

[6] R. Delley, The peak width of nearly Gaussian peaks, Chromatographia. 18 (1984) 374–382.

[7] J.P. Foley, Equations for chromatographic peak modeling and calculation of peak area, Anal. Chem. 59 (1987) 1984–1987.

[8] B. Spangenberg, C.F. Poole, C. Weins, Quantitative Thin-Layer Chromatography, Springer Berlin Heidelberg, Berlin, Heidelberg, 2011.

[9] G.E. Morlock, C. Oellig, L.W. Bezuidenhout, M.J. Brett, W. Schwack, Supporting Informaton: Miniaturized planar chromatography using office peripherals, Anal. Chem. 82 (2010) 2940–6.

[10] S. Kirchert, Z. Wang, M.T. Taschuk, S.R. Jim, M.J. Brett, G.E. Morlock, Inkjet application, chromatography, and mass spectrometry of sugars on nanostructured thin films, Anal. Bioanal. Chem. (2013).

7 Surfaces modified by atomic layer deposition[1]

Stationary phase morphology and surface chemistry dictate the properties of UTLC media and interactions with analytes in sample mixtures. This chapter describes the combination of two powerful thin film deposition techniques to create composite chromatography nanomaterials [1]. Previous chapters demonstrated that high surface area columnar GLAD microstructures with aligned macropores are well-suited for UTLC. Atomic layer deposition (ALD) augments these capabilities by providing unprecedented control over the thickness and conformity of very thin coatings [2–5]. Self-limited gas phase chemical reactions produce coatings monolayer-by-monolayer that are appealing in nanofabrication,

[1] Portions of this chapter were published in: S.R. Jim, A. Foroughi-Abari, K.M. Krause, P. Li, M. Kupsta, M.T. Taschuk, K.C. Cadien, and M.J. Brett, Ultrathin-layer chromatography nanostructures modified by atomic layer deposition, Journal of Chromatography A. 1299 (2013) 118–125. Adapted with permission from [1]. Copyright (2013) Elsevier.

GLAD/ALD fabrication and UTLC separations were performed by A. Foroughi-Abari; porosimetry measurements were performed by K.M. Krause; TEM characterization was performed by P. Li and M. Kupsta. S.R. Jim was involved in experiment design, data analysis and interpretation, and paper preparation.

microelectronics, and other applications that require uniform coatings only a few nanometres thick. ALD has been used to modify GLAD films for magnetic storage [6] and sensor [7] applications. The approach is also useful in tuning the surface chemistry of GLAD chromatography stationary phases by coating media with very thin layers of different materials [1].

Approximately 5 μm thick SiO_2 vertical post GLAD UTLC media were coated with < 10 nm thick ALD metal oxides (Al_2O_3, ZrO_2, and ZnO) to decouple surface chemistry from the underlying GLAD scaffold microstructure (**Figure 7-1**). The conformal ALD coatings covered GLAD columns uniformly along their height including the various surface corrugations (insets). The effects of ALD coatings on GLAD UTLC media were investigated using transmission electron microscopy (TEM), gas adsorption porosimetry, and lipophilic dye separations. The results collectively show that the most significant changes occur over the first few nanometres of ALD coating. They further demonstrate independent control of film microstructure and surface characteristics. ALD coatings can enhance complex GLAD microstructures to engineer new composite nanomaterials potentially useful in analytical chromatography.

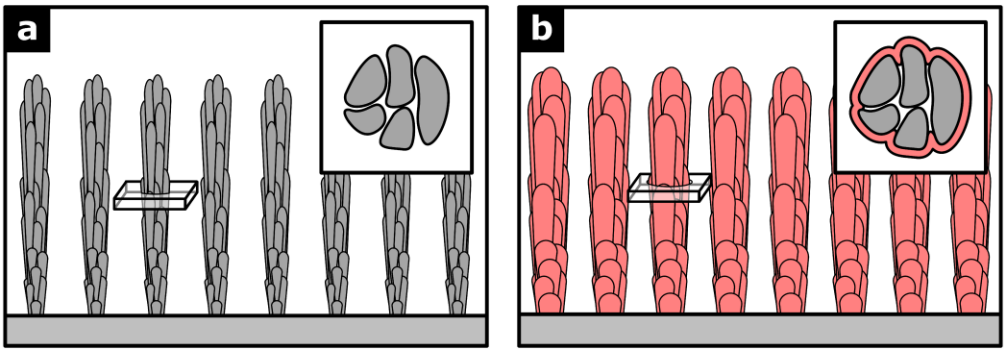

Figure 7-1 Schematics of GLAD UTLC layers (a) before and (b) after ALD coating. Each GLAD column is composed of nanofibres. Cross-sections (insets) of these media were characterized using TEM. Adapted with permission from [1]. Copyright (2013) Elsevier.

7.1 Fabrication of GLAD and GLAD ALD composite UTLC layers

7.1.1 Vertical post SiO_2 and Al_2O_3

The ~ 5 μm thick SiO_2 and Al_2O_3 GLAD UTLC layers used in this study were fabricated at a constant deposition angle of α = 87° and possessed vertical post morphologies (see **3.1.3 Studied GLAD UTLC morphologies** for details). Although sublimated SiO_2 films are stoichiometric, as-evaporated aluminum oxide films tend to be oxygen deficient (AlO_x, $x < 3/2$) and dark yellow in colour. These AlO_x films were oxidized in the annealing furnace (200 °C for 24 hours with atmospheric ambient) before use to improve the stoichiometry of the surface (to Al_2O_3). The oxidized films had a lighter colour that was closer to that of stoichiometric Al_2O_3. The resultant media are assumed to have a well-oxidized stoichiometric surface and incompletely oxidized sub-stoichiometric interior.

7.1.2 Atomic layer deposition coating

A. Foroughi-Abari coated the GLAD UTLC films using a dedicated ALD system in K.C. Cadien's laboratory (see **3.2.3 Atomic layer deposition (ALD)** for details). System recipes (processes) had been optimized for this system by members of his research group. Real-time coating thicknesses were measured on silicon wafers that accompanied the UTLC media during ALD processing. *In-situ* ellipsometry measurements from these "witness" pieces were compared against those of previously-fabricated reference coatings with known thicknesses (on silicon substrates). The thickness of the ALD metal oxide coating on the UTLC media was approximated as that calculated for the witness silicon pieces.

For brevity, GLAD SiO_2 films coated with ALD Al_2O_3 are hereafter denoted as "SiO_2 | Al_2O_3". Media comprised of GLAD SiO_2 films with double ALD coatings of Al_2O_3/ZrO_2 are similarly denoted as "SiO_2 | Al_2O_3/ZrO_2". Similar notation is used for other GLAD ALD composite nanomaterials.

7.2 Transmission electron microscopy analysis[2]

Scanning electron microscopy verified that columnar GLAD films of the expected vertical column morphology and thickness were obtained. Since SEM is a surface characterization technique, it could not be used to distinguish the < 10 nm thick ALD coatings assumed to completely cover column exteriors. Furthermore, poor elemental contrast (Al versus Si) was expected between the Al_2O_3 coatings and SiO_2 films in SEM.

Transmission electron microscopy (2200FS TEM/STEM, JEOL) was used to characterize GLAD SiO_2 | Al_2O_3 column cross-sections. This imaging mode best resolved the morphology of the ALD coatings. TEM samples were prepared in a SEM/FIB dual beam instrument (NB5000 SEM/FIB dual beam system, Hitachi High-Technologies Canada, Rexdale, Ontario, Canada). Samples of SiO_2 and SiO_2 | Al_2O_3 films were filled with photoresist (HPR 504, VWR International) so that cross-sectional slices could be cut through the columns using the instrument's focused ion beam (FIB). Photoresist was applied twice by spin-coating (spin coater, Solitec, Milpitas, California, USA) to improve filling and column immobilization. In each application, the photoresist was poured onto the sample, spun at 500 RPM for 10 s, spun at 1500 RPM for 40 s, and baked at 114 °C for 90 s (Solitec hotplate). This procedure produced a ~ 2 μm thick photoresist overburden above the ~ 5 μm thick GLAD films. Thin cross section lamellae (~ 100 nm thick, located ~ 2.5 μm from the GLAD film bottom) were carefully cut from the filled samples using the FIB and mounted onto TEM grids (copper lift-out grid with 5 posts, Omniprobe®, Ted Pella, Redding, California, USA) within the SEM/FIB instrument.

[2] FIB sample preparation and TEM characterization was performed by P. Li and M. Kupsta (technical officers at the NRC National Institute for Nanotechnology).

Two-dimensional distributions of Si and Al in the column cross-sections were obtained using energy-filtered TEM (EFTEM). These concentration mappings were extrapolated using the three-window imaging technique [8] from core-loss EFTEM images at the L-edges of Si and Al, respectively. Detailed energy windows are listed in **Table 7-1**. Scanning TEM electron energy loss spectroscopy (STEM-EELS) line scans provided additional composition information. Collected EELS spectra were analyzed and plotted using customized programming code created in MATLAB. The script used for background correction and plotting is provided in **B.3 TEM_EELS_process_linescan.m.**

Analysis of cross-sections prepared using the FIB-SEM revealed that 5 nm thick ALD Al_2O_3 coatings fully encapsulate and likely smooth the exterior surfaces of GLAD SiO_2 columns (**Figure 7-2** and **Figure 7-3**). However, aluminum elemental mapping (**Figure 7-2b**) and EELS line scans (**Figure 7-3d**) suggest that the coating did not fully penetrate interstitial micropores between the nanofibres from which each column is composed. The ALD coating likely sealed these pores before they could be completely filled. This finding is consistent with other studies of ALD coatings on microporous materials [4].

Table 7-1 TEM energy filters for elemental mappings (used in preparation of **Figure 7-2**). Reproduced with permission from [1]. Copyright (2013) Elsevier.

Mapping	Energy Filter(s)
Silicon	5 eV windows centred about: 84, 94, 114 eV
Aluminum	10 eV windows centred about: 56, 66, 83 eV

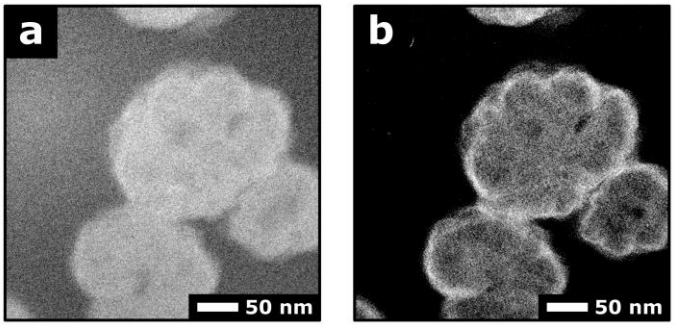

Figure 7-2 (a) Silicon and (b) aluminum TEM elemental mappings of SiO_2 | Al_2O_3 column cross-sections. The 5 nm thick ALD Al_2O_3 coats only the exterior of the GLAD SiO_2 columns. Pixels with stronger signals appear brighter. The film sample was used in a chromatographic run before TEM characterization. See **Table 7-1** for electron energy filters. Reproduced with permission from [1]. Copyright (2013) Elsevier.

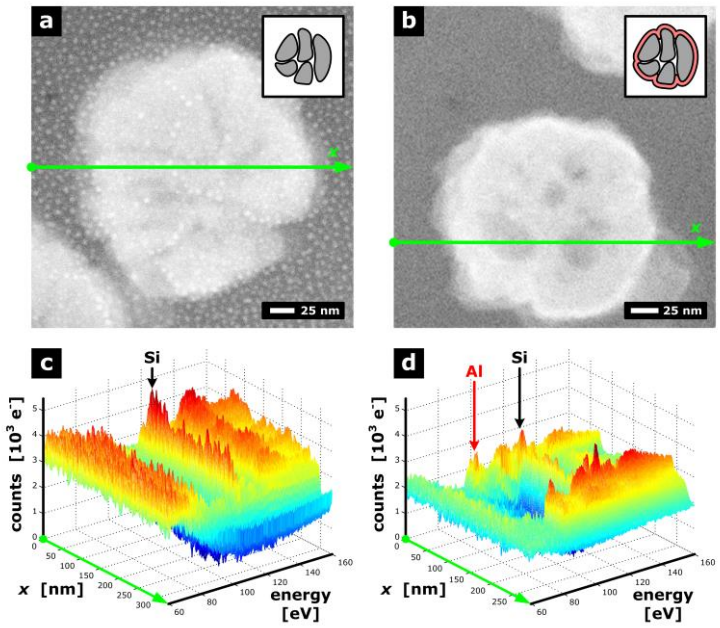

Figure 7-3 (a, b) Dark field TEM images and (c, d) EELS spectra collected across SiO_2 and SiO_2 | Al_2O_3 column cross-sections. The green arrow indicates lines along which EELS data were collected. Silicon (black arrow) and aluminum (red arrow) peaks are shown for each column cross-section. The aluminum signal for the SiO_2 | Al_2O_3 columns (d) indicates that the ALD Al_2O_3 coating did not permeate the micropores in the underlying GLAD SiO_2 column. Spots visible in (a) were FIB-SEM redeposition artifacts created during sample preparation. These spots were independent of the GLAD SiO_2 column sample. Reproduced with permission from [1]. Copyright (2013) Elsevier.

7.3 Density and surface area characterization[3]

Surface areas of GLAD SiO_2 and SiO_2 | Al_2O_3 films were measured using the high-sensitivity Kr gas adsorption porosimetry technique described in previous work [9]. While specific surface areas of GLAD metal oxide films tend to be quite high, the total surface areas of wafer-backed samples testable by gas adsorption porosimetry are low (compared to conventional powder samples). This requires that the adsorbate be Kr gas instead of more common N_2 gas [10].

GLAD SiO_2 films were deposited on five Si wafer pieces, each of footprint area ~ 2200 mm^2. Film mass was measured by weighing each wafer piece before and after deposition (MC5 microbalance, Sartorius AG, Goettingen, Germany). Footprint areas were determined from photographs of each sample beside a ruler using the ImageJ image processing software [11]. Each of the five GLAD samples was coated with a different thickness of ALD Al_2O_3 (uncoated, 1 nm, 2 nm, 3.5 nm, and 5 nm) then reweighed to determine final film mass. The thickness of an uncoated witness GLAD film was measured by SEM and used to calculate each film sample's density.

The five samples were then cleaved into sets of 1 cm x 1.5 cm pieces. Each set was placed into its own 12 mm diameter glass sample bulb (Quantachrome, Boynton Beach, Florida, USA). The bulb and sample pieces were degassed under vacuum at 150 °C for 12-16 hours using a degassing station on the porosimeter (Autosorb-1-MP with liquid N_2 cooled cold trap, Quantachrome) prior to adsorption testing. Adsorption isotherm data was acquired over pressures from 0.05 p_o to 0.3 p_o where p_o = 351 Pa (the saturation pressure of supercooled liquid Kr) using Kr gas (99.999% pure, Praxair, Edmonton, Alberta, Canada) at liquid N_2 (Praxair) temperature (77.3 K). The standard Brunauer-Emmettt-Teller (BET) method [12] was then applied, using the Quantachrome Autosorb software

[3] Density and surface area measurements and calculations were performed by K.M. Krause (Glancing Angle Deposition Laboratory).

(version 1.52) and custom algorithms written in MATLAB to calculate each sample's specific surface area.

Measured densities and surface areas of SiO_2 and SiO_2 | Al_2O_3 films are presented in **Figure 7-4**. Not surprisingly, the ALD Al_2O_3 coatings entered GLAD film macropores, coated column exteriors, and increased overall film density (**Figure 7-4a**). Thicker coatings caused greater increases in film density. However, the specific surface area (**Figure 7-4b**) and surface area enhancement (**Figure 7-4c**) did not change monotonically as Al_2O_3 coatings were applied. Surface areas increased for coatings < 2 nm but decreased for thicker coatings. This result suggests that the ALD coatings nucleated according to the Volmer-Webber (island) growth mode [3] over the < 2 nm thickness regime. The thin discontinuous coatings likely increased column surface roughness and measured film surface area. Meanwhile, thicker coatings were likely continuous over the entire column surface, thus reducing surface roughness, micropore accessibility, and measured film surface area. Differences in the chromatographic properties of SiO_2 and SiO_2 | Al_2O_3 UTLC media are believed to be due to a combination of the changed surface material and surface area accessible to analytes.

7.4 Ultrathin-layer chromatography of dyes

7.4.1 Imaging and numerical analysis

Videos of dye separations were recorded using the custom time-resolved UTLC imaging system described in **6.2 Recording GLAD UTLC separation videos**. Frames extracted from recorded videos were processed using a series of custom image analysis programming scripts prepared for MATLAB. These algorithms perform functions similar to those in the initial time-resolved UTLC report [13] (**6 Time-resolved UTLC**) but were modified for use on individual frames (see **C.14 singleImageUTLC.m** for an updated version of this script).

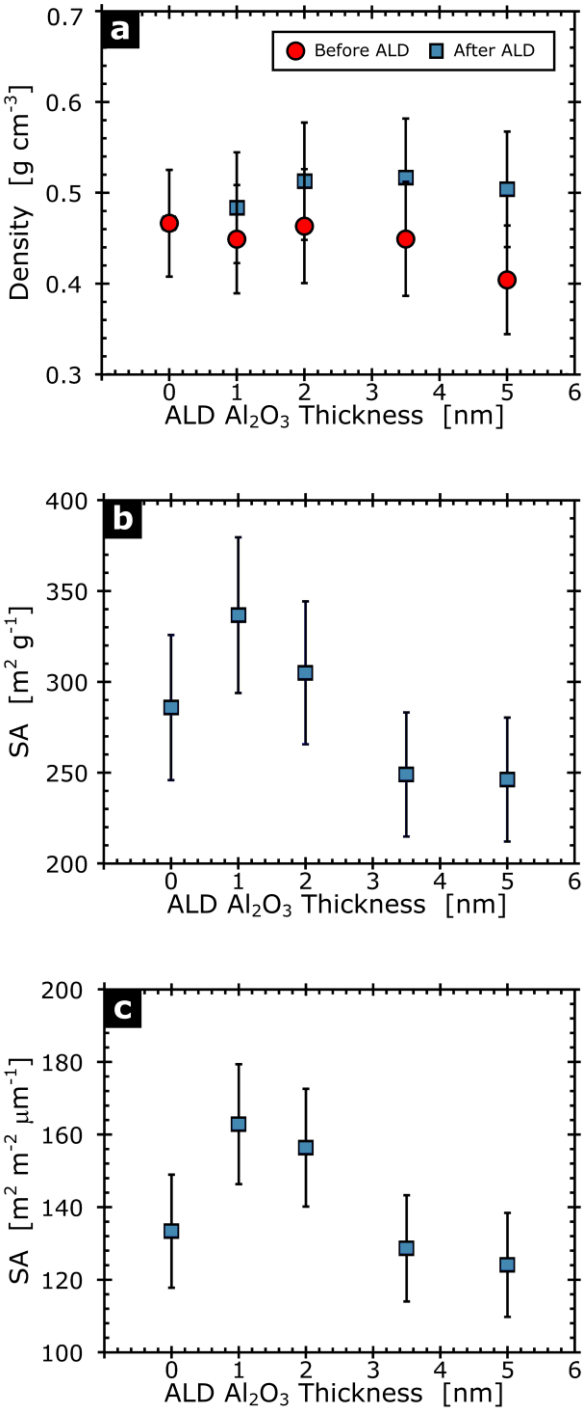

Figure 7-4 Density and surface area characterization. (a) Measured density of GLAD SiO_2 film samples before and after ALD Al_2O_3 coating. (b) Specific surface area and (c) surface area enhancement per unit GLAD SiO_2 film thickness after ALD coating. Applied ALD Al_2O_3 coating thicknesses provided on *x*-axis. Reproduced with permission from [1]. Copyright (2013) Elsevier.

Table 7-2 Hue (colour) filters used to isolate dye components during chromatogram extraction from video frames. Filters defined as inclusive ranges over the interval 0 – 360°. Reproduced with permission from [1]. Copyright (2013) Elsevier.

	Hue Filters (degrees)		
Thickness (nm)	**Dimethyl Yellow**	**Sudan Blue II**	**Ariabel Red**
(uncoated)	25 - 55	195 - 270	300 - 330
0.5	35 - 100	160 - 180	330 - 20
1.0	50 - 90	160 - 200	320 - 0
2.0	35 - 85	160 - 200	345 - 35
3.5	65 - 115	145 - 180	0 - 60
5.0	65 - 115	145 - 185	20 - 70

Numerical analysis was generally restricted to Dimethyl Yellow (DY), Sudan Blue II (SB), and Ariabel Red (AR) which were visible in most separation videos. Other dyes such as Indophenol (IP) were sometimes visible but often too faint for reliable detection. Colour (hue) filtered chromatograms were produced for each dye component on each separation track in a selected video frame. (Hue filter definitions are provided in **Table 7-2**.) Automated Gaussian peak fitting was used to calculate the position and width of the separated dye spots. This analysis was not possible for the GLAD aluminum oxide UTLC plates because the yellow background dominated the coloured dyes.

Standard planar chromatography figures of merit were calculated using the fitted parameters. Of particular interest was the retention factor (hR_F) calculated according to **Equation (2-4)**. It was effective in comparing the interaction strengths between the dyes and GLAD ALD UTLC media.

7.4.2 Chromatographic performance

The chromatographic properties of GLAD Al_2O_3 films changed with the application of a 5 nm thick ALD Al_2O_3 coating (**Figure 7-5a and b; Figure 7-6a and b**). The dye components separated in the same order (DY, SB, AR, IP) as on uncoated media but their retention factors increased by 10-50% on the Al_2O_3 | Al_2O_3 UTLC plate. The relative increases were greatest for analytes with low hR_F

values. The outer surfaces of the oxidized GLAD Al_2O_3 film and the ALD Al_2O_3 coating are assumed to be similarly stoichiometric. Since the surface composition before and after ALD was identical, differences in analyte retention are attributed to changes in GLAD column nanostructure. Reduced surface roughness and micropore accessibility likely decreased the surface area on which analytes could be retained.

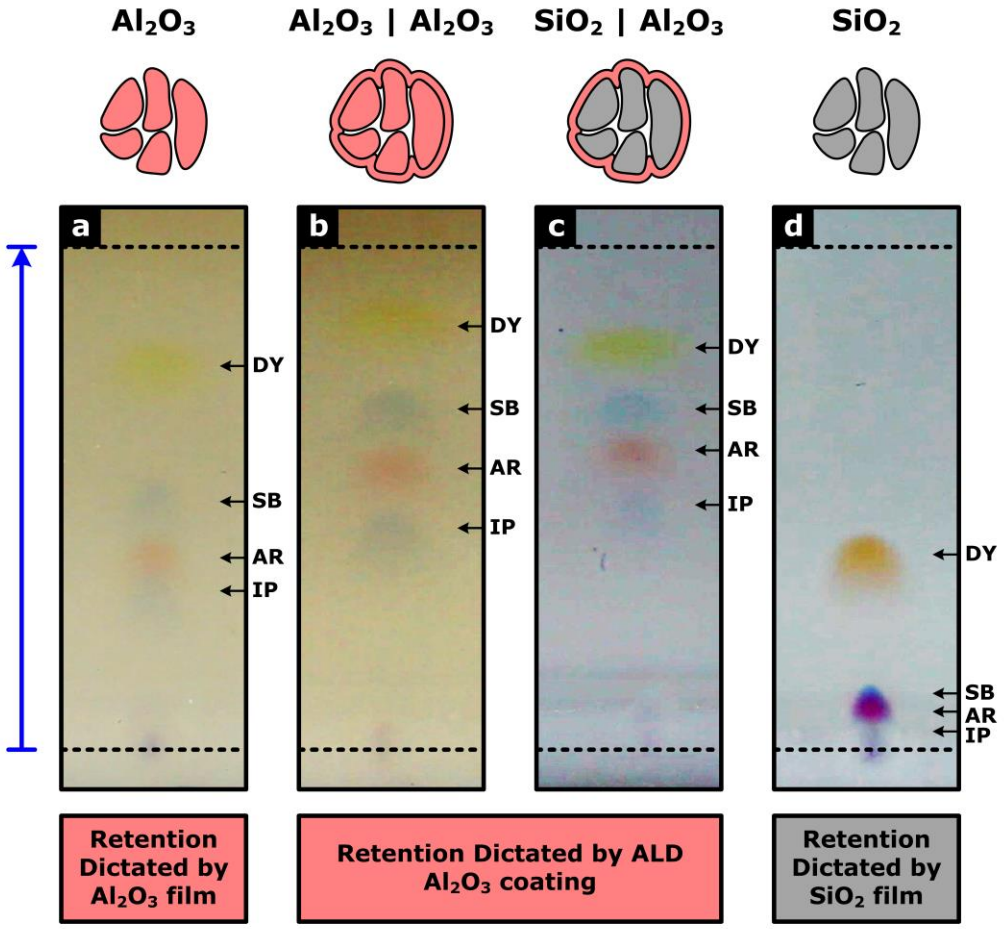

Figure 7-5 Dye separations performed on (a) uncoated Al_2O_3, (b) Al_2O_3 | Al_2O_3, (c) SiO_2 | Al_2O_3, and (d) uncoated SiO_2 media. While the separations (dye hR_F values) on uncoated GLAD Al_2O_3 and SiO_2 were very different, coating both with ALD Al_2O_3 produced similar separations. Blue arrow indicates development vector between the spot application and mobile phase front positions (dashed lines). Dye separation images enhanced for clarity. (Letter labels are consistent with those in **Figure 7-6**.) Reproduced with permission from [1]. Copyright (2013) Elsevier.

The chromatographic properties of GLAD SiO_2 media changed more significantly after coating with ALD Al_2O_3 (**Figure 7-5c and d; Figure 7-6c and d**). The dye separation order was the same on uncoated and coated SiO_2 films as on the Al_2O_3 films. The hR_F values again increased upon ALD coating and relative increases were greatest for low hR_F dyes. However, these increases were significantly larger for media with an initial GLAD SiO_2 film. The IP dye spot had $hR_F \gg 0$ and the hR_F values of the other dyes increased by 200-700 % on the SiO_2 | Al_2O_3. In fact, dye retention factors on Al_2O_3 | Al_2O_3 and SiO_2 | Al_2O_3 media were similar despite their different underlying GLAD column materials (**Figure 7-5b and c**). This indicates that the surface material played a dominant role in defining the chromatographic properties of these hybrid media.

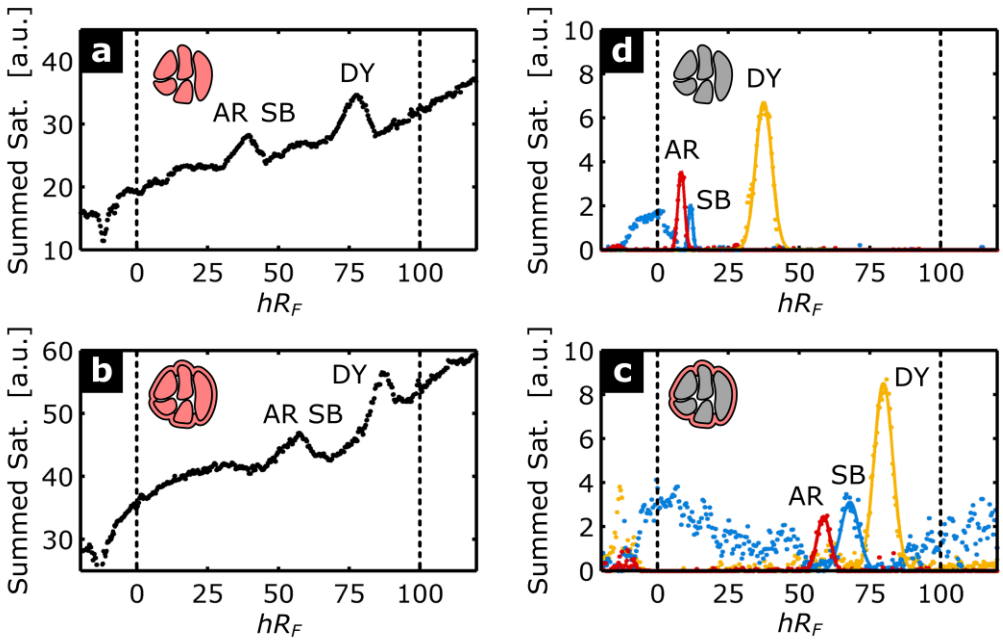

Figure 7-6 Dye separation chromatograms obtained on (a) uncoated Al_2O_3, (b) Al_2O_3 | Al_2O_3, (c) SiO_2 | Al_2O_3, and (d) uncoated SiO_2. (Letter labels are consistent with those in **Figure 7-5**.) The yellow background of the GLAD Al_2O_3 films prevented colour-filtered chromatogram extraction and peak fitting in (a, b); unfiltered signals are shown. Raw and fitted colour-filtered chromatograms for DY (yellow), SB (blue), and AR (red) are shown in (c, d). Reproduced with permission from [1]. Copyright (2013) Elsevier.

ALD Al_2O_3 coating thickness affected analyte retention on SiO_2 | Al_2O_3 media (**Figure 7-7**). hR_F values changed most dramatically within the < 2 nm ALD Al_2O_3 coating range. Over these small thicknesses, the surface composition of the UTLC layer changed from that of the highly-retentive underlying GLAD SiO_2 film to that of the less-retentive ALD Al_2O_3 coating, dominating modest increases in surface roughness. No significant changes in hR_F values were observed for thicker coatings. (Separations on GLAD SiO_2 media with ALD Al_2O_3 coatings of 8 nm and 10 nm thickness produced similar hR_F values, not shown.)

Dye separations on single and double ALD metal oxide coatings demonstrated complete decoupling of surface chemistry from the underlying film. **Figure 7-8** shows separation tracks for GLAD SiO_2 films covered in single coatings of (a) ZrO_2, (c) Al_2O_3, and (e) ZnO; and double coatings of (b) Al_2O_3/ZrO_2 and (d) Al_2O_3/ZnO. Surface area reductions induced by the second coating had a limited effect on chromatographic performance. Separations were instead dictated by the surface chemistry of the outermost material, rather than that of the underlying GLAD film or first ALD coating.

7.5 Opportunities for GLAD ALD Nanocomposites in Chromatography

Although most TLC and HPTLC media are composed of normal-phase silica gel, other materials may be better for some samples. For example, alumina TLC plates exhibit good selectivity for hydrocarbon analytes with carbon-carbon double bonds [14]. In spite of their lower separation efficiency (increased spot broadening), alumina TLC plates are also more effective at separating analytes based on their Lewis acid-base interactions [15]. Alumina HPTLC plates with improved morphology (smaller sorbent particles) may increase performance but are not commercially available [15]. Recent work exploring GLAD UTLC separations of carotenoids (such as β-carotene) indicated that Al_2O_3 thin films performed better than SiO_2 thin films but that their lower surface areas caused increased spot broadening [16].

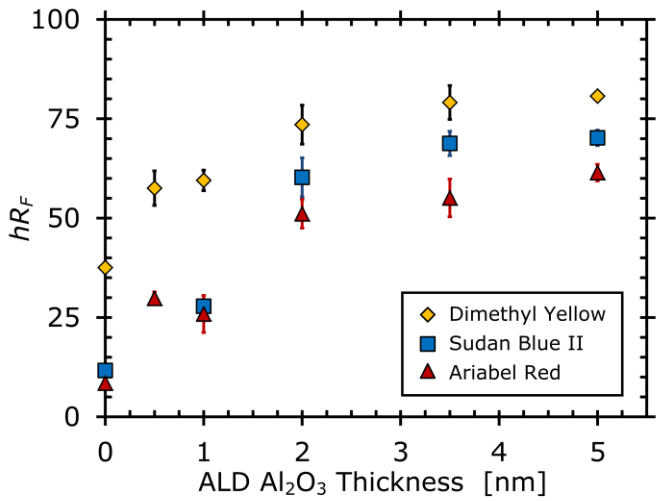

Figure 7-7 Effects of ALD Al_2O_3 coating thickness on DY, SB, and AR dye retention factors for GLAD SiO_2 media. Thin coatings (< 2 nm) caused large changes in hR_F. Error bars reflect variation across 2-4 parallel separation tracks from the same UTLC run. Reproduced with permission from [1]. Copyright (2013) Elsevier.

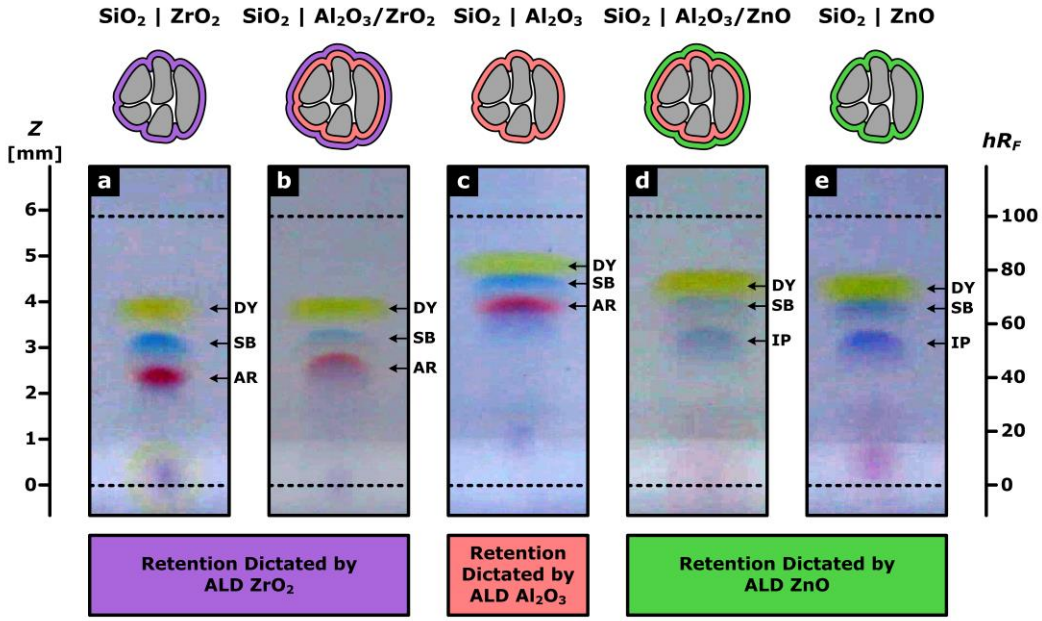

Figure 7-8 Dye separations on GLAD SiO_2 media functionalized with single (a, c, e) and double (b, d) ALD metal oxide coatings (5 nm per coating). The similarity between (a, b) and (d, e) indicates that chromatographic behaviours were dominated by the outermost metal oxide surface rather than the GLAD column core. Dye separation images enhanced for clarity. Modified with permission from [1]. Copyright (2013) Elsevier.

The approach described in this chapter may be used to engineer better performing SiO_2 | Al_2O_3 UTLC media with optimized microstructure (by GLAD) and desirable surface chemistry (by ALD). Combining an Al_2O_3 surface with the underlying GLAD SiO_2 scaffolding provides advantages unachievable with a GLAD Al_2O_3 film alone. This approach can readily produce layers with desirable neutral colour backgrounds. GLAD SiO_2 films also exhibit some of the highest specific surface areas; ~ 4 times greater than GLAD Al_2O_3 films [17]. UTLC media composed of SiO_2 | Al_2O_3 would reduce overloading by providing more active sites at which analytes interact with the stationary phase.

Other unconventional metal oxides such as the ZnO and ZrO_2 studied here may be appropriate for analyte mixtures requiring retention mechanisms impossible on traditional layers. Incorporating ALD metals (such as Pt or Pd) could also catalyze chemical reactions before, during, or after sample separations that were previously too expensive for regular use. Other coatings may make subsequent layer functionalization with specific molecules easier or improve coupling with advanced detection modes (such as mass spectrometry). Composite nanomaterials engineered by leveraging the high surface areas, tunable porosities, and varied architectures of GLAD scaffolds with engineered ALD coatings potentially expand the selection of chromatographic media available to chemists.

7.6 Conclusions

This chapter described UTLC stationary phases derived from ~ 5 μm thick GLAD columnar films and < 10 nm thick conformal ALD metal oxide coatings. The microstructures of SiO_2 | Al_2O_3 media were characterized by electron microscopy and Kr gas adsorption porosimetry. TEM characterization of film cross-sections revealed that 5 nm thick ALD Al_2O_3 coatings fully encapsulate GLAD SiO_2 columns but do not fully penetrate micropores contained within. Surface areas measured using porosimetry depended upon ALD coating thickness; coatings < 2 nm thick increased film surface areas while thicker coatings produced lower surface areas. The effects of ALD modification were studied through normal-

phase separations of lipophilic dyes. Surface polarity alterations occurring over the first ~ 2 nm of ALD coating caused the most significant changes in chromatographic properties on SiO_2 | Al_2O_3 media. Such thin coatings caused retention factors to increase by a factor of ~ 2 for Dimethyl Yellow (from ~ 38 to ~ 73) and a factor of ~ 6 for Ariabel Red (from ~ 8 to ~ 50). Further coating did not cause substantial changes in chromatographic performance. Other experiments showed that dye separations performed on GLAD films with double coatings (SiO_2 | Al_2O_3/ZrO_2 and SiO_2 | Al_2O_3/ZnO) were dictated by the surface chemistry of the outermost material.

This investigation demonstrates that the properties of the film surface can be decoupled from the properties of the interior. The combined GLAD ALD technique may be used to study surface chemistries never before explored in chromatography. High surface area media too difficult or costly to produce using GLAD or other methods alone may be realized by ALD coating appropriate GLAD SiO_2 films. In principle, this approach expands the scope of available chromatography materials to include all those under development in the highly-active ALD materials science field. Surface polarity, carbon-carbon double bond affinity [14], Lewis acidity [15], and other material attributes affecting chromatographic interactions between the analyte and stationary phase surface can be engineered over high surface area scaffolds. GLAD ALD composite nanomaterials may enable future innovations in UTLC and other applications requiring unconventional surface chemistries over complex microstructures.

References

[1] S.R. Jim, A. Foroughi-Abari, K.M. Krause, P. Li, M.R. Kupsta, M.T. Taschuk, et al., Ultrathin-layer chromatography nanostructures modified by atomic layer deposition, J. Chromatogr. A. 1299 (2013) 118–125.

[2] M. Knez, K. Nielsch, L. Niinistö, Synthesis and Surface Engineering of Complex Nanostructures by Atomic Layer Deposition, Adv. Mater. 19 (2007) 3425–3438.

[3] S.M. George, Atomic layer deposition: an overview, Chem. Rev. 110 (2010) 111–31.

[4] C. Detavernier, J. Dendooven, S.P. Sree, K.F. Ludwig, J.A. Martens, Tailoring nanoporous materials by atomic layer deposition, Chem. Soc. Rev. 40 (2011) 5242–5253.

[5] A. Foroughi-Abari, K.C. Cadien, Atomic Layer Deposition for Nanotechnology, in: M. Stepanova, S. Dew (Eds.), Nanofabrication Tech. Princ., Springer Vienna, Vienna, 2012: pp. 143–161.

[6] O. Albrecht, R. Zierold, C. Patzig, J. Bachmann, C. Sturm, B. Rheinländer, et al., Tubular magnetic nanostructures based on glancing angle deposited templates and atomic layer deposition, Phys. Status Solidi B. 247 (2010) 1365–1371.

[7] M.T. Taschuk, K.D. Harris, D.P. Smetaniuk, M.J. Brett, Decoupling sensor morphology and material: Atomic layer deposition onto nanocolumn scaffolds, Sensors Actuators B Chem. 162 (2012) 1–6.

[8] R. Egerton, Applications of Energy-Loss Spectroscopy, in: Electron Energy Loss Spectrosc. Electron Microsc., 2nd ed., Plenum, New York, 1996: p. 301.

[9] K.M. Krause, M.T. Taschuk, K.D. Harris, D.A. Rider, N.G. Wakefield, J.C. Sit, et al., Surface area characterization of obliquely deposited metal oxide nanostructured thin films., Langmuir. 26 (2010) 4368–4376.

[10] S. Lowell, J.E. Shields, M.A. Thomas, M. Thommes, Characterization of Porous Solids and Powders: Surface Area, Pore Size, and Density, Springer, Dordecht, The Netherlands, 2006.

[11] W.S. Rasband, ImageJ, http://imagej.nih.gov/ij [online], (2009).

[12] S. Brunauer, P. Emmett, E. Teller, Adsorption of gases in multimolecular layers, J. Am. Chem. Soc. 60 (1938) 309–319.

[13] A.J. Oko, S.R. Jim, M.T. Taschuk, M.J. Brett, Time resolved chromatograms in ultra-thin layer chromatography, J. Chromatogr. A. 1249 (2012) 226–232.

[14] J. Sherma, Basic TLC Techniques, Materials, and Apparatus, in: J. Sherma, B. Fried (Eds.), Handbook of Thin Layer Chromatography, 3rd ed., Marcel Dekker [Taylor and Francis], New York, 2003: pp. 1–61.

[15] E. Reich, A. Schibli, High-Performance Thin Layer Chromatography for the Analysis of Medicinal Plants, Thieme Medical Publishers, New York, 2007.

[16] J. Wannenmacher, S.R. Jim, M.T. Taschuk, M.J. Brett, G.E. Morlock, Ultrathin-layer chromatography on SiO2, Al2O3, TiO2, and ZrO2 nanostructured thin films, J. Chromatogr. A. 1318 (2013) 234–243.

[17] J.B. Sorge, M.T. Taschuk, N.G. Wakefield, J.C. Sit, M.J. Brett, Metal oxide morphology in argon-assisted glancing angle deposition, J. Vac. Sci. Technol. A. 30 (2012) 021507.

8 Customized GLAD UTLC chamber

The work described in previous sections focussed on advancing GLAD UTLC stationary phases and characterization techniques. Several studies described performance improvements possible through nanostructuring [1,2], post-processing [3,4], precise sample application [4–7], and time-resolved UTLC characterization [8]. This chapter describes an attempt to fabricate and evaluate a chromatographic chamber optimized for GLAD UTLC media.

8.1 Motivation and objective

Conventional development chambers have changed little over the past several decades. Typical ascending development HPTLC chambers are simple glass tanks (commercially available through CAMAG, for example). Solvents sitting at the bottom of the tank supply mobile phase to the bottom edge of the upright HPTLC plate and produce a quasi-saturated vapour in the relatively large

remaining "dead volume." Horizontal development chambers (such as those produced by Desaga and CAMAG) offer many improvements [1,8]. Mobile phase is supplied by a porous glass frit dipped into a primary reservoir at a rate dependent primarily upon the liquid level, frit porosity, and contact area between the frit and chromatography plate. A separate conditioning trough located beneath the face-down chromatography plate produces more uniform mobile phase vapour when required. The reduced dead volume reaches a quasi-saturated state more rapidly and with less change in vapour composition. (The importance of mobile phase vapour saturation is discussed further in **3.4.2 Mobile phase optimization**.)

A Desaga horizontal development chamber (designed for 50 mm x 50 mm HPTLC plates) was used in the majority of this work but had to be modified for use with the miniaturized GLAD UTLC plates (25.4 mm x 25.4 mm or 50.8 mm x 25.4 mm) [1]. (For details see **3.4.3 Ultrathin-layer chromatography development**.) Previous experience found that separation performance was highly dependent upon precise UTLC plate loading and that manipulation of the tiny plates could be cumbersome. Slight misalignment between the plate and the glass frit could cause mobile phase flow non-uniformities; major misalignment would entirely ruin the separation result.

Potential improvements in performance, quantification of performance, and ease of use motivated design of a new custom GLAD UTLC chamber. The refined chamber aimed to ease plate manipulation, enhance compatibility with time-resolved UTLC, reduce variability, and increase overall utility. Fabrication details and revised engineering drawings are provided in **D Custom GLAD UTLC chamber schematics**.

8.2 Design and fabrication

The new horizontal development chamber was engineered specifically for GLAD UTLC media (**Figure 8-1**). It was designed to accommodate 50.8 mm wide x 25.4 mm x 1 mm thick GLAD UTLC plates because these wider plates

have improved mobile phase flow uniformity. Other design criteria specific to GLAD UTLC and the time-resolved UTLC imaging system included:

1. **Material selection**
2. **Constant glass frit positioning**
3. **Precise GLAD UTLC plate positioning**
4. **Rapid loading of GLAD UTLC plates**
5. **Mobile phase liquid level**
6. **Pre-development vapour conditioning**
7. **Reflective illumination and shadows**
8. **Transmission illumination**
9. **In-frame size standard**

8.2.1 Material selection

Materials were selected to ensure compatibility with the organic solvents (such as toluene and *n*-hexane) often used in mobile phases. This criteria prevented use of most plastics, rubbers, and some metals. The numerous parts of the chamber were

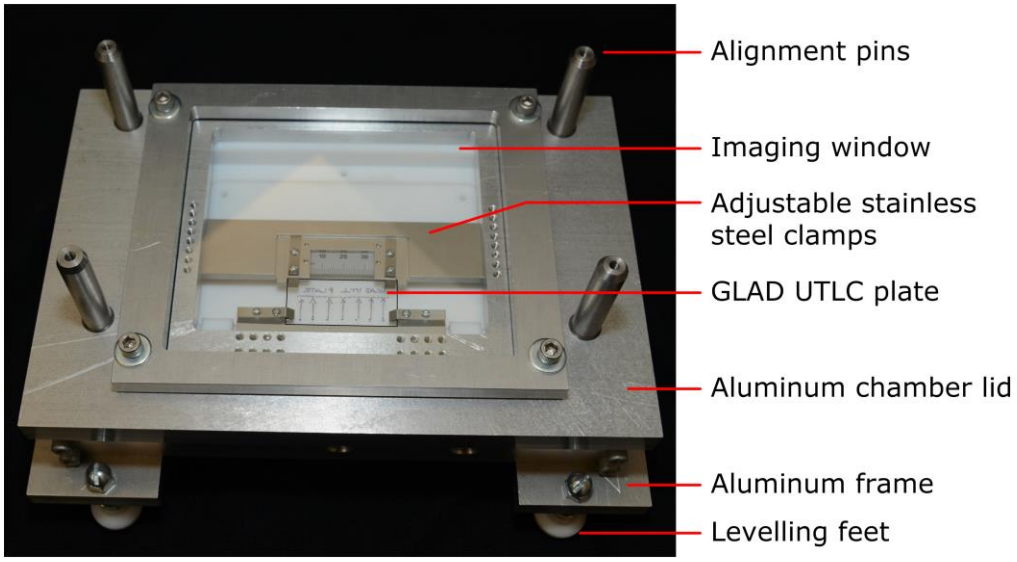

Figure 8-1 Completed development chamber engineered for 50.8 mm wide x 25.4 mm x 1 mm GLAD UTLC plates. Alignment pins ensure that the lid slides precisely onto the bottom of the chamber.

accordingly machined from polytetrafluoroethylene (PTFE; main chamber), stainless steel (clips and clamps), and aluminum (chamber lid, front, and frame). Perfluoroalkoxy (PFA) tubing and tube fittings were used to deliver solvent from glass syringes into the chamber. Chemical-resistant fluorosilicone rubber was cut into gaskets and parts were secured with stainless steel hardware whenever possible. A buna-N o-ring was adequate in the lid because it was only in contact with solvent vapours and could be easily replaced. Glass windows were used at the top and bottom of the chamber.

Fabricating the main chamber part (**Figure 8-2**) from PTFE posed several changes worth noting. This material possesses excellent chemical compatibility but its relative softness makes it notoriously difficult to machine. Great care was taken by expert machinist Reiner Schwarze (Electrical and Computer Engineering Machine Shop, University of Alberta) to precisely mill the solid block of PTFE into the intricate chamber part without warping it. Its softness again caused problems during assembly. The flexibility of the machined part permitted it to be easily over stressed when other rigid metal parts were attached to it. Managing these stresses was important to achieving the precise positioning demanded by the chamber.

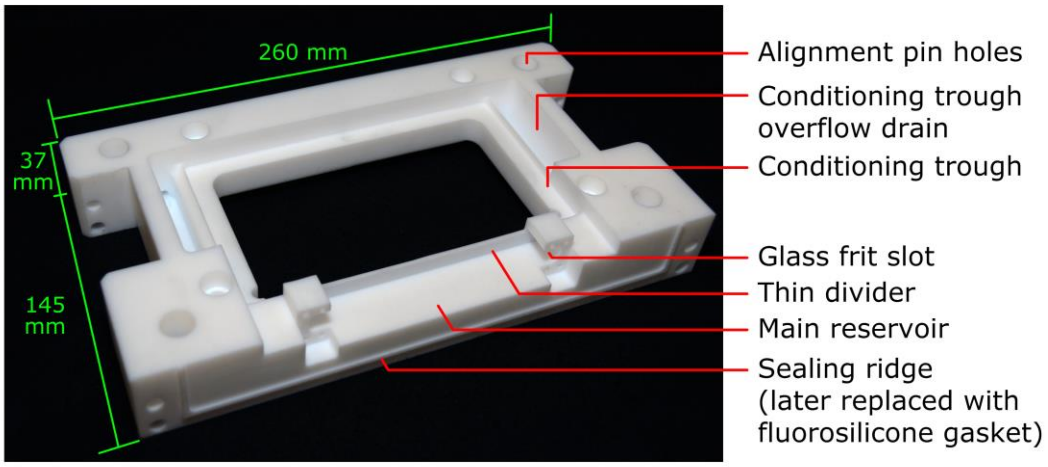

Figure 8-2 Main chamber part machined from PTFE. The front ridge on the chamber was later filed down and replaced with a fluorosilicone seal during assembly (not shown).

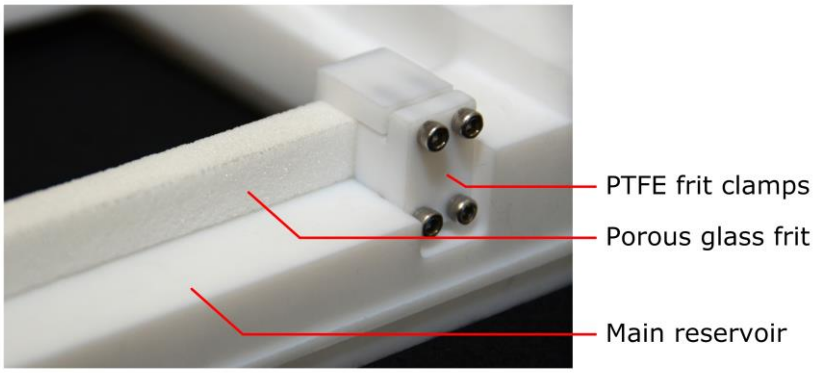

Figure 8-3 Machined PTFE clamps and stainless steel screws used to secure custom cut glass frit.

8.2.2 Constant glass frit positioning

A custom glass frit was purchased for this chamber (porosity "P2," calculated 40-100 μm pore sizes, Adams-Chittenden Scientific Glass, Berkeley, California, USA). The frit was deliberately oversized to accommodate the UTLC plate clamps and make alignment easier. (A wider base is more stable.) Edges were machined smooth by the supplier. The frit was clamped into the chamber's main reservoir so that it would always be in the proper position when the UTLC plate was lowered onto it (**Figure 8-3**). The glass frit is pushed against the thin machined divider between the reservoir and conditioning troughs. The thickness of this divider was minimized to reduce its intrusion into the imaging field.

8.2.3 Precise GLAD UTLC plate positioning

The interface between the GLAD UTLC plate and the glass frit significantly affects the velocity and uniformity of mobile phase flow during development. Repeatable contact was ensured by clamping the UTLC plate to the underside of the chamber lid and ensuring that the lid could slide smoothly along the alignment pins (**Figure 8-4**). The clamps can be adjusted to change the overlap between the frit and plate in discrete values (1.00, 1.50, 1.75, and 2.00 mm). Metal clips apply pressure to the face-down UTLC plate so that the GLAD film is always in the same plane even if the thickness of the glass substrate varies slightly.

8.2.4 Rapid loading of GLAD UTLC plates

Slots cut into the bottommost clamps allow them to be quickly slid into place and tightened when mounting an undeveloped GLAD UTLC plate (**Figure 8-4**). Quickly loading undeveloped and unloading developed plates reduces the total experiment time. This reduces the variations that occur over the course of the separation experiment such as changes in mobile phase composition and degradation (fading) of sample components.

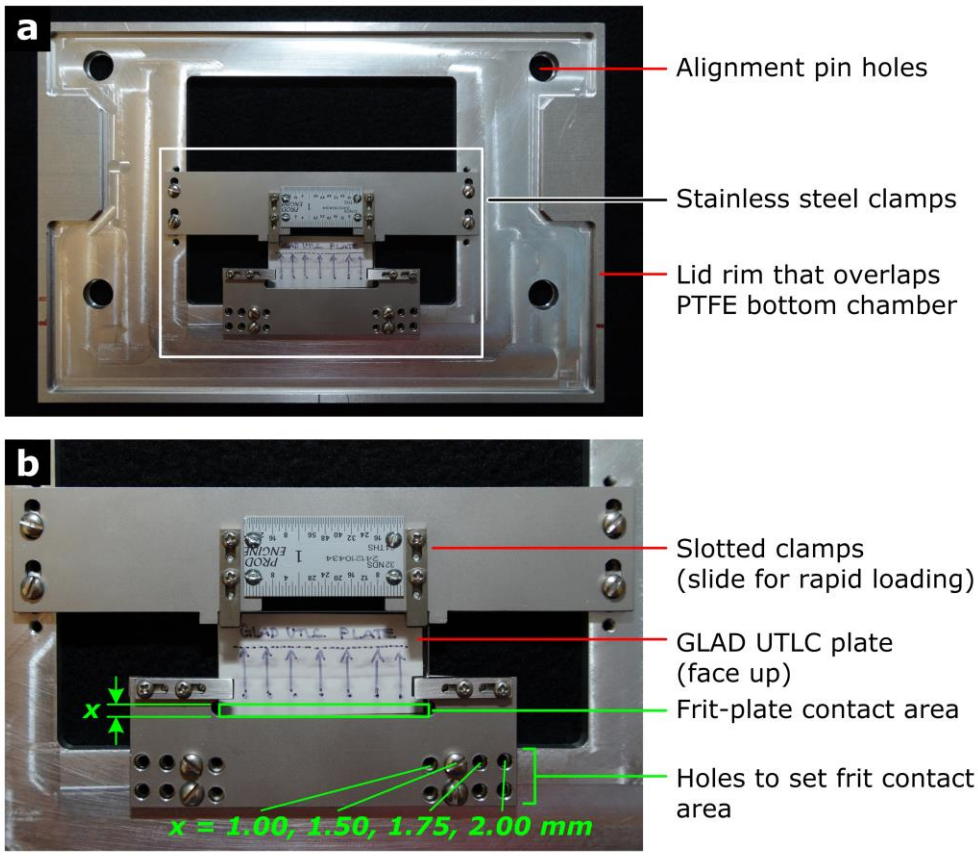

Figure 8-4 (a) Underside of machined aluminum lid and adjustable stainless steel clamps used to precisely mount GLAD UTLC plates. The ~ 6 mm tall lid rim overlaps the chamber bottom so that a quasi-saturated vapour phase can be achieved prior to development. The region marked by the white rectangle is magnified below. (b) Large stainless steel clamps precisely position the GLAD UTLC plate (film side face up in photo) while small slotted clamps enable rapid loading. The desired frit-plate overlap (contact area width x) is set discretely by selecting appropriate screw hole pairs. The innermost pairs give a x = 1 mm overlap while the outermost pairs give a x = 2 mm overlap.

8.2.5 Mobile phase liquid level

The solvent level in the main reservoir affects flow through the glass frit and ultimately also the migration velocities across the UTLC plate. The level in the conditioning trough affects the gas volume beneath the developing plate that must be saturated. These considerations motivated several features of the chamber (**Figure 8-5**). Tubing attached to the chamber allows the user to top-up the main reservoir and conditioning trough from outside of the TR-UTLC imaging booth using large glass syringes attached to the PFA tubing. Overflow drains ensure liquid levels in the main reservoir and conditioning trough are a constant distance below the surface of the GLAD UTLC plate. Adjustable feet attached to the frame ensure that the entire chamber is level (**Figure 8-1**).

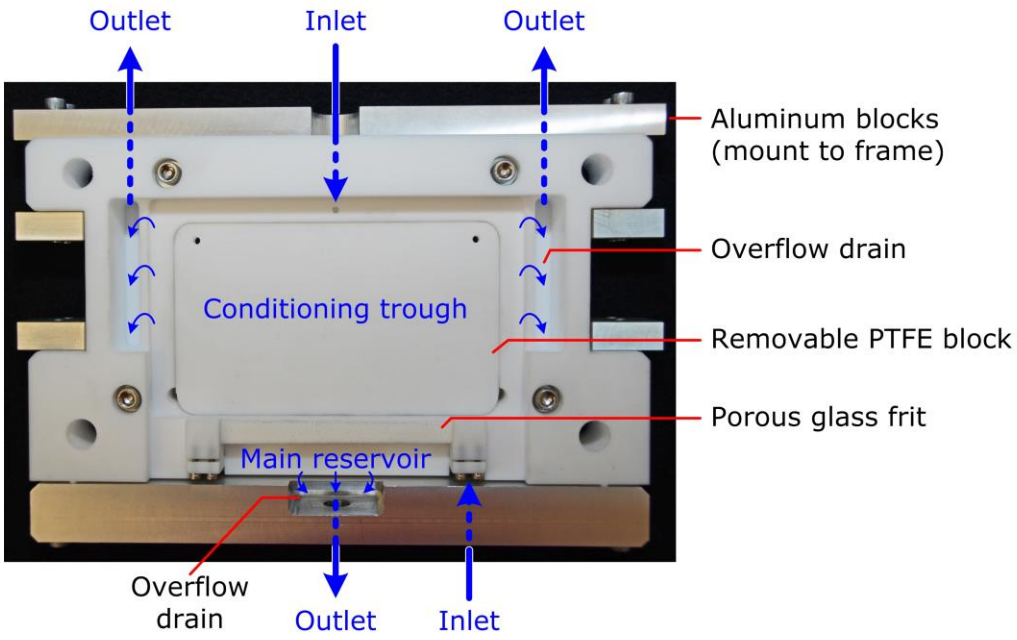

Figure 8-5 Top view of PTFE main chamber part. Overflow drains beside the conditioning trough (left and right; cut into PTFE piece) and next to the main reservoir (cut into front aluminum piece) ensure consistent mobile phase liquid levels. Removable PTFE block in conditioning trough blocks bottom window during reflection mode imaging. Additional aluminum blocks secure the chamber to aluminum frame shown in **Figure 8-1**.

8.2.6 Pre-development vapour conditioning

A rim built into the aluminum lid allows the chamber to be closed without the UTLC plate touching the glass frit (**Figure 8-4a**). Although the seal is not air-tight, it improves mobile phase vapour equilibration before development, if required. The chamber lid can be suspended so that the UTLC plate is a few millimetres above the glass frit until a quasi-saturation vapour is produced. Development then starts when the lid is lowered the remaining few millimetres.

8.2.7 Reflective illumination and shadows

A window in the lid of the chamber ensures that the entire UTLC plate can be imaged from above against a solid white PTFE block. This plate is illuminated by strips of white LEDs located to the left and right of the chamber directed ~ 45° with respect to the plate normal [8] (**Figure 8-6a**). The incident light can potentially cast shadows beneath the GLAD UTLC plate that affect imaging. A large chamber width was selected to minimize shadows cast by the rims (**Figure 8-6b**). Shadows from clamps attached to the GLAD UTLC plate were unavoidable but mitigated by minimizing their size and bevelling larger clamps.

8.2.8 Transmission illumination

Removing the centre PTFE block (**Figure 8-5**) reveals a window beneath the UTLC chamber's conditioning trough (**Figure 8-2**). This window was intended for future incorporation of transmission mode UTLC plate imaging schemes [9]. The large size of the window ensures that an appropriate light source beneath the chamber will produce uniform illumination across the imaging field. The open space designed into the top clamp that grasps the top edge of the plate is intended to serve as a region of known 100% transmission (relative to the UTLC plate) (**Figure 8-7**). Coloured [9] or UV light illumination from below may improve the optical detection of some analytes during time-resolved UTLC development.

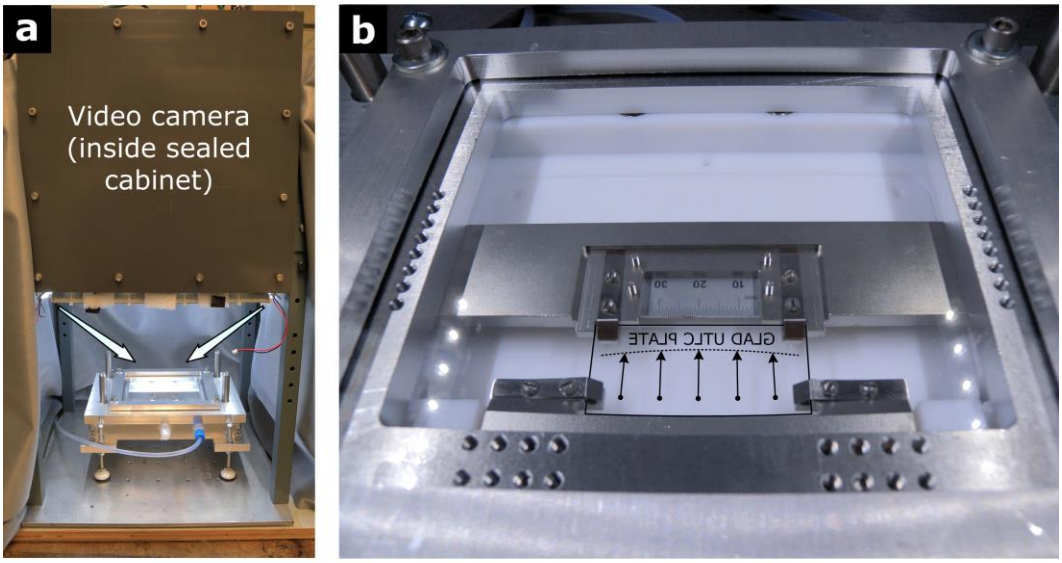

Figure 8-6 Reflection mode UTLC plate illumination and shadows. (a) White LED strips direct light (white arrows) onto the chamber while the GLAD UTLC plate is imaged from above. (b) Shadows cast by the chamber rim do not enter the imaging field.

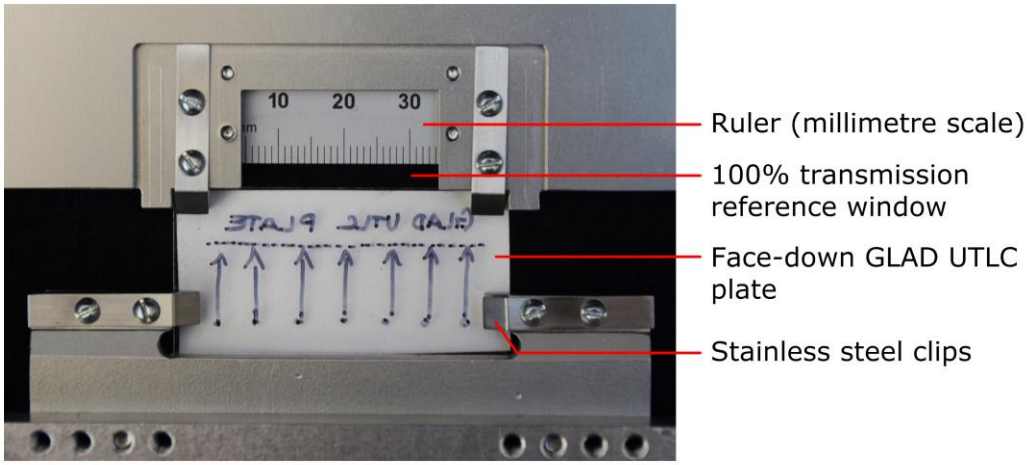

Figure 8-7 GLAD UTLC plate and stainless steel clamps viewed from above. The millimetre scale on the certified ruler is in the same plane as the surface of the face-down GLAD UTLC plate. The gap between the ruler and the top edge of the plate serves as a 100% transmission reference region.

8.2.9 In-frame size standard

A certified stainless steel ruler attaches to the top clamp so that its edge is just inside of the imaging field (**Figure 8-7**). The millimetre scale on the top of the ruler is in the same focus plane as the bottom (film) side of the face-down GLAD UTLC plate. By having a certified scale inside of every frame extracted from the development videos, the user can always be certain of physical sizes (migration distance and spot width).

8.3 Chamber testing

The performance of the customized GLAD UTLC chamber was compared to that of the original Desaga horizontal chamber (**Figure 3-6**) using CAMAG dye separations. Notable differences in the chambers and testing conditions are listed in **Table 8-1**. Each experiment involved 9 identically loaded separation tracks on 5 GLAD UTLC plates:

- **GLAD UTLC film type[1]:** SiO_2, 5 μm thick, α = 87.5°, anisotropic SBD (24 nm period) nominal structure, developed in along-channel direction.
- **Dye sample spots:** 50 nL of CAMAG test dye, diluted to 20% in *n*-hexane, applied by Hamilton syringe.
- **Mobile phase:** 4:3 mixture of toluene:*n*-hexane (v/v).
- **Vapour phase:** Mobile phase mixture was added to the conditioning troughs beneath each developing GLAD UTLC plate.

Dye separations were documented and analyzed using the enhanced time-resolved UTLC approach described in **6 Time-resolved UTLC**. Intra-plate variation was assessed by considering the 9 tracks on a given GLAD UTLC plate while inter-plate variation studied all 5 plates (45 tracks total) in aggregate.

[1] Both films had the same nominal structure but slight differences in porosity are possible due to subtle variation in α between deposition dates. Although direct comparisons between the two sets of GLAD UTLC plates may be difficult, comparisons within each set of 5 plates can be performed.

Table 8-1 Testing details and differences in development chambers.

	Desaga Chamber	Custom GLAD UTLC Chamber
GLAD UTLC film deposition date	May 31, 2012	Nov. 1, 2012
Oxidation heat treatment	200 °C for 24 hr	None
Testing date	June 22, 2012	May 7, 2013
Ambient relative humidity (% RH)	36	17
Ambient temperature (°C)	23	23
Required mobile phase volume (mL)	21	210
Pre-development chamber vapour phase saturation time (min)[2]	0	3
Length of glass frit between reservoir liquid level and UTLC plate (mm)	2	4
Separation between UTLC plate and conditioning trough liquid level (mm)[3]	4	< 4
Glass frit porosity	Not provided	"P2"
Frit-plate interface length (mm)	1.3	1.5

8.3.1 Intra-plate variation

Mobile phase flow non-uniformities are believed to be one of the largest causes of chromatographic figure of merit variations on a single GLAD UTLC plate. The greatest flow uniformity can be expected nearest to the centre of the plate and lowest uniformity closest to the edges. These effects were first probed by comparing separation tracks progressively further from the centre track (track 5). **Figure 8-8** describes signals produced by averaging the Dimethyl Yellow figures of merit for first, second, third, and fourth nearest neighbour separation tracks. (Similar but weaker effects were observed for the other components in the CAMAG dye mixture with shorter migration and lower hR_F.)

Performing this analysis on the fourth plate in each set of five GLAD UTLC plates highlighted interesting differences in Dimethyl Yellow migration distances and FWHMs (**Figure 8-9**). The significantly faster migration observed on plates

[2] The time for which the spotted GLAD UTLC plate sits in the enclosed chamber before chromatographic development.

[3] The surface tension of the mobile phase filling the custom chamber conditioning trough beneath the GLAD UTLC plate produced a convex meniscus. The liquid level rose slightly above the PTFE edges of the overflow troughs and produce a plate-liquid separation less than the designed 4 mm. However, the liquid level in the Desaga chamber conditioning trough was measured directly.

developed in the Desaga chamber (**Figure 8-9a, b**) is likely due to a combination of differences in GLAD UTLC film porosity, glass frit porosity, and the shorter distance along which the mobile phase must flow from the reservoir along the frit (2 mm versus 4 mm, **Table 8-1**). However, this effect is less interesting than that apparent after normalizing migration distances against that of the centre track (**Figure 8-9c, d**). Although very consistent across the separation tracks in the Desaga chamber, progressively slower migration on tracks further from the centre indicate that the plate developed in the custom chamber had a convex migration profile (see a video frame from this run in **Figure 8-8**). Slightly faster migration in the outermost tracks ("Edges Average" signal) suggests that clamps used to hold the GLAD UTLC plate in place disrupted mobile phase flow on the plate in the custom chamber. However, overall good agreement in migration distances (< 5 %) indicates relatively uniform migration across both plates.

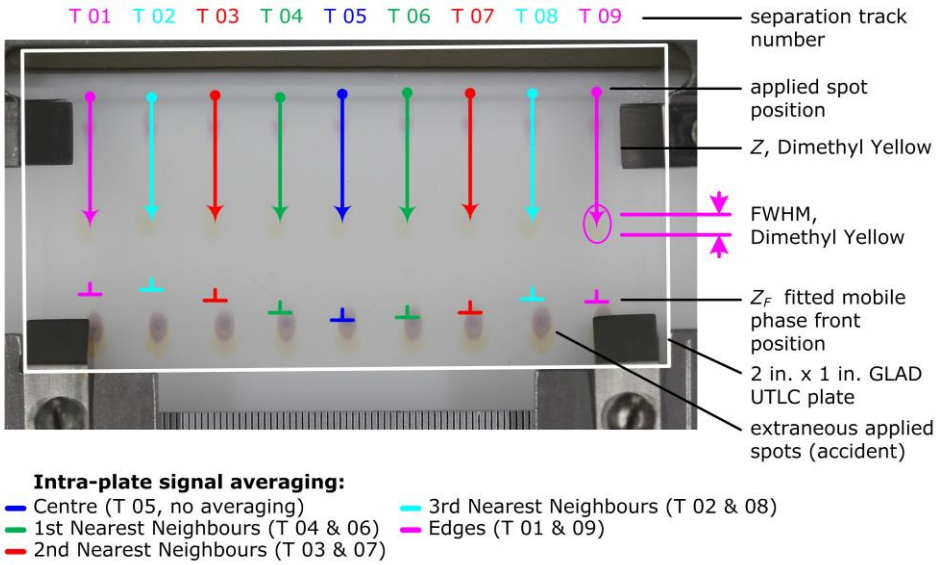

Figure 8-8 Signals used to assess intra-plate figure of merit variation. The migration distance *Z* and FWHM of the Dimethyl Yellow spot was evaluated on 9 tracks across the width of a SBD GLAD UTLC plate. Measured figures of merit were averaged at different distances from the centre track. The sample video frame is from the fourth GLAD UTLC plate used in the custom UTLC chamber. (Sample spots accidentally applied using the wrong sample solvent present at the bottom of the image can be ignored since they were not developed.)

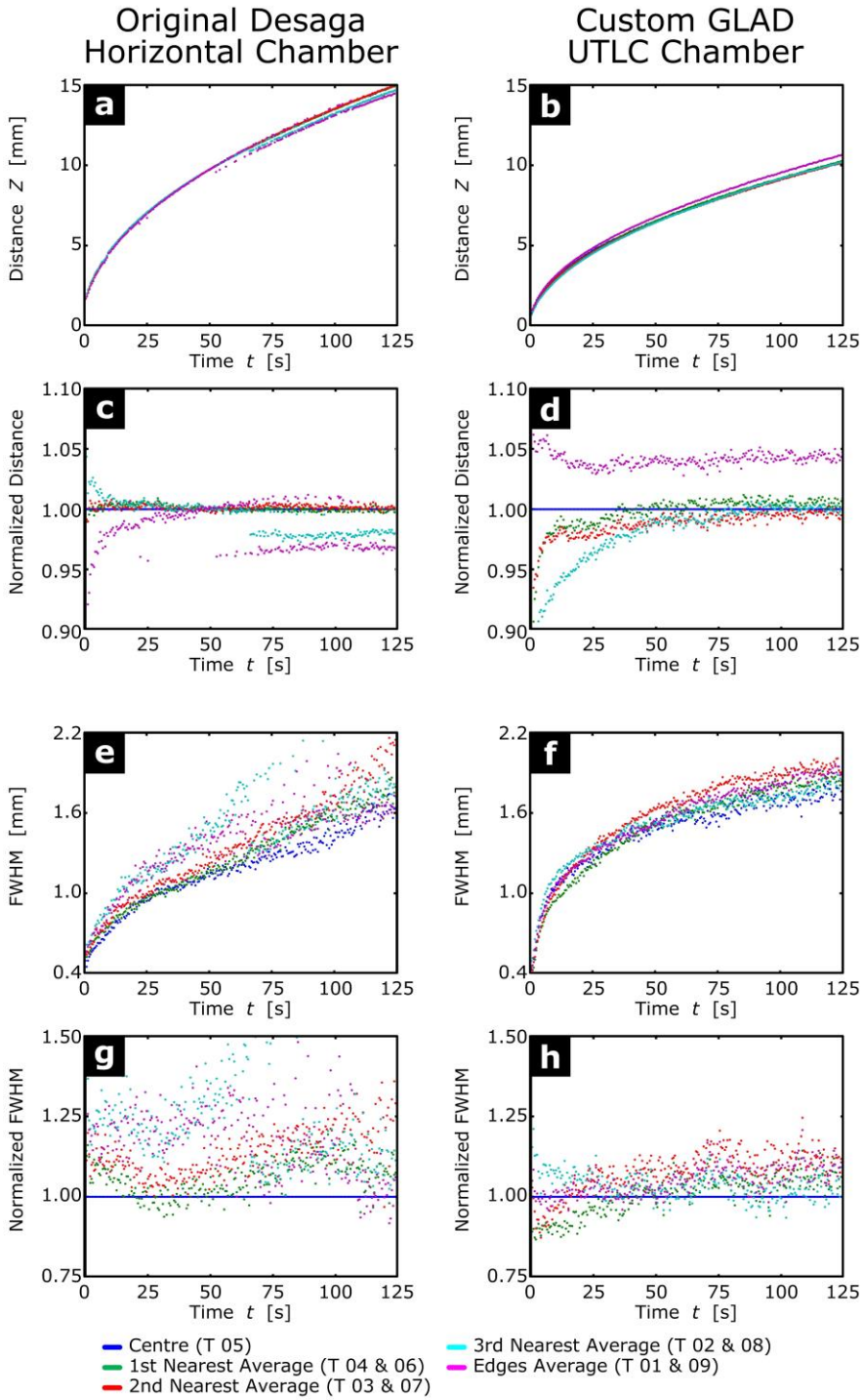

Figure 8-9 Track-averaged Dimethyl Yellow (a,b) migration distance and (e,f) FWHM on a GLAD UTLC plate developed in the Desaga chamber and another developed in the custom chamber. Normalizing these averaged signals against those of the centre track (track 5) enables comparison of (c,d) distance and (g,h) FWHM. Signal averaging is described in **Figure 8-8**.

Similar analysis of the Dimethyl Yellow dye peak FWHMs on plates developed in the chambers also provides valuable insight. Not surprisingly, the calculated spot widths on plates in both chambers are comparable since they are most dependent upon applied spot size – a parameter common in both experiments (**Figure 8-9e, f**). Normalization of the FWHMs indicates that dye spots on tracks further from the centre are broadest, but that greater broadening occurs on the plate developed in the Desaga chamber (**Figure 8-9g, h**). This result seems to contradict the above indication that mobile phase flow uniformity is better on plates in the Desaga chamber. A possible reason for this discrepancy may be that this dye had higher hR_F in the Desaga chamber than in the custom chamber (~ 80 versus ~ 60, **Figure 8-11e, f**) and that broadening tends to be pronounced for high hR_F analytes [10].

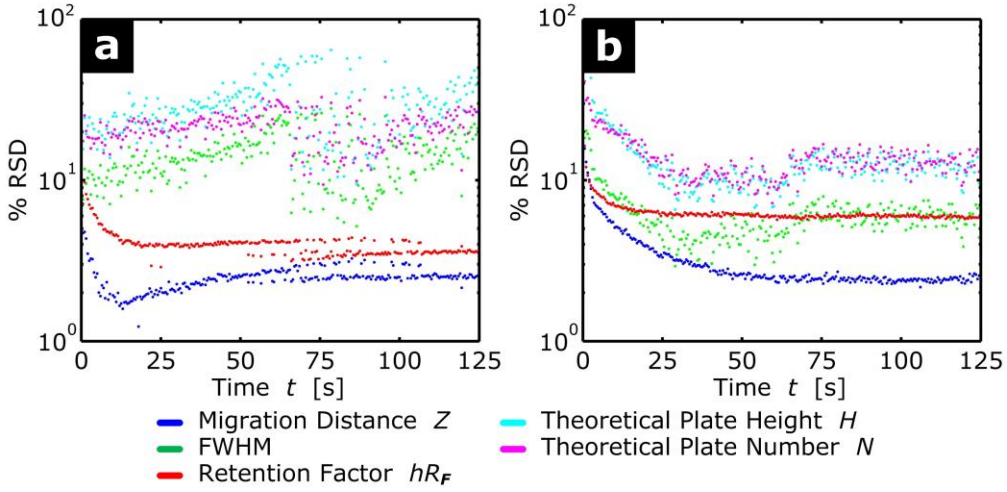

Figure 8-10 Calculated Dimethyl Yellow spot figure of merit relative standard deviations (% RSDs) for a plate developed in (a) the Desaga chamber and in (b) the custom chamber. % RSDs were calculated by averaging all 9 tracks across a single GLAD UTLC plate. Note the logarithmic scale for % RSD.

Figure 8-11 (Next page) Averaged chromatography figures of merit for the Dimethyl Yellow dye spot separated on GLAD UTLC plates in the Desaga and custom UTLC chambers. (a,b) Migration distance, (c,d) FWHM, (e,f) retention factor, (g,h) plate height, and (i,j) plate number were averaged across all 9 tracks in each of the 5 sequential runs.

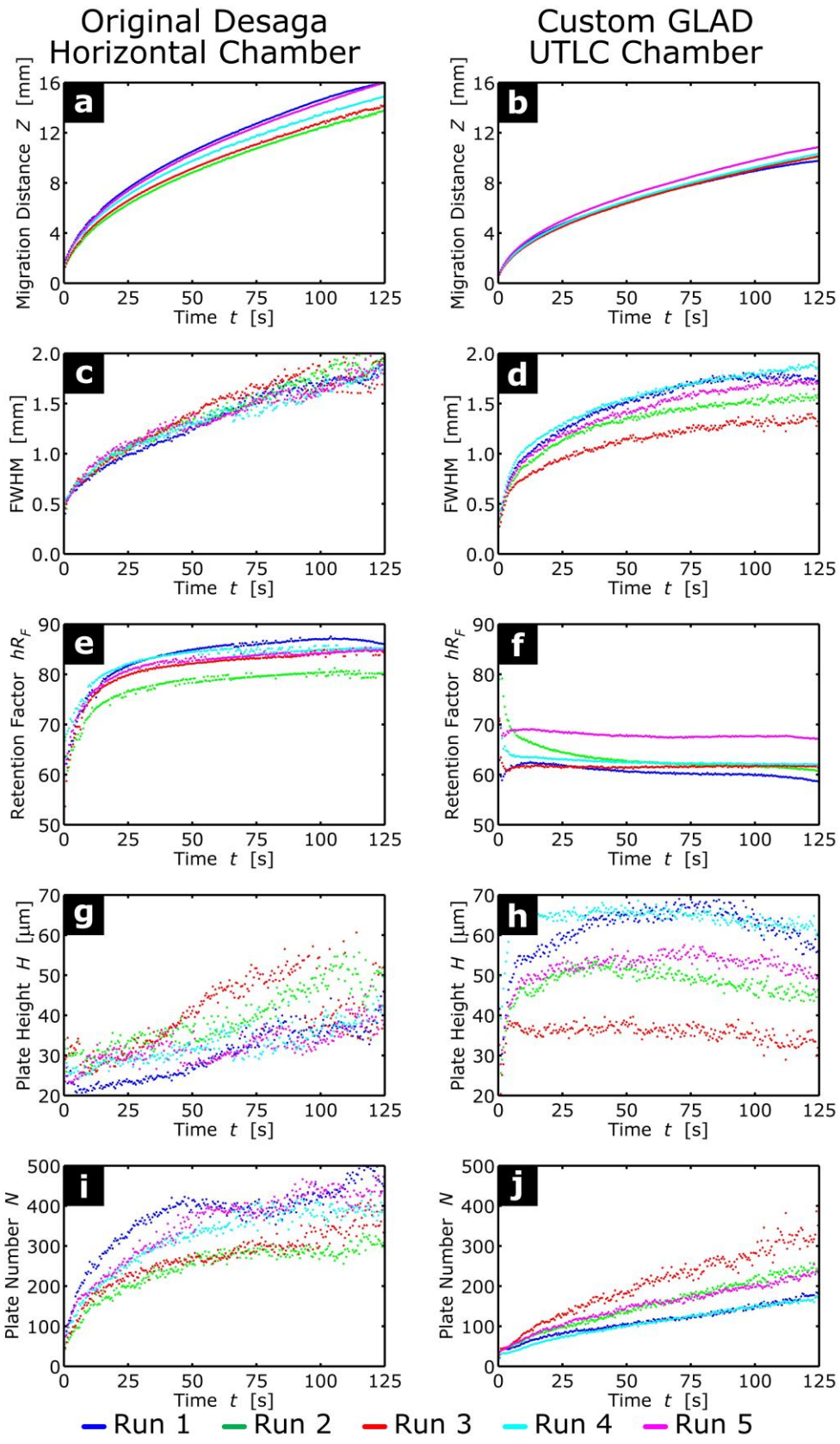

(Caption for **Figure 8-11** on previous page.)

Understanding flow uniformity effects on migration distance and FWHM in the Desaga and custom chambers provides insight into the variation of performance metrics across the whole plate. **Figure 8-10** plots the relative standard deviations for figures of merit across all 9 separation tracks on each plate. Higher migration distances and hR_F values for the separation in the Desaga chamber resulted in slightly lower relative variations (% RSDs) in these measurements. Meanwhile, lower FWHM variation on the plate in the custom chamber produce correspondingly reduced variations in plate height (H) and number (N). These results suggest that the custom GLAD UTLC chamber enables slightly lower intra-plate variation than the modified Desaga chamber used in previous work.

8.3.2 Inter-plate variation

Although variation between separation tracks on the same GLAD UTLC plate may have been slightly improved by the custom chamber, variation between plates appears to be worse. **Figure 8-11** shows the calculated Dimethyl Yellow migration distance, FWHM, hR_F, H, and N averaged across all 9 tracks for each of the five GLAD UTLC plates. Differences in migration distance, retention factor, plate height, and plate number between the two chamber types are not surprising. These changes can easily result from the differences listed in **Table 8-1** and the understanding that parameters optimizing separations in the custom chamber are likely different from those optimized for the Desaga chamber. However, the spread in the figures of merit between plates indicates unimproved control over inter-plate variation.

Comparison of the relative standard deviations in the figures of merit calculated when averaging all 45 available separation tracks together also demonstrate that little improvement in overall figure of merit variation was achieved (**Figure 8-12**). Performance appears similar for both the Desaga and custom GLAD UTLC chambers.

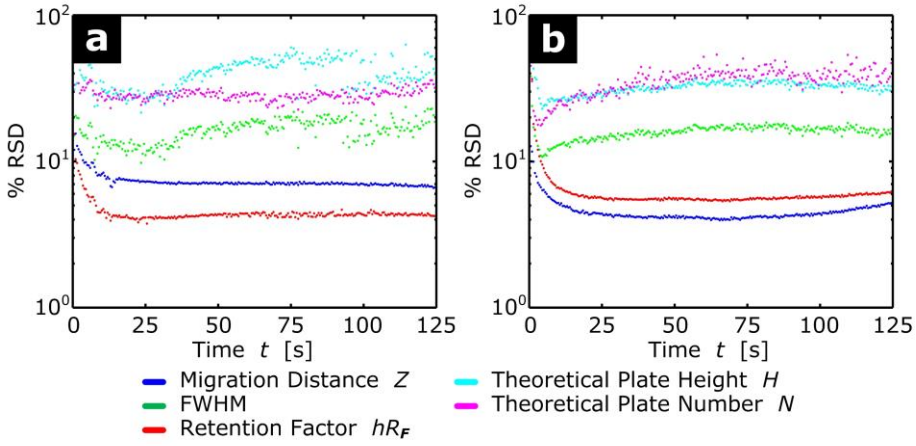

Figure 8-12 Calculated Dimethyl Yellow spot figure of merit relative standard deviations (% RSDs) for plates developed in (a) the Desaga chamber and in (b) the custom chamber. The % RSDs were calculated for figures of merit on all 9 tracks across all 5 plates. In other words, each of the % RSDs considers measurements on 45 separation tracks. Note the logarithmic scale for % RSD.

8.4 Evaluation and suggested improvements

The custom GLAD UTLC chamber satisfied many but not all of the specified objectives. Careful design and expert fabrication produced a device very similar to that specified. Clamps securely fixed the glass frit in the chamber and the chromatography plate into the chamber lid. These features made handling and positioning these delicate pieces easier, faster, and more reliable. Oversized chamber dimensions and in-frame size standards were highly compatible with the time-resolved UTLC characterization approach. The large dimensions enabled maximum use of the video frame while minimizing extraneous shadows. However, these capabilities come at the cost of a significantly more complicated apparatus that is more difficult to set up and requires ten times more mobile phase (210 mL versus 21 mL, **Table 8-1**). Such limitations negate UTLC's claimed advantages of simplicity, low reagent use, and cost effectiveness [1,11–13].

Most importantly of all, the custom GLAD UTLC chamber failed to significantly reduce performance variation within and between subsequent separations. Two of the most likely causes for this are the clamps required to stabilize the GLAD UTLC plates and the deliberately oversized chamber dimensions. As described previously, the clamps slightly distorted mobile phase migration uniformity and resultant separation tracks. The oversized chamber dimensions increased the size of the mobile phase reservoir, conditioning trough, and dead volume requiring vapour saturation whenever the chamber was opened and closed. Changes in mobile phase liquid and vapour composition permitted by the large open reservoirs may have produced some of the observed figure of merit variations. (For example, preferential evaporation of *n*-hexane enriches the toluene fraction in the mobile phase and increases hR_F.)

An improved chamber would incorporate improvements in frit and UTLC plate placement achieved by the present design while minimizing chamber dead volume and contact with the stationary phase surface. Utilizing smaller fluid reservoirs and clamping devices would be essential. Employing transmission mode illumination from below the UTLC plate would eliminate the shadows produced by reflection mode illumination within the smaller chamber.

8.5 Conclusions

The absence of planar chromatography chambers optimized for miniaturized UTLC plates is a large obstacle affecting the utility, performance, and popularity of the technique [1,7]. Work described in this chapter summarized a preliminary attempt to engineer a chamber optimized for the specific needs of GLAD UTLC. Enhanced time-resolved UTLC methods produced the rich analysis required to compare the effectiveness of the previously-used Desaga chamber to that of the custom apparatus. Although the resultant chamber met several of the required design criteria, this analysis demonstrated that it failed to significantly improve the intra-plate and inter-plate variation in measured separation figures of merit. Clamps used to ensure GLAD UTLC plate positioning may have introduced

mobile phase flow non-uniformities and oversized dimensions optimized for time-resolved UTLC may have made mobile phase (and vapour phase) composition less constant. The lessons learned in this attempt provide guidelines for future GLAD UTLC chambers.

References

[1] S.R. Jim, M.T. Taschuk, G.E. Morlock, L.W. Bezuidenhout, W. Schwack, M.J. Brett, Engineered anisotropic microstructures for ultrathin-layer chromatography, Anal. Chem. 82 (2010) 5349–5356.

[2] A.J. Oko, S.R. Jim, M.T. Taschuk, M.J. Brett, Analyte migration in anisotropic nanostructured ultrathin-layer chromatography media, J. Chromatogr. A. 1218 (2011) 2661–2667.

[3] S.R. Jim, A.J. Oko, M.T. Taschuk, M.J. Brett, Morphological modification of nanostructured ultrathin-layer chromatography stationary phases, J. Chromatogr. A. 1218 (2011) 7203–7210.

[4] S.R. Jim, A. Foroughi-Abari, K.M. Krause, P. Li, M.R. Kupsta, M.T. Taschuk, et al., Ultrathin-layer chromatography nanostructures modified by atomic layer deposition, J. Chromatogr. A. 1299 (2013) 118–125.

[5] G.E. Morlock, C. Oellig, L.W. Bezuidenhout, M.J. Brett, W. Schwack, Miniaturized planar chromatography using office peripherals, Anal. Chem. 82 (2010) 2940–2946.

[6] S. Kirchert, Z. Wang, M.T. Taschuk, S.R. Jim, M.J. Brett, G.E. Morlock, Inkjet application, chromatography, and mass spectrometry of sugars on nanostructured thin films, Anal. Bioanal. Chem. (2013).

[7] J. Wannenmacher, S.R. Jim, M.T. Taschuk, M.J. Brett, G.E. Morlock, Ultrathin-layer chromatography on SiO2, Al2O3, TiO2, and ZrO2 nanostructured thin films, J. Chromatogr. A. 1318 (2013) 234–243.

[8] A.J. Oko, S.R. Jim, M.T. Taschuk, M.J. Brett, Time resolved chromatograms in ultra-thin layer chromatography, J. Chromatogr. A. 1249 (2012) 226–232.

[9] A.J. Oko, Advanced Materials and Detection Methods in Ultrathin-Layer Chromatography, University of Alberta, 2013.

[10] B. Spangenberg, C.F. Poole, C. Weins, Quantitative Thin-Layer Chromatography, Springer Berlin Heidelberg, Berlin, Heidelberg, 2011.

[11] H.E. Hauck, O. Bund, W. Fischer, M. Schulz, Ultra-thin layer chromatography (UTLC) — A new dimension in thin-layer chromatography, J. Planar Chromatogr. 14 (2001) 234–236.

[12] H.E. Hauck, M. Schulz, Ultrathin-layer chromatography, J. Chromatogr. Sci. 40 (2002) 550–552.

[13] H.E. Hauck, M. Schulz, Ultra thin-layer chromatography, Chromatographia. 57 (2003) S313–S315.

9 Summary, evaluation, future directions, and remarks

Planar chromatography is often the 'Rodney Dangerfield[1]' of analytical chemistry – *it don't get no respect*. Too many dismiss the technique as an antiquated "quick and dirty" method capable of only qualitative results. They fail to appreciate the merits of this reasonably simple but exceptionally powerful approach to rapidly analyzing complex samples. This dissertation serves as just one example of continued progress in this often underappreciated field. It attacked the method's shortcomings from many angles and identified a couple of new opportunities along the way. The described research aims to demonstrate ongoing advancements and help planar chromatography earn back some of its due respect.

[1] American actor and comedian (1921-2004) well-respected for his famous monologues about the misfortunes he experienced.

9.1 Summary

9.1.1 Anisotropic microstructures

Glancing angle deposition is a powerful platform for engineering ultrathin-layer chromatography microstructures of numerous architectures. The thin film deposition technique can produce planar stationary phases impossible or impractical using other techniques. Of particular interest are the unique media described in **4 Anisotropic UTLC microstructures**. Channel features between the blade-like SBD structures strongly influenced, but did not entirely dictate, analyte migration and separation performance on anisotropic GLAD UTLC film. These behaviours were quantified by introducing new migration anisotropy (*MA*) and separation track deviation angle ($\Delta\theta$) metrics. Development characteristics were also evaluated on media of varied porosity (as controlled by α) and with other morphologies (anisotropic chevron and isotropic vertical post) morphologies.

9.1.2 Modified morphology and development

The strong dependence of chromatographic performance on GLAD UTLC layer microstructure motivated consideration of post-deposition enhancement techniques. Fluorocarbon reactive ion etching and subsequent heat treatments used to tune development characteristics were described in **5 Modified morphology and development**. As RIE duration increased, a smooth transition through three different modification regimes was observed: short durations widened pores, intermediate durations collapsed the GLAD columns, and long durations rarified the columns. Increased film porosity and reduced specific surface area produced higher migration velocities and lower analyte retention after etching. Etching through a simple shadow mask (stencil) patterns regions with different morphologies. This technique enabled fabrication of a rarified concentration zone adjacent to a denser separation zone. The resultant GLAD UTLC-CZ plates increased the separation performance for large applied sample spots.

9.1.3 Atomic layer deposition modification

Atomic layer deposition produces highly conformal coatings with unprecedented thickness control. **7 Surfaces modified by atomic layer deposition** describes GLAD UTLC media enhanced using this technique. Chromatographic separations, gas adsorption porosimetry, and transmission electron microscopy probed the manner in which ALD coatings of Al_2O_3, ZrO_2, and ZnO applied to GLAD SiO_2 films adjust physical properties, analyte retention, and separation performance. The most significant changes in surface area and surface chemistry occurred over only the first ~ 2 nm of coating. This indicates that incorporating ALD with GLAD can decouple the properties of the surface from those of the underlying scaffold microstructure; composites can express the most useful attributes of each. The combined approach can therefore produce high surface area media unachievable by GLAD alone. GLAD ALD composite nanomaterials potentially expand the selection of chromatography materials to include all those under development in the highly-active ALD field.

9.1.4 Custom instrumentation and analysis

Mismatches between equipment and chromatographic materials generally limit overall separation performance. In the specific case of miniaturized GLAD UTLC plates, instruments that enable precise sample spotting, high resolution imaging, and careful chromatography plate handling are necessary. **6 Time-resolved UTLC** describes techniques to extract and analyze colour-filtered chromatograms from high-definition videos of chromatographic separations on GLAD UTLC plates. Enhancements generalized the previously reported TR-UTLC platform to any number of coloured analytes, improved automation, enabled high-level data set comparisons, and increased user-friendliness.

The powerful toolset was applied to studies of alternative GLAD UTLC oxide materials and to evaluation of a new chromatographic chamber. **8 Customized GLAD UTLC chamber** discusses efforts to custom engineer this new horizontal development chamber for miniaturized GLAD UTLC plates. The device was

designed to make these tiny media easier to handle, reduce variations in separation performance, and improve compatibility with TR-UTLC techniques. Testing results indicate that not all of these objectives were satisfactorily met and that a subsequent design iteration is needed to address additional challenges.

9.2 Comparison of GLAD UTLC to UTLC

Appropriate comparison between GLAD UTLC media and the first monolithic UTLC media reported by Hauck *et al.* [1–3] provides some context to the research conducted during this dissertation. Although imperfect, this planar chromatography comparison is most suitable given the similarities in layer thickness and testing method. **Table 9-1** lists differences in layer properties, **Table 9-2** evaluates factors affecting chromatography plate utility, and **Table 9-3** describes representative performance. These tables amalgamate GLAD UTLC results described in chapters **4 Anisotropic UTLC microstructures** (published in [4,5]), **5 Modified morphology and development** (published in [6]), and **7 Surfaces modified by atomic layer deposition** (published in [7]). Results not discussed in detail in this thesis but published with coauthors are also included (J. Wannenmacher [8], S. Kirchert [9], and A.J. Oko [10]). Although insightful, it is important to recognize the limitations of these comparisons and avoid over-generalization. The stationary phase properties, instrumentation, and example separations are both unoptimized and vastly different for the two types of media. Furthermore, recurring use of the CAMAG lipophilic dye mixture (**3.4.1 Model dye system**) throughout this dissertation should not imply that this mixture is of particular importance in planar chromatography or that separation efficiency of these specific dye components indicates universal performance. The CAMAG dye simply served as a convenient standard throughout the GLAD UTLC studies.

9.2.1 Layer properties

(See **Table 9-1**.) The GLAD physical vapour deposition approach enables a significantly broader selection of microstructures and surface chemistries than possible with UTLC monolithic silica gels. Isotropic and anisotropic GLAD

UTLC media of many different metal oxides have been demonstrated. Further flexibility is achieved through the post-deposition RIE processing and ALD coating. However, the fragility of the thinner GLAD films can make handling more difficult. Both media are sensitive to analyte overloading because they exhibit similar specific surface areas (350 m^2g^{-1} for UTLC and 250-340 m^2g^{-1} for GLAD UTLC) that are lower than TLC and HPTLC layers (480-540 m^2g^{-1}) [11,12].

Table 9-1 Comparison of the layer properties of monolithic layers reported by Hauck *et al.* to GLAD UTLC layers produced in dissertation.

	Monolithic UTLC [1–3]	GLAD UTLC
Stationary Phase Material	Silica sol-gel	• SiO_2 [4–9] • Al_2O_3 [7,8] • TiO_2 and ZrO_2 [8] • SiO_2 functionalized with ALD Al_2O_3, ZrO_2, and ZnO (< 10 nm) [7]
Typical Thickness (μm)	10	• 1.3, 2.6 [8] • 4.5-5.4 [4–7,9]
Morphology	Isotropic; sponge-like macroporous monolith	Isotropic or anisotropic; ~100-400 nm thick columns or blades separated by 100-800 nm: • Chevrons [4] • Vertical posts [4,6,7,9] • Blade-like [4,5,8,9] • (Also reactive ion etched columns [6])
Characteristic Size (μm)	1-2 (macropore size)	0.1-0.8 (intercolumn void) [4–9]
Pore Size (nm)	3-4	2-6 [2] [13]
Specific Surface Area (m^2g^{-1})	350	SiO_2 vertical posts [7]: 300 (uncoated); 250-340 (with ALD Al_2O_3 coatings)
Mechanical Stability	Robust	Easily scratched

[2] Pore size was not measured for GLAD UTLC media in this dissertation. Estimated size included above is that reported by K.M. Krause *et al*. [13] for similar films.

9.2.2 Practical considerations

(See **Table 9-2**.) The miniature size of monolithic UTLC plates (typically 36 mm x 60 mm) and GLAD UTLC plates (typically ~ 25 mm x 25-50 mm) introduces significant challenges. Adequate separation performance requires sufficiently small applied sample volumes. Improved spotting equipment (namely, inkjet printers [8,9,14]) now enables precisely-applied low volume spots that were unavailable to Hauck *et al.* a decade ago [1–3]. Vapour phase saturation of organic mobile phases was often required to limit evaporation from the exceptionally thin monolithic and GLAD UTLC media. Both UTLC media require only small mobile phase volumes (1-4 mL) and are compatible with several offline (digital photography and scanning densitometry) and online (TR-UTLC) evaluation modes.

9.2.3 Representative separation performance

(See **Table 9-3**.) Fewer types of sample separations were performed on GLAD UTLC media during this dissertation than reported for monolithic UTLC media. Chromatography of steroids, pesticides, phenols, plasticizers, pharmaceuticals, and amino acids on nanostructured thin film media is likely possible but has not yet been demonstrated. Faster observed migration and separation of several samples on GLAD UTLC layers suggest that these columnar media are more permeable than the monolithic silica gels. Nonetheless, differences in analyte application (volume, instrument) and detection inhibit definitive comparison of absolute separation efficiencies. For example, the extraordinary separation efficiencies (low H) of the aqueous dyes are products of GLAD nanostructuring, precise inkjet printing, and TR-UTLC detection. Comparable relatively low unoptimized LODs (single nanograms) were achieved on both media in spite of differences in analyte type and detection mode. Results summarized in **Table 9-3** suggest that GLAD UTLC media have overall separation performance similar to monolithic silica gel UTLC layers. However further work with additional analytes, instrumentation, and GLAD thin films is required to better quantify the potential performance of this advanced technique.

Table 9-2 Practical considerations affecting monolithic UTLC and GLAD UTLC layer utility. Reported sample spotting methods, development details, and detection modes are provided. (Table also includes some relevant monolithic UTLC reports not written by Hauck *et al*.)

	Monolithic UTLC	GLAD UTLC
Sample Application Volume; Spotting Instrument	• 10 nL; Hamilton 0.5 µL syringe [1–3] • Unknown; I&J Fisnar robot with blunt needle tips, contact mode [3] [10] • 6.8-10.6 nL; piezoelectric PipeJet Nanodispenser P9 [4] [14] • 10-20 nL [2,3], 100-160 nL [4] [14]; CAMAG ATS 4 robot • 0.8-9.6 nL; modified Canon inkjet printer [4] [14]	• 50 nL; Hamilton 0.5 µL syringe, contact mode [7] • Unknown; I&J Fisnar robot with blunt needle tips, contact mode [5,6,8] • 25 nL; modified CAMAG ATS 4 robot, aerosol spray [4] • 3-27 nL; modified Canon inkjet printer [8,9]
Development Chamber; Vapour Saturation	• Ascending (upright) development in "normal" chamber (flat-bottomed tank); with saturation [1–3] • Desaga horizontal chamber; with saturation [3] [10]	• Desaga horizontal chamber; with and without saturation [4–9] • Large volume custom GLAD UTLC chamber, with chamber saturation [5].
Mobile Phase Consumption	1-4 mL [1–3]	1.4-2.5 mL [4,8,9]
Detection and Documentation	• Desaga ProVidDoc [6] (visible) [1]; also after staining [2] • CAMAG TLC Scanner II [7] (visible, UV 200 nm, and UV 254 nm) [1–3] • J&M diode array spectrometer [7] (UV 200 nm and UV 234 nm) [2,3] • Hewlett-Packard flatbed scanner (reflection mode, visible) [4,6] [14] • TR-UTLC system (visible) [3,8] [10]	• Canon flatbed film scanner (transmission mode; visible) [6] [4–6] • Canon DSLR camera [6] (visible) [7]; also after post-separation derivatization [9] • TR-UTLC system (visible) [8] [8]

[3] Used by A.J. Oko *et al*. [10] (prior to the enhancements described in **6 Time-resolved UTLC**).
[4] Used by Morlock *et al.* [14] in performance comparisons with Office Chromatography.
[5] Unpublished custom chamber described in **8 Customized GLAD UTLC chamber**.
[6] Records digital images after development. Densitograms may be generated from these images.
[7] Records only densitogram curves after development by scanning densitometry.
[8] Records digital videos of development and generates time-resolved chromatograms. See also **6 Time-resolved UTLC**.

Table 9-3 Representative sample separation performance on monolithic UTLC and GLAD UTLC layers.

	Monolithic UTLC	GLAD UTLC
Tested Analytes; Mobile Phase Used	• Lipophilic dyes; toluene [1] • Steroids; ethyl acetate / cyclohexane [1,3] • Pesticides; petroleum ether / acetone [1] or petroleum benzene / acetone [2] • Phenols; toluene / chloroform / methanol [2,3] • Plasticizers; petroleum benzene / acetone [2,3] • Pharmaceutically-active ingredients; *n*-hexane / ethyl acetate [2,3] • Amino acids; water / acetonitrile / acetic acid [2] • Caffeine and acetaminophen; ethyl acetate / methanol [2]	• Lipophilic dyes; toluene / *n*-hexane [4–7] • Aqueous dyes; ethyl acetate / methanol / water [8] • Carotenoid pigments; toluene / *n*-hexane / acetic acid [8] • Sugars; ethyl acetate / methanol / formic acid / water [9]
Development Distance (Z_F) and Time	• Lipophilic dyes [1]: 15 mm in 165 s • Steroids [1,3]: 20 mm in 345 s • Pesticides [1,2]: 20 mm in 225-260 s • Phenols; plasticizers; and pharmaceutically-active ingredients [2,3]: 20 mm in 240-250 s • Amino acids [2]: 20 mm in 210 s • Separation of caffeine and acetaminophen [2]: 10 mm in 105 s	• Lipophilic dyes [4–6]: 5-23 mm in 45-90 s • Aqueous dyes [8]: 10-13 mm in 110-160 s • Sugars [9]: 15 mm in 180 s

Table 9-3 Representative sample separation performance on monolithic UTLC and GLAD UTLC layers. (Continued.)

	Monolithic UTLC	GLAD UTLC
Plate Height (H, μm) [9]	• Caffeine: 104 (1.5 mm) [2] • Acetaminophen: 80 (4.5 mm) [2] • Lipophilic dyes [10] [10]: Dimethyl Yellow: ~ 40 (< 12 mm); Ariabel Red: ~ 67 (< 4 mm)	• Lipophilic dyes: Dimethyl Yellow: 20-50 (<16 mm) [11]; Dimethyl Yellow: 8-28 (3-16 mm) [4–6]; Ariabel Red: ~ 17 (1-5 mm) [4–6] • Aqueous dyes [12] [8]: Acid Red 14: 2-3 (< 5 mm); Tartrazine: ~ 3 (< 5 mm)
Plate Number (N) [9]	• Caffeine: 14 (1.5 mm) [2] • Acetaminophen: 56 (4.5 mm) [2] • Lipophilic dyes [10] [10]: Dimethyl Yellow: < 300 (< 12 mm); Ariabel Red: < 60 (< 4 mm)	• Lipophilic dyes: Dimethyl Yellow: 250-400 (<16 mm) [11]; Dimethyl Yellow: 150-1200 (3-16 mm) [4–6]; Ariabel Red: < 300 (1-5 mm) [4–6] • Aqueous dyes [12] [8]: Acid Red 14: < 3000 (< 5 mm); Tartrazine: < 2000 (< 5 mm)
Limit of Detection for Given Analyte and Detector (Absorption)	• Caffeine (CAMAG TLC scanner, UV 200 nm) [2]: 1 ng	• Lipophilic dye (Canon flatbed film scanner, transmission imaging) [4]: Dimethyl Yellow < 10 ng • Aqueous dye (TR-UTLC system) [8]: Tartrazine < 2 ng; Acid Red < 7 ng • Sugars (derivatized and photographed) [13] [9]: Lactose ~ 3 ng; Sucrose ~ 4 ng; Fructose ~ 5 ng

[9] Analyte migration distance Z provided in parentheses.
[10] Measured H and N were not calculated by Hauck *et al*. These measurements were attained using TR-UTLC in A.J. Oko *et al.* [10].
[11] These unpublished Dimethyl Yellow Z, H, and N measurements were obtained using TR-UTLC and are plotted in **Figure 8-11**.
[12] These unpublished Z, H, and N measurements were obtained using TR-UTLC after publication of [8] and are plotted in **Figure 6-8** and **Figure 6-10**.
[13] Separated sugars were visualized using a derivatization reaction. Chromatograms were generated from digital photographs of the resultant plates. Subsequent densitogram analysis produced the listed extrapolated LOD estimates.

9.3 Recommended future directions

9.3.1 Optimized instrumentation and methods

Requirements for effective UTLC plate utilization are more stringent than those demanded by HPTLC. Serious limitations posed by HPTLC instrumentation incompatible with UTLC make optimized equipment design necessary. Continued attempts to customize development chambers for UTLC or to make UTLC media compatible with existing development chambers may achieve the desired separation reproducibility. Planar chromatography in general could also benefit from time-resolved methods that incorporate transmission mode imaging, UV excitation, 3D peak extraction and fitting, and automated calculation of additional chromatographic figures of merit (such as separation number and limits of detection). Further advancement of the Office Chromatography concept [8,9,14] may eventually permit any sample mixture to be inkjet printed with exceptional precision. Devices and methods that increase the reproducibility and performance of miniaturized chromatography media would yield many benefits. Improved quantification would allow other investigation and optimization efforts to be targeted specifically on stationary phase engineering and mobile phase selection. Furthermore, instruments that make spotting, development, documentation, and general use of miniaturized plates easier and more reliable would also ultimately increase the utility, acceptance, and popularity of UTLC.

9.3.2 Coupled techniques

This thesis described several orthogonal methods of improving GLAD UTLC stationary phase performance: nanostructuring, reactive ion etch modification, and atomic layer deposition coating. Combining these capabilities could produce a highly useful new type of UTLC plate, for example an "anisotropic GLAD SBD SiO_2 | Al_2O_3 UTLC-CZ" plate. Channel features incorporated into this anisotropic serial bideposition (SBD) film would permit rapid development along several closely-spaced separation tracks; patterning a concentration zone (CZ)

would compress (large) applied spots into sharp well-separated bands; and ALD coating would achieve useful surface chemistry alternatives (such as Al_2O_3). Utilizing these media in an optimized GLAD UTLC chamber compatible with TR-UTLC imaging would also include the benefits of advanced instrumentation.

Incorporating other areas of research may also improve the utility of GLAD UTLC plates. Exploration of hydrophobic functionalization [15] or other ALD coatings untested in UTLC may enable separations of additional types of samples. Driving mobile phase flow with an electric field (planar electrochromatography [16,17]) may increase performance. Further analytical power could be achieved by hyphenating GLAD UTLC with many existing post-development characterization techniques [18,19] such as surface enhanced Raman spectroscopy (SERS) [20] or mass spectroscopy (electrospray ionization [8,9,21], laser desorption ionization [22,23], or direct analysis in real time [24]). Adding a fluorescence indicator to the nanostructured sorbent could extend utility to UV active (absorbing) analytes.

9.3.3 Advanced analytical separation devices

The methods and types of GLAD layers developed for UTLC in this dissertation may be applicable to other analytical separation fields. Incorporating these structures into microfluidic channels may produce faster separations of biomolecules such as proteins and DNA [25,26].

Reactive ion etching planar GLAD films through shadow masks may also enable simple patterning of complex macroporous elements. Porous millimetre-scale channels patterned in relatively dense columnar thin films could produce useful passive fluidic devices driven only by capillary forces. Quantitative analysis may be improved by confining UTLC separations to narrow channels. Other elements designed to condense, mix, and split streams of fluids wicking through these devices could enable additional capabilities. This concept could combine the benefits of UTLC with those of lab-on-a-chip microfluidics.

9.4 Overall UTLC method evaluation[14]

Ultrathin and nanostructured planar chromatography layers have progressed significantly since UTLC's invention in 2001 by Hauck *et al.* [1] and its commercialization by Merck Darmstadt in 2002 [27]. **Table 9-4** summarizes the properties of some of these new stationary phases, including GLAD media. Relatively simple chemical reactions can produce monolithic silica gels and porous polymer sorbents of varied thickness; sometimes as thick as traditional TLC and HPTLC layers. In new approaches, nanofibrous mats rapidly prepared using electrospinning enable highly efficient separations [21,28–30]. Planar chromatography media templated onto patterned carbon nanotube forests produce tunable geometries by leveraging established microfabrication processes [31–33]. This dissertation demonstrates that GLAD is a powerful platform for engineering nanostructured thin films of varied material, porosity, and architecture that are well-suited for UTLC. Initial reports of new UTLC media produced from layers of coated < 1 μm silica particles [34], brush-gel polymers [35], and microfabricated pillar arrays [36] were not discussed in detail in this thesis but demonstrate that new approaches to producing alternative sorbents continue to emerge and evolve.

Although each ultrathin and nanostructured stationary phase has its own merits, there are several similarities. Miniaturized plates utilize these layers to achieve faster separations over shorter distances with high sensitivity and reduced reagent requirements [2]. However, their smaller size, thinness, and reduced specific surface areas prevent direct transfer of HPTLC methods to UTLC [2,9]. Smaller total surface areas often result in lower analyte retention and higher susceptibility to overloading. Shorter development distances can reduce sample capacity and resolution [11]. Their miniature format can make manual handling awkward and HPTLC instrument limitations can stifle overall separation

[14] Portions of this section are in-press as Chapter 3 "Ultrathin and Nanostructured Stationary Phases" by S.R. Jim and M.J. Brett in *Instrumental Thin Layer Chromatography* (Ed: C.F. Poole), Elsevier, 2014.

performance [11]. These obstacles slowed widespread adoption of monolithic UTLC plates by analytical chromatographers and contributed to Merck Darmstadt's decision to remove them from product catalogues after 2011 [37]. Improved equipment for precise small sample application, development, and documentation (as per Office Chromatography [14] or TR-UTLC [10], for example) are required before UTLC's full separation power can be realized. As a whole, the UTLC (and broader planar chromatography) community recognize that success is contingent upon creation of this infrastructure. Nonetheless, the significant potential performance benefits motivate continued parallel development of miniature nanostructured stationary phase layers and instrumentation optimized for these media.

9.5 Final remarks

This dissertation described the mutually beneficial partnership between two relatively recent fields of study: ultrathin layer chromatography and glancing angle deposition. The success of this pairing relied on the invention of new experimentation and characterization methods. Threads through nanofabrication, apparatus design, and numerical analysis were needed to tie the disciplines together. Once bound, GLAD functioned as an excellent platform for fabricating unique morphologies previously untested in UTLC. Original, intriguing, and potentially useful chromatographic capabilities were achieved. At the same time, UTLC served GLAD as an application within which new morphologies and approaches to modification could be studied. Micro and nano scale material properties could be related to observable macroscopic phenomena. Investigations described in this dissertation facilitated encounters between these remarkable fields of study that contributed to the knowledge, understanding, and capabilities of each.

Table 9-4 Comparison of GLAD UTLC thin films to other ultrathin and nanostructured stationary phases. (This is a version of **Table 2-2** modified to include GLAD UTLC data.).

	Monolithic Silica Gel [15]	Monolithic Polymer	Electrospun Polymer	Carbon Nanotube-Templated Silica	Nanostructured GLAD UTLC Thin Films
Stationary Phase Material	Silica sol-gel [1–3,38–40]	Photopolymerized poly(butyl methacrylate-*co*-ethylene dimethacrylate) [41,42]; poly(glycidyl methacrylate-*co*-ethylene dimethacrylate) [43]	Polyacrylonitrile [21,28–30]; Glassy carbon [29]; Polyvinyl alcohol [44]; Cellulose acetate [45]	SiO_2 nanowire hedges [31,46]; (also functionalized with 3-aminopropyltriethoxysilane, APTES [32,33])	SiO_2 [4–9,14,47]; Al_2O_3 [7,8]; TiO_2 and ZrO_2 [8]; SiO_2 functionalized with C18 [15]; SiO_2 functionalized with ALD Al_2O_3, ZrO_2, and ZnO (< 10 nm thick) [7]; Ag [20]
Thickness	10-12 μm [1–3,38]; ~ 100 μm [40]	50-200 μm [41–43]	5-25 μm [21,28–30,44,45]	~50 μm [31–33,46]	2.6-9 μm [4–9,14,15,47]; 200 nm Ag thin film [20]
Morphology [16]	Isotropic monolith; macroporous and mesoporous [2,39,40]; SSA ~ 350 m^2g^{-1} [2]	Isotropic monolith; macroporous and mesoporous [41–43]	Isotropic [21,28–30,44,45] or anisotropic [30]; mat composed of nanofibres (width 150-600 nm [21,28–30,44,45]); SSA 21.7 m^2g^{-1} [28]	Anisotropic; herring-bone (zig-zag) pattern [31–33,46]; composed of 3-4 μm wide hedges spaced 4-6 μm apart [32,33,46]; with 100-120 nm diameter SiO_2 nanowires [33]; SSA 19-27 m^2g^{-1} for oxidized SiCNTs [46]	Isotropic or anisotropic; ~100-400 nm thick columns or blades separated by ~100-800 nm: Hexagonal helices [14,47]; Chevrons [4,47]; Vertical posts [4,6,7,9,15]; Blade-like [4,5,8,9]; Incline posts [20]; (also reactive ion etched columns [6]) SSA ~300 m^2g^{-1} (SiO_2 vertical posts) and ~ 250-340 m^2g^{-1} (SiO_2 coated in ALD Al_2O_3) [7]

[15] The monolithic silica gel properties listed here include those of Merck UTLC plates and others. **Table 2-1** includes only Merck UTLC plate data.

Table 9-4 Comparison of GLAD UTLC thin films to other ultrathin and nanostructured stationary phases. (This is a version of **Table 2-2** modified to include GLAD UTLC data.). (Continued.)

	Monolithic Silica Gel [15]	Monolithic Polymer	Electrospun Polymer	Carbon Nanotube-Templated Silica	Nanostructured GLAD UTLC Thin Films
Substrate	Glass [1–3,38–40]	Glass [41–43]	Al [21,28,44,45]; Stainless steel [29,30]	Si wafer [31–33,46]	Glass [4–9,14,15,20,47]
Substrate Size	25-40 mm x 30-100 mm [1–3,38–40]	26-30 mm x 33-76 mm [41–43]	20-40 mm x 40-85 mm [21,28–30,44,45]	Limited by 100 mm circular wafer [31–33,46]	20-25 mm x 25-100 mm [4–9,14,15,47]
Development Distance and Time	10-30 mm in 1-8 min [1–3,39,40,48]	30-60 mm in < 6 min [41,43]	25-35 mm in 3-12 min [21,28–30,44] or 70 mm in 30-45 min [45]; 25 mm in 1-1.5 min for aligned nanofibres [30]	25-45 mm in 1-4.5 min [31–33,46]	5-12 mm in < 6 min [4–6,8,9,14,20,47]
Tested Analytes	Dyes [1,39,40]; Pharmaceutically active ingredients [2,3,22,48,49]; Phenols and plasticizers [2,3]; Amino acids and pesticides [2]; Steroids [3]; Triazoles [48]	Proteins and peptides [41–43]; Dyes [41]	UV fluorescent laser dyes [28–30]; Steroids [28,30,45]; Amino acids [29,44]; β-blockers [30]; Beverage preservatives [21]; Aspartame hydrolysis products (aspartic acid, phenylalanine) [44]	Dyes [31–33,46]; Analgesics [46]	Dyes [4–8,14,15,20,47]; Sugars and chocolate samples [9]; Melamine and Trans-1,2-bis(4-pyridyl)ethylene [20]

[16] The reported specific surface areas (SSA) were measured using the Brunauer, Emmett and Teller (BET) method [50], where available. (Previous page.)

References

[1] H.E. Hauck, O. Bund, W. Fischer, M. Schulz, Ultra-thin layer chromatography (UTLC) — A new dimension in thin-layer chromatography, J. Planar Chromatogr. 14 (2001) 234–236.

[2] H.E. Hauck, M. Schulz, Ultrathin-layer chromatography, J. Chromatogr. Sci. 40 (2002) 550–552.

[3] H.E. Hauck, M. Schulz, Ultra thin-layer chromatography, Chromatographia. 57 (2003) S313–S315.

[4] S.R. Jim, M.T. Taschuk, G.E. Morlock, L.W. Bezuidenhout, W. Schwack, M.J. Brett, Engineered anisotropic microstructures for ultrathin-layer chromatography, Anal. Chem. 82 (2010) 5349–5356.

[5] A.J. Oko, S.R. Jim, M.T. Taschuk, M.J. Brett, Analyte migration in anisotropic nanostructured ultrathin-layer chromatography media, J. Chromatogr. A. 1218 (2011) 2661–2667.

[6] S.R. Jim, A.J. Oko, M.T. Taschuk, M.J. Brett, Morphological modification of nanostructured ultrathin-layer chromatography stationary phases, J. Chromatogr. A. 1218 (2011) 7203–7210.

[7] S.R. Jim, A. Foroughi-Abari, K.M. Krause, P. Li, M.R. Kupsta, M.T. Taschuk, et al., Ultrathin-layer chromatography nanostructures modified by atomic layer deposition, J. Chromatogr. A. 1299 (2013) 118–125.

[8] J. Wannenmacher, S.R. Jim, M.T. Taschuk, M.J. Brett, G.E. Morlock, Ultrathin-layer chromatography on SiO2, Al2O3, TiO2, and ZrO2 nanostructured thin films, J. Chromatogr. A. 1318 (2013) 234–243.

[9] S. Kirchert, Z. Wang, M.T. Taschuk, S.R. Jim, M.J. Brett, G.E. Morlock, Inkjet application, chromatography, and mass spectrometry of sugars on nanostructured thin films, Anal. Bioanal. Chem. (2013).

[10] A.J. Oko, S.R. Jim, M.T. Taschuk, M.J. Brett, Time resolved chromatograms in ultra-thin layer chromatography, J. Chromatogr. A. 1249 (2012) 226–232.

[11] S.K. Poole, C.F. Poole, High performance stationary phases for planar chromatography, J. Chromatogr. A. 1218 (2011) 2648–2660.

[12] Merck KGaA ChromBook 2008|09, (2008).

[13] K.M. Krause, M. Thommes, M.J. Brett, Pore analysis of obliquely deposited nanostructures by krypton gas adsorption at 87K, Microporous Mesoporous Mater. 143 (2011) 166–173.

[14] G.E. Morlock, C. Oellig, L.W. Bezuidenhout, M.J. Brett, W. Schwack, Miniaturized planar chromatography using office peripherals, Anal. Chem. 82 (2010) 2940–2946.

[15] J.Z. Hall, M.T. Taschuk, M.J. Brett, Polarity-adjustable reversed phase ultrathin-layer chromatography., J. Chromatogr. A. 1266 (2012) 168–174.

[16] D. Nurok, Planar electrochromatography, J. Chromatogr. A. 1044 (2004) 83–96.

[17] T.H. Dzido, P.W. Płocharz, P. Slazak, A. Hałka, Progress in planar electrochromatography., Anal. Bioanal. Chem. 391 (2008) 2111–8.

[18] G.E. Morlock, Detection, Identification, and Documentation, in: Handbook of Thin Layer Chromatography, 2003.

[19] G.E. Morlock, W. Schwack, Hyphenations in planar chromatography, J. Chromatogr. A. 1217 (2010) 6600–6609.

[20] J. Chen, P. Abgrall, Y.-W. Huang, Y.-P. Zhao, On-chip ultra-thin layer chromatography and surface enhanced Raman spectroscopy., Lab Chip. 12 (2012) 3096–3102.

[21] P. Kampalanonwat, P. Supaphol, G.E. Morlock, Electrospun nanofiber layers with incorporated photoluminescence indicator for chromatography and detection of ultraviolet-active compounds, J. Chromatogr. A. 1299 (2013) 110–117.

[22] P.K. Salo, S. Vilmunen, H. Salomies, R.A. Ketola, R. Kostiainen, Two-dimensional ultra-thin-layer chromatography and atmospheric pressure matrix-assisted laser desorption/ionization mass spectrometry in bioanalysis, Anal. Chem. 79 (2007) 2101–2108.

[23] A.B. Jemere, L.W. Bezuidenhout, M.J. Brett, D.J. Harrison, Matrix-free laser desorption/ionization mass spectrometry using silicon glancing angle deposition (GLAD) films., Rapid Commun. Mass Spectrom. 24 (2010) 2305–11.

[24] G.E. Morlock, E.S. Chernetsova, Coupling of planar chromatography with Direct Analysis in Real Time mass spectrometry, Cent. Eur. J. Chem. 10 (2012) 703–710.

[25] K.D. Harris, M.J. Brett, T.J. Smy, C. Backhouse, Microchannel Surface Area Enhancement Using Porous Thin Films, J. Electrochem. Soc. 147 (2000) 2002.

[26] L.W. Bezuidenhout, E. Flaim, A.L. Elias, M.J. Brett, PDMS microchannels with embedded silicon dioxide nanostructures, in: Proc. microTAS 2009 13th Int. Conf. Miniaturized Syst. Chem. Life Sci., Jeju, Korea, 2009.

[27] J. Sherma, G.E. Morlock, Chronology of thin-layer chromatography focusing on instrumental progress, J. Planar Chromatogr. 21 (2008) 471–477.

[28] J.E. Clark, S. V Olesik, Technique for ultrathin layer chromatography using an electrospun, nanofibrous stationary phase, Anal. Chem. 81 (2009) 4121–4129.

[29] J.E. Clark, S. V Olesik, Electrospun glassy carbon ultra-thin layer chromatography devices, J. Chromatogr. A. 1217 (2010) 4655–4662.

[30] M.C. Beilke, J.W. Zewe, J.E. Clark, S. V Olesik, Aligned electrospun nanofibers for ultra-thin layer chromatography., Anal. Chim. Acta. 761 (2013) 201–208.

[31] J. Song, D.S. Jensen, D.N. Hutchison, B. Turner, T. Wood, A.E. Dadson, et al., Carbon-Nanotube-Templated Microfabrication of Porous Silicon-Carbon Materials with Application to Chemical Separations, Adv. Funct. Mater. 21 (2011) 1132–1139.

[32] D.S. Jensen, S.S. Kanyal, V. Gupta, M.A. Vail, A.E. Dadson, M. Engelhard, et al., Stable, microfabricated thin layer chromatography plates without volume distortion on patterned, carbon and Al(2)O(3)-primed carbon nanotube forests., J. Chromatogr. A. 1257 (2012) 195–203.

[33] D.S. Jensen, S.S. Kanyal, N. Madaan, A.J. Miles, R.C. Davis, R. Vanfleet, et al., Ozone priming of patterned carbon nanotube forests for subsequent atomic layer deposition-like deposition of SiO2 for the preparation of microfabricated thin layer chromatography plates, J. Vac. Sci. Technol. B. 31 (2013) 031803.

[34] Z. Zhang, S.N. Ratnayaka, M.J. Wirth, Protein UTLC-MALDI-MS using thin films of submicrometer silica particles, J. Chromatogr. A. 1218 (2011) 7196–202.

[35] F. Costantini, F. Domenici, F. Mura, R. Scipinotti, S. Sennato, C. Manetti, et al., A New Nanostructured Stationary Phase for Ultra-Thin Layer Chromatography: A Brush-Gel Polymer Film, Nanosci. Nanotechnol. Lett. 5 (2013) 1155–1163.

[36] T.B. Kirchner, N.A. Hatab, N. V Lavrik, M.J. Sepaniak, Highly ordered silicon pillar arrays as platforms for planar chromatography, Anal. Chem. 85 (2013) 11802–11808.

[37] Merck KGaA ChromBook 2012, (2012).

[38] M. Tsionsky, A. Vanger, O. Lev, Macroporous thin films for planar chromatography, J. Sol-Gel Sci. Technol. 2 (1994) 595–599.

[39] A.M. Frolova, M.A. Chukhlieb, A. V. Drobot, A.P. Kryshtal, L.P. Loginova, A.P. Boichenko, Producing of Monolithic Layers of Silica for Thin-Layer Chromatography by Sol-Gel Synthesis, Open Surf. Sci. J. 1 (2009) 40–45.

[40] A.M. Frolova, O.Y. Konovalova, L.P. Loginova, A. V Bulgakova, A.P. Boichenko, Thin-layer chromatographic plates with monolithic layer of silica: Production, physical-chemical characteristics, separation capabilities, J. Sep. Sci. 34 (2011) 2352–2361.

[41] R. Bakry, G.K. Bonn, D. Mair, F. Svec, Monolithic porous polymer layer for the separation of peptides and proteins using thin-layer chromatography coupled with MALDI-TOF-MS, Anal. Chem. 79 (2007) 486–493.

[42] Y. Han, P. Levkin, I. Abarientos, H. Liu, F. Svec, J.M.J. Fréchet, Monolithic superhydrophobic polymer layer with photopatterned virtual channel for the separation of peptides using two-dimensional thin layer chromatography-desorption electrospray ionization mass spectrometry, Anal. Chem. 82 (2010) 2520–2528.

[43] I. Urbanova, F. Svec, Monolithic polymer layer with gradient of hydrophobicity for separation of peptides using two-dimensional thin layer chromatography and MALDI-TOF-MS detection, J. Sep. Sci. 34 (2011) 2345–2351.

[44] T. Lu, S. V Olesik, Electrospun polyvinyl alcohol ultra-thin layer chromatography of amino acids, J. Chromatogr. B. 912 (2013) 98–104.

[45] T. Rojanarata, S. Plianwong, K. Su-uta, P. Opanasopit, T. Ngawhirunpat, Electrospun cellulose acetate nanofibers as thin layer chromatographic media for eco-friendly screening of steroids adulterated in traditional medicine and nutraceutical products, Talanta. 115 (2013) 208–213.

[46] S.S. Kanyal, D.S. Jensen, A.J. Miles, A.E. Dadson, M.A. Vail, R. Olsen, et al., Effects of catalyst thickness on the fabrication and performance of carbon nanotube-templated thin layer chromatography plates, J. Vac. Sci. Technol. B. 31 (2013) 031203.

[47] L.W. Bezuidenhout, M.J. Brett, Ultrathin layer chromatography on nanostructured thin films, J. Chromatogr. A. 1183 (2008) 179–185.

[48] P.K. Salo, H. Salomies, K. Harju, R.A. Ketola, T. Kotiaho, J. Yli-Kauhaluoma, et al., Analysis of small molecules by ultra thin-layer chromatography-atmospheric pressure matrix-assisted laser desorption/ionization mass spectrometry., J. Am. Soc. Mass Spectrom. 16 (2005) 906–915.

[49] T.J. Kauppila, N. Talaty, P.K. Salo, T. Kotiaho, R. Kostiainen, R.G. Cooks, New surfaces for desorption electrospray ionization mass spectrometry: porous silicon and ultra-thin layer chromatography plates, Rapid Commun. Mass Spectrom. 20 (2006) 2143–2150.

[50] S. Brunauer, P. Emmett, E. Teller, Adsorption of gases in multimolecular layers, J. Am. Chem. Soc. 60 (1938) 309–319.

A Names and faces

Dissertations are primarily intended to summarize and highlight the academic contributions made over the course of a research program. However, the agencies, institutions, and people that made this work possible often appear only in written word. This appendix is devoted to matching faces to the names of those that made my research program instructive and enjoyable.

Agencies and institutions

Several institutions and organizations enabled the expensive research, collaboration visits (to Germany), and attendance at international symposia (in the USA, Czech Republic, and Switzerland).

Glancing Angle Deposition (GLAD) Research Group

Professor Mike Brett has collected an excellent group of undergraduate and graduate student, post-doctoral fellows, research associates, and staff. Whether through experiment design, deposition system maintenance, lunch time card games, or simply chatting, I've had the honour and pleasure to know and work with many of them during my program. Below is a complete a list of members from the GLAD and Engineered Nanomaterials Lab (ENL) I met and worked with during my program.

GLAD and ENL group members missing from below photos:

GLAD: Mark Summers, Nathan Gerein, Nicole Beckers, Zhifeng (Jeff) Huang, Doug Gish, Josh Siewert, and Nathanael Wu.

ENL: Jeremy Sit (supervisor and GLAD alumnus), Martin Kupsta, Graham Hunt, and Jocelyn Westwood.

GLAD Research Group (with alumni) and ENL members, Summer 2010. Josh LaForge, Scott Kennedy (2003), Matt Hawkeye, Mike Taschuk, Andy van Popta, Josh Krabbe, Nick Wakefield, Steven Jim, Ryan Schewchuk, Mike Brett, Dan Smetaniuk, Abeed (Al) Lalany, Jaron Van Dijken, Graeme Dice, Jonathan Kwan, Louis Bezuidenhout, Mike Fleischauer, Sumudu Fernando, Mike Thomas, Jason Sorge, Anthony Oko, Viktor Leontyev, Mike Colgan (2003), and James Gospodyn (2008).

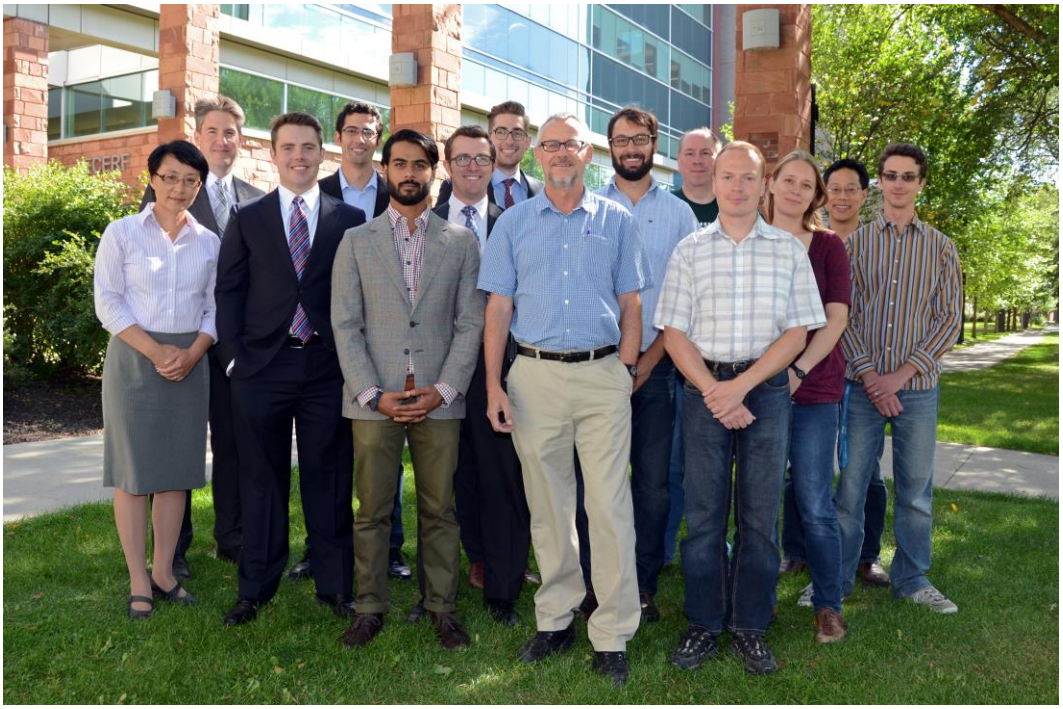

Glancing Angle Deposition (GLAD) Research Group, Fall 2013. Audrey Lin (administrative assistant), Mike Taschuk, Allan Beaudry, Ryan Schewchuk, Abeed (Al) Lalany, Matt Hawkeye, Ryan Tucker, Mike Brett, Mike Fleischauer, Ben Bathgate (laboratory technician), Viktor Leontyev, Katie Krause, Steven Jim, and Josh LaForge. (Missing Jason Sorge.)

Professor Mike Brett holds the NSERC / AITF / Micralyne Senior Industrial Research Chair, an AITF Professorship, is a NRC NINT program coordinator, and is the Canada Research Chair in Nanostructured Films and Devices. In spite of his impressive academic record and daunting reputation, it would be difficult to find another man as kind, humble, and personable. Expressive, knowledgeable, approachable, funny, encouraging, and insightful, he is an excellent teacher and supervisor. Any past or present group member would happily express their gratitude for the environment he creates and the opportunities he provides to motivated people. Nobody is perfect however; he takes guilty pleasure in the occasional chocolate bar.

Dr. Mike Taschuk is the GLAD group's thoroughly capable Research Associate and Mike Brett's "Chief Lieutenant." More than just a lab manager, he draws from his wealth of experience and undeniable technical background to provide exceptional guidance and mentorship whenever needed. He dedicates considerable time and energy to helping group members remain focussed, efficient, and productive. Intelligent, witty, funny, and demanding but kind, his interactions with students encourage them to develop as both researchers and professionals. Group members credit and appreciate his work for elevating the success of each student and the productivity of the research group as whole.

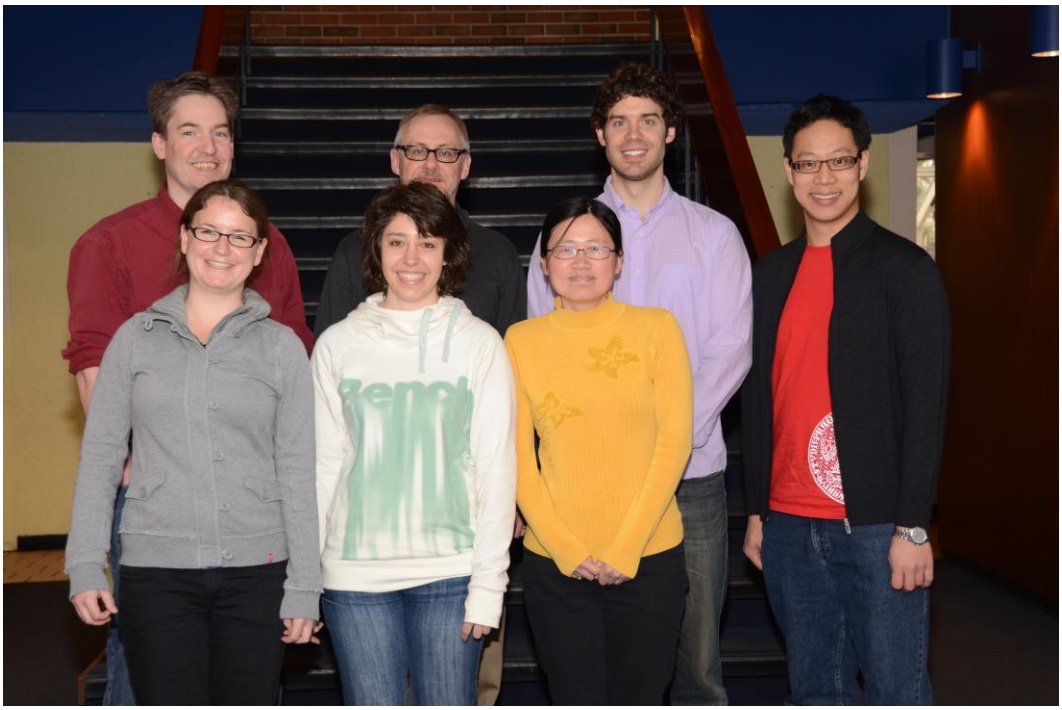

GLAD UTLC Team, Winter 2012. Back row: Mike Taschuk, Mike Brett, Anthony Oko, Steven Jim; front row: Julia Wannenmacher, Simone Kirchert, and Jane Hall (née Zhen Wang). The team would later include Ali Foroughi-Abari and Viktor Leontyev, not shown. Louis Bezuidenhout had graduated (2011) before the team had grown to this size and this photo was taken.

Universität Hohenheim

Professors Gerda Morlock and Wolfgang Schwack. Both are experts in planar chromatography and were my gracious hosts when I visited the Institut für Lebensmittelchemie (Institute for Food Chemistry, directed by Professor Schwack) at Universität Hohenheim (Stuttgart, Germany). Gerda Morlock supervised diplom thesis students Julia Wannenmacher and Simone Kirchert during and after their 2012 visit to the GLAD laboratory.

Electrical and Computer Engineering Machine Shop

ECE machine shop. Martin Riedner, Reiner Schwarze, Herbert Dexel, and Terry Kugler. These expert machinists have extensive experience, strict standards, and are actively involved in the design and fabrication of prototype devices. Their skill is often in creating what researchers wanted instead of what they requested.

University of Alberta NanoFab Facilities

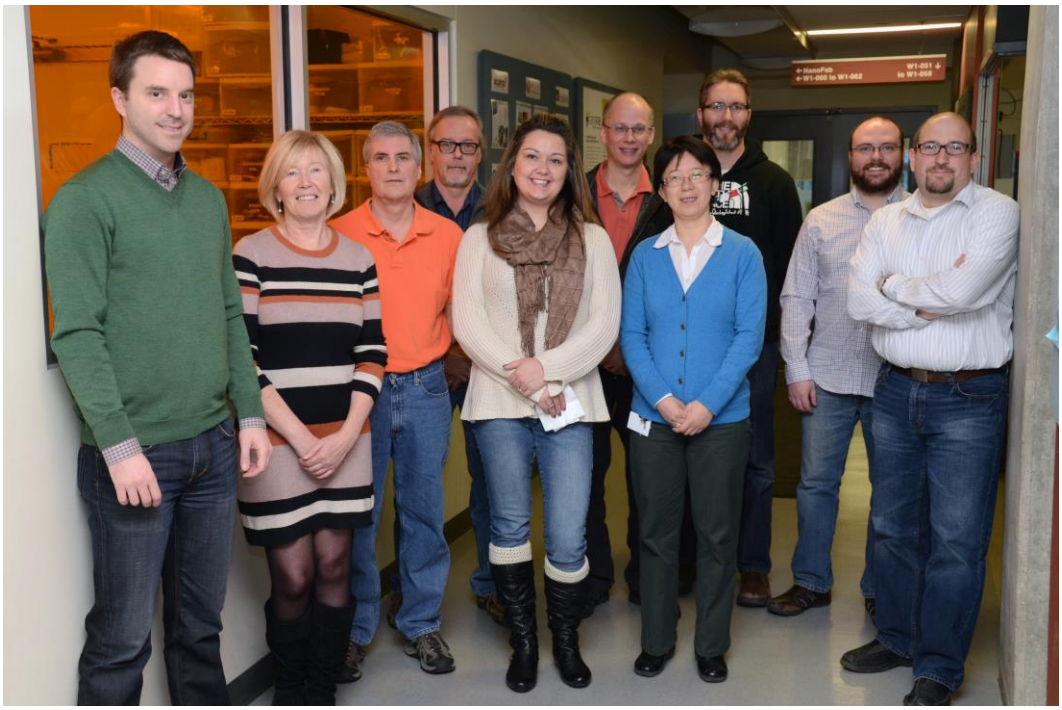

NanoFab staff. Eric Flaim, Stephanie Bozic, Les Scholwalter, Bob Brebber, Melissa Hawrelechko, Glenn Elaschuk, Nancy Zhang, Scott Munro, Jonathan Clark, and Keith Franklin. (Missing Michael Hume and Shiau-Yin Wu; former staff Ken Westra and Jolene Jalota.) The world-class open access U of A NanoFab cleanroom facility is one of the best in Canada and boasts tens of millions of dollars in equipment and infrastructure. Successful operation of the facility requires numerous full-time technicians, trainers, managers, and administrators. Their expertise and diligence ensure that the facility's resources are available to hundreds of academic and industrial users with various backgrounds and projects.

B Numerical analysis scripts

This appendix contains unedited MATLAB scripts written for chromatogram extraction and STEM EELS analysis:

- **B.1 ExtractChromaSJ20100128.m** was used to extract unfiltered darkness chromatograms from single diagonal dye separation tracks in [1].
- **B.2 ExtractChroma20101012.m** was used to extract hue-filtered chromatograms from single, possibly diagonal, tracks in [2].
- **B.3 TEM_EELS_process_linescan.m** was used to process STEM EELS data analyzed in [3]. (Complete script provided.)

For brevity, only excerpts of the first two scripts are provided. Full versions of all three scripts are available at **http://hdl.handle.net/10402/era.38217**. Note also that the below chromatogram extraction scripts are inferior to **`singleImageUTLC.m`** in all ways except for in their ability to process diagonal separation tracks.

References

[1] S.R. Jim, M.T. Taschuk, G.E. Morlock, L.W. Bezuidenhout, W. Schwack, M.J. Brett, Engineered anisotropic microstructures for ultrathin-layer chromatography, Anal. Chem. 82 (2010) 5349–5356.

[2] S.R. Jim, A.J. Oko, M.T. Taschuk, M.J. Brett, Morphological modification of nanostructured ultrathin-layer chromatography stationary phases, J. Chromatogr. A. 1218 (2011) 7203–7210.

[3] S.R. Jim, A. Foroughi-Abari, K.M. Krause, P. Li, M.R. Kupsta, M.T. Taschuk, et al., Ultrathin-layer chromatography nanostructures modified by atomic layer deposition, J. Chromatogr. A. 1299 (2013) 118–125.

B.1 ExtractChromaSJ20100128.m

```
% ExtractChromaSJ20100128.m (Revision 2010-01-28)

% This function is used to extract chromatogram information from cropped
% images of UTLC plates. It assumes that the cropped image contains a
% single separation track that had been developed upwards and that regions
% outside of the separation track are masked by "PURE" black
% (R,G,B)=(0,0,0). (The masked region is assumed to have only pixels with
% R+G+B <= 32/255.) Averages across the track width are taken at different
% positions along the length of the IMAGE. Note that for diagonal
% separation tracks, these positions are NOT the same as the distances
% along the angled separation tracks.

% The image is first rotated clockwise. The region of interest is then
% automatically cropped from the image. Values are then averaged across the
% width of the track contained within the cropped image. Black pixels
% outside of the track (ie. in the masked region) are NOT included in the
% averages. Calculated values are not manually rounded. The function also
% calculates the darkness for each pixel within the track. (Regions outside
% of the track are forced to have darkness = 0.) The function does
% not calculate retention factors, perform background subtraction, find
% peaks, or evaluate peak height/area/volume.

% This script is modified from: "ExtractChromaSJ20091211.m"

% INPUTS: image file name (RGB with *.jpg suffix; developed upwards); 3
% RGB channel weights (for weighted average "greyness"); base name for
% exported figures and files (does not contain a suffix); 'y' or 'n' value
% used to determine if files (figures, *.txt, and *.csv) should be
% exported; 'y' or 'n' value to determine if manipulated images should
% be exported; 'y' or 'n' value to determine if darkness at each pixel on
% track should be exported (surface plots as *.jpg and *.fig; numerical
% data as *.csv).

% OUTPUTS: (rotated, cropped) image array; 3 column vectors with mean RGB
% channel values ([0,255]; pure red has R=255); 1 vector with weighted
% average "greyness" values ([0,255]; pure black has value 255); 1
% vector with average "darkness" values ([0,1]; pure black has value 1).

% EXPORTS:
% If export == 'y':
    % 6 large *.jpg figures containing plots of the data; *.csv file
    % containing columns for position (from bottom in input image; from
```

```
    % left in rotated and cropped image), RGB channel levels, "greyness"
    % level, "darkness" value, start/end rows defining track position in
    % rotated (UNCROPPED) image, and track width; and  *.txt log file
    % containing image sizes and output messages.
% If ImgExp == 'y'
    % A *.jpg file of rotated, cropped image; and a *.jpg file of the
    % rotated, cropped, and shifted image (all track pixels aligned to top
    % of image), and a greyscale *.jpg representation of track darkness.
% If DtrackExp == 'y'
    % Surface plots of darkness at each pixel on track as *.jpg and *.fig;
    % and numerical data as a *.csv. If and only if the rotated croped
    % image has width greater than 1 pixel.

% Define function outputs and inputs
function [A,R,G,B,grey,dark,D_track] = ExtractChromaSJ20100128...
    (img,r,g,b,OutName,export,ImgExp,DtrackExp)
```

B.2 ExtractChroma20101012.m

```
% ExtractChroma20101012.m (Revision 2010-10-12)

% Written by: S. Jim

% Based in-part on script: "ExtractChroma20100805.m"

% This function is used to extract chromatogram information from cropped
% images of UTLC plates. It permits colour filtering by restricting the
% lightness ([0,1]) and the hue ([0,360)) of permitted pixels.

% It assumes that the cropped image contains a single separation track
% that had been developed upwards and that regions outside of the
% separation track are masked by "PURE" black (R,G,B)=(0,0,0).
% (The masked region is assumed to have only pixels with R+G+B <= 32/255.)
% Averages and sums across the track width are taken at different
% positions along the length of the IMAGE. Note that for diagonal
% separation tracks, these positions are NOT the same as the distances
% along the angled separation tracks.

% The input image is rotated clockwise. The region of interest is then
% automatically cropped from the image. A reference matrix is defined to
% force all values off of the track (ie. black pixels in the masked region)
% to 0 (and therefore exclude them from any averaging or summing). The
% function does not calculate retention factors, perform background
% subtraction, find peaks, or evaluate peak height/area/volume.

% RED, GREEN, BLUE, HUE, SATURATION, LIGHTNESS, and DARKNESS values are
% averaged across the the track width. These signals are not filtered.

% FILTERED signals are calculated by summing SATURATION values of pixels
% with permitted LIGHTNESS and HUE. One lightness filter is used. An
% unrestricted number of hue filters may be used. One signal is generated
% for each hue filter.

% INPUTS: (img,OutName,Lfilter,Hfilter,Hfilterlabel,NumExp,FigExp,ImgExp)
    % 1: Image file name string (RGB with *.jpg suffix; developed upwards);
    % 2: Base name string for exported figures and files (without suffix);
    % 3: Lightness filter 1x2 row vector defining permitted pixels as
    %     those within L=[L_min,L_max];
    % 4: HFx2 hue filter vector. Each row in the vector represents one hue
    %     filter and restricts the hue values of the permitted pixels to
    %     those within the arc defined counterclockwise (ccw) between
    %     Hfilter(hf,1) and Hfilter(hf,2).
    %     Ex: Green hues: H values in ccw arc between 90 and 150 deg.
    %     Ex: Red hues: H values in ccw arc between 330 and 30 deg.
    %     Ex: Exclude red hues: H values in ccw arc betwene 30 and 330 deg.
```

```
    % 5: HFLx1 hue filter label vector. Each entry is a cell string defined
    %     using cellstr('filtername') used to label the corresponding hue
    %     filter. The number of labels (HFL) may be different from the
    %     number of filters. However, the last labels are excluded if
    %     HFL>HF and added if HFL<HF.
    % 6: Export numerical data to *.csv? 'y' or 'n' string input.
    % 7: Export figures? 'y' or 'n' string input.
    % 8: Export generated images? 'y' or 'n' string input.

% OUTPUTS: [A,R,G,B,H,S,L,D]
    % 1: Array representing rotated, cropped image. (Unshifted.)
    % 2-4: Arrays for RED, GREEN, BLUE values at each pixel position
    %     ([0,1]). (Pixels off of track have forced values of 0.)
    % 5-8: Arrays for HUE, SATURATION, LIGHTNESS, DARKNESS values at each
    %     pixel position ([0,360), [0,1], [0,1]). (Pixels off of the track
    %     have forced values of 0.)

% EXPORTS:
% If NumExp == 'y':
    % *.csv file containing pixel position, track width information, RGB
    % averages, HSL averages, D (darkness) averages, and filtered
    % saturation sums.
% If FigExp == 'y':
    % All figures exported to *.fig.
    % Figures with filtered signal exported also to *.jpg.
% If ImgExp == 'y': *.jpg's of:
    % 1: Rotated, cropped track image
    % 2: Image with all track pixel rows shifted to one edge.
    % 3: Greyscale representation of SATURATION of track pixels.
    % 4: Greyscale representation of LIGHTNESS of track pixels.
    % 5: Greyscale representation of DARKNESS of track pixels.

% Define function outputs and inputs
function [A,R,G,B,H,S,L,D] = ExtractChroma20101012...
    (img,OutName,Lfilter,Hfilter,Hfilterlabel,NumExp,FigExp,ImgExp)
```

B.3 TEM_EELS_process_linescan.m

```
% TEM_EELS_process_linescan.m  (Revised 2013-03-04)
%
% Purpose:  This script is designed to process a 2D array representing
% TEM EELS spectra collected at different points along a line scan.  The
% background in these spectra (associated with the zero-loss peak and
% phonon scattering) is often modelled by a power law.  The script fits a
% power law (BG = b1*energy^b2) to the spectum collected at each position.
%     This script is used for the specific processing of TEM EELS data
% collected across GLAD SiO2 columns without/with ALD Al2O3 coatings.
% (Fitting and clipping regions selected accordingly.)
%
% Inputs:
% - sig0 : Array of electron counts at different positions along
% the line scan (rows) at different energies (columns):
%     c(x1,e1) c(x1,e2) ... c(x1,eN)
%     c(x2,e1) c(x2,e2) ... c(x2,eN)
%     .        .            .
%     .        .            .
%     .        .            .
%     c(xM,e1) c(xM,e2) ... c(xM,eN)
% - poslim : Range of positions over which spectra was originally collected
%   (Example: 0 - 291.464 nm)
% - elim : Range of energies over which spectra was originally collected
%   (Example: 30.5 - 169.4 eV)
%
% Output:
```

```
% - sig : Background-corrected array
% - BG : Fitted background array

function [sig,BG] = TEM_EELS_process_linescan(sig0)

%% User inputs and vector definitions
disp(' ')
disp('SPECTRA COLLECTION PARAMETERS')
disp('Input 2-element row vector for range')
poslim = input('    of positions in array (nm): ');
elim = input('    of energy values in array (eV): ');

% Background fitting and signal clipping values (for plots)
efitlim = [60 70];      % Region over which BG should be fit (eV)
eclip = [60 160];       % Energy levels over which spectra are plotted (eV)

% Additional parameters
[H W] = size(sig0);                     % Height and width of array
pos = linspace(poslim(1),poslim(2),H)'; % Position (column) vector
e = linspace(elim(1),elim(2),W);        % Energy (row) vector

% Extract energy vector and array used in background fitting
% (eselect is used to select approriate energies and region from signal)
eselect = (e >= efitlim(1)) & (e <= efitlim(2));
efit = e(eselect);                  % Energies used during fitting
sig0fit = sig0(:,eselect);          % Region of array used in fitting

%% Fit background

% Suppress warnings expected from this fitting.
warning('off','stats:nlinfit:ModelConstantWRTParam');
warning('off','stats:nlinfit:IterationLimitExceeded');
warning('off','stats:nlinfit:IllConditionedJacobian');

% Power law function with parameters
power_law = @(A,e) A(1)*e.^A(2);

% Initialize vector for fitted power law function
b1 = zeros(H,1);        % Vector of multipliers for each position
b2 = zeros(H,1);        % Vector of exponents for each position
BG = zeros(size(sig0)); % Array to represent calculated background

for m = 1:H
    % Spectrum at row m (row vector)
    y = sig0fit(m,:);

    % Initial guesses for b1 and b2
    % Suppose y_mean = b1_guess*e_mean^(b2_guess) then,
    % b1_guess = y_mean*e_mean^(-b2_guess).
    b2_guess = -2;
    b1_guess = mean(y)*mean(elim)^(-b2_guess);

    % Perform power law fit
    params = nlinfit(efit,y,power_law,[b1_guess b2_guess]);
    b1(m) = params(1);
    b2(m) = params(2);

    % Calculate background signal
    BG(m,:) = b1(m)*(e).^b2(m);  % Row in array
end

% Restore warnings expected from this fitting.
warning('on','stats:nlinfit:ModelConstantWRTParam');
warning('on','stats:nlinfit:IterationLimitExceeded');
warning('on','stats:nlinfit:IllConditionedJacobian');

%% Apply background correction and generate plots
```

```
% Processed signal to be plotted
sig = sig0 - BG;

% Smooth signal
h = 1/9*ones(3,3);              % Nearest neighbour averaging
sig_smooth = filter2(h,sig);

% Clip signals, offset, scale for plotting
e_plot = e( e>=eclip(1) & e<=eclip(2) );
sig_plot = sig_smooth(:,e>=eclip(1) & e<=eclip(2));
sig_plot = sig_plot - min(sig_plot(:));     % Offset so all values are > 0
sig_plot = sig_plot/1000;                   % Scale magnitude of counts
sig_plot_zlim = [0 5.5];

figure(1); clf; mesh(e_plot,pos,sig_plot);              % Surface plot
xlim(eclip); ylim(poslim); zlim(sig_plot_zlim);
set(gca,'YDir','reverse');

figure(2); clf; imagesc(pos,e,sig_plot',sig_plot_zlim); % Coloured image
xlim(poslim); ylim(eclip); zlim(sig_plot_zlim); colorbar;
set(gca,'YDir','normal');

end
```

C Time-resolved UTLC scripts

The time-resolved UTLC numerical analysis package involves numerous custom MATLAB programming scripts. These scripts are collectively designed to extract numerical data from a directory of video frames and calculate chromatographic figures of merit. Excerpts of relevant scripts are provided below (listed in alphabetical order):

- **C.1 amalgamatefomUTLC.m**
- **C.2 batchAnalyzeVideoUTLC.m**
- **C.3 combinePlateUTLCfom.m**
- **C.4 createRecipeUTLC.m**
- **C.5 filteredChromaPlotVideo.m**
- **C.6 filteredDensitogram.m**
- **C.7 fomUTLC.m**
- **C.8 fomUTLCavg.m**

- **C.9 fomUTLCcsv.m**
- **C.10 frontFit.m**
- **C.11 iterativeGaussFit.m**
- **C.12 mainUTLC.m**
- **C.13 sampleSpots.m**
- **C.14 singleImageUTLC.m**[1]

The excerpts describe the purpose of their respective scripts but for brevity, none of the functional programming code is provided. The complete TR-UTLC package can instead be downloaded from **http://hdl.handle.net/10402/era.38218**. Prospective users are welcome to copy these scripts into their MATLAB root directory and use them with appropriate attribution.

C.1 amalgamatefomUTLC.m

```
function amalgamatefomUTLC

% Written by S.R. Jim, (C) October 2013
% Glancing Angle Deposition (GLAD) Laboratory, PI: M.J. Brett
% University of Alberta, Edmonton, Canada
%
% Purpose:  This script is designed to amalgamate the figure of merit *.mat
% files output by the UTLC video analysis script fomUTLC.m.  It loads data
% arrays in order into a cell array in which each cell is a structure:
%
% FOMs produced by combinePlateUTLCfom.m (See Note 1):
%   fom*, group, nfom, plateref, subset
%
% Basic FOMs produced by fomUTLC.m:
%   ampSpot, chi, firstFrame, frameRate, frameRes, hueRange1,
%   hueRangeLabel1, intLength, lastFrame, LODtVect, middleFrame, nFrames,
%   noisefloorLOG, nSpots1, nTracks1, RealPH, RealPN, relConc, resSpot,
%   rfLimits1, sigSpot, SN, SNfit, SNsVect, spotFWHM, spotHRF, spotLOD,
%   spotLOD0, spotLocationX1, spotLocationY1, stdevBlank, stdevBlankScaled,
%   stdevBlankScaledLOG, stdevBlankTrk, spotMass1, spotPH, spotPN, spotSNR,
%   spotVolume1, stdResiduals, stdSpot, sVect, t, tVect, undilutedConc,
%   zf1, zSpot
%
% Averaged FOMs from fomUTLCavg.m:
%   avgSigTrk, avgSigName, avg_*, stdev_*
%
% Note 1:
% It also can be used to amalgamate data produced by combinePlateUTLCfom.m.
% These data include:
%    fom* : All of the above data produced in a first pass through this
%       script.  Note that combinePlateUTLCfom.m requires an amalgamation
%       file produced by this script since it requires fom{}.variable
%       arrays.  To access data extracted during the first pass, use
%       "fom{}.fom{}.variable" (ie. nested structures.)
```

[1] **singleImageUTLC.m** is not formally a part of the TR-UTLC package as it was designed to analyze a single extracted video frame.

```
%    group : Relevant foms from all fom{} cells combined together.
%    nfom : Number of fom{} cells used by combinePlateUTLCfom.m
%    plateref : Vector used to record plate from which each track's data
%       was extracted.
%    subset : Array used to select data from fom{} cells.
% If present, these variables will be listed at beginning of new fom{}
% structure.
%
% Note 2:
% If they exist, the script can import averaged FOMs produced by
% fomUTLCavg.m.  (Files output by fomUTLCavg.m also contain all those from
% fomUTLC.m.)  These data signals are imported if 'script_fomUTLC_avg'
% exists.
```

C.2 batchAnalyzeVideoUTLC.m

```
function batchAnalyzeVideoUTLC

% Written by S.R. Jim, (C) October 2013
% Glancing Angle Deposition (GLAD) Laboratory, PI: M.J. Brett
% University of Alberta, Edmonton, Canada
%
% Purpose:  Batch process a directory of UTLC video recipe files.  These
% recipe files uniquely define the parameters required in the analysis of
% each UTLC development video.  This function processes all recipe files in
% a given directory (*-recipe.mat suffix) using the following functions:
%     - mainUTLC.m:  Process and fit densitogram signals extracted from a
%     directory of images.  (Directory specified in each video's recipe
%     file.)
%     - fomUTLC.m:  Given the fitted densitogram peak locations and
%     widths, noise, and other data generated by the above script,
%     calculate relevant figures-of-merit.
%     - fomUTLCcsv.m:  Calculated FOMs are exported to *.csv by this
%     script.
%
% Notes:
%   - This script does not calculate limits of detection (LODs).
%   - This script does not calculate separation numbers, real plate numbers
%   or real plate heights.
```

C.3 combinePlateUTLCfom.m

```
function combinePlateUTLCfom

% Written by S.R. Jim, (C) October 2013
% Glancing Angle Deposition (GLAD) Laboratory, PI: M.J. Brett
% University of Alberta, Edmonton, Canada
%
% Purpose:  This script is designed to compare the figures of merit
% measured for similarly loaded GLAD UTLC plates.  Videos are analyzed
% using createRecipeUTLC.m --> mainUTLC.m --> fomUTLC.m --> (*OPTIONAL:
% fomUTLCavg.m -->) amalgamatefomUTLC.m.  The last script is used to create
% a 1-D cell array.  Each cell contains all relevant data for one
% run/video.  (*OPTIONAL:  The averaged FOMs produced by fomUTLCavg.m are
% not required by this script.  However, the data file output by that
% script also contains the required data from fomUTLC.m.)
%
% The script assumes that all development videos are equivalent in loading
% (same analyte, concentration, spot volume, etc.) and processed
% similarly (same frame extraction rate, frame resolution, hue filters,
% signal integration region length, etc.)  Although the number of tracks
% per plate does not need to be the same between plates, it is important to
% note that ALL tracks from EACH plate will be used.
```

```
%
% Notes:
%   - Also calculates relative standard deviations.
%   - Only data for the same number of spots are combined.   (Example: If
%   fom{1} only has data for 3 spots, ensure that only 3 spots from fom{2}
%   are added into the group arrays.
%   - Arrays generated by mainUTLC.m and reduced in fomUTLC.m are copied
%   and corrected if necessary.  Example: Suppose mainUTLC.m generates data
%   for 4 spots and 3 tracks but only 3 spots (sVect = [1 3 4]) and 2
%   tracks (tVect = [1 2]) are considered in fomUTLC.m.  Then generate a
%   new array with this subset and append this to the group arrays.
```

C.4 createRecipeUTLC.m

```
function createRecipeUTLC

% Written by S.R. Jim, (C) October 2013
% Based on createRecipeUTLCv2.m written by A.J. Oko, September 2011
% Glancing Angle Deposition (GLAD) Laboratory, PI: M.J. Brett
% University of Alberta, Edmonton, Canada
%
% Purpose:  This script is used to define the parameters required for GLAD
% UTLC video analysis.  It enables input of an existing recipe file
% (oldRecipe) and output of a recipe file with a new filename (newRecipe).
% This recipe file is then input into a mainUTLCv* script for subsequent
% video analysis.
%
% Subfunctions:  frontFit.m
%
% Notes:
%   - Note 1:  PART 8 is used to define regions in frames from which blank
%   signals may be calculated.  Future work with signals may enable
%   estimation of system noise and limits of detection (LOD).  This feature
%   is not fully functional in the current time-resolved UTLC package.
```

C.5 filteredChromaPlotVideo.m

```
function filteredChromaPlotVideo

% Written by S.R. Jim, (C) October 2013
% Glancing Angle Deposition (GLAD) Laboratory, PI: M.J. Brett
% University of Alberta, Edmonton, Canada
%
% Purpose:  Consider the colour filtered densitograms for a given track and
% their evolution over the course of a chromatographic development.  Use
% this movie to assess the appropriateness of the selected colour filters
% and the gaussian fits.  This script does not calculate any signals and
% only plots hue-filtered densitogram signals already produced by
% mainUTLC.m.  It allows multiple separation track videos to be generated.
%
% Inputs:  Data file generated by mainUTLC.m, original directory of frames
% used to generate this data file.
%
% Outputs: Videos of chromatograms plotted along side their cropped track
% image.
```

C.6 filteredDensitogram.m

```
function [D,avg_px,stdev_px,avg_D,stdev_D] = ...
    filteredDensitogram(img,hueRange)

% Written by S.R. Jim, (C) October 2013
% Glancing Angle Deposition (GLAD) Laboratory, PI: M.J. Brett
% University of Alberta, Edmonton, Canada
%
% Purpose:  This script is designed to analyze an input UTLC track image
% (img, developed top to bottom) or a blank track region given a set of
% colour filters (hueRange).  It then outputs a 2D array (D) whose
% columns contain colour-filtered densitograms.  It also outputs the mean
% and standard deviation row vectors calculated in two different ways:
%
%   - avg_px, stdev_px : Mean and standard deviation in the saturation
%   values of all PIXELS in img with hues inside of the filter.  The
%   saturation values of pixels with hue outside of the filter are excluded
%   from this analysis.
%
%   - avg_D, stdev_D : Mean and standard deviation in the calculated
%   DENSITOGRAM signal.  Recall that the signal 'D' is determined both by
%   the number of pixels with hue inside of the filter as well as the
%   saturation values of those pixels.  Pixels with hue outside of the
%   filter have their saturation values set to 0 before signal summing.
%
% Notes:
%   - Unfiltered densitograms are possible when hueRange(i,1) ==
%   hueRange(i,2).  (Ex. [0 0]; special case: [0 360] --> [0 0])
```

C.7 fomUTLC.m

```
function fomUTLC(spec,inFile,outFile)

% Written by S.R. Jim, (C) October 2013
% Glancing Angle Deposition (GLAD) Laboratory, PI: M.J. Brett
% University of Alberta, Edmonton, Canada
%
% Purpose:  Given information produced by the recipe file (output by
% createRecipeUTLC.m) and calculated/fitted data file (output by
% mainUTLC.m), this script calculates several figures of merit (FOM) that
% are used to evaluate performance from a UTLC development video.  This
% script can be called by batchAnalyzeVideoUTLC.m.
%
% Input:  Specify the *.mat file that contains information produced by the
% aformentioned scripts.
%
% Optional Inputs (those from batchAnalyzeVideoUTLC.m):
%   - spec:  A structure containing predefined values for inputs required
%   by this script.
%   - inFile:  Full filepath and name of the input recipe file.
%   - outFile:  Full filepath and name of the output main file.
%
% Outputs:  Relevant figures of merit saved in a new *.mat file.
%
% Notes:
%   - Based on figuresOfMerit.m written by A.J. Oko, September 2011
%   - This script attempts to calculate the signal-to-noise ratio and
%   limits of detection (LODs).  Noise is calculated from signals generated
%   on the blank tracks.  These values should not be used without further
%   verification.  Improved understanding of noise behaviours must be
%   performed.
%   - This script attempts to calculate the separation number (SN), real
```

```
%   plate number (RealPN), and real plate height (RealPH). These values are
%   valid only if typical spot broadening occurs:  Higher RF spots broaden
%   more than lower RF spots.  Spot focussing and other effects can cause
%   nonsensical values.
```

C.8 fomUTLCavg.m

```
function fomUTLCavg

% Written by S.R. Jim, (C) October 2013
% Glancing Angle Deposition (GLAD) Laboratory, PI: M.J. Brett
% University of Alberta, Edmonton, Canada
%
% Purpose:  Average the figures-of-merit from "similarly" loaded tracks.
% This script processes a file output by fomUTLC.m.  Basic figures-of-
% merit (zSpot, stdSpot, spotFWHM, spotHRF, spotPN, spotPH, etc.) and
% optional figures-of-merit (spotLOD, etc.) are considered.  Means and
% standard deviatons are calculated at each instant in time.
%
% The output file contains all fomUTLC.m variables (unaltered) and all
% variables generated in this script.
```

C.9 fomUTLCcsv.m

```
function fomUTLCcsv(inFile,outFilePrefix)

% Written by S.R. Jim, (C) October 2013
% Glancing Angle Deposition (GLAD) Laboratory, PI: M.J. Brett
% University of Alberta, Edmonton, Canada
%
% Purpose:  Export already calculated UTLC figures-of-merit as *.csv files.
% These FOMs were calculated from UTLC development videos using MATLAB
% scripts createRecipeUTLC.m, mainUTLC.m, and fomUTLC.m.  This script can
% be called by batchAnalyzeVideoUTLC.m.
%
% Input:  A file generated by fomUTLC.m that contains 2D, 3D, or 4D arrays
% of calculated figures of merit.
%
% Optional Inputs (those from batchAnalyzeVideoUTLC.m):
%   - Full file path (including file name) to an exisiting *.mat file
%   containing the FOMs to be exported to *.csv.
%   - Full file path and file name prefix for exported *.csv files
%
% Outputs:
%   - This script exports one *.csv file for each FOM contained in the
%   input file (if it exists).  The file name is of the form:
%               *_(fomname)-(dim1)-(dim2)-(dim3).csv
%   with:
%       - (fomname):  Name of the FOM variable (ex. spotHRF)
%       - (dim1), (dim2), (dim3):  Dimensions of (3D) output array before
%       flattening into a *.csv (ex. 300, 3, 6)
%   example: test_spotHRF-300-3-6.csv
%   - It also exports a *.txt file containing information about the
%   all performed analysis
```

C.10 frontFit.m

```
function  [chi,zStart,tStart,zf_measured,time] = ...
    frontFit(filepath,filename,zStart_guess,tStart_guess,...
    chitrkloc1,chitrkloc2,nSteps,enh)

% Written by S.R. Jim, (C) October 2013
% Glancing Angle Deposition (GLAD) Laboratory, PI: M.J. Brett
% University of Alberta, Edmonton, Canada
%
% Purpose:  This script is designed to calculate the migration constant chi
% (in units px^2/frame).  It considers a region (defined by chitrkloc1)
% cropped from select frames in a given directory (filepath).  The user
% identifies the migration front by eye.  These measurements are used to
% fit the required chi, zStart, and tStart scalar values.  (Another larger
% region, chitrkloc2, is shown above the R,G,B,L curves generated using the
% region defined by chitrkloc1.)
%
% Notes:
%   - Based on getChi2.m written by A.J. Oko, October 2011
%   - This revision uses an equation form that includes parameters (chi,
%   zStart, tStart) to satisfy the equation zf(t):
%       zf = sqrt(chi .* (t + tStart)) + zStart
%   This equation acknowledges that:
%       - the immersion line from which the solvent flows (~ zStart)
%       depends on the position of the UTLC plate.
%       - the solvent started flowing before the first frame.  It started
%       ~ tStart frames ago.
```

C.11 iterativeGaussFit.m

```
function [params,roi,res,resStdev,status] = ...
    iterativeGaussFit(x,y,roi0,iter,crit)

% Written by S.R. Jim, (C) October 2013
% Glancing Angle Deposition (GLAD) Laboratory, PI: M.J. Brett
% University of Alberta, Edmonton, Canada
%
% Purpose:  This script is used to fit a Gaussian peak to a region of an
% input data vector.  It returns numerical parameters for the Gaussian fit
% if the following criteria are satisfied:
%   1. The fitted amplitude is more than 6 times greater than the standard
%   deviation of the residuals (calculated over fitting region).
%   2. The fitting region is wide enough to ensure that, with 99% (3
%   sigma) certainty, at least the top half of the fitted peak is within
%   the fitting region.  ie.  The FWHM is contained within the fitting
%   region.  (The standard deviation of the residuals are used to estimate
%   this error, sigma.)
% If the criteria are not satisfied, a new broader fitting region is
% defined (based on the old fitted parameters) and fitting is attempted
% again over this region.  The difference between subsequently fitted peak
% standard deviations is used as a convergence criteria.
%
% Inputs:
%   x    : Input position column vector
%   y    : Raw signal column vector to be fit
%   roi0 : Row vector defining inclusive x-bounds on y over which the first
%       fitting iteration is performed.
%   iter : Maxiumum number of fitting iterations
%   crit : Covergence criteria for the fitted peak standard deviations
%       (crit = abs( ( stdev_N - stdev_(N-1) ) / stdev_(N-1) )
%       ex. crit = 0.01 means that the current and previous stdevs differ
%       by less than 1%.
```

```
%
% Outputs:
%   params : Array containing fitted values for each iteration.  Columns
%       represent fitted Gaussian parameters [mu stdev amp].  One row for
%       each fitting iteration (ordered final 1, 2, ..., N, ..., iter) so
%       that the final *non-zero* row contains the final fitted values:
%       [stdev mu amp].  1 row padded with zeros for each incomplete
%       iteration exists below the final fitted values.
%   roi : Array defining the inclusive x-bounds on y over which fitting was
%       performed (1 row for each iteration like for params). If
%       successful, the last non-zero row is also the region over which the
%       standard deviation in the residuals is calculated.
%   res : Residuals (fit - raw) calculated over ENTIRE signal.  Reported
%       only for the final fit.  (No NaNs present.)
%   resStdev : Standard deviation in residuals (fit - raw) calculated ONLY
%       over the fitting region.  Reported only for final fit.
%   status : A cell array containing strings to report status of iterative
%       fitting.  Rows contain:
%           'fail 1: insufficent data within roi0' : Cannot be fit, too
%               little data in roi0.
%           'fail 2: fitted peak centre outside x' : Nonsensical fitted
%               peak centre that would cause divergence of subsequent
%               fitting attempts.
%           'fail 3: amp<#*stdev' : Unacceptable fit, too noisy.
%           'fail 4: roi too small' : Unacceptable fit, roi too small
%               for reliable fit.
%           'fail 1-4: repeat of failed iteration' : Previous fitting
%           region limits were tried already.
%           'iter # failed, revert to last acceptable iter #' : Use last
%           acceptable iteration.
%           'acceptable, continue iter' : Fit statisfies both acceptance
%               criteria but continue improving fitted values.
%           'stop: iter = max iter' : Stop fitting, reached max iterations.
%           'stop: conv crit satisfied' : Stop iteration; fitted values
%               stable.
```

C.12 mainUTLC.m

```
function mainUTLC(spec,inFile,outFile)

% Written by S.R. Jim, (C) October 2013
% Glancing Angle Deposition (GLAD) Laboratory, PI: M.J. Brett
% University of Alberta, Edmonton, Canada
%
% Purpose:  This script is used to analyze a directory of frame *.jpg or
% *.tif files extracted from a UTLC development video.  It is used to
% extract colour-filtered chromatograms from tracks defined on each frame
% in the directory.  This script can be called by batchAnalyzeVideoUTLC.m.
%
% Input:  A recipe file prepared using createRecipeUTLC.m is selected.
% This contains all variables that may be relevant for this analysis.  The
% filepath to the directory of images is assumed to be the same as that
% identified in the recipefile (filepath).
%
% Optional Inputs (those from batchAnalyzeVideoUTLC.m):
%   - spec:  A structure containing predefined values for inputs required
%   by this script.
%   - inFile:  Full filepath and name of the input recipe file.
%   - outFile:  Full filepath and name of the output main file.
%
% Outputs:  This script produces one output file.  This contains all data
% produced in this script and that included in the recipe file.
%
% Subfunctions:  filteredDensitogram.m, iterativeGaussFit.m
%
```

```
% Notes:
%   - Based on mainUTLCv7.mat written by A.J. Oko, September 2011
%   - Saving the Densitogram and fitDensitogram signals is optional. These
%   output signals may have lower sampling frequency than the frame rate.
%   (Ex. Only data from every 5 frames is selected, etc.)
%   - This script can also be used to save the raw blank pixel signals for
%   subsequent analysis (ex. histograms, etc.)
%   - Calculated blank track saturation value means and standard deviations
%   are calculated using filteredDensitogram.m using two different methods
%   (below).  They may be used in future system noise and LOD calculations.
%       - Consider all pixels in blank track.  Exclude pixels with hue
%       outside of the given hue filter.  Calculate mean and standard
%       deviation in remaining pixels' staturation values.
%       - Calculate a hue-filtered densitogram for the blank track as
%       usual.  Calculate the mean and standard deviation in this resultant
%       signal.
```

C.13 sampleSpots.m

```
function [spotLoc,satSum] = sampleSpots(refFrame,spotLoc,...
    plot_data,exp_dir,exp_data,exp_plots,expName)

% Written by S.R. Jim, (C) March 2014
% Glancing Angle Deposition (GLAD) Laboratory, PI: M.J. Brett
% University of Alberta, Edmonton, Canada
%
% This script can be used to identify the spot locations and hue ranges
% required during colour-filtered chromatogram extraction in the subsequent
% scripts:  createRecipeUTLC.m, mainUTLC.m, (fomUTLC.m)
% It is also a subfunction of singleImageUTLC.m
%
% INPUTS:
%   - refFrame:  Reference image array of RGB (uint8) values.
%   - spotLoc:  Array used to define the regions from which spot pixels
%   should be cropped.
%   - plot_data:  Should data be displayed on plots ('y','n')?  (Must =
%   'y' in order to export plots below.)
%   - exp_dir:  Directory into which data *.mat and/or *.fig/*.png figures
%   will be exported.  (Skip by setting to 'n'.)
%   - exp_data:  Should data be exported as *.mat ('y','n')?
%   - exp_plots:  Should plots be exported as *.fig and *.png ('y','n')?
%   - expName:  Prefix of exported files (a string).
```

C.14 singleImageUTLC.m

```
function singleImageUTLC

% Written by S.R. Jim, (C) March 2014
% Glancing Angle Deposition (GLAD) Laboratory, PI: M.J. Brett
% University of Alberta, Edmonton, Canada
%
% Purpose:  This script is designed to analyze a single image of a UTLC
% plate to produce chromatograms and relevant figures-of-merit.  It
% incorporates many of the same TR-UTLC functions in createRecipeUTLC.m,
% mainUTLC.m, filteredChromaPlotVideo.m, and fomUTLC.m.  Before analysis,
% it also allows for calibration of the input image (rotation and
% cropping).
%
% Subfunctions:  sampleSpots.m
%
% Inputs/outputs:  Data file (*.mat) that stores configurations and output
% data.
%
```

```
% Exports:
%   - Rotated and cropped version of the UTLC plate image (*.jpg)
%   - Figures demonstrating hue measurement/selection (*.fig/*.jpg) and
%   *.mat data file containing this data.
%   - Chromatogram figures (isolated track, raw/fitted peaks)
%   (*.fig,*.jpg)
%   - Tables of calculated FOMs (*.csv)
%   - Data file with all configuration/calculated data
```

D Custom GLAD UTLC chamber schematics

The custom GLAD UTLC horizontal development chamber involved a combination of parts that were commercially available and parts that were carefully machined from PTFE, aluminum, and stainless steel. This appendix provides details and engineering drawings for the required pieces.

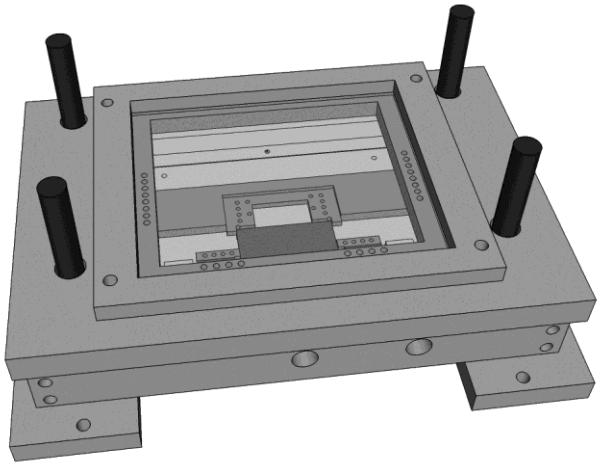

D.1 Listing of custom machined parts

Drawings are provided on the listed pages in **D.3 Engineering drawings**.

Part Name	Quantity	Description	Page
1: Main PTFE Layer	1	Chromatography chamber.	**209**
2A: Chamber front (aluminum)	1	Seals 1's main reservoir; secures chamber to *7A*. Cut fluorosilicone gasket required.	**224**
2B: PTFE clamps	2	Secures a porous glass frit into slot in *1*.	**226**
2C: PTFE insert	1	Rests inside conditioning trough milled in *1*.	**227**
3A: Stainless steel clamp A	1	Mounts glass piece to *4*.	**228**
3B: Stainless steel clamp B	1	Mounts glass piece to *4*.	**229**
3C: Stainless steel clamp C	4	Secures glass piece to *3A* (also for *3B*).	**230**
3D: Stainless steel clips	4	Secures glass piece to *3A* (also for *3B*). Cut from stainless steel shim stock.	**231**
4: Chamber lid (aluminum)	1	Rests on PTFE chamber. *1* and *2* sit within its rim.	**232**
5: Top window frame (aluminum)	1	Presses top window against *4*.	**236**
6: Bottom window frame (aluminum)	1	Presses bottom window against bottom of *1*. Cut fluorosilicone gasket required.	**237**
7A: Frame rail A (aluminum)	2	Left and right rails that form base for chamber.	**238**
7B: Frame rail B (aluminum)	1	Secures *1* against *7A*.	**239**
7C: Mounting blocks (aluminum)	4	Secures *1* against *7A*.	**240**

D.2 Listing of purchased parts

Item	Quantity	Description
Porous glass frit[1]	1	Sits in main reservoir of *1* and held in place using *2B*. Porosity P2; custom machined to 110 x 10 x 8 mm by supplier.
Alignment posts, stainless steel[2]	4	Screwed into 7A and used to align *4* with *1*. Optical posts, 1/2" diameter, 4" length; TR4.
Top window, glass[3]	1	For imaging from above.
Bottom window, glass[3]	1	For illumination from below.
Tube fittings[4]	5	Threaded into *1* and used to connect PFA tubing. Swagelok; PFA-420-1-4.
PFA tubing[4]	20 feet	Delivers and drains solvents from *1*. PFA-T4-062-100.
Glass syringes[5]	2	30 cc, Luer-Lok tips; Micro-Mate (Cadence Scientific); 14-825-10A.
Luer-tubing adapters, stainless steel[5]	5	Connects Luer tips to 1/8"-3/16" inner diameter tubing; Cadence Scientific 6452.
Fluorosilicone rubber sheet[6]	1	Cut and folded into gaskets between *1* and *2A*, and between *1* and bottom window. Corrosion-resistant, 1/32" thick, 12" square; 2183T12. Fold placed along longest edge.
Certified precision ruler, stainless steel[6]	1	Cut down and screwed into *3B*. 150 mm length; 2056A22.
Levelling feet[6]	4	1/4"-20 thread, 1" diameter base with swivel ball-and-socket design; 6103K24.
Assorted hardware		Screws, bolts, and washers; stainless steel when possible.

D.3 Engineering drawings

Schematics for all custom parts are provided on the following pages.

[1] Adams & Chittenden (Berkeley, California, USA)
[2] Thorlabs (Newton, New Jersey, USA)
[3] Crystal Glass Canada (Edmonton, Alberta, Canada)
[4] Edmonton Valve and Fitting - Swagelok (Edmonton, Alberta, Canada)
[5] Fisher Scientific (Ottawa, Ontario, Canada)
[6] McMaster-Carr Supply Company (Elmhurst, Illinois, USA)

PROJECT: CHROMATOGRAPHY CHAMBER
STEVEN JIM, GLAD LAB
(SJIM@UALBERTA.CA; 780 492 7926)

PART 1: MAIN PTFE LAYER

OBLIQUE: TOP

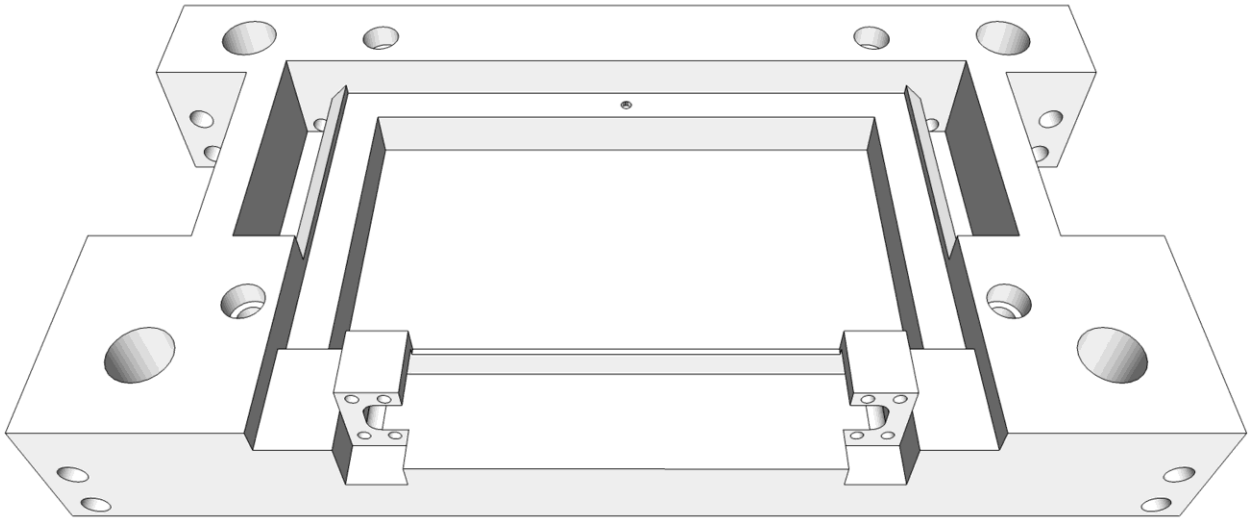

FILENAME: "UTLC Chamber-Part1-MainPTFE-update20130424.vsd" PAGE: 1 OF 15

PROJECT: CHROMATOGRAPHY CHAMBER
STEVEN JIM, GLAD LAB
(SJIM@UALBERTA.CA; 780 492 7926)

PART 1: MAIN PTFE LAYER

OBLIQUE: FRONT

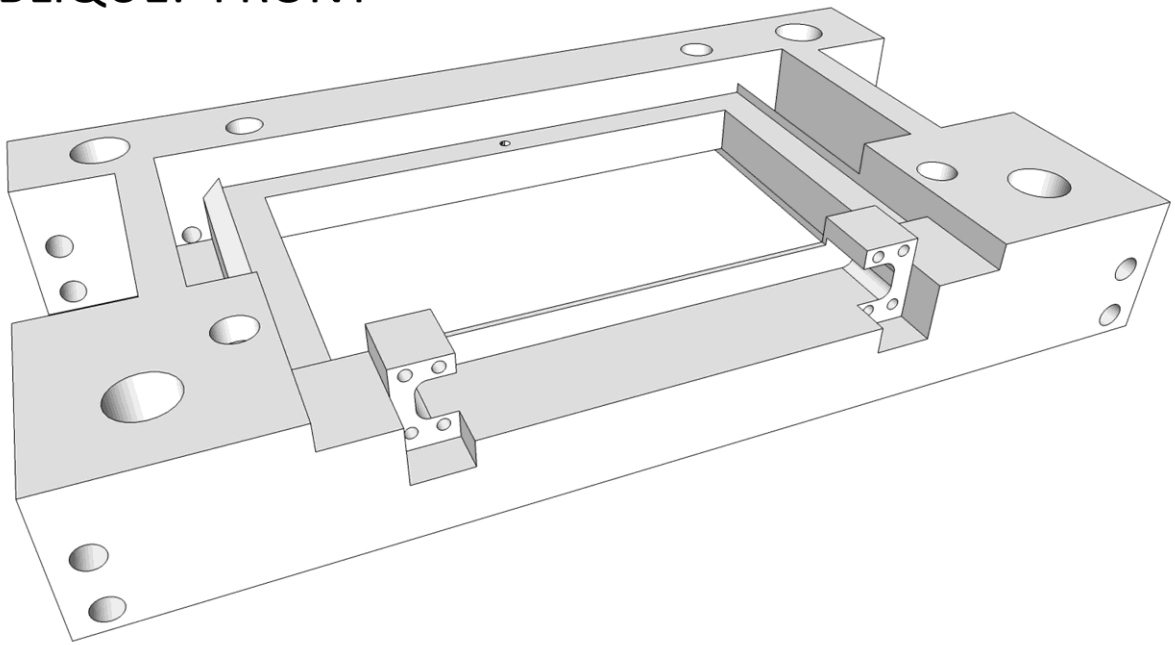

FILENAME: "UTLC Chamber-Part1-MainPTFE-update20130424.vsd" PAGE: 2 OF 15

PROJECT: CHROMATOGRAPHY CHAMBER
STEVEN JIM, GLAD LAB
(SJIM@UALBERTA.CA; 780 492 7926)

PART 1: MAIN PTFE LAYER

OBLIQUE: BACK

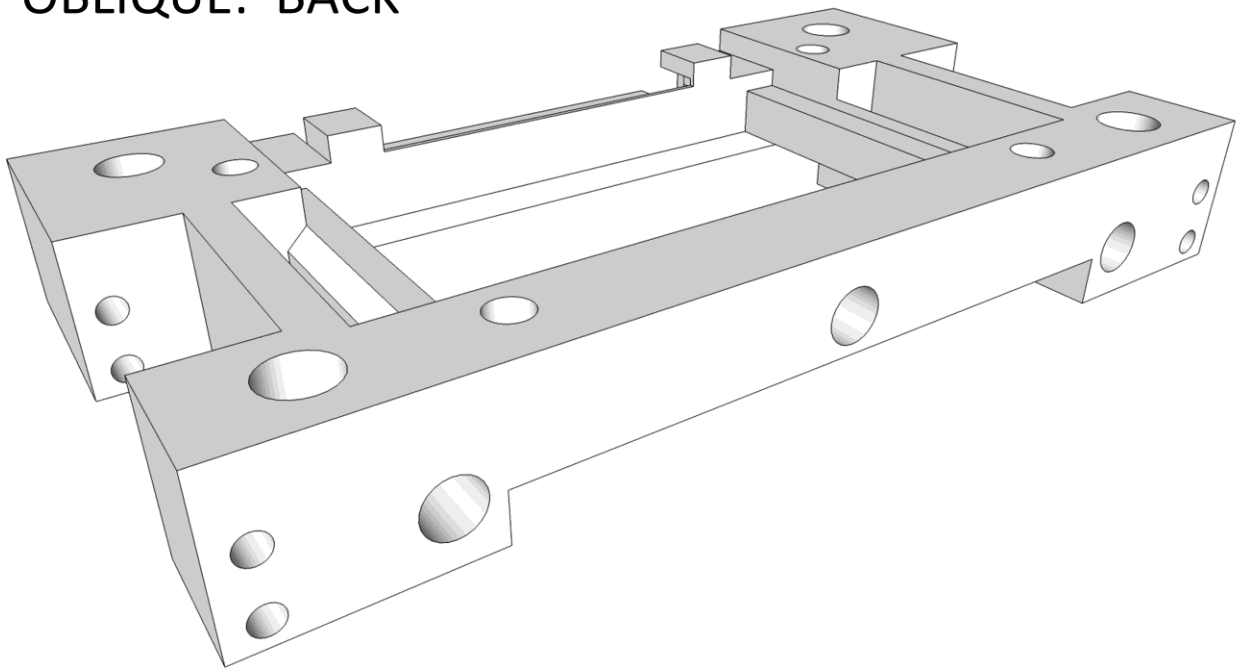

FILENAME: "UTLC Chamber-Part1-MainPTFE-update20130424.vsd" PAGE: 3 OF 15

PROJECT: CHROMATOGRAPHY CHAMBER
STEVEN JIM, GLAD LAB
(SJIM@UALBERTA.CA; 780 492 7926)

PART 1: MAIN PTFE LAYER

OBLIQUE: BOTTOM

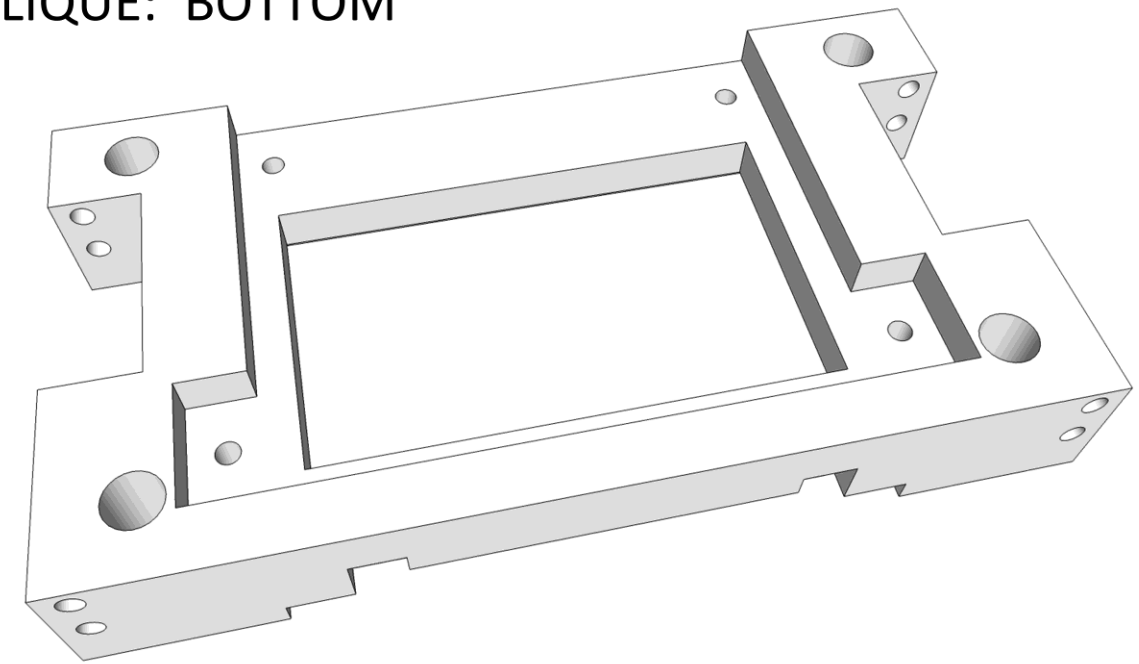

FILENAME: "UTLC Chamber-Part1-MainPTFE-update20130424.vsd" PAGE: 4 OF 15

PROJECT: CHROMATOGRAPHY CHAMBER
STEVEN JIM, GLAD LAB
(SJIM@UALBERTA.CA; 780 492 7926)

PART 1: MAIN PTFE LAYER

TOP (SECTION PLANES)

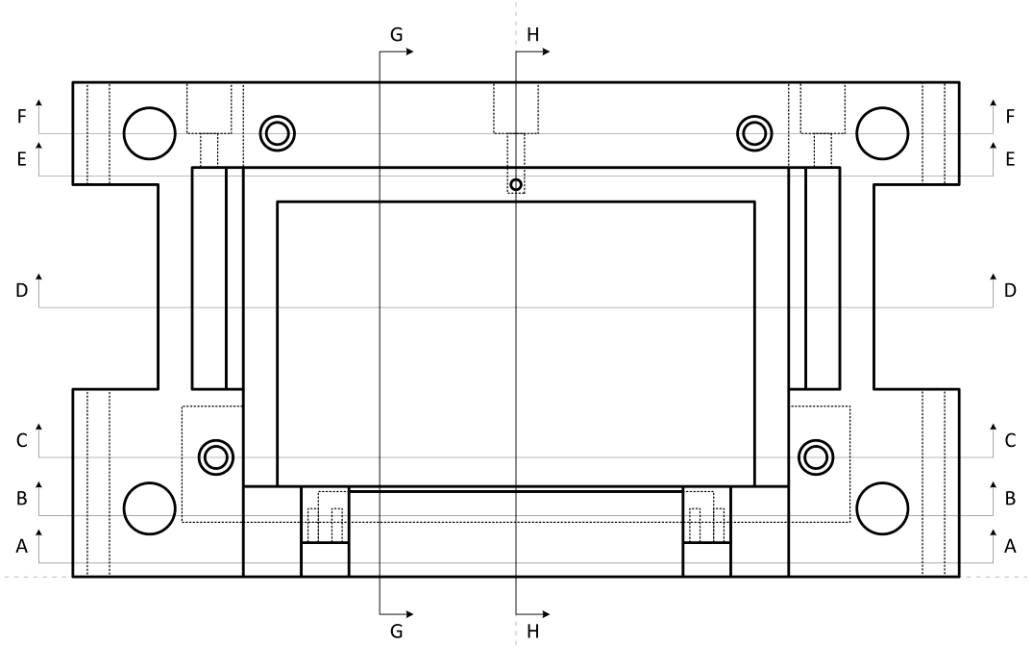

FILENAME: "UTLC Chamber-Part1-MainPTFE-update20130424.vsd" PAGE: 5 OF 15

PROJECT: CHROMATOGRAPHY CHAMBER
STEVEN JIM, GLAD LAB
(SJIM@UALBERTA.CA; 780 492 7926)

PART 1: MAIN PTFE LAYER

TOP

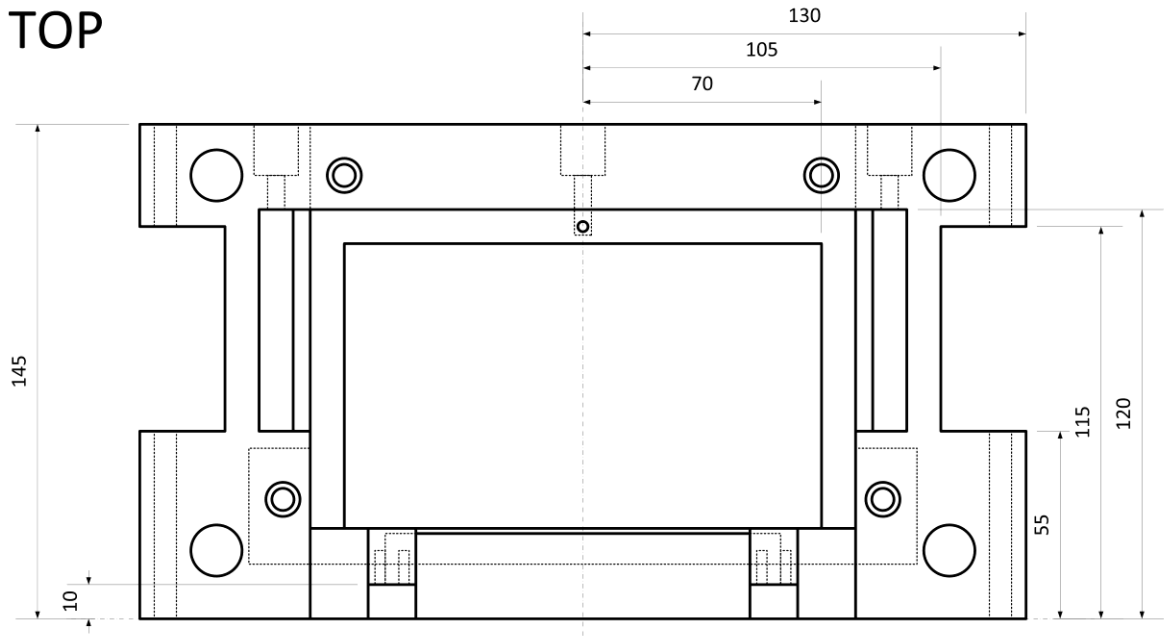

NOTE: THE BOTTOM SURFACE (IN THIS VIEW) IS SEALED AGAINST
THE ALUMINUM PIECE PART 2A USING A FLUOROSILICONE SHEET.

FILENAME: "UTLC Chamber-Part1-MainPTFE-update20130424.vsd" **PAGE: 6 OF 15**

PROJECT: CHROMATOGRAPHY CHAMBER
STEVEN JIM, GLAD LAB
(SJIM@UALBERTA.CA; 780 492 7926)

PART 1: MAIN PTFE LAYER

TOP (HOLES)

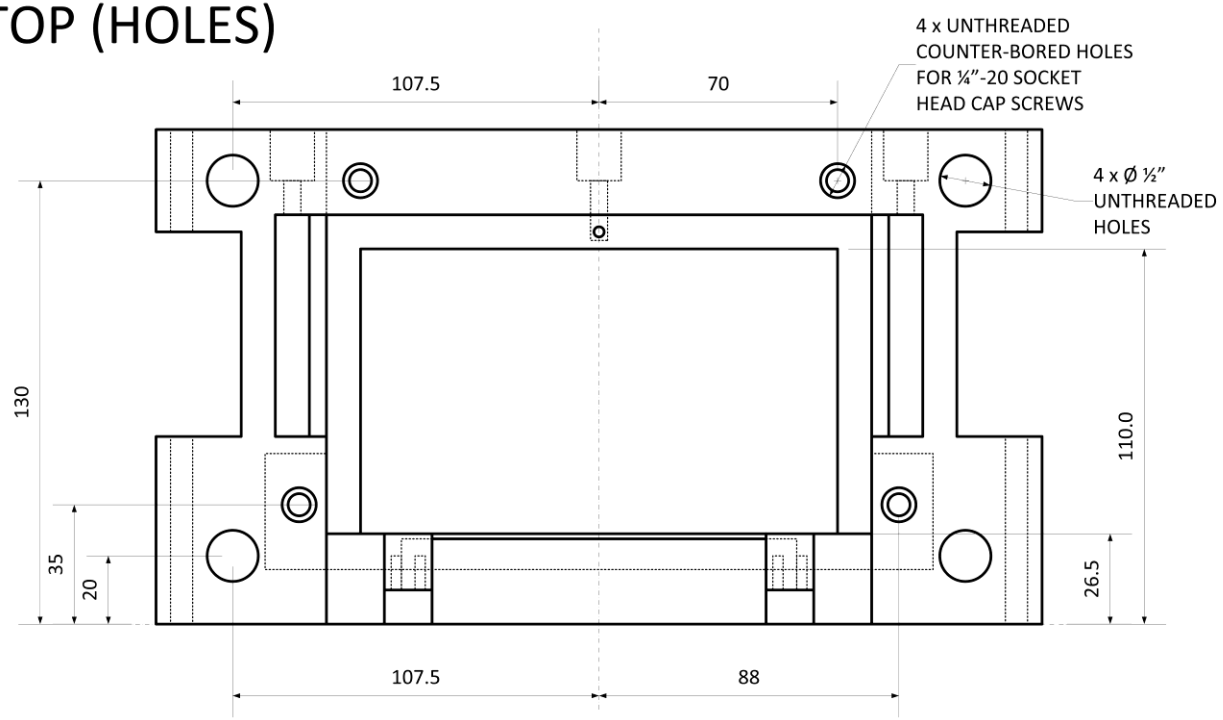

FILENAME: "UTLC Chamber-Part1-MainPTFE-update20130424.vsd" PAGE: 7 OF 15

PROJECT: CHROMATOGRAPHY CHAMBER
STEVEN JIM, GLAD LAB
(SJIM@UALBERTA.CA; 780 492 7926)

PART 1: MAIN PTFE LAYER

BOTTOM

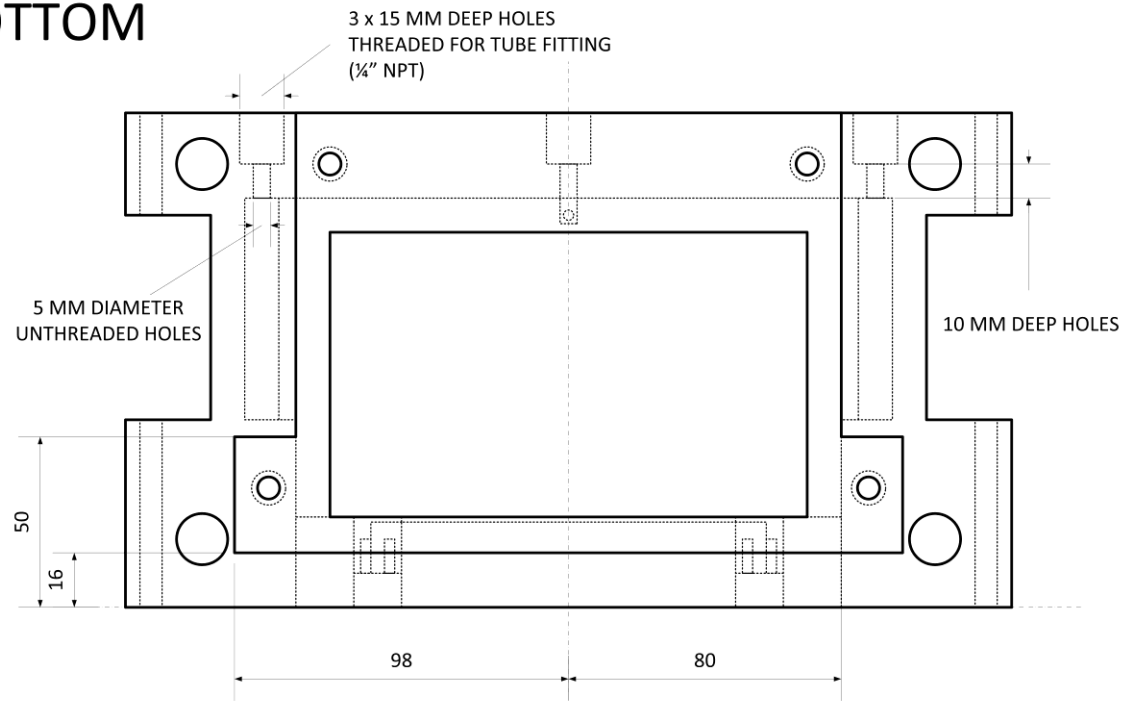

FILENAME: "UTLC Chamber-Part1-MainPTFE-update20130424.vsd" **PAGE: 8 OF 15**

PROJECT: CHROMATOGRAPHY CHAMBER
STEVEN JIM, GLAD LAB
(SJIM@UALBERTA.CA; 780 492 7926)

PART 1: MAIN PTFE LAYER

FRONT

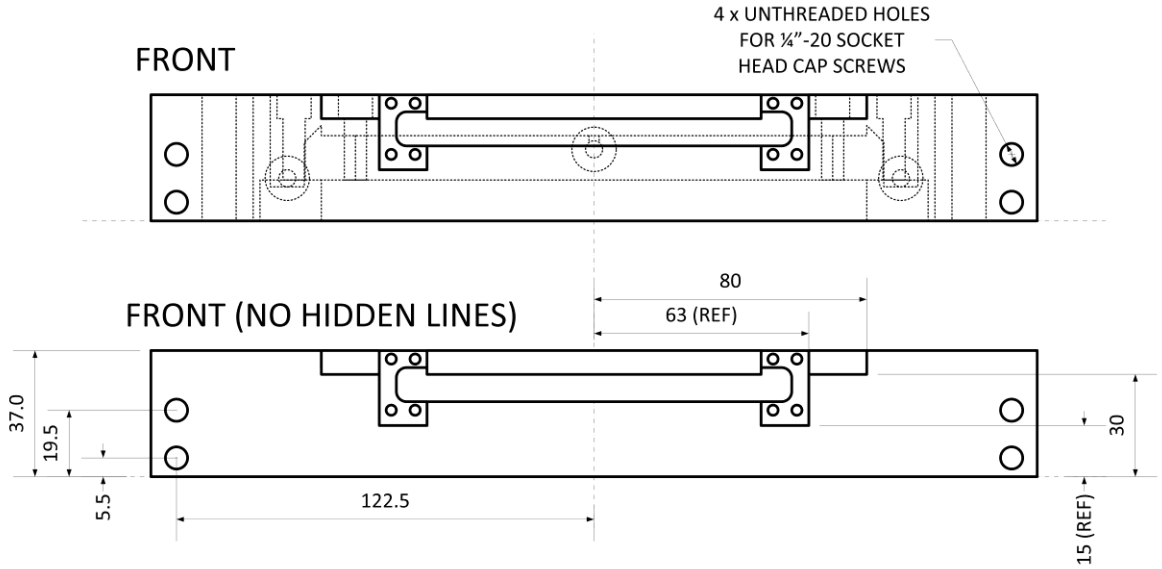

FILENAME: "UTLC Chamber-Part1-MainPTFE-update20130424.vsd" **PAGE: 9 OF 15**

PROJECT: CHROMATOGRAPHY CHAMBER
STEVEN JIM, GLAD LAB
(SJIM@UALBERTA.CA; 780 492 7926)

PART 1: MAIN PTFE LAYER

BACK

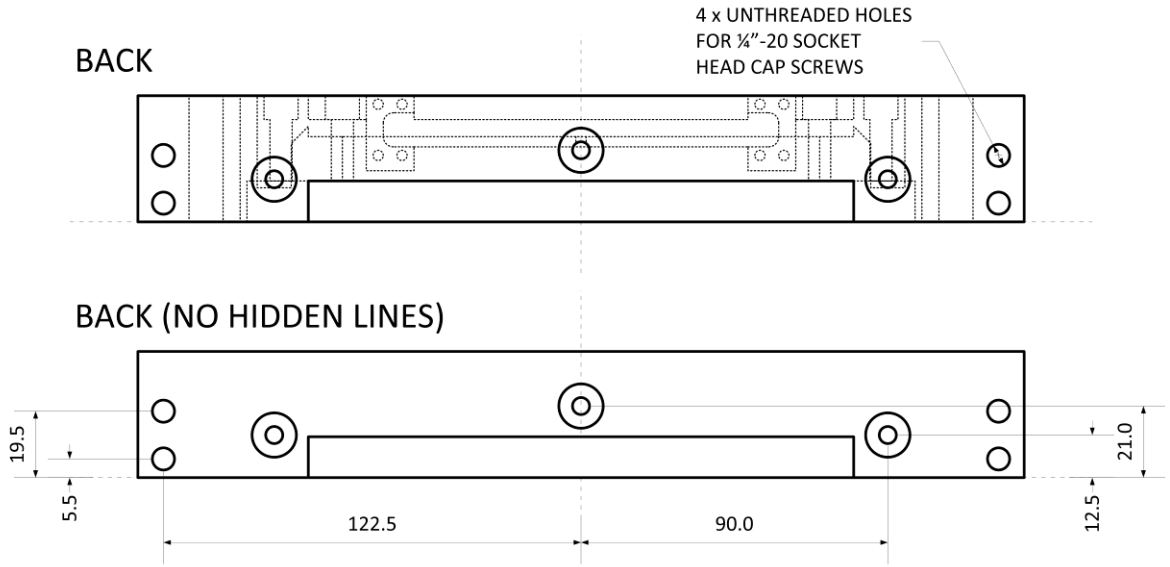

FILENAME: "UTLC Chamber-Part1-MainPTFE-update20130424.vsd" **PAGE: 10 OF 15**

PROJECT: CHROMATOGRAPHY CHAMBER
STEVEN JIM, GLAD LAB
(SJIM@UALBERTA.CA; 780 492 7926)

PART 1: MAIN PTFE LAYER

SECTIONS AA, BB

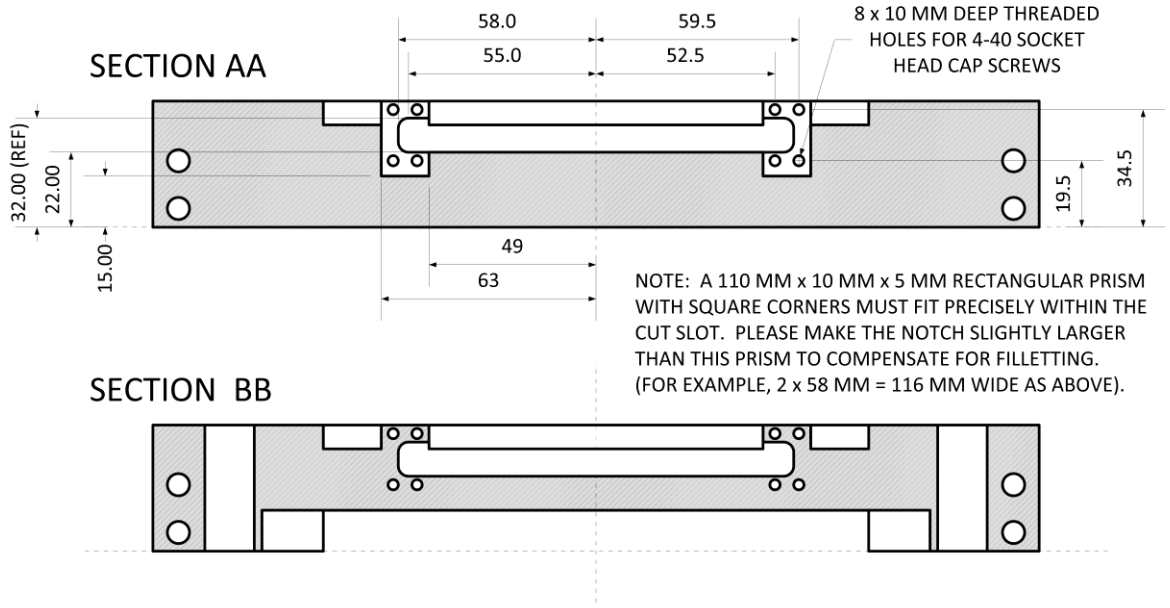

FILENAME: "UTLC Chamber-Part1-MainPTFE-update20130424.vsd" PAGE: 11 OF 15

PROJECT: CHROMATOGRAPHY CHAMBER
STEVEN JIM, GLAD LAB
(SJIM@UALBERTA.CA; 780 492 7926)

PART 1: MAIN PTFE LAYER

SECTIONS CC, DD

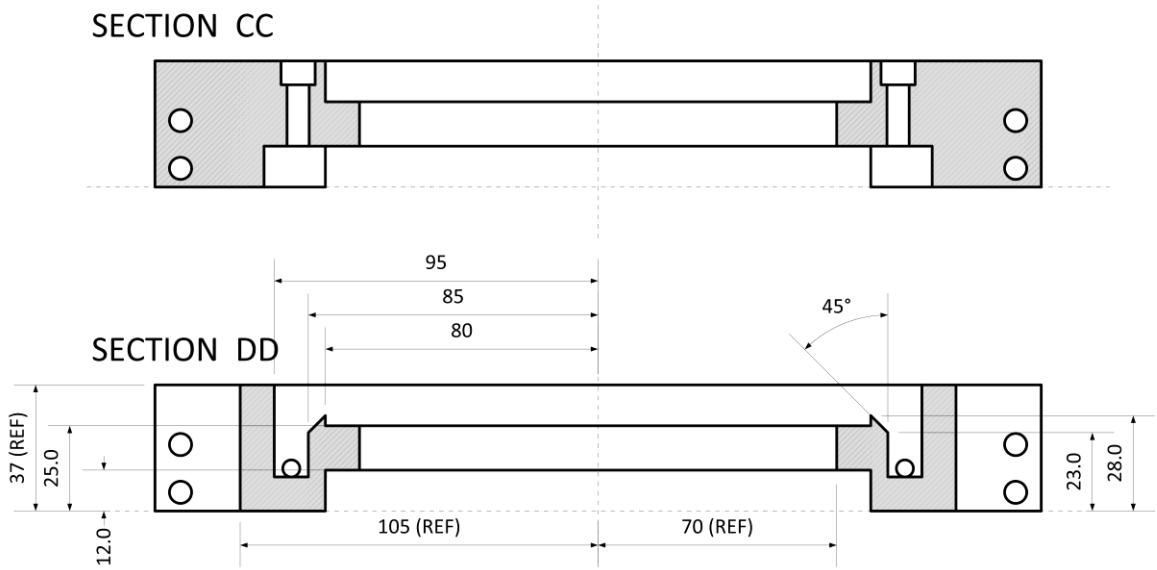

FILENAME: "UTLC Chamber-Part1-MainPTFE-update20130424.vsd" PAGE: 12 OF 15

PROJECT: CHROMATOGRAPHY CHAMBER
STEVEN JIM, GLAD LAB
(SJIM@UALBERTA.CA; 780 492 7926)

PART 1: MAIN PTFE LAYER

SECTIONS EE, FF

SECTION EE

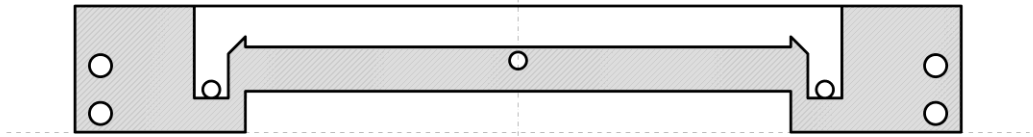

SECTION FF

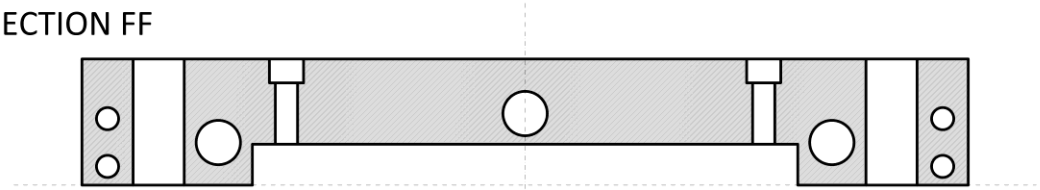

FILENAME: "UTLC Chamber-Part1-MainPTFE-update20130424.vsd" PAGE: 13 OF 15

PROJECT: CHROMATOGRAPHY CHAMBER
STEVEN JIM, GLAD LAB
(SJIM@UALBERTA.CA; 780 492 7926)

PART 1: MAIN PTFE LAYER

SECTION GG

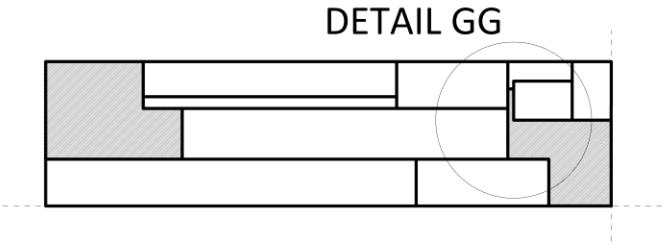

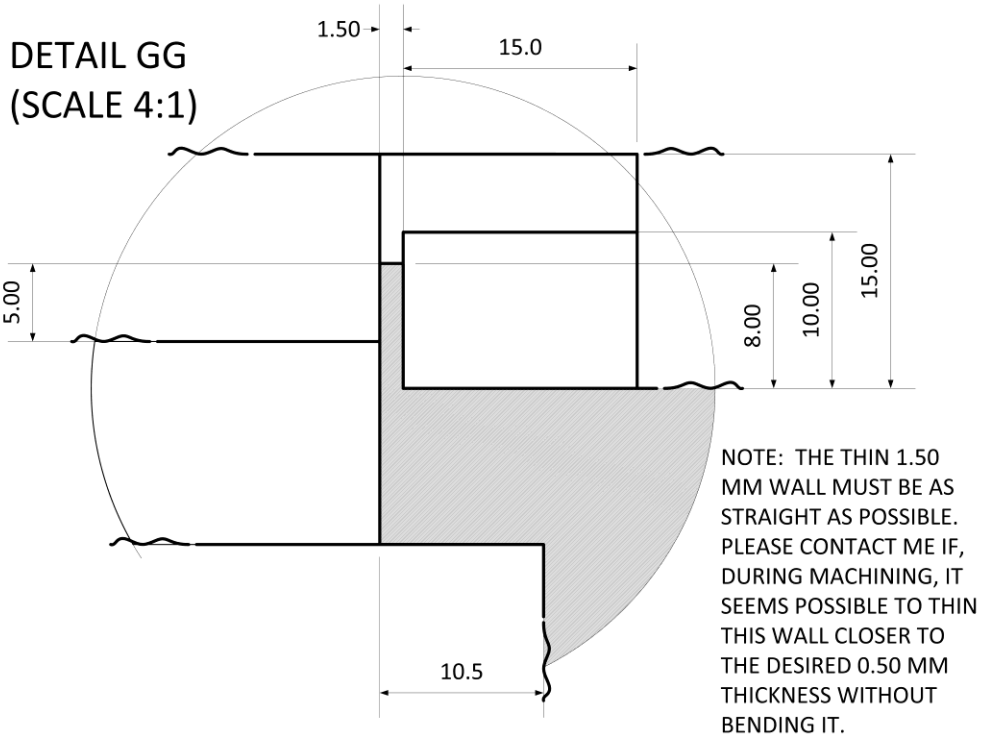

NOTE: THE THIN 1.50 MM WALL MUST BE AS STRAIGHT AS POSSIBLE. PLEASE CONTACT ME IF, DURING MACHINING, IT SEEMS POSSIBLE TO THIN THIS WALL CLOSER TO THE DESIRED 0.50 MM THICKNESS WITHOUT BENDING IT.

FILENAME: "UTLC Chamber-Part1-MainPTFE-update20130424.vsd"

PAGE: 14 OF 15

PROJECT: CHROMATOGRAPHY CHAMBER
STEVEN JIM, GLAD LAB
(SJIM@UALBERTA.CA; 780 492 7926)

PART 1: MAIN PTFE LAYER

SECTION HH

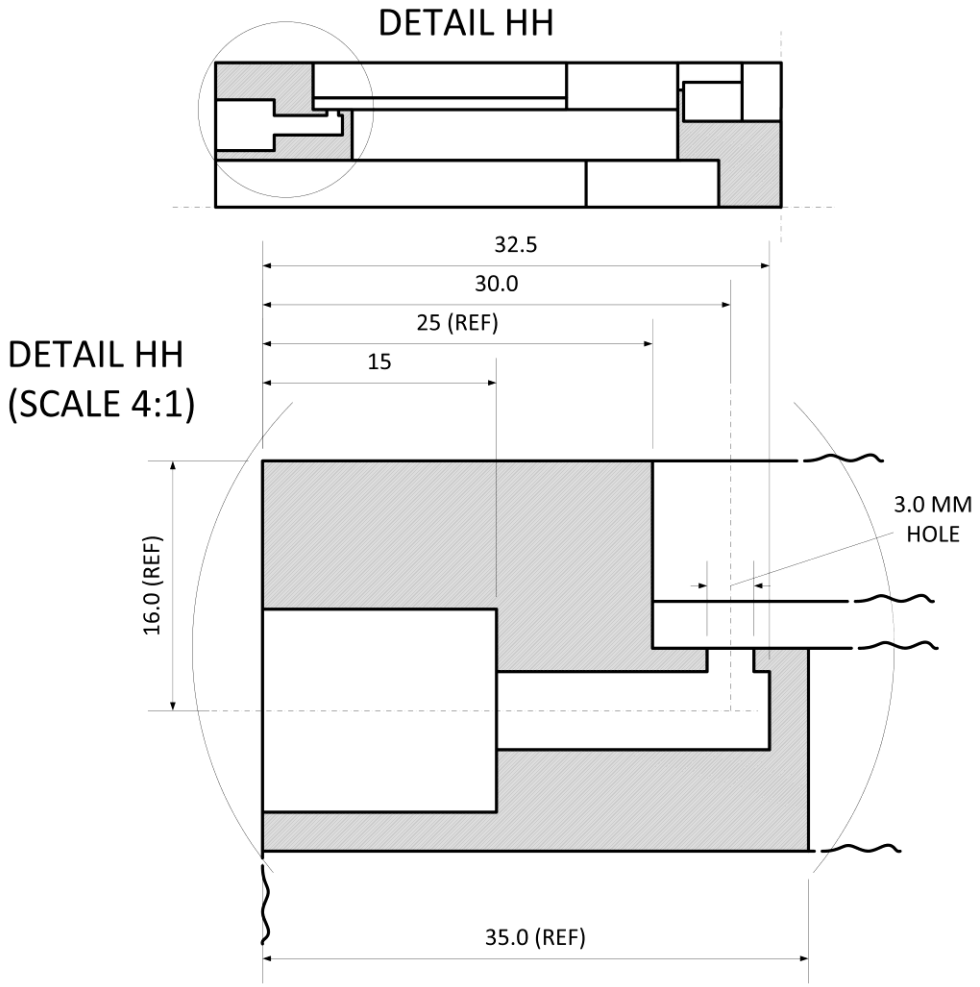

FILENAME: "UTLC Chamber-Part1-MainPTFE-update20130424.vsd"

PAGE: 15 OF 15

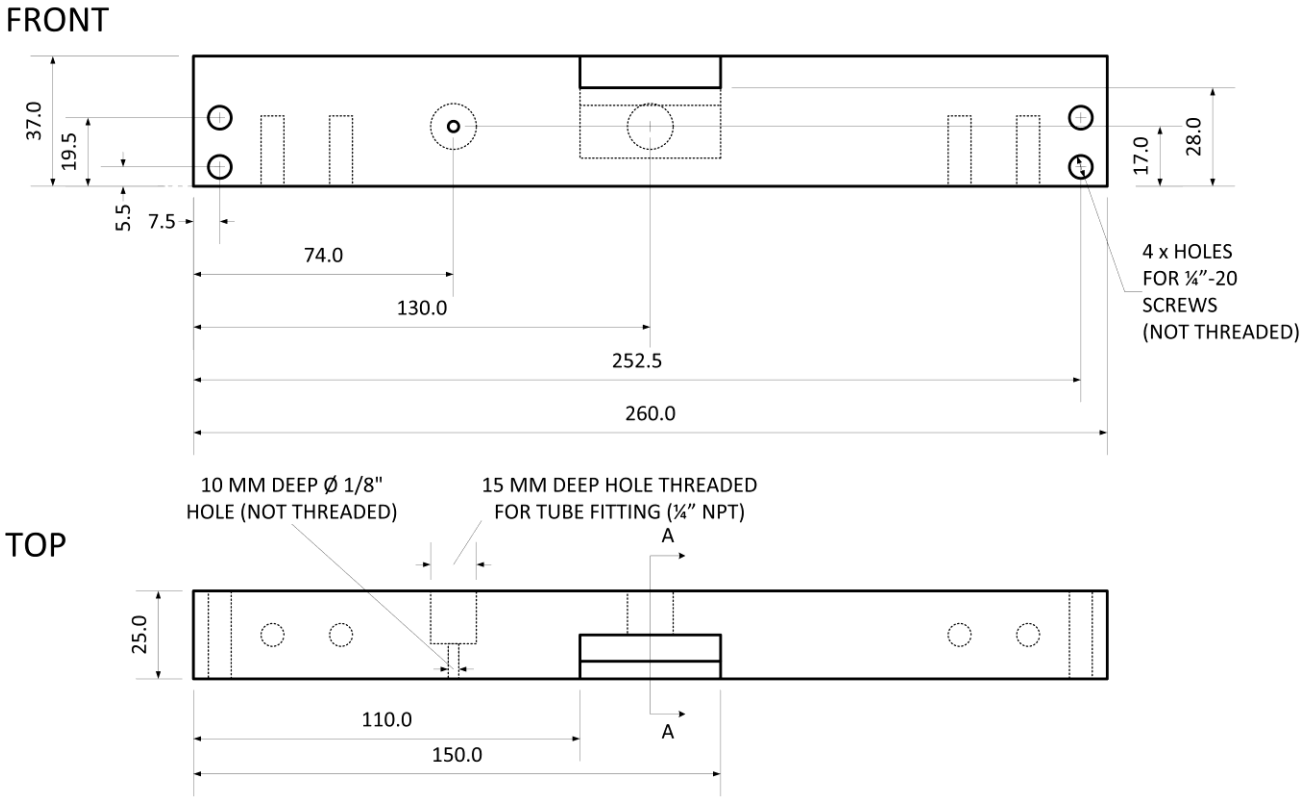

PROJECT: CHROMATOGRAPHY CHAMBER
STEVEN JIM, GLAD LAB
(SJIM@UALBERTA.CA; 780 492 7926)

PART 2A: Chamber Front (Aluminum)

FILENAME: "UTLC Chamber-Part2A-ChamberFront-update20131030.vsd" PAGE: 1 OF 2

BOTTOM

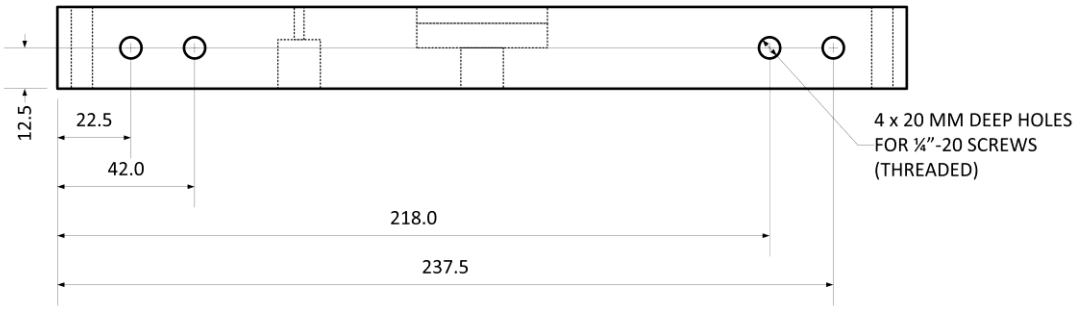

SECTION AA (2:1)

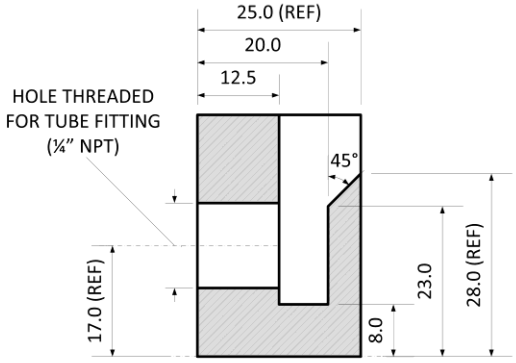

OBLIQUE (FRONT/TOP)

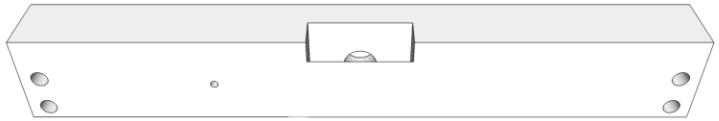

OBLIQUE (BACK/BOTTOM)

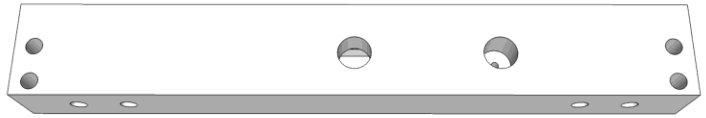

PROJECT: CHROMATOGRAPHY CHAMBER
STEVEN JIM, GLAD LAB
(SJIM@UALBERTA.CA; 780 492 7926)

PART 2A: Chamber Front (Aluminum)

FILENAME: "UTLC Chamber-Part2A-ChamberFront-update20131030.vsd" PAGE: 2 OF 2

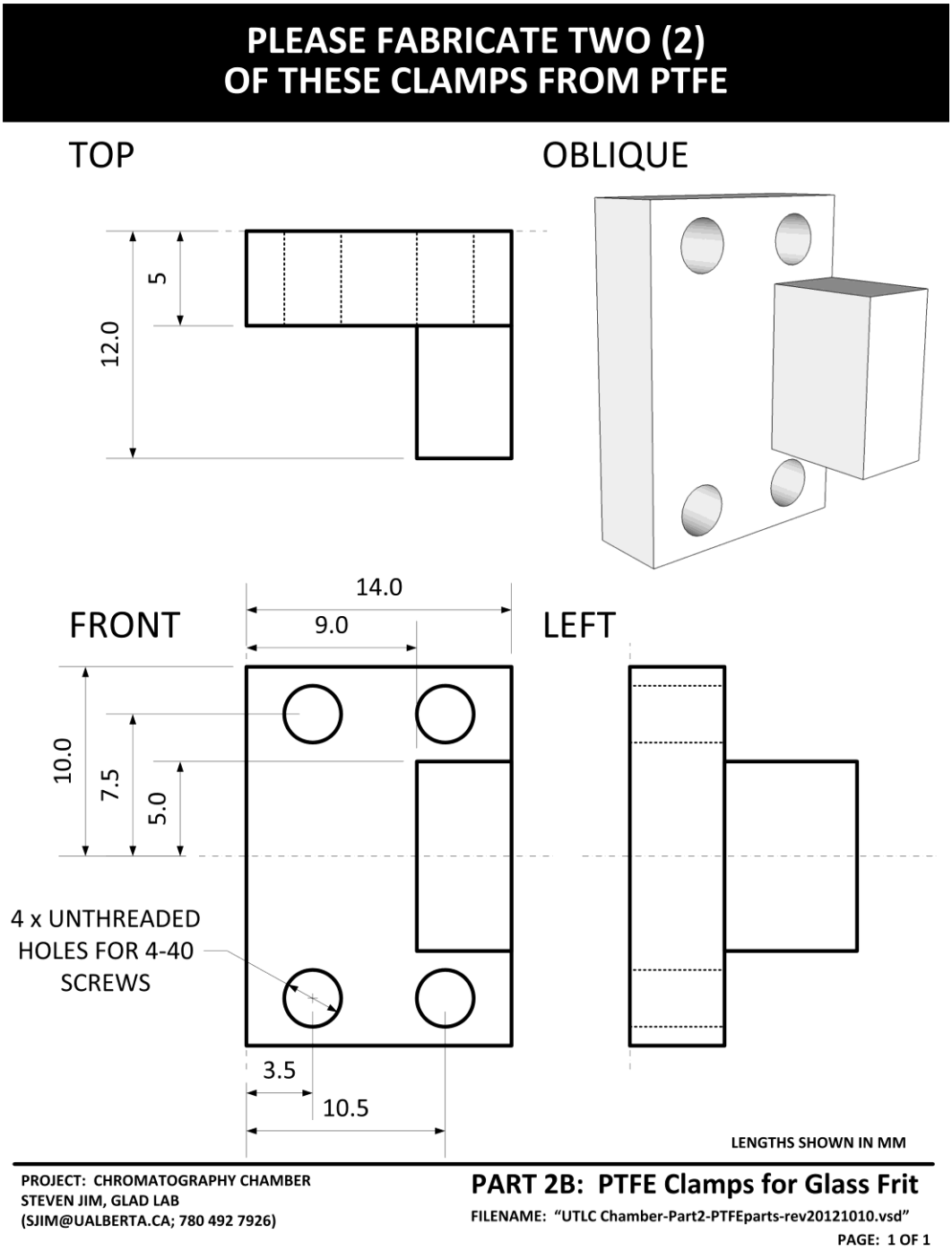
PLEASE FABRICATE TWO (2)
OF THESE CLAMPS FROM PTFE
TOP
OBLIQUE
5
12.0
14.0
9.0
FRONT
LEFT
10.0
7.5
5.0
4 x UNTHREADED
HOLES FOR 4-40
SCREWS
3.5
10.5
LENGTHS SHOWN IN MM
PROJECT: CHROMATOGRAPHY CHAMBER
STEVEN JIM, GLAD LAB
(SJIM@UALBERTA.CA; 780 492 7926)
PART 2B: PTFE Clamps for Glass Frit
FILENAME: "UTLC Chamber-Part2-PTFEparts-rev20121010.vsd"
PAGE: 1 OF 1

OBLIQUE

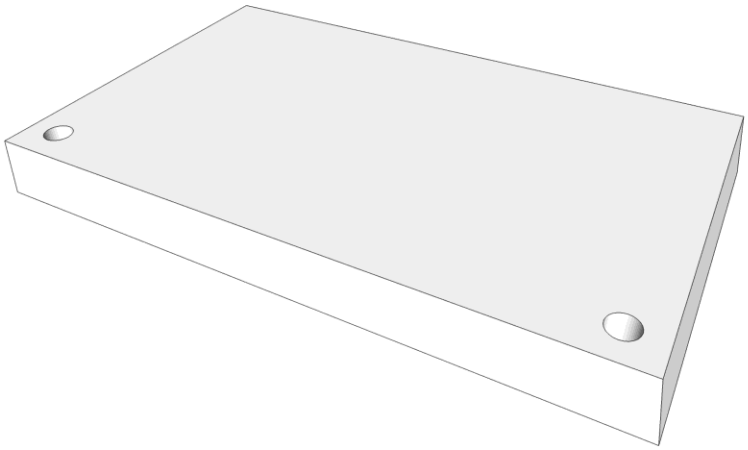

TOP

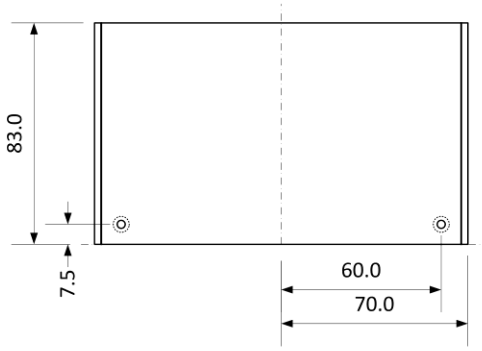

FRONT

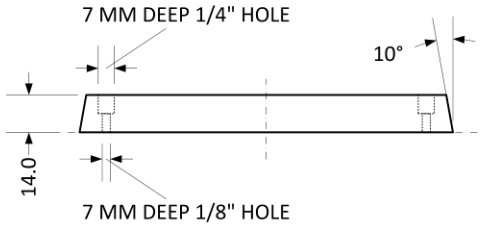

NOTES

1. THIS PTFE INSERT IS DESIGNED TO FIT (UPSIDE DOWN) WITHIN THE LARGE RECTANGULAR HOLE CUT INTO THE BOTTOM OF **PART 1: MAIN PTFE LAYER**. PLEASE ROUND THE CORNERS OF THIS INSERT TO COMPENSATE FOR FILLETING IN THE CORNERS OF THIS HOLE.

2. THIS INSERT MUST BE REMOVABLE FROM THE HOLE. A BEVEL AND COUNTER-BORED HOLE SHOULD MAKE THIS PIECE EASIER TO LIFT WITH A WIRE HOOK.

LENGTHS SHOWN IN MM

PROJECT: CHROMATOGRAPHY CHAMBER
STEVEN JIM, GLAD LAB
(SJIM@UALBERTA.CA; 780 492 7926)

PART 2C: PTFE Insert
FILENAME: "UTLC Chamber-Part2-PTFEparts-rev20121010.vsd"
PAGE: 1 OF 1

FRONT (OBLIQUE)

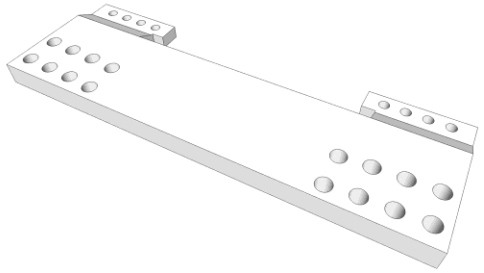

BACK (OBLIQUE)

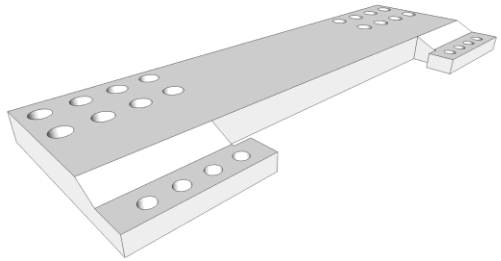

TOP

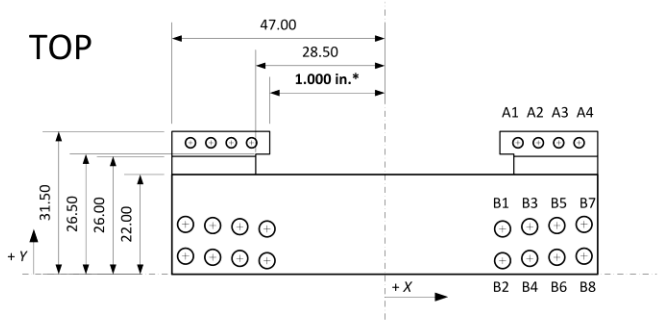

RIGHT (SCALE 2:1)

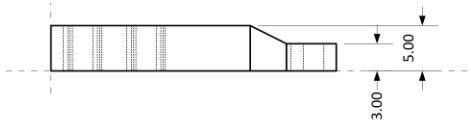

HOLE SET A: FOR 2-56 SCREWS; THREADED

TAG	X LOC (MM)	Y LOC (MM)
A1	29.40	29.00
A2	33.90	29.00
A3	38.40	29.00
A4	42.90	29.00

HOLE SET B: FOR 6-32 SCREWS; NOT THREADED

TAG	X LOC (MM)	Y LOC (MM)
B1	26.00	10.00
B2	26.00	3.00
B3	32.00	10.50
B4	32.00	3.50
B5	38.00	10.75
B6	38.00	3.75
B7	44.00	11.00
B8	44.00	4.00

* NOTE: 2.000 IN. WIDE GLASS PIECES MUST FIT PRECISELY WITHIN THE CLAMP GAP (LABELLED AS 2 x 1.000 IN. ABOVE).

PROJECT: CHROMATOGRAPHY CHAMBER
STEVEN JIM, GLAD LAB
(SJIM@UALBERTA.CA; 780 492 7926)

PART 3A: Stainless Steel Clamp A

FILENAME: "UTLC Chamber-Part3-stainless clamps-rev20121101.vsd" PAGE: 1 OF 1

FRONT (OBLIQUE)

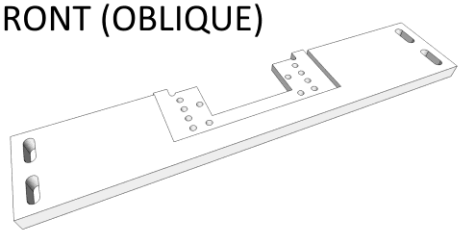

BACK (OBLIQUE)

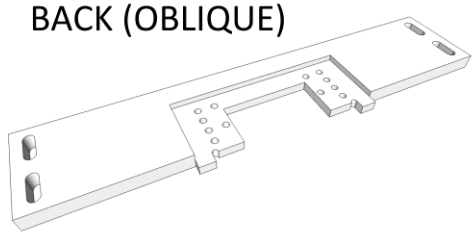

TOP

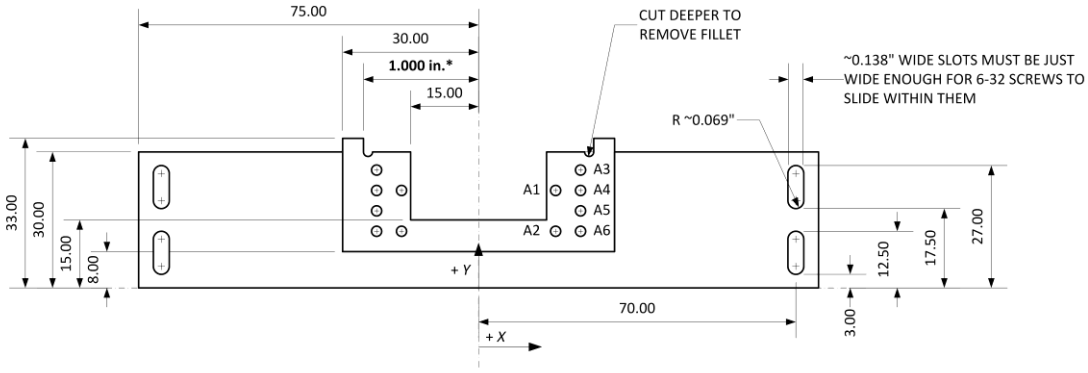

RIGHT (SCALE 2:1)

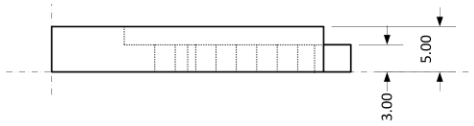

HOLE SET A: FOR 2-56 SCREWS; THREADED		
TAG	X LOC (MM)	Y LOC (MM)
A1	17.00	21.50
A2	17.00	12.50
A3	22.50	26.00
A4	22.50	21.50
A5	22.50	17.00
A6	22.50	12.50

* NOTE: 2.000 IN. WIDE GLASS PIECES MUST FIT PRECISELY WITHIN THE CLAMP GAP (LABELLED AS 2 x 1.000 IN. ABOVE).

PROJECT: CHROMATOGRAPHY CHAMBER
STEVEN JIM, GLAD LAB
(SJIM@UALBERTA.CA; 780 492 7926)

PART 3B: Stainless Steel Clamp B

FILENAME: "UTLC Chamber-Part3-stainless clamps-rev20121101.vsd" PAGE: 1 OF 1

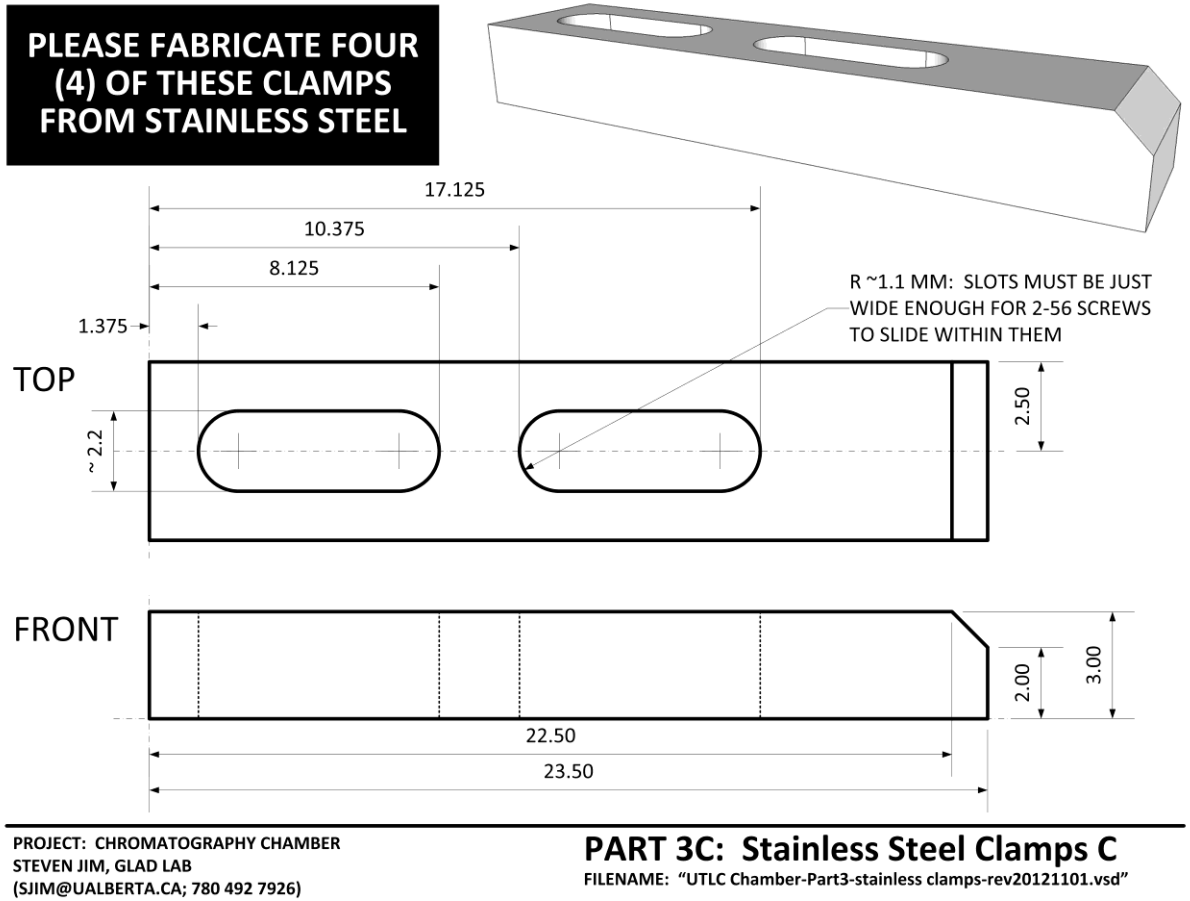
PLEASE FABRICATE FOUR (4) OF THESE CLAMPS FROM STAINLESS STEEL
17.125
10.375
8.125
1.375
R ~1.1 MM: SLOTS MUST BE JUST WIDE ENOUGH FOR 2-56 SCREWS TO SLIDE WITHIN THEM
TOP
~ 2.2
2.50
FRONT
2.00
3.00
22.50
23.50
PROJECT: CHROMATOGRAPHY CHAMBER
STEVEN JIM, GLAD LAB
(SJIM@UALBERTA.CA; 780 492 7926)
PART 3C: Stainless Steel Clamps C
FILENAME: "UTLC Chamber-Part3-stainless clamps-rev20121101.vsd"

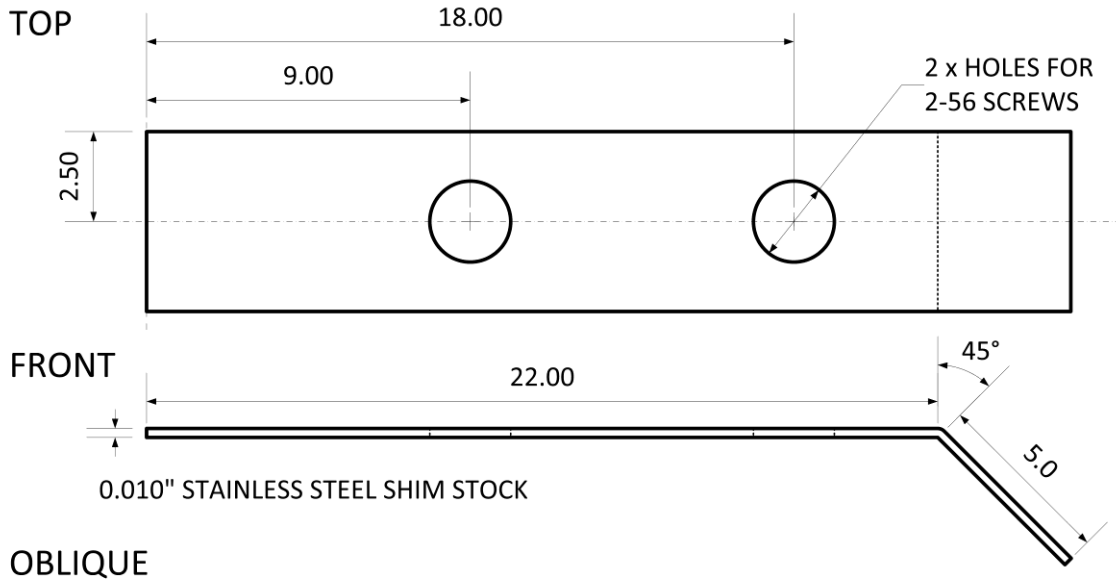

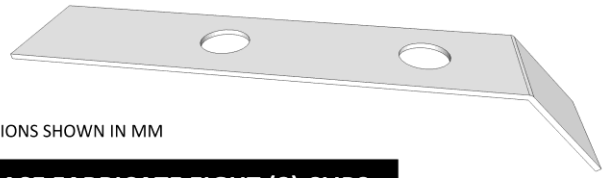

DIMENSIONS SHOWN IN MM

PLEASE FABRICATE EIGHT (8) CLIPS

NOTE 1: BEND THESE SPRINGY CLIPS FROM 27 MM STRIPS OF STAINLESS STEEL SHIM STOCK (0.010" THICK)

NOTE 2: EXAMPLE RAW MATERIAL FROM MCMASTER-CARR: TYPE 301 STAINLESS STEEL ROLLS—1/2 HARD TEMPER; ITEM: 2316K18.
HOWEVER, OTHER LESS EXPENSIVE TYPES OF STAINLESS STEEL MAY BE USED INSTEAD.

PROJECT: CHROMATOGRAPHY CHAMBER
STEVEN JIM, GLAD LAB
(SJIM@UALBERTA.CA; 780 492 7926)

PART 3D: Stainless Steel Clips

FILENAME: "UTLC Chamber-Part3D-stainless clips-update20131030.vsd" PAGE: 1 OF 1

TOP
(OBLIQUE)

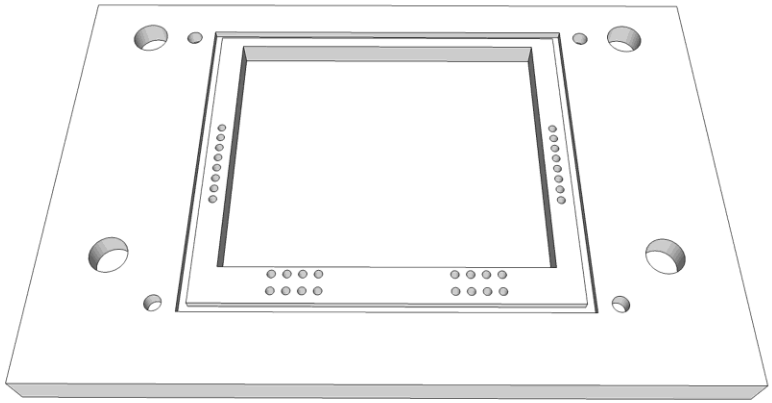

BOTTOM
(OBLIQUE)

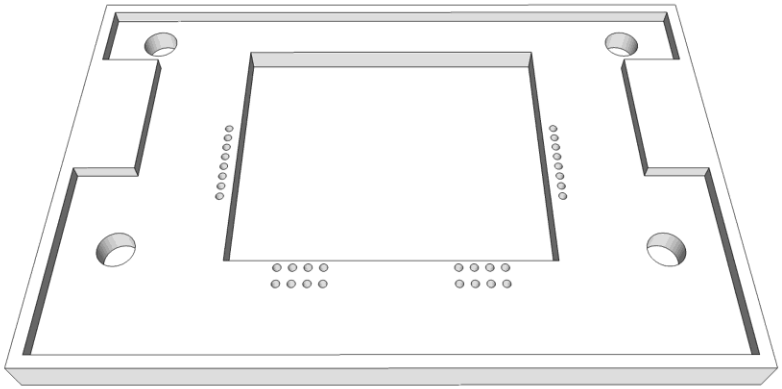

PROJECT: CHROMATOGRAPHY CHAMBER
STEVEN JIM, GLAD LAB
(SJIM@UALBERTA.CA; 780 492 7926)

PART 4: Chamber Lid (Aluminum)

FILENAME: "UTLC Chamber-Part4-aluminum lid-update20130424.vsd" PAGE: 1 OF 4

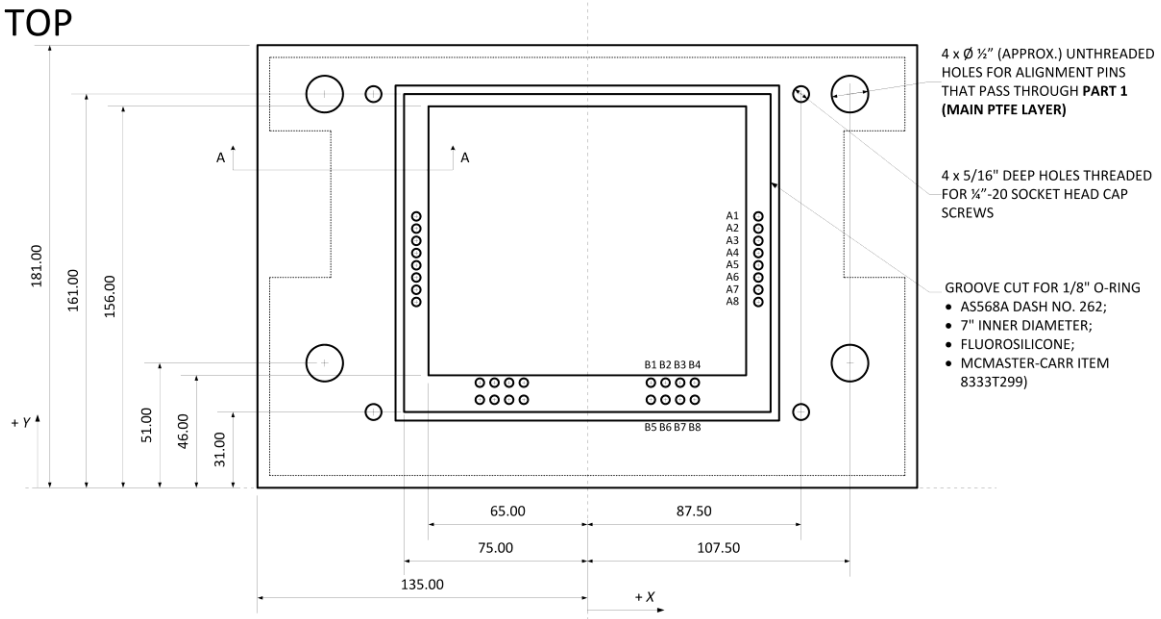

HOLE SET A: FOR 6-32 SCREWS, THREADED

TAG	X LOC (MM)	Y LOC (MM)
A1	70.00	111.00
A2	70.00	106.00
A3	70.00	101.00
A4	70.00	96.00
A5	70.00	91.00
A6	70.00	86.00
A7	70.00	81.00
A8	70.00	76.00

HOLE SET B: FOR 6-32 SCREWS, THREADED

TAG	X LOC (MM)	Y LOC (MM)
B1	26.00	43.00
B2	32.00	43.00
B3	38.00	43.00
B4	44.00	43.00
B5	26.00	36.00
B6	32.00	36.00
B7	38.00	36.00
B8	44.00	36.00

DIMENSIONS SHOWN IN MM

PROJECT: CHROMATOGRAPHY CHAMBER
STEVEN JIM, GLAD LAB
(SJIM@UALBERTA.CA; 780 492 7926)

PART 4: Chamber Lid (Aluminum)

FILENAME: "UTLC Chamber-Part4-aluminum lid-update20130424.vsd"

PAGE: 2 OF 4

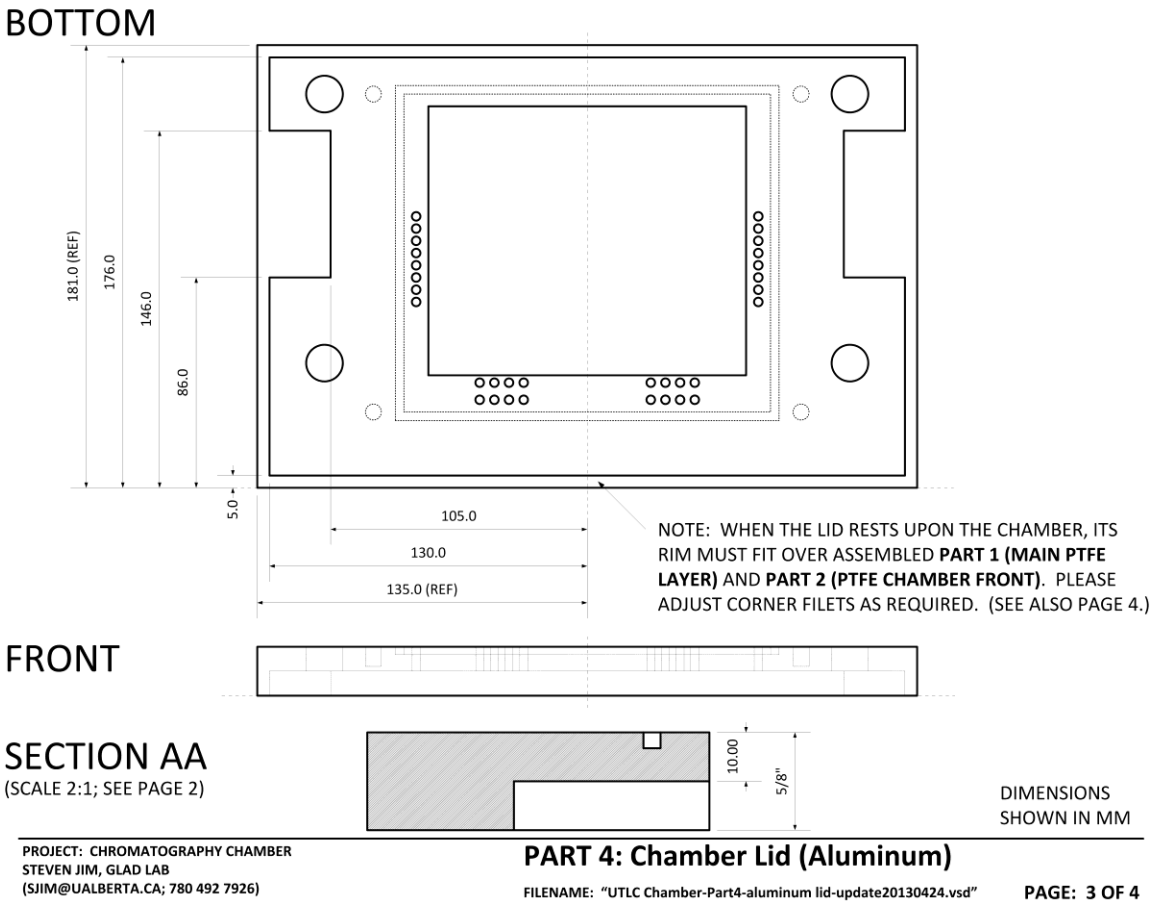
BOTTOM
181.0 (REF)
176.0
146.0
86.0
5.0
105.0
130.0
135.0 (REF)
NOTE: WHEN THE LID RESTS UPON THE CHAMBER, ITS RIM MUST FIT OVER ASSEMBLED PART 1 (MAIN PTFE LAYER) AND PART 2 (PTFE CHAMBER FRONT). PLEASE ADJUST CORNER FILETS AS REQUIRED. (SEE ALSO PAGE 4.)
FRONT
SECTION AA
(SCALE 2:1; SEE PAGE 2)
10.00
5/8"
DIMENSIONS SHOWN IN MM
PROJECT: CHROMATOGRAPHY CHAMBER
STEVEN JIM, GLAD LAB
(SJIM@UALBERTA.CA; 780 492 7926)
PART 4: Chamber Lid (Aluminum)
FILENAME: "UTLC Chamber-Part4-aluminum lid-update20130424.vsd"
PAGE: 3 OF 4

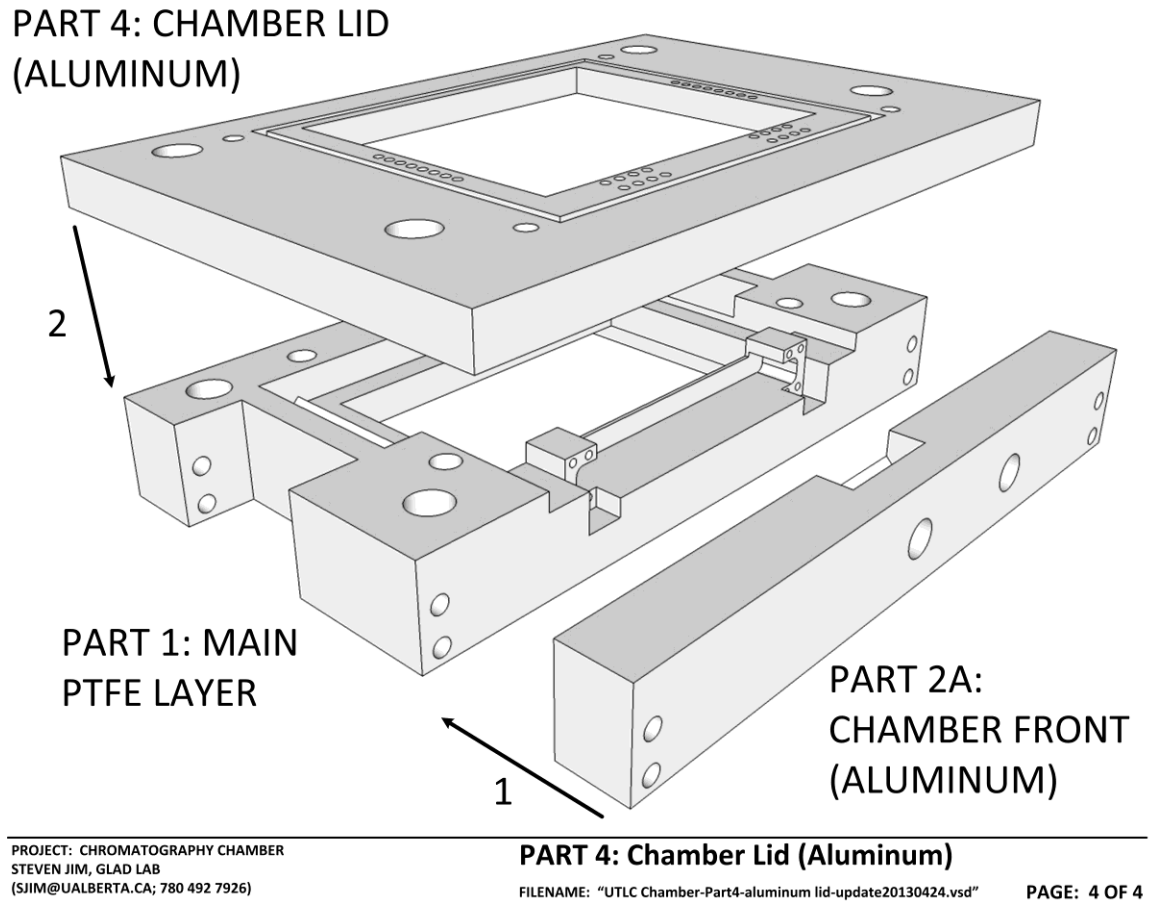
PART 4: CHAMBER LID
(ALUMINUM)
2
PART 1: MAIN
PTFE LAYER
1
PART 2A:
CHAMBER FRONT
(ALUMINUM)
PROJECT: CHROMATOGRAPHY CHAMBER
STEVEN JIM, GLAD LAB
(SJIM@UALBERTA.CA; 780 492 7926)
PART 4: Chamber Lid (Aluminum)
FILENAME: "UTLC Chamber-Part4-aluminum lid-update20130424.vsd"
PAGE: 4 OF 4

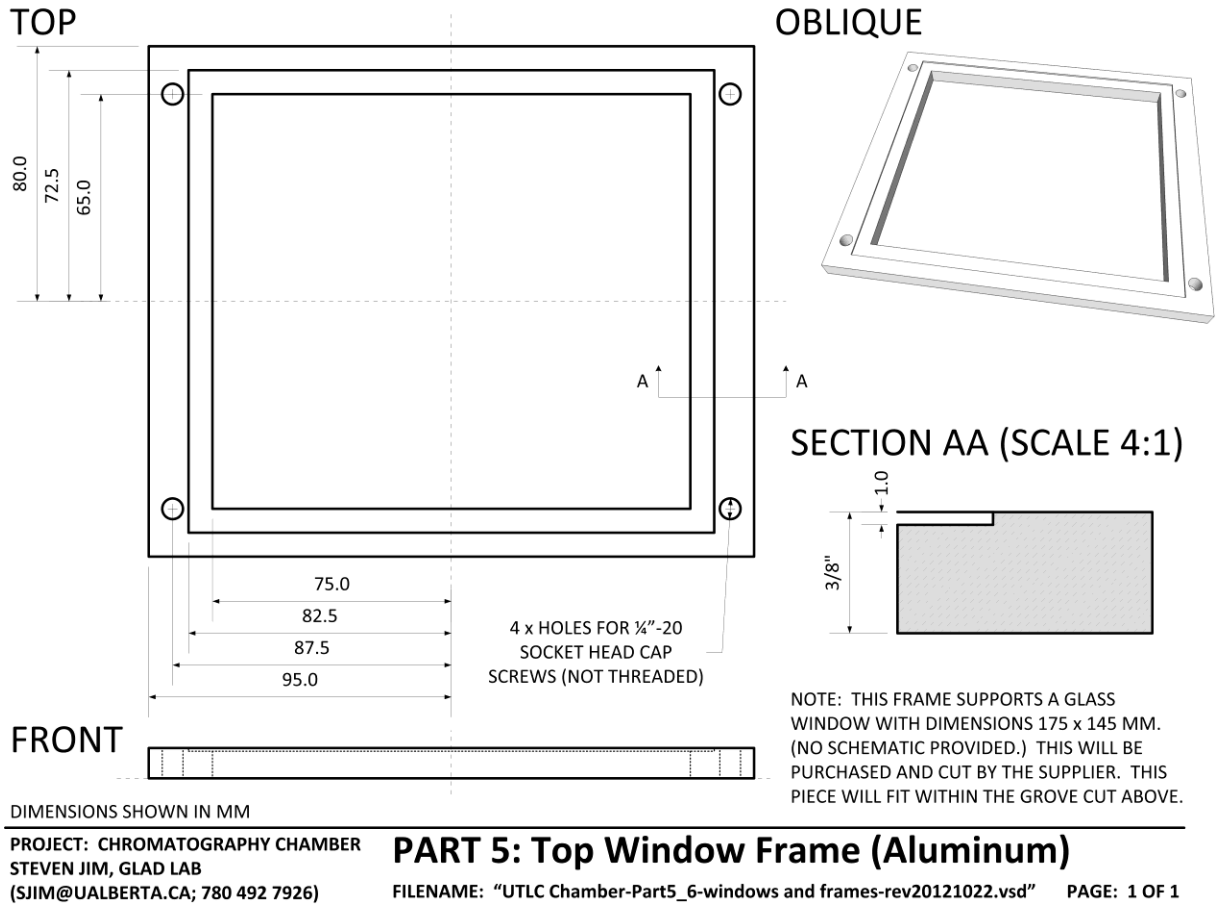
TOP
OBLIQUE
80.0
72.5
65.0
A
A
SECTION AA (SCALE 4:1)
1.0
3/8"
75.0
82.5
87.5
95.0
4 x HOLES FOR ¼"-20
SOCKET HEAD CAP
SCREWS (NOT THREADED)
NOTE: THIS FRAME SUPPORTS A GLASS WINDOW WITH DIMENSIONS 175 x 145 MM. (NO SCHEMATIC PROVIDED.) THIS WILL BE PURCHASED AND CUT BY THE SUPPLIER. THIS PIECE WILL FIT WITHIN THE GROVE CUT ABOVE.
FRONT
DIMENSIONS SHOWN IN MM
PROJECT: CHROMATOGRAPHY CHAMBER
STEVEN JIM, GLAD LAB
(SJIM@UALBERTA.CA; 780 492 7926)
PART 5: Top Window Frame (Aluminum)
FILENAME: "UTLC Chamber-Part5_6-windows and frames-rev20121022.vsd"
PAGE: 1 OF 1

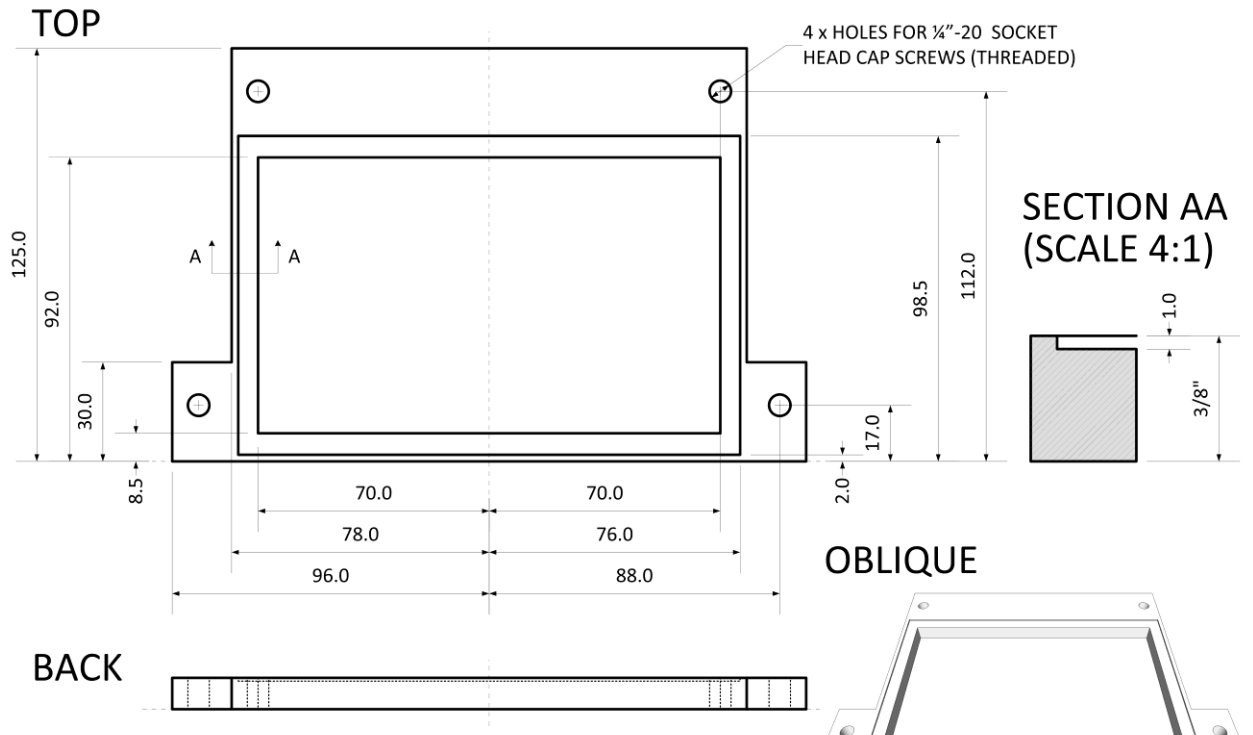
TOP
4 x HOLES FOR ¼"-20 SOCKET
HEAD CAP SCREWS (THREADED)
A
A
125.0
92.0
30.0
8.5
98.5
112.0
17.0
2.0
70.0
70.0
78.0
76.0
96.0
88.0
SECTION AA
(SCALE 4:1)
1.0
3/8"
OBLIQUE
BACK
NOTE: THIS FRAME SUPPORTS A GLASS WINDOW WITH DIMENSIONS 152 x 96.5 MM.
(NO SCHEMATIC PROVIDED.) THIS WILL BE PURCHASED AND CUT BY THE SUPPLIER. THIS
PIECE WILL FIT WITHIN THE GROVE CUT ABOVE.
DIMENSIONS SHOWN IN MM
PROJECT: CHROMATOGRAPHY CHAMBER
STEVEN JIM, GLAD LAB
(SJIM@UALBERTA.CA; 780 492 7926)
PART 6: Bottom Window Frame (Aluminum)
FILENAME: "UTLC Chamber-Part5_6-windows and frames-rev20121022.vsd"
PAGE: 1 OF 1

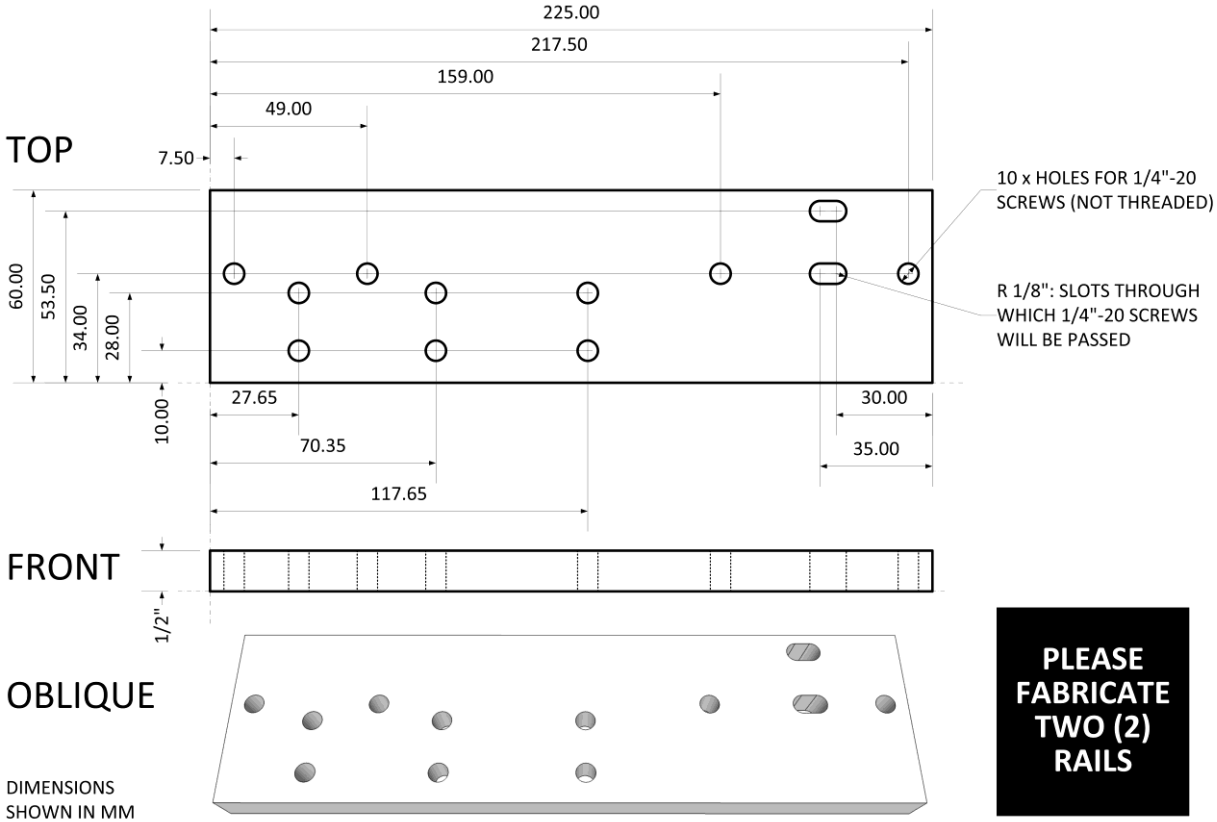
225.00
217.50
159.00
49.00
TOP
7.50
10 x HOLES FOR 1/4"-20
SCREWS (NOT THREADED)
R 1/8": SLOTS THROUGH
WHICH 1/4"-20 SCREWS
WILL BE PASSED
60.00
53.50
34.00
28.00
10.00
27.65
70.35
117.65
30.00
35.00
FRONT
1/2"
OBLIQUE
DIMENSIONS
SHOWN IN MM
PLEASE
FABRICATE
TWO (2)
RAILS
PROJECT: CHROMATOGRAPHY CHAMBER
STEVEN JIM, GLAD LAB
(SJIM@UALBERTA.CA; 780 492 7926)
PART 7A: Frame Rail A (Aluminum)
FILENAME: "UTLC Chamber-Part7-frame-rev20121024.vsd"
PAGE: 1 OF 1

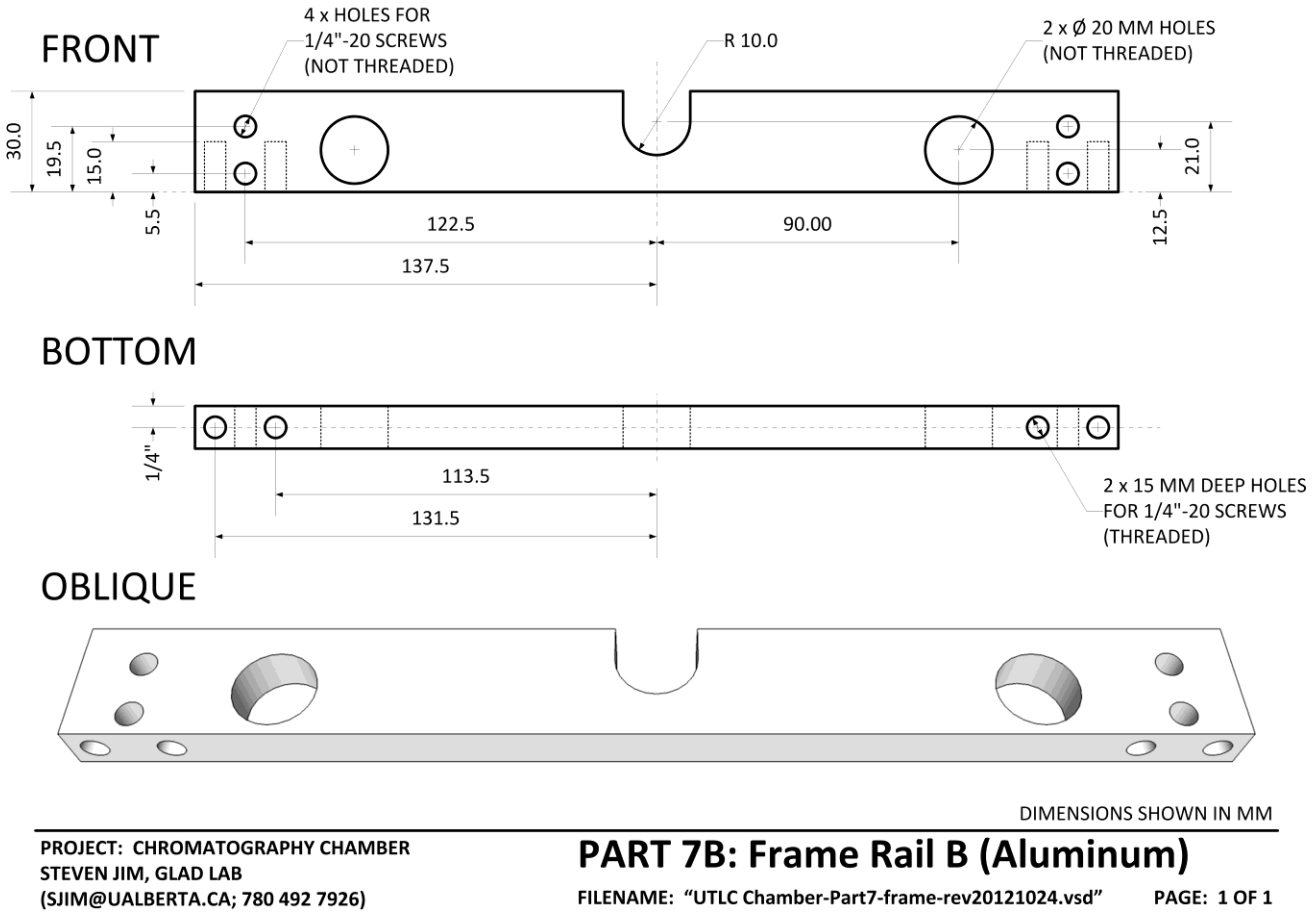
FRONT
4 x HOLES FOR
1/4"-20 SCREWS
(NOT THREADED)
R 10.0
2 x Ø 20 MM HOLES
(NOT THREADED)
30.0
19.5
15.0
5.5
21.0
12.5
122.5
90.00
137.5
BOTTOM
1/4"
113.5
131.5
2 x 15 MM DEEP HOLES
FOR 1/4"-20 SCREWS
(THREADED)
OBLIQUE
DIMENSIONS SHOWN IN MM
PROJECT: CHROMATOGRAPHY CHAMBER
STEVEN JIM, GLAD LAB
(SJIM@UALBERTA.CA; 780 492 7926)
PART 7B: Frame Rail B (Aluminum)
FILENAME: "UTLC Chamber-Part7-frame-rev20121024.vsd"
PAGE: 1 OF 1

PLEASE FABRICATE FOUR (4) MOUNTING BLOCKS

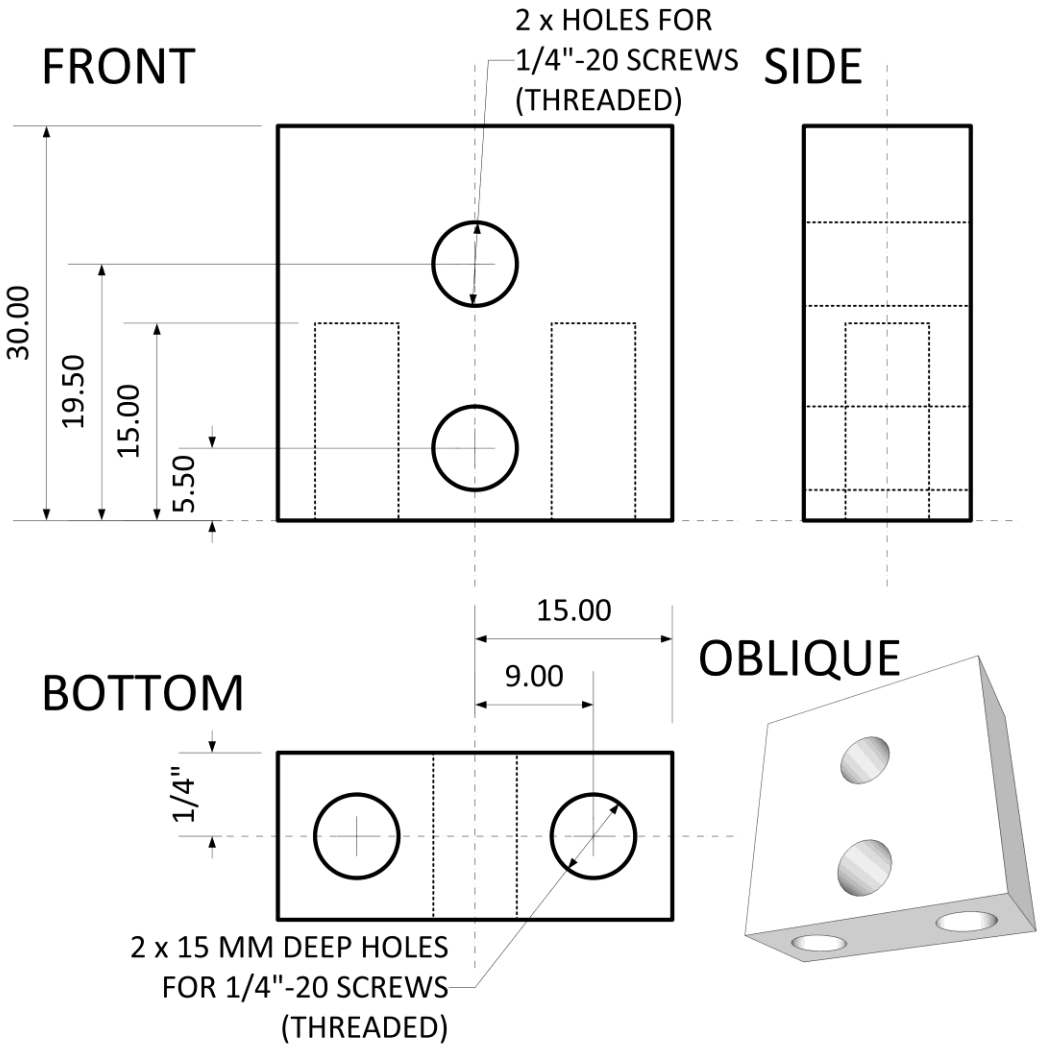

DIMENSIONS SHOWN IN MM

PROJECT: CHROMATOGRAPHY CHAMBER
STEVEN JIM, GLAD LAB
(SJIM@UALBERTA.CA; 780 492 7926)

Part 7C: Mounting Blocks (Aluminum)
FILENAME: "UTLC Chamber-Part7-frame-rev20121024.vsd"
PAGE: 1 OF 1